


6-23-2014

Paleoenvironments and Geochemical Signals from the Late Barremian to the Middle Aptian in a Tethyan Marginal Basin, Northeast Spain: Implications for Carbon Sequestration in Restricted Basins

Yosmel Sanchez Hernandez Mr.
Florida International University, ysanc016@fiu.edu

DOI: 10.25148/etd.FI14071122

Follow this and additional works at: <https://digitalcommons.fiu.edu/etd>

 Part of the [Geochemistry Commons](#), [Geology Commons](#), [Paleontology Commons](#), [Sedimentology Commons](#), and the [Stratigraphy Commons](#)

Recommended Citation

Sanchez Hernandez, Yosmel Mr., "Paleoenvironments and Geochemical Signals from the Late Barremian to the Middle Aptian in a Tethyan Marginal Basin, Northeast Spain: Implications for Carbon Sequestration in Restricted Basins" (2014). *FIU Electronic Theses and Dissertations*. 1421.

<https://digitalcommons.fiu.edu/etd/1421>

This work is brought to you for free and open access by the University Graduate School at FIU Digital Commons. It has been accepted for inclusion in FIU Electronic Theses and Dissertations by an authorized administrator of FIU Digital Commons. For more information, please contact dcc@fiu.edu.

FLORIDA INTERNATIONAL UNIVERSITY

Miami, Florida

PALEOENVIRONMENTS AND GEOCHEMICAL SIGNALS FROM THE LATE
BARREMIAN TO THE MIDDLE APTIAN IN A TETHYAN MARGINAL BASIN,
NORTHEAST SPAIN: IMPLICATIONS FOR CARBON SEQUESTRATION IN
RESTRICTED BASINS

A dissertation submitted in partial fulfillment of

the requirements for the degree of

DOCTOR OF PHILOSOPHY

in

GEOSCIENCES

by

Yosmel Sanchez-Hernandez

2014

To: Interim Dean Michael R. Heithaus
College of Arts and Sciences

This dissertation, written by Yosmel Sanchez-Hernandez, and entitled Paleoenvironments and Geochemical Signals from the Late Barremian to the Middle Aptian in a Tethyan Marginal Basin, Northeast Spain: Implications for Carbon Sequestration in Restricted Basins, having been approved in respect to style and intellectual content, is referred to you for judgment.

We have read this dissertation and recommend that it be approved.

Laurel Collins

Rosemary Hickey-Vargas

Rudolf Jaffé

Florentin Maurrasse, Major Professor

Date of Defense: June 23, 2014

The dissertation of Yosmel Sanchez-Hernandez is approved.

Interim Dean Michael R. Heithaus
College of Arts and Sciences

Dean Lakshmi N. Reddi
University Graduate School

Florida International University, 2014

DEDICATION

To my family for their love and encouragement, to my grandmother.

ACKNOWLEDGMENTS

Exploring the boundaries between scientific disciplines while learning the secrets stored for millions of years in the rocks of the Spanish Pyrenees have been both challenging and thrilling. For this experience I am extremely grateful to a number of people.

First, to my advisor, Dr. Florentin J. Maurrasse, for his invaluable teachings on general science, for his extraordinary leadership, his altruism and contagious love and dedication to the geosciences, for his economic support through the Goodfriend Memorial Funds. Dr. Maurrasse mentorship has been extremely valuable not only for academic purposes but also as life lessons.

To my committee members for their teachings, time, and support. Dr. Laurel Collins for my first steps into the study of paleoenvironments and for constructive review of my work. Dr. Rosemary Hickey for providing me with valuable knowledge in geochemistry and for her helpful and supportive comments along my doctorate. To Dr. Rudolf Jaffe for his helpful lessons on organic geochemistry that improved my understanding of geochemical processes related to organic matter preservation, for his important support with the biomarker analyses.

I am also most grateful to Dr. William Anderson for his contribution with the carbon isotopic analyses; and Dr. Greenville Draper for allowing me to use his lab facilities. Special thanks go to Diane Pirie for her commitment to the functionality of the department's lab facilities and her efficient logistic support; to Tom Beasley for opening me the doors to SEM with EDS microscopy which is a substantial part of my dissertation. Dr. Tatiana Trejos is also kindly acknowledged for her training and support with the

sample preparation, LA-ICPMS procedures and data processing. I want to also thank Ding He and Sarah Jantzy for their assistance with biomarker and trace element analyses, respectively. Carrie Rebenack and John Harris are also acknowledged for their help with the carbon isotope analyses.

A special acknowledgment to Yaya for her encouragement, understanding and love.

I am very grateful to Florida International University, the University Graduate School and the Department of Earth and Environment for supporting me through a teaching assistantship and the Doctoral Evidence Acquisition fellowship. Chemical Geology and Cretaceous Research both from Elsevier are graciously acknowledge for copyright release of the published articles.

ABSTRACT OF THE DISSERTATION

PALEOENVIRONMENTS AND GEOCHEMICAL SIGNALS FROM THE LATE
BARREMIAN TO THE MIDDLE APTIAN IN A TETHYAN MARGINAL BASIN,
NORTHEAST SPAIN: IMPLICATIONS FOR CARBON SEQUESTRATION IN
RESTRICTED BASINS

by

Yosmel Sanchez-Hernandez

Florida International University, 2014

Miami, Florida

Professor Florentin Maurrasse, Major Professor

The hallmark of oceanic anoxic event 1a (OAE1a) (early Aptian ~125 Ma) corresponds to worldwide deposition of black shales with total organic carbon (TOC) content > 2% and a $\delta^{13}\text{C}$ positive excursion up to ~5‰. OAE1a has been related to large igneous province volcanism and dissociation of methane hydrates during the Lower Cretaceous. However, the occurrence of atypical, coeval and diachronous organic-rich deposits associated with OAE1a, which are also characterized by positive spikes of the $\delta^{13}\text{C}$ in epicontinental to restricted marine environments of the Tethys Ocean, indicates localized responses decoupled from complex global forcing factors.

The present research is a high-resolution, multiproxy approach to assess the paleoenvironmental conditions that led to enhanced carbon sequestration from the late Barremian to the middle Aptian in a restricted, Tethyan marginal basin prior to and during OAE1a. I studied the lower 240 m of the El Pui section, Organyà Basin, Spanish Pyrenees. The basin developed as the result of extensional tectonism linked to the

opening of the Atlantic Ocean. At the field scale the section consists of a sequence of alternating beds of cm – m-scale, medium-gray to grayish-black limestones and marlstones with TOC up to ~4%.

The results indicate that the lowest 85 m of the section, from latest Barremian – earliest Aptian, characterize a deepening phase of the basin concomitant with sustained riverine flux and intensified primary productivity. These changes induced a shift in the sedimentation pattern and decreased the oxygen levels in the water column through organic matter respiration and limited ventilation of the basin.

The upper 155 m comprising the earliest – late-early Aptian document the occurrence of OAE1a and its associated geochemical signatures (TOC up to 3% and a positive shift in $\delta^{13}\text{C}$ of ~5‰). However, a low enrichment of redox-sensitive trace elements indicates that the basin did not achieve anoxic conditions. The results also suggest that a shallower-phase of the basin, coeval with platform progradation, may have increased ventilation of the basin at the same time that heightened sedimentation rates and additional input of organic matter from terrestrial sources increased the burial and preservation rate of TOC in the sediment.

TABLE OF CONTENTS

CHAPTER	PAGE
1 INTRODUCTION	1
1.1 The record of OAE1a.....	3
1.2 Geochemical and stratigraphic particularities in marginal basins prior to OAE1a ...	6
1.3 Main Hypothesis	8
1.4 Objectives	9
1.5 Summary of the methods and issues addressed	9
1.6 Dissertation Structure.....	10
1.7 References.....	12
2 GEOLOGIC AND STRATIGRAPHIC SETTING OF THE ORGANYÀ BASIN	19
2.1 Overall stratigraphic framework of the Organyà Basin.....	21
2.2 The El Pui section	22
2.3 References.....	24
3 MATERIAL AND METHODS	27
3.1 Field measurement and sampling of the stratigraphic section.....	27
3.2 Laboratory analyses	28
3.2.1 Petrographic analysis	28
3.2.2 Micropaleontology and age.....	29
3.2.3 Scanning Electron Microscopy	31
3.2.4 Total carbon/carbonate – TC, TIC, TOC	32
3.2.5 C-stable isotope on the organic fraction ($\delta^{13}\text{C}_{\text{org}}$).....	33
3.2.6 Major and trace element analyses	33
3.2.7 Biomarker analysis.....	35
3.2.8 Bulk and clay mineral analysis	36
3.3 References.....	38
4 GEOCHEMICAL CHARACTERIZATION AND REDOX SIGNALS FROM THE LATEST BARREMIAN TO THE EARLIEST APTIAN IN A RESTRICTED MARINE BASIN: EL PUI SECTION, ORGANYÀ BASIN, SOUTH-CENTRAL PYRENEES	42
Abstract.....	42
4.1 Introduction.....	43
4.2 Geographic and geologic setting.....	47
4.3 Material and Methods	50
4.3.1 Petrographic analysis	50
4.3.2 Total carbon/carbonate –TC, TIC, TOC	52
4.3.3 C-stable isotope on the organic fraction ($\delta^{13}\text{C}_{\text{org}}$).....	53
4.3.4 Major and trace element analyses	53
4.3.5 SEM and EDS analyses	55
4.4 Results.....	55

4.4.1	Petrographic analysis	55
4.4.2	TOC, TIC, and $\delta^{13}\text{C}_{\text{org}}$	58
4.4.3	Major and trace elements analyses	60
4.5	Discussion	66
4.5.1	Carbon isotope chemostratigraphy and age correlation	66
4.5.2	Role of basin physiography on nutrient-driven productivity	71
4.5.3	Redox conditions	75
4.6	Conclusions	82
4.7	Acknowledgments	84
4.8	References	85
5	ASSESSING THE FACTORS CONTROLLING HIGH SEDIMENTATION RATES FROM THE LATEST BARREMIAN–EARLIEST APTIAN IN THE HEMIPELAGIC SETTING OF THE RESTRICTED ORGANYÀ BASIN, NE SPAIN	101
	Abstract	101
5.1	Introduction	102
5.2	Geological setting and paleoceanography of the study area	105
5.3	Materials and methods	108
5.3.1	Carbon analysis	108
5.3.2	Biomarker analysis	108
5.3.3	Bulk and clay mineral analysis	109
5.3.4	Microscopy	110
5.4	Results	112
5.4.1	Carbon geochemistry	112
5.4.2	Biomarkers	115
5.4.3	Clay and bulk mineral assemblages	118
5.4.4	Microscopy: light microscope, SEM and EDS	121
5.5	Discussion	123
5.5.1	Biochronology and paleontological significance of calcareous nannofossils in the El Pui section.	123
5.5.2	Assessing the provenance of sediment components in the El Pui section	126
5.5.3	Significance of $\delta^{13}\text{C}/\text{TOC}/\text{TIC}/\text{Biomarkers}$ in assessing productivity rates	132
5.5.4	Assessing sediment accumulation rate	136
5.5.5	Characterization of terrestrial fluxes in the Organyà Basin	139
5.6	Conclusions	142
5.7	Acknowledgments	143
5.8	References	144
6	MICROFACIES CHARACTERIZATION AND FAUNAL VARIATIONS IN THE UPPER BARREMIAN–LOWER APTIAN HEMIPELAGIC SEDIMENTS OF THE ORGANYÀ BASIN: PALEOENVIRONMENTAL IMPLICATIONS	161
	Abstract	161
6.1	Introduction	162
6.2	Physiographic and geologic settings	165

6.3	Materials and Methods.....	168
6.4	Results and discussion	174
6.4.1	Overall lithology and macrofacies.....	174
6.4.2	Microfacies description, intervals of occurrence and interpretation.....	175
6.4.3	Paleoecologic significance of micro-ammonoids and roveacrinids in the El Pui sediments.....	193
6.5	Conclusions.....	196
6.6	Acknowledgments.....	197
6.7	References.....	197
7	THE RECORD OF OCEANIC ANOXIC EVENT 1a (OAE1a) IN THE SEMI-RESTRICTED ORGANYÀ BASIN: IMPLICATIONS FOR UNDERSTANDING THE INFLUENCE OF REGIONAL FACTORS IN THE EXPRESSION OF OAE1a	207
	Abstract.....	207
7.1	Introduction.....	208
7.2	Geological setting	210
7.3	Materials and Methods.....	212
7.3.1	Sampling and petrographic analysis	212
7.3.2	Carbon analyses (TOC, TIC, $\delta^{13}\text{C}_{\text{org}}$).....	213
7.3.3	Bulk and clay mineral analyses.....	214
7.3.4	Major and trace element analysis.....	215
7.3.5	Biomarker analysis.....	216
7.4	Results.....	217
7.4.1	Lithostratigraphy, and petrographic analysis.....	217
7.4.2	Inorganic, organic and isotopic carbon analyses (TIC, TOC and $\delta^{13}\text{C}_{\text{org}}$).....	220
7.4.3	Bulk and clay mineral analyses.....	221
7.4.4	Major and trace elements	223
7.4.5	Biomarker analysis.....	227
7.5	Discussion	229
7.5.1	Constraints from the integrated $\delta^{13}\text{C}_{\text{org}}$ record of the El Pui section	229
7.5.2	Facies variability, geochemical proxies as paleoenvironmental indicators	231
7.5.3	Main Controlling factors on the expression of OAE1a in the El Pui section	237
7.6	Conclusions.....	239
7.7	Acknowledgments.....	240
7.8	References.....	241
8	GENERAL CONCLUSIONS.....	251
	APPENDICES	254
	VITA.....	272

LIST OF FIGURES

FIGURE	PAGE
Figure 1-1 Global paleogeography and paleotectonics of the Late Jurassic ~150 Ma.	2
Figure 1-2 Global paleogeography and paleotectonics of the Early Cretaceous ~120 Ma; (from http://cpgeosystems.com/paleomaps.html).	2
Figure 1-3 Paleogeographic distribution (120 Ma) of black shales deposited during OAE1a (after Wang et al., 2011).	4
Figure 1-4 Comparative $\delta^{13}\text{C}$ profile of three Subalpine sections showing a broad positive excursion indicative of intensified ^{12}C burial in the latest Barremian.	6
Figure 1-5 Integrated model for enhanced preservation of OM in extensional basins.	7
Figure 2-1 The opening of the Bay of Biscay during the Mesozoic with the main tectonic features and adjacent terrains. After García-Mondejar (1996).	20
Figure 2-2 Synthetic stratigraphic column of the Organyà Basin with the geochronological distribution of the five more important lithologic groups. After García-Senz (2002). The black arrow indicates the studied interval.	22
Figure 2-3 Field view of the first ~30 m of the El Pui section showing the bedding of the sequence. See geologist in the extreme left and right along the road for scale.	23
Figure 2-4 Lower part of the El Pui section that shows the continuous parallel bedding that favors excellent outcrop conditions for high resolution sampling.	24
Figure 3-1 Comparative sketch of the diffractograms obtained for the El Pui samples. The number of peaks and their corresponding intensity can be used to assess the presence of mixed layered clay.	38
Figure 4-1 A) Simplified geologic map of the Organyà Basin (modified from Bernaus et al., 2003) showing the location of the study area, the overall age and lithologies in the southern flank of Sierra de Prada. Short lines symbol (└) show the strike and dip of the homoclinal sequence. B) Simplified geologic cross section of the studied area through X-Y drawn from a 1:50.000 topographic map of Cabó from the Institut Cartogràfic de Catalunya (http://www.icc.cat)	46
Figure 4-2 A) Synthetic stratigraphic column and age distribution of the lower Cretaceous of the Organyà Basin (from García Senz, 2002), the Barremian-Aptian boundary has been modified after Moreno-Bedmar (2010). B) Chronostratigraphic column of the 85 m studied at El Pui with fossil and lithologic characterization. All the facies studied correspond to the mudstone classification of Dunham (1962).	

Circled numbers to the right of the fossil content indicate the bioturbation index after Taylor and Goldring (1993). See legend for explanation of symbols..... 48

Figure 4-3 El Pui section: A) Panoramic view of the lower 25 m (sediment thickness) of the sampled area showing a continuous succession. B) Close up view of the yellow oval that corresponds to the stratigraphic interval from ~15 m to ~20 m showing the lithology along a road cut to the top of Sierra de Prada; note the well-consolidated dark limestone beds..... 50

Figure 4-4 SEM micrograph of samples at different levels within the studied section. C10-19 left: Arrow points to coccolith fragments. C10-19 right: Lower arrow points to small calcite spheres, remains of coccoid bacteria; upper arrow indicates dispersive pyrite. C10-30: Arrow points to a relatively well preserved calcareous nannofossil. C10-48: Arrow indicates dispersive pyrite in a carbonate matrix of calcareous nannofossil fragments. C10-50: Cyanobacterial structure. C11-87: Arrows point to abundant framboidal pyrite less than 10 μm in size; black circles enclose calcareous nannofossils..... 56

Figure 4-5 Illustrations of *G. blowi*. A: picture taken with a Leica reflected light microscope of a relatively well-preserved whole specimen obtained at ~16 m; B and C: photomicrograph of *G. blowi* in thin section at 12 m and 33 m respectively. 57

Figure 4-6 Figure 6. SEM with EDS analysis performed on samples showing the presence of siliciclastic material. Diagrams show the qualitative elemental composition of the grains analyzed. Micrographs show the texture of the fine matrix and the random distribution of the grains. Arrows pointing to the elemental diagram originate at small squares where EDS was performed..... 58

Figure 4-7 Lithostratigraphy and carbon chemostratigraphy: A) Simplified chronostratigraphic column of the studied section. B) Vertical variation in TOC. Star symbols indicate levels of high TOC concurrent with positive excursions in $\delta^{13}\text{C}_{\text{org}}$. C) Vertical variation in TIC. D) Vertical variation in $\delta^{13}\text{C}_{\text{org}}$ including the characteristic late Barremian – lower Aptian carbon isotope segments C1-C3 from Menegatti et al. (1998). The C segments define patterns in the $\delta^{13}\text{C}_{\text{org}}$ curve that are widely used for chemostratigraphic correlation..... 59

Figure 4-8. Stratigraphic correlation of major and trace elements normalized to Al concentration (\dagger represents values $\times 10^{-4}$). C1- C3 corresponds to $\delta^{13}\text{C}_{\text{org}}$ carbon isotope segments in the El Pui section based on the “Cismon” carbon isotope subdivision proposed by Menegatti et al. (1998). The studied 85 m correspond to the *G. blowi* Zone. The two far right columns in the chart show the redox indices Ni/Co and U/Th, and are included for vertical comparison. Dashed lines represent the Al normalized concentration of each corresponding element in the average shale from Wedepohl (1971, 1991). Dashed lines in the Ni/Co and U/Th plots indicate the redox fields proposed by Jones and Manning (1994) (see also Fig. 4-10). Dotted line to the left in the U/Th plot reflects the standard value suggested by Wignall and Myers

(1988) for normal mudstones. The asterisks (*) for the redox indices in this figure indicate dysoxia as a general term for oxygen limited conditions as proposed by Wignall and Myers (1988). The shaded interval refers to recurrent oxygen deficient conditions within the lower 31 m of the section.	61
Figure 4-9 Linear plots of selected elements versus Al, showing the correlation coefficient used to support the interpretation on provenance. A) Silicon; B) Titanium; C) Phosphorous; D) Iron ; E) Nickel; F) Chromium ; G) Uranium; H) Vanadium.....	64
Figure 4-10 Redox fields classification based on oxygen levels after Tyson and Pearson (1991) and redox indices after Jones and Manning (1994). The suggested limits for the Ni/Co and U/Th are not of strict application in this work.....	65
Figure 4-11 Geochemical correlation of $\delta^{13}\text{C}$ for several Tethys sections: A) Cismon (Menegatti et al., 1998); B) Cassis-La Bédoule (Stein et al., 2012); C) Pădurea Craiului (Papp et al., 2013); D) Igaratza (Millán et al., 2009); E) chemostratigraphic synthesis of the late Barremian - Aptian from Erba (2004); and F) El Pui, this study. The light blue areas indicate intervals of correlation. Gray shaded rectangles correspond to the interval of OAE1a. The approximate Barremian-Aptian boundary at El Pui is proposed based on geochemical correlation with calibrated sections. C1- C8 segments represent trends in the $\delta^{13}\text{C}_{\text{carb}}$ and $\delta^{13}\text{C}_{\text{org}}$ defined by Menegatti et al. (1998).....	69
Figure 5-1 General geographic location and simplified geologic map of the Organyà area modified from García-Senz (2002). The arrow next to El Pui represents the approximate location of the studied section.....	105
Figure 5-2 (A) Overview of the first ~30 m of the section showing distinct continuous interbeds of limestones and marls characteristic of the entire studied sequence at El Pui. (B) Black limestone facies are more common in the lowest 15 m of the section. (C) Marly facies are more characteristic of the upper 40 m of the section.....	106
Figure 5-3 Paleooceanographic reconstruction of the western Tethys during the early Aptian modified from Masse et al. (1993). Also, details of bathymetry and paleoenvironments are incorporated from Mancinelli and Chiocchini, (2006), and Godet et al. (2013). Red star shows the relative position of the Organyà Basin in the paleophysiographic context of the Early Cretaceous of Western Tethys.	107
Figure 5-4 Simplified lithological log and geochemical variations in the 85 m El Pui section. (A) Simplified chronostratigraphic column including lithological variations, oxic, dysoxic levels, and relevant nannofossil events. (B) TOC. (C) TIC. (D) $\delta^{13}\text{C}_{\text{org}}$. The “C” Subdivisions correspond to the carbon isotopic segments after Menegatti et al. (1998) that have been proposed for the El Pui section in Sanchez-Hernandez and Maurrasse (2014).	113

Figure 5-5 SEM micrographs of calcareous nannofossils including the sample code and corresponding stratigraphic position. The carbonate matrix is dominated by disaggregated calcareous nannofossil fragments at any level in the studied section. At higher magnification the fragments surrounding better preserve <i>Nannoconus sp.</i> on B resemble those shown in C.	114
Figure 5-6 Microfacies of selected samples at different levels of the stratigraphic column showing texture and composition characteristic of a hemipelagic setting with dominant calcareous nannofossils shown in Fig. 5. A-) sample C10-05 at ~1.2 m, dark micritic matrix with small planktonic foraminifera in the center; B-) sample C10-16 at ~ 4.9 m, abundant calcispheres and small planktonic foraminifera in a fine, dark carbonate matrix with traces of kerogen; C-) sample C10-42 at ~16.8 m, fine micritic matrix; and D-) sample C10-87 at ~32.3 m, fine micritic matrix with coiled benthic foraminifera in the center. Pictures B, C, and D were taken using a white polarized light source. Scale bar represents 0.5 mm.....	115
Figure 5-7 Relative stratigraphic position of 10 of the 24 samples analyzed for <i>n</i> -alkanes and their corresponding bar diagrams: <i>n</i> -alkanes abundance in ng/g (y axis) with respect to the carbon chain length (x axis). Notice the absence of even or odd carbon number preference.....	116
Figure 5-8 Chromatograms of selected samples along the studied section. Notice the absence of <i>n</i> -alkanes with carbon chain number > C ₂₀ . For relative position of the samples, see Figure 5-7.....	118
Figure 5-9 Characteristic diffractograms of XRD analyses for sample C10-58 (glycolated (GLY) and heated (HTD)). Qualitative identification of a small amount of mixed-layered clay is represented by the small peak near 5.2° 2θ on the EG solvated sample. The broad peak near 17.7° 2θ points to a most likely illite/smectite random interlayering. Heating the sample produces a pattern lacking the small peak near 5.2° 2θ with an overall resemblance to that of a pure illite pattern with a weakened 003 peak.	119
Figure 5-10 Relative percentages of clay minerals at different levels of the studied section. Notice that the assemblages are dominated by illite with minor variations in the concentration of illite/smectite mixed layer, chlorite and kaolinite. Because of the consistency in the concentrations these measurements are considered to represent the general average variation of the 85 m studied.	120
Figure 5-11 Pie diagram of the average mineral composition of limestones and marls in the El Pui section from bulk mineral measurements and EDS analyses.	120
Figure 5-12 (A) Simplified lithological log and nannofossil events in the studied 85 m of El Pui section. Chemostratigraphic correlation and relative position of the Barremian-Aptian boundary discussed in the text suggest that the <i>R. angustus</i> appearance at El Pui coincides with its true first occurrence. B, C, D, and E: vertical	

variation in the relative abundances of <i>Watznaueria barnesae</i> , <i>Nannoconus sp.</i> , narrow canal <i>nannoconids</i> , and wide canal <i>nannoconids</i> , respectively. All the samples represented were analyzed using light microscope and SEM with EDS.	122
Figure 6-1 Geologic map of the Organyà area showing the relative position of the El Pui section (Adapted from Bachmann and Willens, 1996).....	164
Figure 6-2 Distant view of the basal ~40 m of the El Pui section. Yellow arrows point to geologists seen on the site for scale. Note the well-defined, continuous interbeds of limestones and marlstones characteristic of the lower 85 m studied.	165
Figure 6-3 Near field view of the lower ~17 m of the stacked limestones and marlstones of the El Pui section. Note facies intervals as described in the text.	167
Figure 6-4 Close-up view of part of the succession shown in Fig. 6-3 and immediately above. Note the Dark yellowish orange (10YR 6/6) of the weathered surface in contrast to the true Bluish gray (5B 6/1) of the unaltered rock.	168
Figure 6-5 Close-up view higher up the sequence showing part of the outcrop of microfacies MF5.	170
Figure 6-6 Close-up view of the outcrop comprising microfacies MF5 showing the transition from massive well consolidated limestones to marlstones.	171
Figure 6-7 A) Simplified lithologic column of the lower 85 m of the El Pui section with partial sample location and microfacies distribution. Color assignment to microfacies follows the same pattern throughout the column. B) Total organic carbon curve (TOC), and C) total inorganic carbon (TIC) as wt % CaCO ₃	173
Figure 6-8 SEM micrographs of samples showing characteristic components of the matrix in the 85m section studied. A) C10-52, 19 m; B) C10-77, 28 m; C) C11-87, 32 m); and D) C11-137, 49 m. Calcareous nannofossil remains are consistently abundant and are the main components of the calcareous matrix throughout the studied sequence. Note framboidal pyrite (FP) in micrograph B.	177
Figure 6-9 Photomicrographs illustrating microfacies MF1. A) Sample C10-01, micritic matrix with a larger unidentified skeletal grain. B) Sample C10-04, bioturbated matrix with kerogen filling in interparticle pore spaces. C) Sample C10-05, very fine micritic matrix with a small planktonic foraminifera (Pk) (cf. <i>G. blowi</i> ?). D) Sample C10-06, very fine micritic matrix with roveacrinid fragments. E) Sample C10-06, undetermined roveacrinid fragment in a fine carbonate mud. F) Sample C10-09, with well-preserved coiled benthic foraminifera in a carbonate mud with additional carbonate microfragments. G) Sample C10-09, undetermined roveacrinid fragment.	178

Figure 6-10 Photomicrographs illustrating microfacies MF1A. A) Sample C10-64, benthic foraminifera in a very fine carbonate mud with dispersive amorphous OM. B) Sample C10-65, cross section of a small echinoid spine in a very fine carbonate mud with dispersive amorphous OM. C) Sample C11-19, roveacrinid fragment next to a microfracture in a fine matrix. D) Sample C11-191, planktonic foraminifera *G. blowi*. E) Sample C11-193, biserial benthic foraminifera (Bt) and microcarbonate fragments floating in a micritic matrix. F) Sample C11-189, undetermined bioclast, possibly an ostracod? 181

Figure 6-11 Photomicrographs illustrating microfacies MF2. A) Sample C10-16, fine carbonaceous matrix with benthic (Bt) slightly below center, planktonic (Pk) foraminifera, and abundant calcispheres (cs). B) Magnified view of part of photomicrograph shown previously in A. C) Sample C10-17, abundant microcarbonate fragments and skeletal components in a fine matrix. D) Sample C10-18, inferred section of a radial plate of an undetermined roveacrinid. The microcarbonate particles are thought to be from disintegration of these planktonic micro-echinoderms. E) Sample C10-20, biserial benthic (Bt) foraminifera. F) Sample C10-18, slightly bioturbated carbonate matrix with abundant comminuted skeletal debris. G) Sample C10-20, molds of planktonic (Pk) foraminifera replaced with kerogen in a micritic matrix. H) Sample C10-19, undetermined fossil remain embedded in a fine carbonate matrix (copepod ?, loricifera ? van der Wielen et al. 2005, Yakimov et al. 2007)..... 183

Figure 6-12 Photomicrographs illustrating microfacies type MF2, continued. A) Sample C10-31, oblique section of small echinoderm spine. B) Sample C10-31, undetermined roveacrinid fragment in a fine, dark carbonate mud. C) Sample C10-32, planktonic foraminifera. D) Sample C10-32, biserial benthic foraminifera (Bt) with chambers filled with OM. E, F) Sample C10-39, undetermined roveacrinid fragments in a fine micrite. G) Sample C11-153, comminuted ammonite shells. H) Sample C11-155, cross section of a small echinoid spine in a fine carbonate matrix with occasional subparallel fabric. I) Sample C11-161, undetermined roveacrinid fragment in a dark carbonate mud with dispersive amorphous OM. J) sample C11-165, echinoderm fragment. K) Sample C11-173, biserial benthic foraminifera in a micritic matrix..... 184

Figure 6-13 Photomicrographs illustrating microfacies MF3. A) Sample C10-21, lateral cut of a small planktonic foraminifera in a very fine, dark carbonate mud. B) Sample C10-24, partial view of a biserial benthic foraminifera in the same type of matrix as C10-21. C) Sample C10-25, roveacrinid skeletal fragment. D, E) sample C10-42, benthic foraminifera in a dark carbonate matrix. F, G, H) Sample C10-43, (F) transversal section of a roveacrinid cup; (G) undetermined bioclast; (H) oblique to transverse section of an undetermined roveacrinid. I) Sample C10-44, benthic foraminifera in a fine carbonate mud. J) Sample C11-203, ammonoid skeletal fragment in a fine carbonate mud (field of view is rotated relative to the normal bedding plane)..... 186

Figure 6-14 Photomicrographs illustrating microfacies MF4. A, B, C, D) sample C10-22, (A, B) abundant acicular to microtabular carbonate particles in a fine-dark matrix; (C) planktonic foraminifera *G. blowi*; (D) unidentified bioclast (? possibly a fragment of the brachial plate of a roveacrinid). E) Sample C10-23, benthic foraminifera in a very fine matrix, chambers filled with kerogen. F) Sample C10-29, unidentified bioclast in a dark matrix with traces of kerogen. G) Sample C11-129, fine micrite with sub-anisotropic fabric. H) Sample C11-131, unidentified bioclast in a dark matrix with traces of OM. Arrows point to calcispheres (cs) and planktonic foraminifera (Pk)..... 188

Figure 6-15 Photomicrographs illustrating microfacies MF5. A, B, C) Sample C10-46, (A) micritic matrix with interparticle pores filled with OM; (B) longitudinal section of the brachial plate of an undetermined roveacrinid; (C) roveacrinid fragment. D, E, F, G) Sample C10-47, D) R in the center: transversal section of a brachial plate of a roveacrinid (?), center and above: coiled benthic foraminifera (Bt), left upper corner: roveacrinid fragment; (E) ammonoid shell fragment (?); (F) planktonic foraminifera *G. blowi* ? (G) bioclast. H, I) Sample C10-50, (H) planktonic foraminifera in a dark micritic matrix with subparallel alignment; (I) roveacrinid fragment. J) Sample C10-55, tangential thecal section of a roveacrinid. K) Sample C10-56, relatively large biserial benthic foraminifera. L) Sample C10-59, oblique section of small echinoid spine in a matrix with abundant dispersive OM and pyrite. M) Sample C10-69, unidentified bioclast. N) Sample C10-74, abundant acicular fragments from disintegration of ammonite nacreous layer. O, P) Sample C10-75, (O) brachial fragment of roveacrinid, (P) section of a small ammonite shell. Q) Sample C10-83, small echinoid spine..... 191

Figure 6-16 Photomicrographs illustrating microfacies MF5A. A) Sample C10-64, planktonic foraminifera in a fine micritic matrix with dispersive OM. B) Sample C10-65, uniserial benthic foraminifera in a very fine carbonate mud rich in OM. C) Sample C10-84, comminuted skeletal fragments in a fine micrite with small planktonic foraminifera (Pk) and calcispheres. D) Sample C10-85, small echinoid spine in a dark matrix of carbonate mud rich in OM and very fine skeletal grains..... 192

Figure 6-17 Thin section of sample C10-51 at 18.8 m (MF5) showing a dislocated roveacrinid arm with pinnules. Magnified views shown below were taken at the point indicated by the arrows. Note the microtabular structure of the shell, which may account for at least 10% of the allochemical constituents. 195

Figure 7-1 A) Paleooceanographic map of the lower Aptian with the location of the Organyà Basin and the relative position of Iberia in the Western Tethys (after Masse et al., 1993; 2000). B) Simplified geologic map of the Organyà area with the relative position of the studied section (modified from Bernaus et al., 2003)..... 211

Figure 7-2 A) Simplified stratigraphic log of the upper 155 m of the El Pui section (85-240 m) showing the relative lithological variations. The M and W on top of the column refer to the mudstone and wackestone classification of Dunham (1962). B)

TIC profile along the studied interval. C) Temporal variation in the TOC correlated with the stratigraphic log and TIC. D) $\delta^{13}\text{C}_{\text{org}}$ profile along the stratigraphic column...	218
Figure 7-3 Field view of part of the studied section at about the 186 m level showing well-stratified pseudo-nodular limestone.....	219
Figure 7-4 Fossil echinoid found at level 187.5 m (sample C12-360). These echinoids are common in the 180 – ~200 m interval.	219
Figure 7-5 Sedimentary microfacies prior to, during and after OAE1a in the El Pui section showing paleodepositional changes. A) Sample C12-216 at 92.5 m; fine carbonate matrix with kerogene content showing subparallel microfabric with low bioturbation. B) Sample C12-280 at 149 m; this level is characterized by an increase in the microcarbonate content and size in a dark carbonate mud. C) Sample C12-286 at ~153 m; showing increase abundance and size of carbonate debris. D) Sample C12-345 at ~182 m; showing a sharp change in microfacies with abundant benthic foraminifera, echinoid and roveacrinid fragments, and other bioclasts. E) Sample C12-418 at ~202 m; a new change in microfacies type takes place at the onset of the positive excursion in $\delta^{13}\text{C}_{\text{org}}$ (Fig. 2D). F) Sample C12-480 at 240 m; a very dark fossiliferous micrite. Scale bar = 500 μm	220
Figure 7-6 Variations in the clay mineral content along the stratigraphic log at discrete levels. Emphasis was given to the interval marked by rapid and pronounced fluctuation in the $\delta^{13}\text{C}_{\text{org}}$ (Fig. 2D) in order to better assess changes in depositional conditions.	222
Figure 7-7 Average mineralogical composition of sediments of the studied interval of the El Pui section.	224
Figure 7-8 Major elements and redox sensitive trace elements concentration normalized with respect to Al. The values are compared to the ASV (fine continuous line) of Wedephol (1971; 1991) to assess partial enrichment indicative of chemically reducing depositional conditions. The small horizontal lines at ~88 m correspond to the average calculated error for each element reported in the plots. ($\delta\text{Al}/\text{Mean Al} + \delta\text{Element}/\text{Mean Element}$). * values $\times 10^{-4}$	226
Figure 7-9 <i>N</i> -alkane distribution measured in 8 samples corresponding to different levels of the stratigraphic column. The presence of organic compounds with carbon chain length >20 indicates contribution of OM from terrestrial sources to the basin.....	228
Figure 7-10 Chemostratigraphic correlation based on $\delta^{13}\text{C}$ of the El Pui section with other Tethyan sections. The C segments correspond to the $\delta^{13}\text{C}$ subdivision as proposed by Menegatti et al. (1998) for the lower Aptian. Shaded intervals correspond to the occurrence of the OAE1a. Note that the expanded character of the sedimentary sequence at El Pui allows for a detail description of the C segments.	231

ABBREVIATIONS AND ACRONYMS

ASV	Average shale value
CaCO ₃	Calcium Carbonate
cm/ky	Centimeters per thousand years
Dysoxia/dysoxic	Qualitative term meaning oxygen restricted conditions unless specified values of oxygen concentration are provided
EDS	Energy Dispersive Spectrometry
EG	Ethylene glycol
FOV	Field of view
g	Gram
GC-MS	Gas chromatography-mass spectrometry
h	Hour
HCl	Hydrochloric acid
LA-ICP-MS	Laser ablation inductively coupled mass spectrometry
LN ₂	Liquid nitrogen
Ma	Million years
n-alkanes	Normal alkanes
ng/g	nano-grams per gram
NIST	National Institute of Standards and Technology
OAE	Oceanic anoxic event
OAE1a	Oceanic anoxic event 1a
OC	Organic carbon
OM	Organic matter

PACS-2	National Research Council of Canada
Phy	Phytane
Pr	Pristane
RSTE	Redox sensitive trace elements
SEM	Scanning electron microscope
TC	Total carbon
TIC	Total inorganic carbon
TOC	Total organic carbon
XRD	X-ray diffraction

1 INTRODUCTION

The Phanerozoic sedimentary record registered various episodes of severe environmental perturbations that impacted geological systems and life at different scales. These episodes were particularly intense during the Mesozoic Era in which the supercontinent Pangaea began to fragment and separate into major north and south land masses (Fig. 1-1, Fig. 1-2), reshaping the ocean-land distribution and oceanic circulation patterns (Barron and Peterson, 1990). However, it was not until the Cretaceous Period when a more developed phase of the proto-Atlantic extending southward concomitant with the expansion of the seaway between Europe and Africa, separated South America and Africa (Fig. 1-2) and further influenced the global marine circulation (Barron et al., 1995).

Numerous studies have provided evidence that during the Cretaceous, in particular the mid-Cretaceous, Earth experienced greenhouse conditions (Barron et al., 1995, Puc at et al., 2003, Ando et al., 2008). This time was also characterized by high atmospheric pCO₂ (Barron and Washington, 1985; Lasaga et al., 1985; Ekart et al., 1999; Beerling and Royer, 2002; Robinson et al., 2002; Huber et al., 2002; Wissler et al., 2003; Herrle and Mutterlose, 2003; Wang et al., 2014), high eustatic sea level (Haq et al., 1987) and a weak temperature gradient between low and high latitudes (Barron and Washington, 1982; Huber et al., 1995).

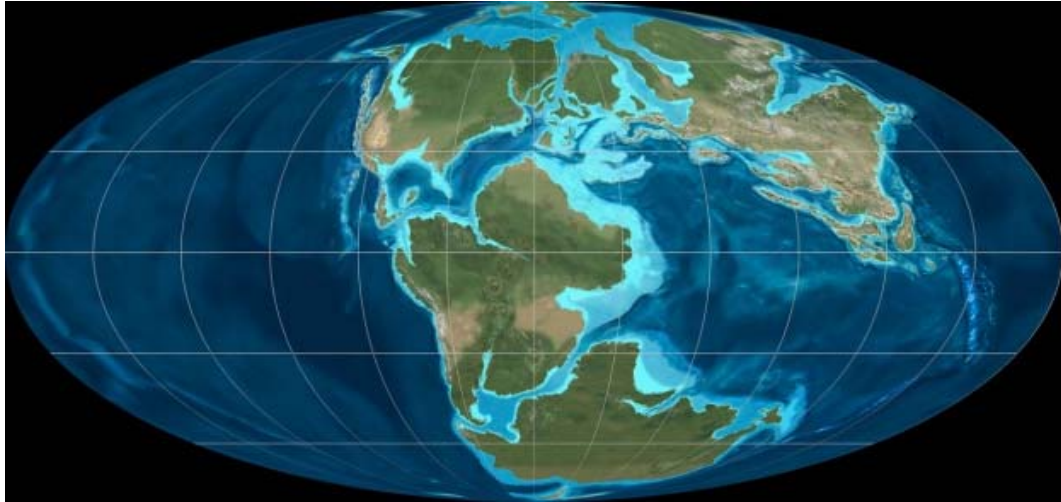


Figure 1-1 Global paleogeography and paleotectonics of the Late Jurassic ~150 Ma; (from <http://cpgeosystems.com/paleomaps.html>).

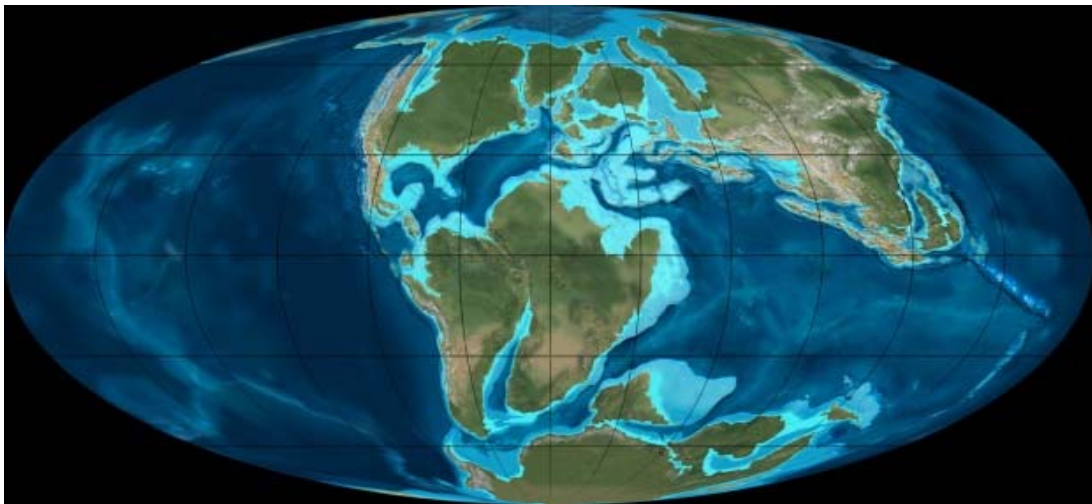


Figure 1-2 Global paleogeography and paleotectonics of the Early Cretaceous ~120 Ma; (from <http://cpgeosystems.com/paleomaps.html>).

One of the most relevant consequences of these global forcing processes during the Cretaceous is the worldwide deposition of sediments of variable carbonate content and unusually rich in organic matter, generally classified as black shales (Arthur, 1979), and related to oceanic conditions of severe oxygen deficiency, and even anoxia, referred to as oceanic anoxic events (OAE's) (Schlanger and Jenkyns, 1976). Such organic-rich marine deposits accumulated at different time intervals under oxygen-depleted conditions

that varied in intensity and extent, depending on the physiography and severity of global forcing mechanisms (e.g., Borrego et al., 1996; Uličný et al., 1997; van de Schootbrugge et al., 2005; Armstrong et al., 2009; Maurrasse et al., 2010). Because of their economic significance as causal factors for the development of important hydrocarbon reservoirs (Arthur and Schlanger, 1979; Sanchez-Hernandez and Maurrasse, 2014) and their potential as models to understand the impact of major alterations of the carbon cycle in the global climate (Jenkyns, 2010), OAE's remain an active topic of research.

1.1 The record of OAE1a

One of the most prominent anoxic episodes of the Cretaceous Period identified as Oceanic Anoxic Event 1a (OAE1a) occurred in the early-Aptian (~120 Ma), and lasted ~1.2 Ma (Li et al., 2008). Organic-rich deposits associated with OAE1a are well documented in different worldwide locations (Figure 1-2) (Sliter, 1989; Sager et al., 1993; Winterer and Sager, 1995; Menegatti et al., 1998; Erba et al., 1999; de Gea et al., 2003; Erba, 2004; Jenkyns, 2010; Föllmi, 2012; Gaona-Narvaez et al., 2013; Elkhazri et al., 2013). The hallmark of OAE1a includes not only deposition of organic-rich sediments with total organic carbon (TOC) >2%, but also a pronounced positive $\delta^{13}\text{C}$ excursion of 4-6‰ in the chemostratigraphic record (Jenkyns, 1980; Arthur and Premoli-Silva, 1982; Arthur et al., 1985; Jenkyns, 1995; Moullade et al., 1998; Erba et al., 1999; Leckie et al., 2002; Méhay et al., 2009; Khunt et al., 2011; Stein et al 2012; Papp et al., 2013; Elkhazri et al., 2013).

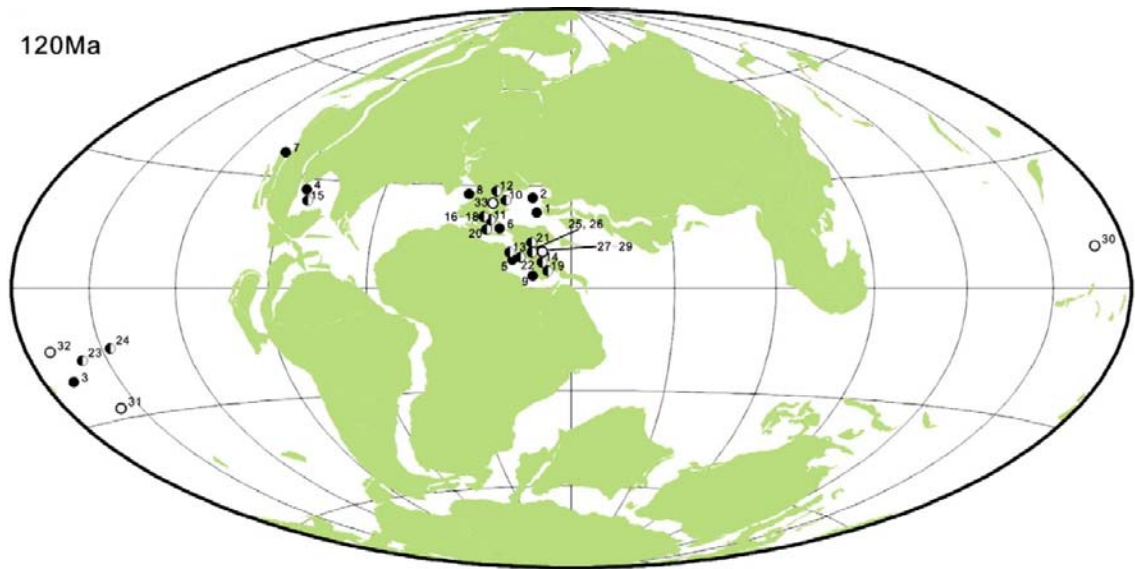


Figure 1-3 Paleogeographic distribution (120 Ma) of black shales deposited during OAE1a (after Wang et al., 2011).

The sharp shift in $\delta^{13}\text{C}$ identified in both organic matter and carbonates is preceded by a large negative excursion of $\sim 4\text{‰}$ that is globally correlated with the initiation of massive deposition of organic-rich beds in the marine environment (Weissert, 1989). Since primary producers preferentially incorporate the lighter isotope of the carbon series (^{12}C), abrupt and large positive excursions in the organic carbon isotopic curve are generally interpreted as the result of rapid burial of organic matter (OM) during episodes of intensified biological productivity (Weissert, 1989; Arthur et al., 1990).

Considering both the vast amount and the light isotopic composition of carbon required to produce the global $\delta^{13}\text{C}$ negative anomaly registered at the onset of OAE1a, the coeval intense submarine volcanic activity in the Pacific Ocean (Larson et al., 1991a, b) was first postulated as the major forcing factor (Menegatti et al., 1998; Tejada et al., 2009). However, the amount of CO_2 released from the mantle at relatively depleted $\delta^{13}\text{C}$

values has been considered insufficient for the amplitude of the negative carbon isotope shift (Jahren et al., 2005). Thus, dissociation of methane hydrates or thermal metamorphism of OM-rich sediments with extremely low $\delta^{13}\text{C}$ values have also been argued as an additional source for such a negative excursion in the carbon isotope record (Jahren et al., 2005; van Breugel et al., 2007; Méhay et al., 2009).

The effects of these processes in the development of global marine anoxia are not completely understood, although an integrated proposed mechanism includes the following postulates: 1) Intense volcanism and the release of CO_2 induced greenhouse conditions, resulting in a higher global average temperature that melted the polar ice and limited oceanic vertical circulation (Larson et al., 1999). 2) Simultaneous interaction of newly formed oceanic crust released chemical elements in the surrounding ocean water; hence the warmer, less dense water upwelled to the surface and acted as a nutrient source (Stinton and Duncan, 1997; Tejada et al., 2009). There is still an active debate concerning to what extent active volcanism in the Pacific Ocean would have been able to alter the World Ocean average water temperature. 3) Intense exothermic processes and mantle out-gassing could have certainly reduced the concentration of dissolved oxygen in the water column. 4) Sustained supply of nutrients from continental weathering associated with high temperature and an accentuated precipitation cycle, coupled with concurrent volcanism, could have benefited opportunistic species blooms in marine surface waters (Sanchez-Hernandez et al., in press.) 5) Intense biological productivity generating large amounts of OM together with impoverished ventilation of bottom water masses could have overcome the bacterial oxidation rate in the water column, thereby resulting in

oxygen depletion with depth and leading to the preservation of extensive organic-rich black layers (Weissert et al., 1985; Bralower et al., 1994; Leckie et al., 2002).

1.2 Geochemical and stratigraphic particularities in marginal basins prior to OAE1a

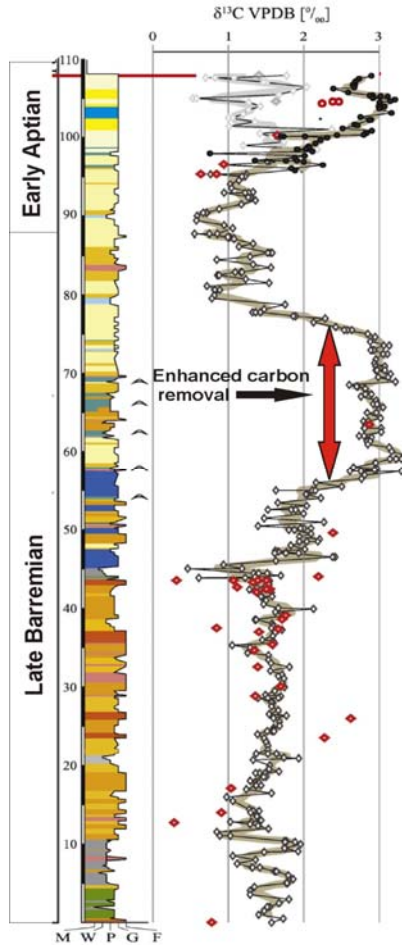


Figure 1-4 Comparative $\delta^{13}\text{C}$ profile of three Subalpine sections showing a broad positive excursion indicative of intensified ^{12}C burial in the latest Barremian.

Globally, the hallmark of OAE1a corresponds to worldwide deposition of black shales with TOC > 2% and a positive excursion up to ~5‰ in $\delta^{13}\text{C}$. However, sedimentological and geochemical characteristics similar to OAE1a have also been identified in deposits corresponding to epicontinental seas and restricted marine environments of the Tethys Ocean prior to OAE1a (Mutterlose et al., 2009b; Huck et al., 2010), thus suggesting an independent paleoenvironmental response to complex regional factors (Mutterlose and Böckel, 1998; Huck et al., 2010) (Fig. 1-4)

As the global climate transitioned to greenhouse conditions through the Barremian–Aptian boundary, it has been argued that the resulting marine transgression

induced differential drowning of preexisting carbonate platforms (Weissert et al., 1998; Erba, 2004; Weissert and Erba, 2004; Föllmi et al., 2006; Barragan and Maurrasse, 2008; Huck et al., 2010), which led to the development of restricted epicontinental seas and stagnation of deep-water masses in the Western Tethys marginal basins (Bralower et al., 1994; Mutterlose et al., 2009b). The concurrent acceleration of

the hydrologic cycle (Hay and DeConto, 1999) periodically intensified continental runoff and strong pulses of fresh water collection in semi-enclosed basins. The vertical density contrast created under such conditions further constrained ventilation of the underlying water masses. Fluvial fluxes also acted as the carrier for the transport of biolimiting elements such as phosphorous (in the form of apatite and/or particulate and dissolved OM) and iron (in ferrous minerals) into the marine environment (Föllmi et al., 1994, Föllmi, 1996; Sanchez-Hernandez and Maurrasse, 2014). Thus, in nutrient-rich environments, enhanced primary productivity may increase the CO₂ sequestration rate in OM, thereby intensifying export production (Fig. 1-5). Given that oxygenation of the water column in restricted basins is limited, intensified bottom export of OM further exacerbates the oxygen demand, which generates lower oxygen levels and enhances OM preservation in sediments.

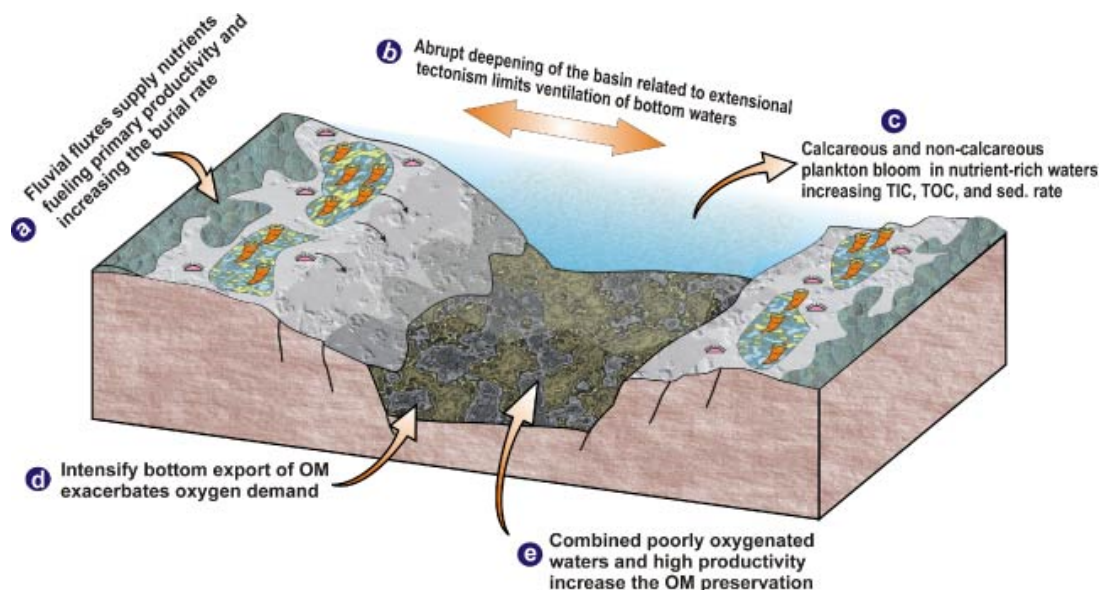


Figure 1-5 Integrated model for enhanced preservation of OM in extensional basins (Sanchez-Hernandez).

Because the sedimentological record of the Tethys marginal basins consistently reveals intermittent black levels with TOC enrichment > 0.5% coincident with positive excursions of the $\delta^{13}\text{C}$ (e.g. Mutterlose and Böckel, 1998, Millán et al., 2009, Stein et al., 2011), a combination of the different factors suggested offers a plausible mechanism to explain short-lived events before the occurrence of the global OAE1a. In addition, the applicability of the $\delta^{13}\text{C}$ profile to further our understanding of the causes of the perturbations in the carbon reservoir has evolved as a powerful tool for worldwide stratigraphic correlation and geochronology, as such variations have a global scope. In particular, the carbon isotopic profile ranging from the latest Barremian to the middle Aptian is commonly used to correlate global geological and biogeochemical events (e.g. major volcanism related to the emplacement of the Ontong Java Plateau (Larson, 1998; Larson and Erba, 1999) and enhanced bio-productivity (Leckie et al., 2002). Menegatti et al. (1998) proposed a subdivision of the $\delta^{13}\text{C}$ record of the latest Barremian to the middle Aptian in eight segments (C1 – C8) that allows for a structured form of correlation and the geochemical definition of the OAE1a occurring interval.

1.3 Main Hypothesis

The occurrence of organic-rich sediments in semi-restricted basins and their geochemical characteristics have been shown to be frequently decoupled from the complex global forcing factors (Mutterlose et al., 2009b; Huck et al., 2010; Khunt et al., 2011) that induced deposition of black shales associated with the Lower Aptian OAE1a elsewhere. On the basis of these findings, it is reasonable to hypothesize that the extensive Barremian-Aptian hemipelagic deposits of the Organyà restricted Basin

(Garrido-Mejias, 1973; Peybernès, 1976; Caus et al., 1990; García-Senz, 2002; Bernaus et al., 2002; Gong et al., 2009) should also have a distinctive record for that time.

1.4 Objectives

To test the main hypothesis my scientific objectives were:

- 1- To determine the causal factors for the deposition of organic-rich sediments in the semi-restricted Organyà Basin prior to OAE1a.
- 2- To characterize the factors involved in the high sedimentation rates in the restricted Organyà Basin from the late Barremian to the early Aptian.
- 3- To assess the influence of basin physiography and regional paleoenvironmental factors in the local expression of the global OAE1a.
- 4- To develop a high-resolution $\delta^{13}\text{C}_{\text{org}}$ profile for the Organyà Basin that can be used as a possible reference for global correlation for the latest Barremian to the middle Aptian.

1.5 Summary of the methods and issues addressed

To test my hypotheses and accomplish the proposed objectives I developed the following methodology:

- a- Extensive fieldwork and high-resolution sampling in order to understand the tectonic and structural setting of the Organyà Basin, as well as to identify field scale sedimentary features that may serve as depositional indicators.
- b- Thin section, smear slides and SEM analyses for microfossil and mineral content indicative of specific depositional settings and composition of the rock matrix.

- c- Total carbon, total inorganic and total organic carbon to determine the preservation level of organic carbon in the sediment as well as the contribution of carbonate producers to the rock matrix.
- d- Major and trace element analyses to evaluate redox depositional conditions, intensity of terrestrial fluxes and nutrient levels.
- e- Bulk and clay mineral analyses to assess the mineralogical composition of the rock matrix and the provenance of the detrital fraction.
- f- Biomarkers analyses to determine the origin of the organic matter.

1.6 Dissertation Structure

I organized the dissertation in the form of research articles, each representing a chapter, that are either published, or submitted and each addressed one or several objectives:

- Chapter Two covers the tectonic evolution of the Organyà Basin and describes the palaeoceanographic context of the basin within the lower Cretaceous. It also provides a general stratigraphic framework of the studied section and lithostratigraphic description of field and microscopic observations.
- Chapter Three reports in detail the methods and materials applied in order to allow reproducibility of the results presented.
- Chapter Four provides results of a detailed geochemical and stratigraphic assessment of the depositional conditions and controlling factors leading to the intermittent occurrence of organic-rich sediments and faunal variability on the basal 85 m of the El Pui section. The findings reveal a particular basinal response to local conditions

- aside from the influence of global forcing factors and the relevance of restricted basins as carbon sinks (Sanchez-Hernandez and Maurrasse, 2014).
- Chapter Five discusses the role of basin physiography and enhanced productivity in the sedimentation rate and carbon removal. It presents a detailed qualitative and quantitative assessment of the calcareous nannofossils assemblages and discussion of depositional conditions based on their distribution and preservation state. Biomarker analyses are applied to determine the sources of the OM and to explain the trend in the carbon isotopic signal. Comparisons with other well studied basins are included to provide a better understanding of the paleoenvironments of the Organyà Basin (Sanchez-Hernandez et al., 2014).
 - Chapter Six provides a detailed characterization of the microfacies which recorded the variability of the depositional conditions in response to redox and productivity changes in the basal 85 m of the El Pui section. It also covers the novel finding of roveacrinids (planktonic microcrinoids) facies in the Organyà Basin and the faunal assemblages that developed under the described environments (Sanchez-Hernandez and Maurrasse, submitted to Facies)
 - Chapter Seven discusses in detail the upper 155 m of the El Pui section and reveals the geochemical, stratigraphic, and sedimentary record of the OAE1a in the Organyà Basin, for the first time. It provides the identification of the C isotopic segments that define the occurrence of OAE1a, discusses the effect of local environmental conditions in the expression of OAE1a in the El Pui section and establishes the existence of precursory signals to OAE1a.

- Chapter Eight summarises the significance of my dissertation research and states the main accomplishments and conclusions.

1.7 References

- Ando, A., Kaiho, K., Kawahata, H., Kakegawa, T., 2008. Timing and magnitude of early Aptian extreme warming: Unraveling primary delta O-18 variation in indurated pelagic carbonates at Deep Sea Drilling Project Site 463, central Pacific Ocean. *Palaeogeography Palaeoclimatology Palaeoecology* 260, 463-476.
- Armstrong, H. A., Abbott, G. D., Turner, B. R., Makhlof, I.M., Muhammad, A. B., Pedentchouk, N., Peters, H., 2009. Black shale deposition in an Upper Ordovician-Silurian permanently stratified, peri-glacial basin, southern Jordan. *Palaeogeography, Palaeoclimatology, Palaeoecology* 273, 368-377.
- Arthur, M. A., 1979. North Atlantic Cretaceous Black Shales: The Record at Site 398 and a brief comparison with other occurrences. In Sibuet, J.-C, Ryan, W.B.F., et al., *Initial Reports of the Deep Sea Drilling Project*, v. 47, Part 2: Washington (U.S. Government Printing Office), pp. 451-468.
- Arthur, M., Premoli Silva, I., 1982. Development of widespread organic carbon-rich strata in the Mediterranean Tethys, in Schlanger, S.O. and Cita, M.B., (Eds.) *Nature and origin of cretaceous carbon-rich facies*: London, Academic Press Inc. pp. 7-54.
- Arthur, M. A., Brumsack, H.-J., Jenkyns, H. C., Schlanger, S. O., 1990. Stratigraphy, geochemistry, and paleoceanography of organic carbon-rich Cretaceous sequences, in *Cretaceous Resources, Events, and Rhythms*, edited by R. N. Ginsburg and B. Beaudoin, Kluwer Acad., Norwell, Mass. pp. 75–119
- Arthur, M. A., Schlanger S. O., 1979. Cretaceous “oceanic anoxic events” as causal factors in development of reef-reservoired giant oil fields, *AAPG Bull.* 63, 870–885.
- Barragan, R., Maurrasse, F.J-M.R., 2008. Lower Aptian (Lower Cretaceous) ammonites from the basal strata of the La Peña Formation of Nuevo León State, northeast Mexico: biochronostratigraphic implications. *Revista Mexicana de Ciencias Geológicas* 25 (1), 145–157.
- Barron, E. J., Washington, W. M., 1982. Cretaceous climate: A comparison of atmospheric simulations with the geologic record. *Palaeogeography, Palaeoclimatology, Palaeoecology.* 40(1-3), 103–133.
- Barron, E. J., Washington, W. M. 1985. Warm Cretaceous Climates: High atmospheric CO₂ as plausible mechanism. In: Sundquist, E. T., Broecker, W. (Eds), *The Carbon Cycle and Atmospheric CO₂*, Geophysical Monographs series 32. American Geophysical Union, Washington, pp. 546–553.

- Barron, E.J., Fawcett, P.J., Peterson, W.H., Pollard, D., Thompson, S.L., 1995. A simulation of mid-Cretaceous climate. *Paleoceanography* 10, 953–962.
- Barron, E.J., Peterson, W.H., 1990. Mid-Cretaceous ocean circulation: results from model sensitivity studies. *Paleoceanography* 5, 319–337.
- Beerling, D. J., Royer, D. L., 2002. Fossil plants as indicators of the Phanerozoic global carbon cycle. *Annual Review of Earth Science* 30, 527–556.
- Bernaus, J.M., Arnaud-Vanneau, A., Caus, E., 2002. Stratigraphic distribution of Valanginian Early Aptian shallow-water benthic foraminifera and algae, and depositional sequences of a carbonate platform in a tectonically-controlled basin: the Organyà Basin, Pyrenees, Spain. *Cretaceous Research* 23, 25-36.
- Borrego, A. G., Hagemann, H. W., Blanco, C. G., Suarez, M., and Suarez de Centi, C., 1996. The Pliensbachian (Early Jurassic) “anoxic event in Asturias, northern Spain: Santa Mera Member, Rodiles Formation: Organic Geochemistry, 25(5-7), 295–309.
- Bralower, T.J., Arthur, M.A., Leckie, R.M., Sliter, W.V., Allard, D.J., Schlanger, S.O., 1994. Timing and paleoceanography of oceanic dysoxia/anoxia in the Late Barremian to Early Aptian. *Palaios* 9, 335–369.
- Caus, E., García-Senz, J. M., Rodés, D., Simón, A., 1990. Stratigraphy of the Lower Cretaceous (Berriasian-Barremian) sediments in the Organyà Basin, Pyrenees, Spain. *Cretaceous Research* 11, 313–320.
- de Gea, G. A., Castro, J. M., Aguado, R., Ruiz-Ortiz, P. A. & Company, M. 2003. Lower Aptian carbon isotope stratigraphy from a distal carbonate shelf setting; the Cau section, Prebetic Zone, SE Spain. *Palaeogeography, Palaeoclimatology, Palaeoecology* 200, 207–219.
- Ekart, D. D., Cerling, T. E., Montañez, I. P., Tabor, N. J., 1999. A 400 million year carbon isotope record of pedogenic carbonate: implications for paleoatmospheric carbon dioxide. *American Journal of Science* 299, 85–106.
- Elkhazri, A., Abdallah, H., Razgallah, S., Moullade, M., Kuhnt, W., 2013. Carbon-isotope and microfaunal stratigraphy bounding the Lower Aptian Oceanic Anoxic Event 1^a in northeastern Tunisia. *Cretaceous Research* 39, 133–148.
- Erba, E., 2004. Calcareous nannofossils and Mesozoic oceanic events. *Marine micropaleontology* 52, 85–106.
- Erba, E., Channell, J.E.T., Claps, M., Jones, C., Larson, R., Opdyke, B., Premoli Silva, I., Riva, A., Salvini, G., Torricelli, S., 1999. Integrated stratigraphy of the Cismon APTICORE (Southern Alps, Italy): a “reference section” for the Barremian–Aptian interval at low latitudes. *Journal of Foraminiferal Research* 29, 371–392.

- Fischer, A. G. and Arthur M. A., 1977. Secular variations in the pelagic realm. In Cook, H. E. and Enos, P. (Eds.), *Deep water carbonate environments*, SEPM Spec. Publ. 25, 19–50
- Föllmi, K.B., 1996. The phosphorus cycle, phosphogenesis, and marine phosphate-rich deposits. *Earth-Science Reviews* 40, 55–124.
- Föllmi, K. B., 2012. Early Cretaceous life, climate and anoxia. *Cretaceous Research* 35, 230– 257.
- Föllmi, K.B., Weissert, H., Bisping, M., Funk, H., 1994. Phosphogenesis, carbon-isotope stratigraphy, and carbonate-platform evolution along the Lower Cretaceous northern tethyan margin. *Geological Society of America* 106, 729–746.
- Gaona-Narvaez, T., Maurrasse, F.J-M.R., and Moreno-Bedmar, J.A., 2013. Stable carbon-isotope stratigraphy and ammonite biochronology at Madoz, Navarra, northern Spain): implications for the timing and duration of oxygen depletion during OAE-1a. *Cretaceous Research* 40, 143–157.
- García-Senz, J., 2002. Cuencas extensivas del Cretácico Inferior en los Pirineos Centrales: formación y subsecuente inversión. PhD Thesis, University of Barcelona, Barcelona, 310 pp.
- Garrido Mejias, A. 1973. Estudio geológico y relación entre tectónica y sedimentación del Secundario y Terciario de la vertiente meridional pirenaica en su zona central (provincias de Huesca y Lérida). PhD thesis, Universidad de Granada, 320 pp.
- Gong, Z., van Hinsbergen, D. J.J., Vissers R. L.M., Dekkers M. J., 2009. Early Cretaceous syn-rotational extension in the Organyà Basin - New constraints on the palinspastic position of Iberia during its rotation. *Tectonophysics* 473, 312–323.
- Haq, B.U., Hardenbol, J., Vail, P.R., 1987. Chronology of fluctuating sea levels since the Triassic. *Science* 235, 1156–1167.
- Hay, W. W., Deconto R. M., 1999. Comparison of modern and Late Cretaceous meridional energy transport and oceanology, in *Evolution of the Cretaceous Ocean-Climate System*, in: Barrera, E. and Johnson, C. C. (Eds), *Special Papers*, Geological Society of America 332, 283–300.
- Herrle, J.O., Mutterlose, J., 2003. Calcareous nannofossils from the Aptian–Lower Albian of southeast France: palaeoecological and biostratigraphic implications. *Cretaceous Research* 24, 1–22.
- Huber, B.T., Norris, R.D., MacLeod, K.G., 2002. Deep-sea paleo-temperature record of extreme warmth during the Cretaceous. *Geology* 30, 123–126.

- Huber, B.T., Hodell, D.A., Hamilton, C.P., 1995. Mid- to Late Cretaceous climate of the southern high latitudes. Stable isotopic evidence for minimal equator-to-pole thermal gradients. *Geological Society of America* 107, 1164–1191.
- Huck, S., Rameil, N., Korbar, T., Heimhofer, U., Wieczorek, T.D., Immenhauser, A., 2010. Latitudinally different responses of tethyan shoal-water carbonate systems to the early Aptian oceanic anoxic event (OAE1a). *Sedimentology* 57, 1585–1614.
- Jahren, A.H., Conrad, C.P., Arens, N.C., Mora, G., and Lithgow-Bertelloni, C., 2005, A plate tectonic mechanism for methane hydrate release along subduction zones: *Earth and Planetary Science Letters*, 236, 691–704
- Jenkyns, H.C., 1980. Cretaceous anoxic events: from continents to oceans. *Journal of the Geological Society of London* 137, 171–188.
- Jenkyns, H.C., 1995. Carbon-isotope stratigraphy and paleoceanographic significance of the Lower Cretaceous shallow-water carbonates of resolution Guyot, Mid-Pacific Mountains. *Proc. Ocean Drill. Program, Sci. Results*, pp. 99–104.
- Jenkyns, H. C., 2010. Geochemistry of oceanic anoxic events, *Geochemistry, Geophysics and Geosystems* 11(3), 1525–2027.
- Kuhnt, W., Holbourn, A., Moullade, M., 2011. Transient global cooling at the onset of early Aptian oceanic anoxic event (OAE) 1a. *Geology* 39(4), 323–326.
- Lasaga, A. C., Berner, R. A., Garrels, R. M., 1985. An improved geochemical model of atmospheric CO₂ fluctuations over the past 100 million years. In: Sundquist, E. T. (Ed), *The Carbon Cycle and Atmospheric CO₂*, Geophysical Monographs series 32. American Geophysical Union, Washington, pp. 397–411.
- Larson, R.L., 1998. The mid-Cretaceous superplume episode, *Geology* 98/99 Annual Editions, *Duskin/McGraw Hill, Guilford*, Art. 28, p.123–127.
- Larson, R. L., 1991a. Geological consequences of superplumes, *Geology* 19, 963–966.
- Larson, R. L., 1991b. Latest pulse of Earth: Evidence for a mid-Cretaceous superplume, *Geology*, 19, 547–550.
- Larson, R.L., Erba, E., 1999. Onset of the mid-Cretaceous greenhouse in the Barremian - Aptian: igneous events and the biological, sedimentary, and geochemical responses. *Paleoceanography* 14, 663–678.
- Leckie, R.M., Bralower, T.J., Cashman, R., 2002. Oceanic anoxic events and plankton evolution: biotic response to tectonic forcing during the mid-Cretaceous. *Paleoceanography* 17(3), 1–29

- Li, Y.X., Bralower, T.J., Montanez, I.P., Osleger, D.A., Arthur, M.A., Bice, D.M., Herbert, T.D., Erba, E., Premoli Silva, I., 2008. Toward an orbital chronology for the early Aptian Oceanic Anoxic Event (OAE1a, similar to 120 Ma). *Earth and Planetary Science Letters* 271, 88–100.
- Maurrasse, F. J-M. R., Duque-Botero, F., Blanco-Piñon, A., 2010. Oceanic anoxic event 2 (OAE-2) in Cretaceous northeastern Mexico and the effects of paleophysiology on the sediment record. In: Marcos Lamolda, et al., eds. *Geoevents, Geological Heritage, and the Role of the IGCP*, Caravaca de la Cruz, Spain. pp. 54–62.
- Méhay, S., Keller, C. E., Bernasconi, S. M., Weissert, H., Erba, E., Bottini, C., Huchuli, P. A., 2009. A volcanic CO₂ pulse triggered the Cretaceous oceanic anoxic event 1a and a biocalcification crisis. *Geology* 37, 819–822.
- Menegatti, A. P., Weissert, H., Brown, R. S., Tyson, R. V., Farrimond, P., Strasser, A., Caron, M., 1998. High resolution $\delta^{13}\text{C}$ stratigraphy through the Early Aptian “Livello Selli” of the Alpine Tethys. *Paleoceanography* 13(5), 530–545.
- Millán, M.I., Weissert, H.J., Fernández-Mendiola, P.A., García-Mondéjar, J., 2009. Impact of Early Aptian carbon cycle perturbations on evolution of a marine shelf system in the Basque-Cantabrian Basin (Aralar, N Spain), *Earth and Planetary Science Letters* 287(3–4), 392–401.
- Moullade, M., Kuhnt, W., Bergen, J.A., Masse, J.P., Tronchetti, G., 1998. Correlation of biostratigraphic and stable isotope events in the Aptian historical stratotype of La Bedoule (Southeast France). *C. R. Acad. Sci. Paris IIA* 327, 693–698.
- Mutterlose, J., Böckel, B., 1998. The Barremian–Aptian boundary interval in NW Germany:—A synthesis. *Cretaceous Research* 19, 539–568.
- Mutterlose, J., Pauly, S., Steuber, T., 2009b. Temperature controlled deposition of early Cretaceous (Barremian–early Aptian) black shales in an epicontinental sea. *Palaeogeography, Palaeoclimatology, Palaeoecology* 273, 330–345.
- Papp, D.C., Cociuba, I., Lazăr, D.F., 2013. Carbon and oxygen-isotope stratigraphy of the Early Cretaceous carbonate platform of Pădurea Craiului (Apuseni Mountains, Romania): A chemostratigraphic correlation and paleoenvironmental tool. *Applied Geochemistry* 32, 3–16.
- Peybernès, B., 1976. *Le Jurassique et le Crétacé inférieur des Pyrénées franco-espagnoles*. Thèse de doctorat, Laboratoire de Géologie, Université Paul Sabatier, Toulouse, 459 pp.
- Pucéat, E., Lecuyer, C., Sheppard, S.M.F., Dromart, G., Reboulet, S., Grandjean, P., 2003. Thermal evolution of Cretaceous Tethyan marine waters inferred from oxygen isotope composition of fish tooth enamels. *Paleoceanography* 18, 1–12.

- Robinson, S. A., Andrews, J. E., Hesselbo, S. P., Radley, J. D., Dennis, P. F., Harding, I. C., Allen, P., 2002. Atmospheric pCO₂ and depositional environment from stable isotope geochemistry of calcrite nodules (Barremian, Lower Cretaceous, Wealden Beds, England). *Journal of the Geological Society of London* 159, 215–224.
- Sager, W.W., Winterer, E.L., Firth, J.V., et al., 1993. Leg Synthesis. Proceedings of the Ocean Drilling Program, Initial Reports, 143, 13–29.
- Sanchez-Hernandez, Y., Maurrasse, F.J-M.R., 2014. Geochemical characterization and redox signals from the latest Barremian to the earliest Aptian in a restricted marine basin: El Pui section, Organyà Basin, south-central Pyrenees. *Chemical Geology* 372, 12–31.
- Schlanger, S.O., Jenkyns, H.C., 1976. Cretaceous anoxic events: causes and consequences. *Geol. Mijnbouw* 55, 179–184.
- Sliter, W. V., 1989. Aptian Anoxia in the Pacific Basin. *Geology* 17, 909–912.
- Stein, M., Westermann, S., Adatte, T., Matera, V., Fleitmann, D., Spangenberg, J.E. and Föllmi, K.B., 2012. Late Barremian –Early Aptian palaeoenvironmental change: the Cassis-La Bédoule section, southeast France. *Cretaceous Research* 37, 209–222.
- Stein, M., Föllmi, K.B., Westermann, S., Godet, A., Adatte, T., Matera, V., Fleitmann, D., Berner, Z., 2011. Progressive palaeoenvironmental change during the Late Barremian-Early Aptian as prelude to Oceanic Anoxic Event 1a: evidence from the Gorgo a Cerbara section (Umbria-Marche Basin, central Italy). *Palaeogeography, Palaeoclimatology, Palaeoecology* 302, 396–406.
- Stinton, C.W., Duncan, R.A., 1997. Potential links between ocean plateau volcanism and global ocean anoxia at the Cenomanian-Turonian boundary: *Economical Geology* 92, 836–842.
- Tejada, M. L. G., Suzuki, K., Kuroda, J., Coccioni, R., Mahoney, J. J., Ohkouchi, N., Sakamoto, T., Tatsumi, Y., 2009. Ontong Java Plateau eruption as a trigger for the Early Aptian oceanic anoxic event. *Geology* 37, 855–858.
- Uličný, D., Hladíková, J., Moses, J. A. Jr., Čech, S., Hradecká, L., and Svobodová, M., 1997. Sea-level changes and geochemical anomalies across the Cenomanian-Turonian boundary: Pecinov quarry, Bohemia: *Palaeogeography, Palaeoclimatology, Palaeoecology* 132, 265–285.
- van Breugel, Y., Schouten, S., Tsikos, H., Erba, E., Price, G. D., Sinninghe Damsté, J. S., 2007. Synchronous negative carbon isotope shifts in marine and terrestrial biomarkers at the onset of the early Aptian oceanic anoxic event 1a: Evidence for the release of ¹³C-deplete carbon into the atmosphere. *Paleoceanography*, 22, PA1210, 1–13.

- van de Schootbrugge, B., McArthur, J.M., Bailey, T.R., Rosenthal, Y., Wright, J.D., Miller, K.G., 2005, Toarcian oceanic anoxic event: an assessment of global causes using belemnite C isotope records: *Paleoceanography*, 20, PA3008.
- Wang, C., Hu, X., Huang, Y., Wagreich, M., Scott, R.W., Hay, W.W., 2011. Cretaceous oceanic red beds as possible consequence of oceanic anoxic events. *Sedimentary Geology* 235(1–2), 27–37.
- Wang, Y., Huang, C., Sun, B., Quan, C., Wu, J., Lin, Z., 2014. Paleo CO₂ variation trends and the Cretaceous greenhouse climate. *Earth-Science Reviews* 129, 136–47.
- Weissert, H., 1989. C-isotope stratigraphy, a monitor of paleoenvironmental changes: a case study from the Early Cretaceous. *Surveys in Geophysics* 10, 1–16.
- Weissert, H., Lini, A., Föllmi, K. B., Kuhn, O., 1998. Correlation of Early Cretaceous carbon isotope stratigraphy and platform drowning events: a possible link? *Palaeogeography, Palaeoclimatology, Palaeoecology*, 137(3), 189–203.
- Winterer, E. L., Sager, W. W., 1995. Synthesis of drilling results from the mid-Pacific Mountains: Regional context and implications. *In*, Winterer, E.L., Sager, W.W., Firth, J.V., and Sinton, J.M. (Eds.), *Proc. ODP, Sci. Results*, 143, 497–535.
- Wissler, L., Funk, H., Weissert, H., 2003. Response of Early Cretaceous carbonate platforms to changes in atmospheric carbon dioxide levels. *Palaeogeography, Palaeoclimatology, Palaeoecology*, 200, 187–205.

2 GEOLOGIC AND STRATIGRAPHIC SETTING OF THE ORGANYÀ BASIN

The Organyà Basin evolved through the breakup of pre-extensional Jurassic platforms (Seguret, 1972; Caus et al., 1990; Muñoz, 1991; Vergés, 1993) concurrent with the opening of the Atlantic Ocean, and coeval with the opening of the Bay of Biscay during Aptian–Albian times (Berástegui et al., 1990; 1993) (Fig. 2-1). The basin developed a system of depocenters with an E-W trend and irregular margins (Caus et al., 1990) that allowed for the accumulation of shallow marine carbonates and hemipelagic sediments with abrupt facies differences. Geometrically, the depositional setting of the Organyà Basin resembles a graben with estimated dimensions of ~ 80 km along the extensional axis and up to 15 km wide (Dinarès-Turell and García-Senz, 2000). During the Mesozoic the basin filled with ~ 4500-5000 m of sediments, most of it corresponding to the Lower Cretaceous (Bachmann and Willens, 1996), and subsidence increased, providing ample accommodation space for the high sedimentation rate (up to ~20 cm/ky) (García-Senz, 2002; Gong, 2008).

During the upper Albian-Cenomanian the extensional system inverted to transpressive (Puigdefàbregas and Souquet, 1986; Muñoz, 1992; Bond and McClay, 1995) leading to a significant erosion of mainly late Albian deposits and augmented terrigenous input. Shallow-water carbonate platform deposits are also recorded from this time. Later, in Campanian times, a period of compression and subduction started as the result of the interaction between the European and Iberian plates which led to the basin inversion and the development of the Bóixols thrust system and the Santa Fè syncline

(Vergés and Muñoz, 1990). Exposure of Lower Cretaceous sediments (mainly Aptian to Albian) occurs at both limbs of the Santa Fè syncline.

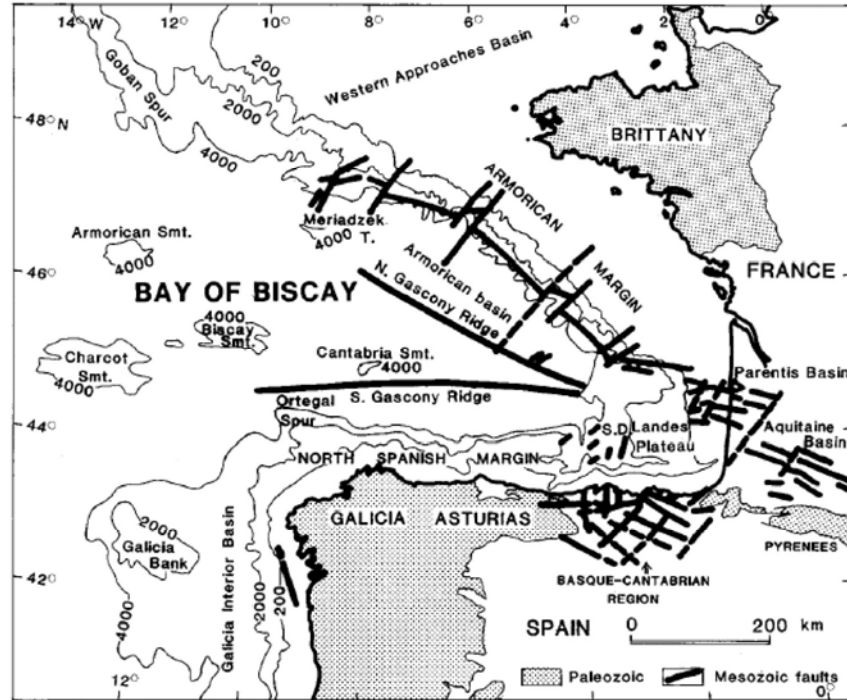


Figure 2-1 The opening of the Bay of Biscay during the Mesozoic with the main tectonic features and adjacent terrains. After García-Mondejar (1996).

The tectonic history of the basin can be summarized in three main phases:

- 1) Early Cretaceous extensional tectonism associated with the opening of the Bay of Biscay (Berástegui et al., 1990, 1993; Vergés, 1993) led to the development of the Organyà Basin as result of the breakup of Jurassic platforms (Caus et al., 1990). It was the time when several other small sedimentary basins also developed along the edges of the Iberian and European plates.
- 2) A Cretaceous phase of development of carbonate platforms characterized by a high subsidence rate and the accumulation of thick carbonate sequences. This phase of

sedimentation also coincides with the accumulation of organic-rich layers suggested to be possibly correlative with OAE1a (Bernaus et al., 2003).

3) Latest Cretaceous /early Cenozoic collision of the Iberian Plate with Europe led to the emergence of the Organyà Basin (García-Senz, 2002). The first stages of tectonic extension modified the paleogeographic configuration of the region as extensional processes caused the formation of a wider seaway between Europe and Iberia. During the Barremian-early Aptian, a phase of intense rifting took place and subsidence and net sedimentation rate approximately doubled (Bachmann and Willems, 1996; García-Senz, 2002). Sediments from that interval reflect a marine setting, and higher influx of terrigenous materials suggests a more elevated topography in the adjacent areas (Gong et al., 2009).

2.1 Overall stratigraphic framework of the Organyà Basin.

The Bòixols thrust sheet comprises three megasequences corresponding to the Triassic- Jurassic, Lower Cretaceous (Berriasian–Cenomanian), and Cenomanian–Maastrichtian (Berástegui et al., 1990). My research section is part of the Lower Cretaceous megasequence that has been studied by several authors (Garrido-Mejias, 1973; Peybernès, 1976; García-Senz, 2002; Bernaus et al., 2002) and stratigraphically subdivided in five major depositional units proposed by Berástegui et al. (1990), García-Senz et al. (1995), and García-Senz, (2002) (Fig. 2-2). The El Pui section which is the object of the present study is part of the Cabó Formation that represents a late Barremian-early Aptian time frame (Fig. 2-3).

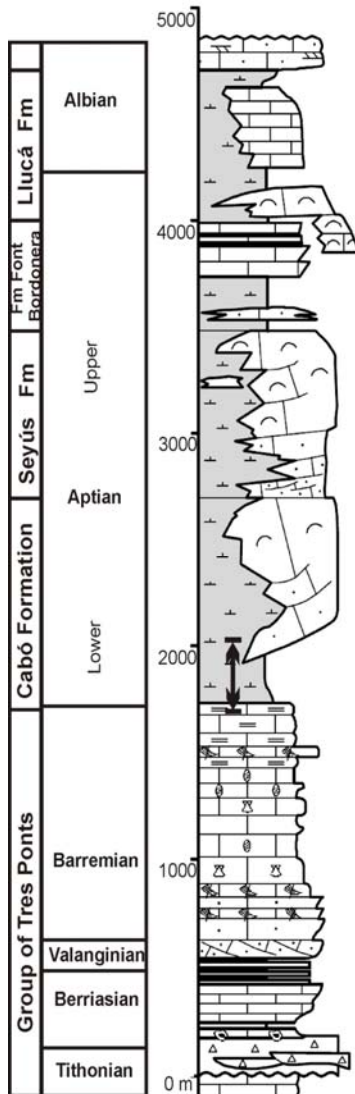


Figure 2-2 Synthetic stratigraphic column of the Organyà Basin with the geochronological distribution of the five more important lithologic groups. After García-Senz (2002). The black arrow indicates the studied interval.

2.2 The El Pui section

The uppermost unit of the south-central Pyrenees of Spain is the Bòixols Thrust Sheet that incorporates the sedimentary succession of the Organyà Basin (Seguret, 1972; Peybernès, 1976; Muñoz et al., 1984; Verges and Muñoz, 1990; García-Senz, 2002). The Sierra de Prada is part of that unit and its southern flank shows a remarkable homoclinal structure with northward vergence and an overall E-W strike (Fig. 2-3) The strata dip uniformly southward with an average angle between 40° and 50° (Fig. 2-3). Typically, the southern flank of the Sierra de Prada has an essentially dip-slope topography that is further affected by differential lithification of the strata, which are generally planar with a dip parallel to bedding.

My study comprises the lower part of ~1100 m of limestone and marls (Fig. 2-3, Fig. 2-4) that are exposed in

the southern flank of the Sierra de Prada often designated as Cabó Marls (Peybernès and Souquet, 1973; Peybernès, 1976; Martínez, 1982; García-Senz, 2002; Bernaus et al., 2002, 2003; Moreno-Bedmar, 2010; Sanchez-Hernandez and Maurrasse, 2014). The studied sedimentary succession including the upper most part of the Prada Formation and the designated Cabó Marls has been assigned an overall latest Barremian to early Aptian age on the basis of paleontological studies of ammonites, and benthic and planktic foraminifera (Peybernès and Souquet, 1973; Peybernès, 1976;

Martínez, 1982; Berástegui et al., 1990; Bachmann and Willems, 1996; Bernaus et al., 2002, 2003; Moreno-Bedmar, 2010).



Figure 2-3 Field view of the first ~30 m of the El Pui section showing the bedding of the sequence. See geologist in the extreme left and right along the road for scale.

More specifically I focus on the El Pui section ($42^{\circ}14' 36.00''\text{N}$, $1^{\circ}13' 33.67''\text{E}$) where differential erosion of the beds along dip slopes facilitated the development of subsequent streams that cut deeply into the layers (Fig. 2-3, Fig. 2-4). These stream valleys form step-like profiles with water gaps that offer excellent spatial and temporal continuity of outcrops. I studied the lower 240 m of the section, named after the local area known as El Pui (Fig. 2-4). At the field scale the section consist of a sequence of alternating beds of cm to m scale of medium gray (N5) to grayish black (N2) consolidated, but somewhat friable, shaly limestones, and marls with no conspicuous primary structures (color is assigned on fresh samples). The carbonate-rich facies include intermittent organic-rich layers ($\text{TOC} > 0.5\%$) that herald conditions of increased

deposition of organic matter, and fluctuating paleoenvironments in the basin, and have been suggested to include the record of the lower Aptian OAE1a (Bernaus et al., 2003). The upper 150 m of the section include intermittent intervals that suggest a cyclic pattern associated with the influence of local as well as global factors environmental (Bachmann and Willems, 1996)



Figure 2-4 Lower part of the El Pui section that shows the continuous parallel bedding that favors excellent outcrop conditions for high resolution sampling.

2.3 References

- Bachmann, M., Willems, H., 1996. High-frequency cycles in the upper Aptian carbonates of the Organyà basin, NE Spain. *Geologische Rundschau* 85(3), 586-605.
- Berástegui, X., García-Senz, J.M., Losantos, M., 1990. Tectonosedimentary evolution of the Organyà extensional basin (Central South Pyrenean Unit, Spain) during the Lower Cretaceous. *Bulletin de la Société Géologique de France* 8, VI, 2, 251- 264.
- Berástegui X., Losantos M., Muñoz J.A., Puig de Fàbregas. C., 1993. Tall geològic del Pirineu central 1:200 000. Map and explanations. Servei Geològic de Catalunya, Barcelona, 58 pp.

- Bernaus, J.M., Arnaud-Vanneau, A., Caus, E., 2002. Stratigraphic distribution of Valanginian Early Aptian shallow-water benthic foraminifera and algae, and depositional sequences of a carbonate platform in a tectonically-controlled basin: the Organyà Basin, Pyrenees, Spain. *Cretaceous Research* 23, 25-36.
- Bernaus, J.M., Arnaud-Vanneau, A., Caus, E., 2003. Carbonate platform sequence stratigraphy in a rapidly subsiding area: the Late Barremian - Early Aptian of the Organyà Basin, Spanish Pyrenees. *Sedimentary Geology* 159 (3-4), 177–201.
- Bond, R.M.G., McClay, K.R., 1995. Inversion of a Lower Cretaceous extensional basin, south central Pyrenees, Spain. In *Basin Inversion* (Eds) Buchanan, J.G. and Buchanan, P.G. Geological society special publication 88, 415–431.
- Caus, E., García-Senz, J. M., Rodés, D., Simón, A., 1990. Stratigraphy of the Lower Cretaceous (Berriasian-Barremian) sediments in the Organyà Basin, Pyrenees, Spain. *Cretaceous Research* 11, 313–320.
- Dinarès-Turell, J., García-Senz, J., 2000. Remagnetization of Lower Cretaceous limestones from the southern Pyrenees and relation to the Iberian plate geodynamic evolution. *Journal of Geophysical Research* 105(B8), 19405–19418.
- García-Mondejar, J., 1996. Plate reconstruction of the Bay of Biscay. *Geology* 24 (7), 635–638.
- García-Senz, J., 2002. Cuencas extensivas del Cretácico Inferior en los Pirineos Centrales: formación y subsecuente inversión. PhD Thesis, University of Barcelona, Barcelona, 310 pp.
- García-Senz, J., Berástegui, X., Caus, E., Losantos, M., Puigdefàbregas, C., 1995. El Cretácico inferior de la Cuenca de Organyà (lamina cabalgante Bóixols), In *El Cretácico Inferior del Nordeste de Iberia, Guia de Campo del III Coloquio del Cretácico de España*, Morella, 1991. Universidad de Barcelona, Barcelona, pp. 95–153.
- Garrido Mejias, A. 1973. Estudio geológico y relación entre tectónica y sedimentación del Secundario y Terciario de la vertiente meridional pirenaica en su zona central (provincias de Huesca y Lérida). PhD thesis, Universidad de Granada, 320 pp.
- Gong, Z., van Hinsbergen, D. J.J., Vissers R. L.M., Dekkers M. J., 2009. Early Cretaceous syn-rotational extension in the Organyà Basin - New constraints on the palinspastic position of Iberia during its rotation. *Tectonophysics* 473, 312–323.
- Gong, Z., 2008. The rotation of Iberia during the Aptian and consequences for pervasive Cretaceous remagnetization. PhD Dissertation, University of Utrecht, Budapestlaan, The Netherlands, 103 pp.

- Martínez, R., 1982. Ammonoideos cretácicos del Prepirineo de la provincia de Lleida. PhD thesis, publicaciones de la Universitat Autònoma de Barcelona, 17, pp. 197.
- Moreno-Bedmar, J.A., 2010. Ammonits de l'Aptià inferior de la península Ibèrica. Biostratigrafia i aportacions a l'estudi del Oceanic Anoxic Event 1a. Universitat de Barcelona, 331 pp.
- Muñoz, J.A., 1991. Evolution of a continental collision belt: ECORS-Pyrenees crustal balanced cross-section, In Thrust Tectonics Ed. K.R. McClay. Chapman and Hall, New York, pp. 235-247.
- Muñoz, J.A., 1992. Evolution of a continental collision belt: ECORS Pyrenees crustal balanced cross-section, in: McClay, K.R. (Eds.), Thrust tectonics. Chapman and Hall, London, pp. 235-246.
- Muñoz, J.A., Puig de Fàbregas, C., Fontboté, J.M., 1984. Orógenos alpinos, in: Ríos, L. J. J. M. (Ed.), El Pirineo. Inst. Geol. Min. España. Geología de España 2, pp. 161–205.
- Peybernès, B., 1976. Le Jurassique et le Crétacé inférieur des Pyrénées franco-espagnoles. Thèse de doctorat, Laboratoire de Géologie, Université Paul Sabatier, Toulouse, 459 pp.
- Peybernès, B. and Souquet, P., 1973. Biostratigraphie des marnes noires de l'Aptien-Albien de la zone sud-pyrénéenne. Comptes Rendus de l'Académie des Sciences Paris 276 (2 Mai 1976), Séries D, 2501-2504.
- Puigdefàbregas, C., Souquet, P., 1986. Tecto-sedimentary cycles and depositional sequences of the Mesozoic and Tertiary from the Pyrenees. Tectonophysics 129, 173–203.
- Seguret, M., 1972. Étude tectonique des nappes et séries décollées de la partie centrale du versant sud des Pyrénées Pub. Ustela, Série Géologie Structurale 2, 155 pp.
- Vergés J., Muñoz, J.A., 1990. Thrust sequences in the southern central Pyrenees. Bulletin de la Société Géologique de France 8, VI 2, 265–271.
- Vergés, J., 1993. Estudi tectònic del versant sud del Pirineu oriental i central. Evolució cinemàtica en 3D. Tesis doctoral Universitat de Barcelona, Barcelona, 191 pp.

3 MATERIAL AND METHODS

The multiproxy approach used to assess criteria indicative of temporal environmental changes in the basin was achieved as follows:

3.1 Field measurement and sampling of the stratigraphic section

In order to select a suitable section for the study, the fieldwork started with a preliminary reconnaissance of the geology of the Organyà region, and examination of the entire stratigraphic succession exposed along the southern flank of the Prada Mountain in the El Pui area. The studied section was selected to include the marly sequence of the Cabò Formation (García-Senz, 2002) reported in the published literature as late Barremian to the Late Aptian (Peybernès and Souquet, 1973; Peybernès, 1976; Martínez, 1982; Caus et al., 1990; Berástegui et al., 1993; García-Senz, 2002; Bernaus et al., 2002; 2003; Moreno-Bedmar, 2010).

The field method I used involved systematic bed-by-bed descriptions and sampling (Folk, 1959, 1962, 1980), including the physical stratigraphy, field-scale structures, and measurement of bed thickness with a Jacob's staff and a measuring tape. I used a combined letter and numerical designation for rock colors of dry rocks in reference to the "Rock-color chart" distributed by the Geological Society of America, which is based on the modified Munsell color system (Goddard et al., 1963). Further details of the method are described in Chapter 6 (Sanchez-Hernandez and Maurrasse, submitted). I collected a total of 482 samples for laboratory analyses during three field seasons (2010; 2011; 2012), and samples were labeled in continuous numeric order with the year as reference and common denominator for the batch collected that year. Sample positions were recorded in a continuous series of photographs for further accuracy in

determining their respective points in the stratigraphic column. The samples were collected targeting each apparent bed, giving an average sampling interval of ~50 cm along the 440 m of the studied section. The lowest 87 samples were collected on fresh outcrops along a recently (2 years) built private dirt road leading to the top of the Sierra de Prada. The remaining samples were taken along erosional ridges and valleys, as described in Chapter four (Sanchez-Hernandez and Maurrasse, 2014). In order to ensure lesser influence of weathering, the samples were taken at least 5 cm deep from the surface of the recently exposed rock masses. At least one thin section per sample was made for petrographic analysis.

3.2 Laboratory analyses

3.2.1 Petrographic analysis

Petrographic and microfacies analyses were carried out on all samples with conventional transmitted light microscopy (Olympus BH-2 microscope). Sample selection for these analyses was based on three main factors: color of fresh cut specimen, abundance of benthic fauna, and presence of unidentified grains in thin sections. As a complement to field scale observations, the microscopic study also paid special attention to the presence/absence of benthic fauna, bioturbation and early diagenetic minerals indicative of redox conditions.

The total inorganic carbon (TIC) in most of the rocks of the sequence are above 30% dry weight (Sanchez-Hernandez and Maurrasse, 2014); therefore, for the petrographic analysis, including designation of allochems and assignment of microfacies name, I followed guidelines proposed by numerous authors for classification of carbonate rocks (Folk, 1962; 1974; 1993; Dunham, 1962; Ehlers and Blatt, 1999; Flügel, 2010).

The petrographic analysis of thin sections was also used to determine the bioturbation index, which was assigned a value from 0 to 6, based on previous assessment by Droser and Bottjer (1986) and formulated in description proposed by Taylor and Goldring (1993).

These analyses provide information about sedimentary facies, mineral composition, and concentration and identification of faunas. Because of the scarcity of both benthic and planktic foraminifera throughout the section (less than 15 per 10 cm² of thin section) a specific scale was created to define their relative abundance: more than 10 specimens per 10 square centimeters is equivalent to abundant (>10/10 cm² abundant); between 10 and 4 specimens per 10 cm² (10-4/10 cm²), scarce; and less than 4 specimens per 10 cm² (<4/10 cm²), rare. Visual estimate for allochems versus matrix was used according to the method proposed by Terry and Chillingarian (1955).

3.2.2 Micropaleontology and age

The microscope work on calcareous nannofossils was performed by Dr. Mihaela Melinte (GEOECOMAR, Romania) on an Olympus BH-2 petrographic microscope with a magnification of $\times 1500$. Calcareous nannofossils were examined using simple smear slides (Lamolda et al., 1994) and standard light-microscope techniques (Bown and Young, 1998). In order to achieve quantitative analyses, at least 300 specimens were counted in each smear-slide, in longitudinal transverses, randomly distributed.

The individual abundance of the observed taxa was considered as follows: P - present: 1 specimen (s) />50 fields of view (FOV); R-rare: 1s/21-50 FOV; F-few: 1s/11-20 FOV; C-common: 1s/2-10 FOV; A-abundant: >1s/FOV. The individual taxonomic

diversity, in percentage, was considered from the total counted taxa following the procedure outlined in Lamolda et al. (1994), and Melinte and Lamolda (2007).

Because most of the samples were lithified I achieved only limited success in obtaining individual planktonic foraminifera (Fig. 4.5, Sanchez-Hernandez and Maurrasse, 2014) from partly indurated marl. The few loose specimens obtained were extracted with liquid nitrogen [LN₂] following the treatment proposed by Remin et al (2012). The new LN₂ method falls into the category of freeze-thaw method in which a rock sample previously soaked in water is treated alternately with LN₂, and then boiling water until the sample is sufficiently disintegrated. Depending on the state of induration of the rock, the procedure may necessitate 15–20 cycles in order to obtain a satisfactory of coarse residue for microscopic examination. The effective mechanism of this method resides in the fact that LN₂ [-196°C] causes complete and instantaneous formation of ice crystals in the pore system that expands by approximately 10%. The sudden addition of boiling water [100°C] produces a significant temperature shift of 300°C, and the difference in thermal expansion between rock matrix and the various microfossils leads to partial disintegration and the release of the foraminifera from the matrix (Remin et al., 2012). The micropaleontological analysis for planktonic foraminifera was accomplished primarily with thin sections using the help of illustrations in the published literature (e.g. Caron, 1985; Premoli Silva et al., 1999; Verga and Premoli-Silva, 2002; Premoli Silva and Verga, 2006).

The taxonomic name *Globigerinelloides* is used for the species *G. blowi* based on the works of Verga and Premoli-Silva (2002), and Premoli Silva and Verga (2006), as they clearly establish the validity of the genus *Globierinelloides* to be applied to this

taxon. Also, as discussed in Sanchez and Maurrasse (Chapter 6) these authors defined other taxa such as *G. maridalensis* and *G. paragottisi*, which in the case of the El Pui samples the sediments were too indurated to obtain free specimens that would have allowed unequivocal differentiation with co-occurring *G. blowi*. For chronostratigraphic correlation and paleogeographic reconstruction I used established standard works by Bolli et al. (1985); Caron (1985); Premoli Silva et al. (1999); Verga and Premoli-Silva (2002); Ogg and Ogg, (2008); Blakey (2011); and Walker et al. (2012).

3.2.3 Scanning Electron Microscopy

In order to obtain more detailed paleontological and sedimentological information, 55 small cubes (~1 cm³) of rock were cut and semi-polished for Scanning Electron Microscopy (SEM) and Energy Dispersive Spectrometry (EDS). The analyses were performed at the Florida Center for Analytical Electron Microscopy (FCAEM) located at FIU using a JEOL JSM 5910LV scanning electron microscope with an EDAX energy dispersive spectroscope. Samples for SEM and EDS analyses were selected at levels with different TOC and TIC content along the sedimentary sequence.

Energy dispersive spectroscopy (EDS) was also performed to determine the composition of the rock matrix and non-biogenic grains. For the analyses, samples were carbon coated to the orange thickness (150 Å) and processed in Compo mode under backscattered electron imaging detection. Areas of interest were first determined and inspected in secondary electron imaging and later switched to backscatter for qualitative elemental analysis. Relative composition was determined using the Compo mode and both diffractograms and X-ray maps generated to evaluate the grain size and rock matrix composition.

3.2.4 Total carbon/carbonate – TC, TIC, TOC

Total carbon (TC) and total inorganic carbon (TIC) were measured at Florida International University (FIU) for 420 samples (Appendix 1) following the standard analytical procedures of our carbonate laboratory facility (Sanchez-Hernandez and Maurrasse, 2014). The measurements were performed on a LECO CR-412 carbon analyzer, which uses an infrared cell to measure the CO₂ produced by combustion of 0.250 g of powdered sample placed in a furnace at 1450°C. Calibration of the LECO CR-412 was performed using calcite (C64-500, Fisher Scientific) and dolomite (Dolomitic Limestone NIST 88b) as standard reference materials. The measured carbon was standardized to pure calcite, and the results of TC and TIC are expressed as a percentage by weight of bulk CaCO₃. The analytical precision of the results was of ± 5%.

In preparation for TC measure, every piece of rock was cut using a diamond saw in order to remove the exposed surface. Small pieces (1-2 cm) were cut, dried at 45°C for 24 h and powdered using a Bell-Art micromill with a tungsten-carbide chamber and hardened blade. Powdered samples were later put in the oven at 60°C for 2 h and stored in a desiccator until analysis was carried out. TC was determined from 0.250 ± 0.003 g of rock powder. To obtain the TIC (CaCO₃), an aliquot of the same powdered samples was placed into a furnace at 580°C for 2 h in order to burn off all organic matter, before being processed by the LECO CR-412 analyzer. Given that the instrument provides all results as a CaCO₃ weight percent, the difference (TC-TIC) was divided by 8.33 (molecular weight of CaCO₃ divided by molecular weight of C: 100.086/12.011) to obtain total organic carbon (TOC) expressed as a weight percent of carbon. TIC values are used to assign a lithologic classification based on the nomenclature adopted in our sedimentary

laboratory. Hence, the relative percentage of total measured CaCO_3 (TIC) indicates: limestone, > 65% CaCO_3 ; marly-limestone, 60-65% CaCO_3 ; marlstone, 30-60% CaCO_3 ; calcareous mud-rock/shale, 10-30% CaCO_3 ; and mud-rock/shale, 0-10% CaCO_3 .

3.2.5 C-stable isotope on the organic fraction ($\delta^{13}\text{C}_{\text{org}}$)

Carbon isotope analyses on the organic fraction of 420 samples from the El Pui section (Appendix 1) were conducted on a Finnigan Delta C EA-IRMS (with TC/EA), at the Southeast Environmental Research Center, FIU. The analytical technique uses 0.1-1.0 mg samples of powdered dry rock. The homogenized rock samples require initial dissolution of the inorganic carbon (CaCO_3) in a 1M HCl solution. The carbon isotope ratios are expressed on a per mil (‰) basis relative to the Vienna Pee Dee Belemnite standard (VPDB). Carbon ratios obtained were repeatedly compared with a laboratory reference gas under identical conditions. Precision of isotopic analyses for replicate samples, the international standard IAEA-CH-6 (Sucrose) and our lab standard (glycine) was better than $\pm 0.025\%$.

3.2.6 Major and trace element analyses

The method and calibration applied follow the methodology of Arroyo et al., (2009). Laser Ablation-Inductively Coupled Plasma Mass Spectrometry (LA-ICP-MS) was used in order to determine the concentrations of trace and major elements. ICP-MS analyses were conducted at the FIU Forensic Center using a quadrupole ELAN DRC II (Perkin Elmer LAS, Shelton CT USA), in the standard operation mode. A 266 nm Nd-YAG laser (LSX 500, CETAC, USA) was used for this work. Best ablation results, previously evaluated as the best precision and accuracy for reference standards were obtained using a depth profile ablation mode with a 200 μm spot size and 10 Hz.

Ablations were conducted as discrete scans in previously prepared pressed sample pellets, in four different locations in the same pellet die.

I analyzed 124 small rock fragments of $\sim 1 \text{ cm}^3$ selected from areas with no evidence of weathering, and processed as described for TC preparation. Fine powdered samples were weighed between 0.5 and 1.0 g, and a Scandium solution (1000 ppm in 3% HNO_3) added as internal standard, dried at 80°C overnight, homogenized with a ball-mill for 10 min and converted to pellets using a manual press. As control samples, two sand blanks of known composition were prepared using identical steps and conditions as for the actual samples. Two additional samples (included in the 124 measured) corresponding to the same level as C12-257 and C12-259, respectively but with different lateral position (C12-257A and C12-259A) were analyzed to test the horizontal homogeneity of the trace element concentration (Appendix 2). Although the test was only performed for two samples, the results provided acceptable precision for the elements concentration. Standards and sand blanks were run at the beginning and end of the sample line. Concentrations of Ni, V, Cr, P, Fe, Cu, U, Th, Co, and Mo and major elements such as Al, Si and Ti are reported herein (Appendix 2). No significant external contribution from the sample preparation process was identified. Data processing was performed using the Glitter software (ARC National Center for Geochemical Evolution and Metallogeny of Continents).

Results of every measurement were averaged for each sample and the relative standard deviation (standard deviation/mean) calculated. Percentages of the relative standard deviation were consistently below 10% for all the elements measured, although accuracy of the measurements for every sample is different and depends on factors as

choice of standards and abundance of measured element. The error of the measurements is reported as the average standard deviation per element (Appendix 2). The following soil and sediment standards were used for evaluation of the analytical performance of the method: a) marine sediment reference material, PACS-2 (National Research Council of Canada, Ottawa, Canada); b) soil reference material, SRM NIST2710 (Montana Soil), and c) NIST2704 (Buffalo River Sediment), US Department of Commerce, National Institute of Standards and Technology, Gaithersburg, MD, USA).

3.2.7 Biomarker analysis

Fossil biomarkers or biologically-derived residual compounds found preserved in sediments are increasingly used in sedimentary geology as a critical tool that provides information on the origin and type of organic matter, environmental conditions of deposition and maturity of the carbon compounds affected by subsequent diagenetic processes (Peters et al., 2005). They are reliable because they cannot be synthesized by non-biological processes and can be preserved over long geological times with little change in the original structure of the living organisms or parent molecules (Simoneit, 2004).

In preparation for biomarker determination, small rock slabs corresponding to 36 different samples were powdered in a Bell-Art micromill. A careful cleaning process, with water, detergent, deionized water and acetone, was completed between samples. Biomarkers were analyzed following the procedures described in Jaffé et al. (2001). Samples were subjected to Soxhlet extraction for 24 h with 300 ml 100% methylene chloride (Optima, Fisher, USA) as solvent. HCl (10%) activated copper was added during the extraction to eliminate elemental sulfur. Total extracts were concentrated by rotary

evaporation and saponified with 0.5 N KOH to separate into neutral and acid fractions. The neutral fractions free of elemental sulfur were further fractionated by elution with hexane to obtain saturated hydrocarbon fraction using Pasteur pipette columns packed with silica gel. A known quantity of squalene was added as internal standard for quantification purpose and the hydrocarbon fraction was run on GC/MS with a Hewlett-Packard 6890 GC linked to a HP 5973 quadrupole MS system, fitted with Rtx-1MS columns (30 m long, 0.25 mm ID, 0.25 μm df) from RESTEK, USA. The GC oven was programmed to hold initial temperature of 40°C for 1 min, and then ramped at a rate of 6°C/min to a final temperature of 300°C held for 20 min. Identification of compounds was performed by comparison of chromatographic retention time, comparison with the mass spectra library and previous mass spectra reported in the literature. The concentration of n-alkanes was normalized to organic carbon (OC) as ng/g OC.

3.2.8 Bulk and clay mineral analysis

Mineralogical analyses of 30 samples (Appendix 3) were performed at the Illinois State Geological Survey (ISGS) using X-ray diffraction (XRD) following the methodology described by Moore and Reynolds (1997). For the XRD procedure, the samples were micronized in a McCrone micronizing mill with deionized water for 10 min. Then transferred to 50 mL centrifuge tubes, which were placed in the centrifuge for 20 min at 2000 rpm. The clear supernatant was poured off and the remaining material dried overnight at 40°C. When completely dried the material was mixed lightly with a mortar and pestle and then packed into an end-loading sample holder as a random powder bulk-pack. The random powder bulk-pack was analyzed with a Scintag XDS 2000 diffractometer. Step-scanned data was collected from 2° to 60° 2 θ with a fixed time of 5

sec per $0.05^\circ 2\theta$ for each sample. All resulting traces were analyzed using the semi-quantitative data reduction software from Materials Data Inc. (MDI) known as Jade®.

The clay mineral composition was determined using oriented slides of the clay size $< 2 \mu\text{m}$ fraction with semi-quantitative values of the clay mineral assemblage calculated from ethylene glycol (EG) solvated slides (Hughes and Warren, 1989; Hughes et al, 1994; Moore and Reynolds, 1997).

In preparation for XRD 20 g - 30 g of each sample was soaked for about 10-12 h in deionized water and protected from external agents. As water interacts with the sample small clay particles are released into the solution. Further stirring of the solution mechanically induced clay release from the sample. After settling, about 1/3 of the water was removed from the beaker. The beaker was then refilled with deionized water and two drops of sodium hexametaphosphate is added as a dispersant. The mix was stirred and then allowed to settle for 15 min. The generated supernatant was pipetted and several drops were added onto a glass slide and let to dry overnight.

Alternate treatments with EG for 24 h, and heating to 490°C , were also applied in order to establish a better comparison in peak intensity ratios among the expandable clays. Step-scans from 2° - $34^\circ 2\theta$ with a fixed time of 5 sec per $0.05^\circ 2\theta$ were conducted for each sample. The diffractograms generated were superimposed (Fig. 3-1) for peak identification and mixed layer clay assessment.

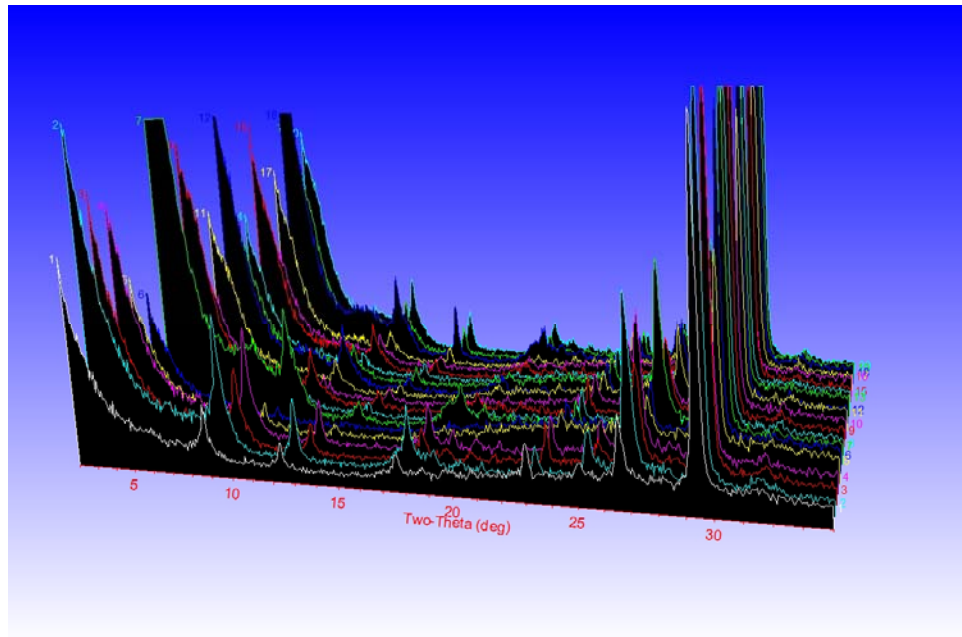


Figure 3-1 Comparative sketch of the diffractograms obtained for the El Pui samples. The number of peaks and their corresponding intensity can be used to assess the presence of mixed layered clay.

3.3 References

- American Association of Petroleum Geologists, 1983. North American Commission on Stratigraphic Nomenclature. North American Stratigraphic Code. AAPG Bulletin 67 (5), 841–875.
- Berástegui X., Losantos M., Muñoz, J.A., Puig de Fàbregas, C., 1993. Tall geològic del Pirineu central 1:200 000. Map and explanations. Servei Geològic de Catalunya, Barcelona, 58 pp.
- Bernaus, J.M., Arnaud-Vanneau, A., Caus, E., 2002. Stratigraphic distribution of Valanginian Early Aptian shallow-water benthic foraminifera and algae, and depositional sequences of a carbonate platform in a tectonically-controlled basin: the Organyà Basin, Pyrenees, Spain. *Cretaceous Research* 23, 25–36.
- Bernaus, J.M., Arnaud-Vanneau, A., Caus, E., 2003. Carbonate platform sequence stratigraphy in a rapidly subsiding area: the Late Barremian – Early Aptian of the Organyà Basin, Spanish Pyrenees. *Sedimentary Geology* 159 (3–4), 177–201.
- Blakey, R., 2011. Colorado Plateau Geosystems Inc. (<http://www.geomapp.org/>)
- Bolli, H.M., Saunders, J.B., Perch-Nielsen, K., 1985, *Plankton Stratigraphy*: Cambridge Earth Science Series, Cambridge University Press 1, 86p.

- Bown, P.R., Young, J.R., 1998. Techniques. In: Bown, P.R. (Ed.), *Calcareous Nannofossil Biostratigraphy*. Chapman and Hall, London, pp. 16–28.
- Caron, M. 1985. Cretaceous planktic foraminifera. In Bolli, H. M., Saunders, J. B., and Perch-Nielsen, K, (eds). *Plankton Stratigraphy*. Cambridge University Press, pp.17–86.
- Caus, E., García-Senz, J. M., Rodés, D., Simón , A., 1990. Stratigraphy of the Lower Cretaceous (Berriasian-Barremian) sediments in the Organyà Basin, Pyrenees, Spain. *Cretaceous Research* 11, 313–320.
- Droser, M.L., Bottjer, D., 1986. A semiquantitative field classification of ichnofabric. *Journal of Sedimentary Petrology* 56(4), 558–559.
- Dunham, R. J., 1962. Classification of carbonate rocks according to depositional textures, *in* Ham, W, E. (ed.), *Classification of carbonate rocks: American Association of Petroleum Geologists Mem. 1*, p. 108–121.
- Ehlers, E. G., Blatt, H. 1999. *Petrology Igneous, Sedimentary, and Metamorphic*. W. H. Freeman & Co. Publisher, 732 p.
- Folk, R. L., 1962. Spectral subdivision of limestone types. *in* Ham, W, E. (ed.), *Classification of carbonate rocks: American Association of Petroleum Geologists Mem. 1*, p. 6 – 84.
- Folk, R.L., 1974, *Petrology of Sedimentary Rocks*: Hemphill Publishing Company, Austin, Texas, 185p.
- Folk, R. L., 1993. SEM imaging of bacteria and nannobacteria in carbonate sediments and rocks. *Journal of Sedimentary Petrology* 63, 990–999.
- Flügel, E., Munnecke, A., 2010. *Microfacies of Carbonate Rocks: Analysis, Interpretation and Application*. Springer-Verlag, Berlin Heidelberg, Germany, Second ed. pp 984.
- García-Senz, J., 2002. *Cuencas extensivas del Cretácico Inferior en los Pirineos Centrales: formación y subsecuente inversión*. PhD Thesis, University of Barcelona, Barcelona, 310 pp.
- Goddard, E.N., Trask, P. D., De Ford, R. K., Rove, O.N., Singewald, J.T., Overbeck, R.M., 1963, *Rock-Color Chart*. Distributed by the Geological Society of America, New York, N.Y. 16 p.
- Jaffé, R., Mead, R., Hernandez, M.E., Peralba, M.C., and DiGuida, O.A., 2001, Origin and transport of sedimentary organic matter in two subtropical estuaries: a comparative, biomarker-based study: *Organic Geochemistry* 32, 507–526.

- Lamolda, M. A., Gorostidi, A., Paul, C. R. C., 1994. Quantitative estimates of calcareous nannofossil changes across the Plenus Marls (latest Cenomanian), Dover, England: implications for the generation of the cenomanian–Turonian Boundary Event. *Cretaceous Research* 14,143–164.
- Martínez, R., 1982. Ammonoideos cretácicos del Prepirineo de la provincia de Lleida. PhD thesis, publicaciones de la Universitat Autònoma de Barcelona, 17, pp. 197.
- Melinte, M.C., Lamolda, M.A., 2007. Calcareous nannofossil biostratigraphy of the Coniacian/Santonian boundary interval in Romania and comparison with other European regions. *Cretaceous Research* 28(1), 119–127.
- Moreno-Bedmar, J.A., 2010. Ammonits de l’Aptià inferior de la península Ibèrica. Biostratigrafia i aportacions a l’estudi del Oceanic Anoxic Event 1a. Universitat de Barcelona, 331 pp.
- Ogg, J.G., Ogg, G., 2008. Early Cretaceous (103-138 Ma time-slice). Update to Geological Time Scale 2004 (Gradstein, F.M., Ogg, J.G., Smith, A.G., et al., Cambridge Univ. Press) and The Concise Geologic Time Scale (Ogg, J.G., Ogg, G., Gradstein, F.M., 2008). URL: https://engineering.purdue.edu/Stratigraphy/charts/Timeslices/4_Mid-Cret.pdf.
- Peters, K.E., Walters, C.C., Moldowan, J.M., 2005. The biomarker guide: II, Biomarkers and isotopes in petroleum systems and Earth history, Cambridge, UK, Cambridge University Press, pp. 475–1155.
- Peybernès, B., Souquet, P., 1973. Biostratigraphie des marnes noires de l’Aptien–Albien de la zone sud-pyrénéenne. *Comptes Rendus de l’Académie des Sciences Paris* 276 (2 Mai 1976), Séries D, 2501–2504.
- Peybernès, B., 1976. Le Jurassique et le Crétacé inférieur des Pyrénées franco-espagnoles. Thèse de doctorat, Laboratoire de Géologie, Université Paul Sabatier, Toulouse, 459 pp.
- Premoli Siva, I., Erba, E., Salvini, G., Locatelli, C., Verga, D., 1999. Biotic changes in Cretaceous oceanic anoxic events of the Tethys. *Journal of Foraminiferal Research*, 29, 352–370.
- Premoli-Silva, I., Verga, D., 2006. Classification of Early Cretaceous trochospiral and planispiral planktonic foraminifera: An update. *Anuário do Instituto de Geociências UFRJ*. 209 (1), 361–362.
- Remin, Z., Dubicka, Z., Kozłowska, A., Kuchta, B., 2012. A new method of rock disintegration and foraminiferal extraction with the use of liquid nitrogen [LN₂]. Do conventional methods lead to biased paleoecological and paleoenvironmental interpretations? *Marine Micropaleontology* 86–87, 11–14.

- Sanchez-Hernandez, Y., Maurrasse, F.J-M.R., 2014. Geochemical characterization and redox signals from the latest Barremian to the earliest Aptian in a restricted marine basin: El Pui section, Organyà Basin, south-central Pyrenees. *Chemical Geology* 372, 12–31.
- Sanchez-Hernandez, Y., Maurrasse, F. J-M. R., Melinte-Dobrinescu, M. C., He, D., Butler, S. K., (submitted). Assessing the factors controlling high sedimentation rates from latest Barremian–earliest Aptian in a restricted marginal basin. *Cretaceous Research* (2014).
- Simoneit, B., 2004, Biomarkers (molecular fossils) as geochemical indicators of life. *Advances in Space Research*, 33 (8), 1255–1261.
- Taylor, A. M., Goldring, R. 1993. Description and analysis of bioturbation and ichnofabric. *Journal of the Geological Society of London* 150, 141–148.
- Terry, R. D., and Chilingarian, G. V. 1955. Summary of “Concerning some additional aids in studying sedimentary formations” by M.S. Shevtsov. *Journal Sedimentary Petrology*, v. 25, p. 229 – 234.
- Verga, D., Premoli Silva, I., 2002. Early Cretaceous planktonic foraminifera from the Tethys. The genus *Leupoldina*. *Cretaceous Research* 23, 189–212.
- Walker, J.D., Geissman, J.W., Bowring, S.A., and Babcock, L.E., compilers, 2012, *Geologic Time Scale v. 4.0*: Geological Society of America.

4 GEOCHEMICAL CHARACTERIZATION AND REDOX SIGNALS FROM THE LATEST BARREMIAN TO THE EARLIEST APTIAN IN A RESTRICTED MARINE BASIN: EL PUI SECTION, ORGANYÀ BASIN, SOUTH-CENTRAL PYRENEES

Sanchez-Hernandez, Y., Maurrasse, F.J-M.R., 2014. Geochemical characterization and redox signals from the latest Barremian to the earliest Aptian in a restricted marine basin: El Pui section, Organyà Basin, south-central Pyrenees. *Chemical Geology* 372, 12–31.

Abstract

The Organyà Basin located in the south-central Spanish Pyrenees developed in the northern part of the Iberian Peninsula mainly during a Barremian to early Albian phase, when Iberia rifted and rotated counter-clockwise away from Europe. Extension was followed by strong subsidence in the basin resulting in the development and accumulation of carbonate platforms and deeper-water hemipelagic sediments.

Here we present the multiproxy results of a high-resolution lithostratigraphic and geochemical study of the lowest 85 m of the El Pui section in the Organyà Basin, Catalunya, Spain. The sequence comprises series of limestone and marlstone interbeds spanning the latest Barremian and the earliest Aptian. Our results show that intermittent dark limestone and marlstone layers associated with extremely low diversity and scarce benthic fauna, low bioturbation index (0-3) and high TOC (up to 1.7 wt%), indicate recurrent oxygen-deficient conditions within the lowest 31 m of the section and more uniform oxygenation in the upper 54 m. SEM analyses reveal a high abundance of calcareous nannofossils as the source of carbonate throughout the section. EDS analyses confirmed the presence of clastics (mainly aluminum silicates) in the matrix. Sustained high primary productivity was the result of a constant supply of nutrients, especially biolimiting elements (P, Fe), from terrestrial fluxes as indicated by excellent linear

correlation with Al, Si and Ti. $\delta^{13}\text{C}_{\text{org}}$ values within the high TOC intervals show excursions of up to 2.0‰ suggesting important isotopic changes in the carbon reservoir. Relatively high enrichment of Ni, and minor of U and Cr with respect to the average shale concurrent with high Ni/Co ratios, and punctuated high U/Th values, suggest the existence of intermittent reducing benthic conditions in these intervals. However, V is depleted, indicating that reducing conditions were weak with the absence of an anoxic/euxinic phase.

In the present study we document that basin physiography along with the nature of the adjacent geologic terranes surrounding the Organyà Basin induced a sustained nutrient supply, thereby enhancing constant productivity, which intensified OM respiration in the water column. Density stratification may have also temporarily exacerbated oxygen deficiency (without an anoxic phase) that enhanced OM preservation from the late Barremian to the earliest Aptian.

4.1 Introduction

The Mesozoic Era recorded severe greenhouse conditions associated with a series of widespread Oceanic Anoxic Events (OAEs) (Schlanger and Jenkyns, 1976; Jenkyns, 1980). The Barremian–Aptian transition was marked by intense tectonic, volcanic, and paleoceanographic changes (Arthur et al., 1985; Bralower et al., 1994; Larson and Erba, 1999; Aguado et al., 1999; Weissert and Erba, 2004; Neal et al., 2008; Tejada et al., 2009; Föllmi, 2012) concurrent with greenhouse conditions (Föllmi et al., 2006; Ando et al., 2008; Méhay et al., 2009), lower temperature gradient between low and high latitudes, and intensified hydrological cycle (Hay and Deconto, 1999). Such conditions may have led to increased continental runoff (that enhanced marine productivity) and

higher eustatic elevations (Barron et al., 1989, 1995). The early Aptian also shows differential drowning of preexisting carbonate platforms (Föllmi & Gainon, 2008; Barragan and Maurrasse, 2008; Godet et al., 2013; Masse and Ferneci-Masse, 2013) development of restricted epicontinental seas, and stagnation of deep-water masses (Bralower et al., 1994) in the Western Tethys.

A combination of these factors produced stressful conditions that contributed to the occurrence of the early Aptian Oceanic Anoxic Event 1a (OAE1a) (~125 Ma, Erba, 2004; Li et al., 2008), which was one of the most intense episodes of widespread marine anoxia in the Cretaceous Period. OAE1a is well documented in different worldwide locations (Menegatti et al., 1998; Larson and Erba, 1999; Erba, 2004; Li et al., 2008; Jenkyns, 2010, among others). Its hallmark in the stratigraphic record includes not only deposition of organic-rich sediment (TOC >2%) that lasted for about 1.2My (Li et al., 2008), but also involves a pronounced positive $\delta^{13}\text{C}$ excursion of 2-5‰ (Jenkyns, 1980; Arthur and Premoli-Silva, 1982; Arthur et al., 1985; Menegatti et al., 1998; Leckie et al., 2002; Méhay et al., 2009; Millán et al., 2009).

Because OAE1a is most significant as an interval of worldwide accumulation of organic-rich sediments, it has been the subject of most scientific investigations of Early Cretaceous anoxic events. While most studies centered essentially on the event, however, the gradual environmental response to the transition between normal conditions in the late Barremian to extreme conditions in the early Aptian (Mutterlose and Böckel, 1998; Godet et al., 2008; Mutterlose et al., 2009; Stein et al., 2011, 2012; Pauly et al., 2013) still remains to be fully understood. Indeed, in order to better discern the mechanisms associated with these changes, biological and environmental responses to changing

conditions prior to OAE1a need to be better known, because several studies have recognized the occurrence of highly positive excursions of $\delta^{13}\text{C}$ not associated with known widespread OAE's. Case in point is the Upper Barremian stage B7 (e.g. Alvier section, Wissler et al., 2003), the C1 segment from Menegatti et al. (1998) (e.g. Cismon section, Erba, 1999; Cassis–La Bédoule section, Stein et al., 2012) and the late Barremian–early Aptian interval at Cluses section (Huck et al., 2011). Such $\delta^{13}\text{C}$ increments suggest enhanced ^{12}C sequestration due to preservation of OM in part recorded in several Tethyan sections (Föllmi et al., 2012). These events are of particular interest to further our understanding of the Earth systems localized response to greenhouse conditions and increased carbon sequestration.

The El Pui section of the Organyà Basin, south-central Spanish Pyrenees (Séguret, 1972; Peybernès, 1976; Muñoz et al., 1984; Berástegui et al., 1990; García-Senz, 2002) (Fig. 4-1A, Fig. 4-2 A, B), contains an expanded continuous sequence of medium gray (N5) to grayish black (N2) hemipelagic sediments (Fig. 4-3 A, B) that offers an excellent opportunity to study the paleoenvironmental response to changing global conditions concomitant with tectonic evolution of the basin between the late Barremian and early Aptian (Fig. 4-1 A, B; Fig. 4-2 A, B). In the present study we integrate high-resolution stratigraphic and geochemical analyses using various proxies: total inorganic carbon (TIC), total organic carbon (TOC), stable isotopes of organic carbon ($\delta^{13}\text{C}_{\text{org}}$), and major and trace element concentrations, in order to reconstruct local paleoenvironmental conditions from the latest Barremian to the earliest Aptian prior to the occurrence of the OAE1a in the Organyà Basin (Fig. 4-2 A, B). In addition, considering the paleogeographic position of the basin (Peybernès, 1976; Berástegui, et

al., 1990, Masse et al., 2000; García-Senz, 2002), the study improves our knowledge of the local response of the restricted Organyà Basin to increasing greenhouse conditions in the development and accumulation of organic-rich sediments. It also reveals the possible causes and mechanisms of enhanced organic carbon (OC) sequestration during the late Barremian—early Aptian interval.

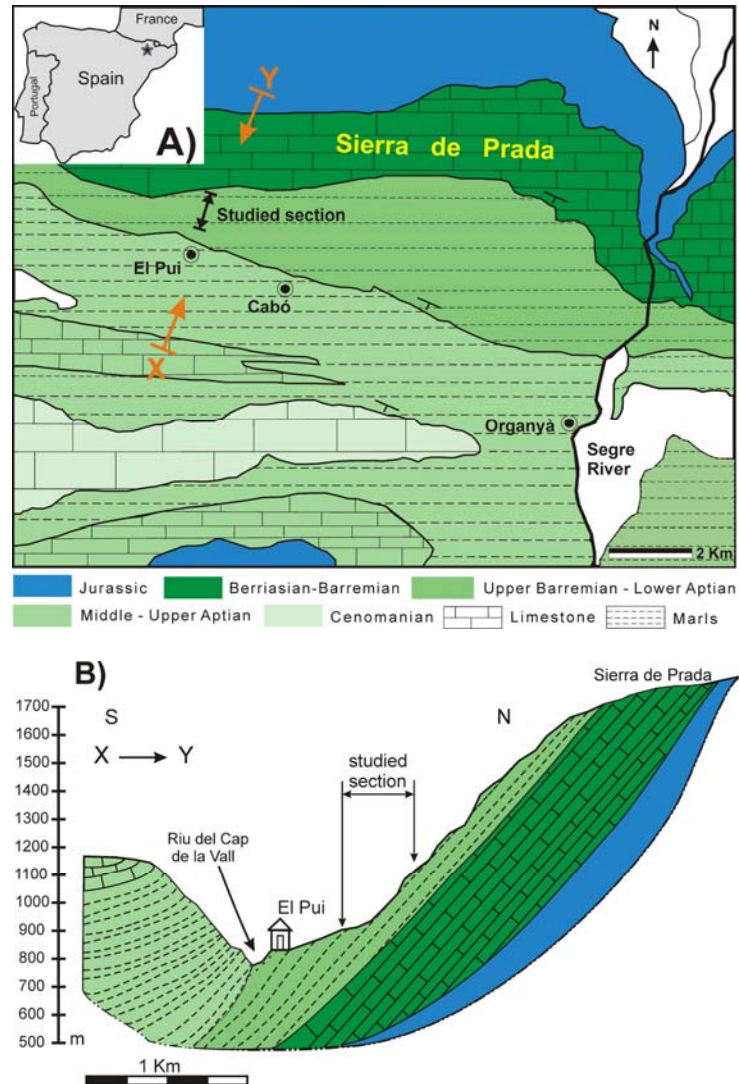


Figure 4-1 A) Simplified geologic map of the Organyà Basin (modified from Bernaus et al., 2003) showing the location of the study area, the overall age and lithologies in the southern flank of Sierra de Prada. Short lines symbol (└) show the strike and dip of the homoclinal sequence. B) Simplified geologic cross section of the studied area through X-Y drawn from a 1:50.000 topographic map of Cabó from the Institut Cartogràfic de Catalunya (<http://www.icc.cat>)

4.2 Geographic and geologic setting

The south-central Pyrenees of Spain comprise numerous thrust sheets whose uppermost unit, the Bòixols Thrust Sheet, incorporates the sedimentary succession of the Organyà Basin (Fig. 4-2A) (Seguret, 1972; Peybernès, 1976; Muñoz et al., 1984; Verges and Muñoz, 1990; García-Senz, 2002). The Sierra de Prada is part of that unit and its southern flank shows a remarkable homoclinal structure with northward vergence and an overall E–W strike. The strata dip uniformly southward with an average angle between 40 and 50° (Fig. 4-1A, Fig. 4-3A). Typically, the southern flank of the Sierra de Prada has an essentially dip-slope topography that is further affected by differential lithification of the strata, which are generally planar with a dip parallel to bedding. The El Pui section (42° 14' 36.00"N, 1° 13' 33.67"E) is situated on the southern limb of the Sierra de Prada (Fig. 4-1 A, B) where differential erosion of the beds along dip slopes facilitated development of subsequent streams that cut deeply into the layers (Fig. 4-3 A, B). These stream valleys form step-like profiles with water gaps that offer excellent spatial and temporal continuity of outcrops (Fig. 4-3A, B). We studied the lower 85 m of the section, named after the local area known as El Pui (Fig. 4-1A, B; Fig. 4-2B). The studied section is part of a continuous sequence extending eastward past the nearby town of Cabó (Fig. 4-1A), the namesake of the marly sequence, coined the Cabó Formation (García-Senz, 2002).

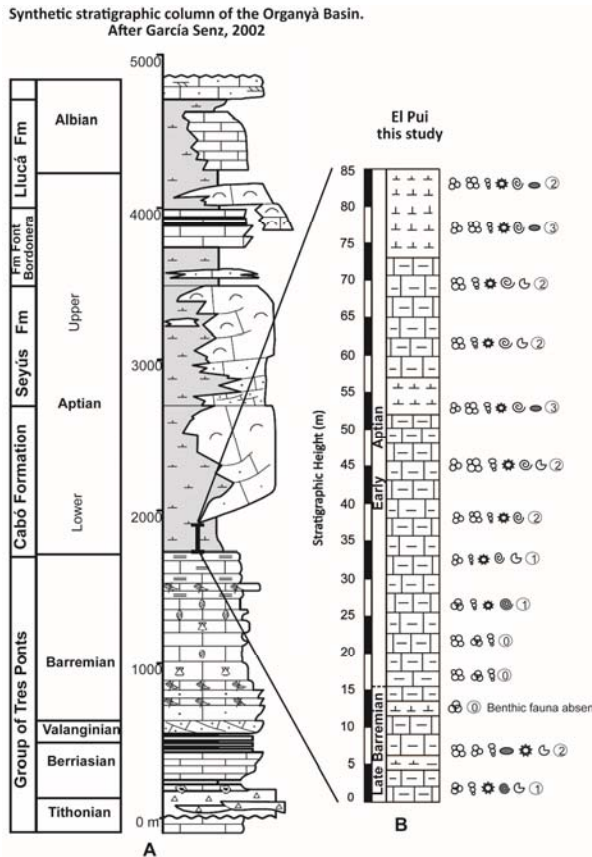


Figure 4-2 A) Synthetic stratigraphic column and age distribution of the lower Cretaceous of the Organyà Basin (from García Senz, 2002), the Barremian-Aptian boundary has been modified after Moreno-Bedmar (2010). B) Chronostratigraphic column of the 85 m studied at El Pui with fossil and lithologic characterization. All the facies studied correspond to the mudstone classification of Dunham (1962). Circled numbers to the right of the fossil content indicate the bioturbation index after Taylor and Goldring (1993). See legend for explanation of symbols.

Previous studies indicate that the basin developed during extensional processes related to counter-clockwise rotation of Iberia from the late Jurassic to early Cretaceous, concurrent with the opening of the Atlantic Ocean leading to the opening of the Bay of Biscay during Aptian-Albian times (Berástegui et al., 1990, 1993). About 4500 m of shallow water to hemipelagic sediments accumulated in the Organyà Basin during the Cretaceous (Fig. 4-2A), with

approximately 1000 m corresponding to the Barremian-early Aptian interval (García-Sens, 2002) (Fig. 4-2A). The studied sedimentary succession including the upper most part of the

Prada Formation and the designated Cabó Marls has been assigned an overall latest Barremian to early Aptian age (Fig. 4-1 A, Fig. 4-2A, B), based on paleontological studies of ammonites, and benthic and planktic foraminifera (Peybernès and Souquet, 1973; Peybernès, 1976; Martínez, 1982; Berástegui et al., 1990; Bachmann and Willems, 1996; Bernaus et al., 2002, 2003; Moreno-Bedmar, 2010).

Three main phases characterized the tectonic evolution of the basin and influenced the variability of the sedimentary sequence:

- 1) Early Cretaceous extensional tectonism associated with the opening of the Bay of Biscay (Berástegui et al., 1990, 1993; Vergés, 1993) led to the development of the Organyà Basin as result of the breakup of Jurassic platforms (Caus et al., 1990). It was the time when several other small sedimentary basins also developed along the edges of the Iberian and European plates.
- 2) A Cretaceous phase of development of carbonate platforms characterized by a high subsidence rate and the accumulation of thick carbonate sequences. This phase of sedimentation also coincides with the accumulation of organic-rich layers above the studied 85 m, suggested to be possibly correlative with OAE1a (Bernaus et al., 2003).
- 3) Latest Cretaceous /early Cenozoic collision of the Iberian Plate with Europe led to the emergence of the Organyà Basin (García-Senz, 2002).

The first stages of tectonic extension modified the paleogeographic configuration of the region as extensional processes caused the formation of a wider seaway between Europe and Iberia. During the Barremian–early Aptian, subsidence rates increased and the net sedimentation rate approximately doubled (Bachmann and Willems, 1996; García-Senz, 2002). Sediments from that interval reflect a marine setting, and higher influx of terrigenous materials suggests a more elevated topography in the adjacent areas (Gong et al., 2009).

The segment studied comprises only the lower part of the Cabó Marls, reported to reach an estimated total thickness of ~800 m of gray to black limestones and marls (Fig. 4-3B) (Caus et al., 1990; Berástegui et al., 1990, Bernaus et al., 2003). At the field scale

the lower 85 m consist of a sequence of alternating beds (0.15-3.0 m) of medium gray (N5) to grayish black (N2) consolidated, but somewhat friable, shaly limestones, and marls with no conspicuous primary structures (color is assigned on fresh samples). Certain levels of recurrent black, well-consolidated limestone beds (Fig. 4-3B) herald conditions of increased deposition of organic matter, and fluctuating paleoenvironments in the basin.

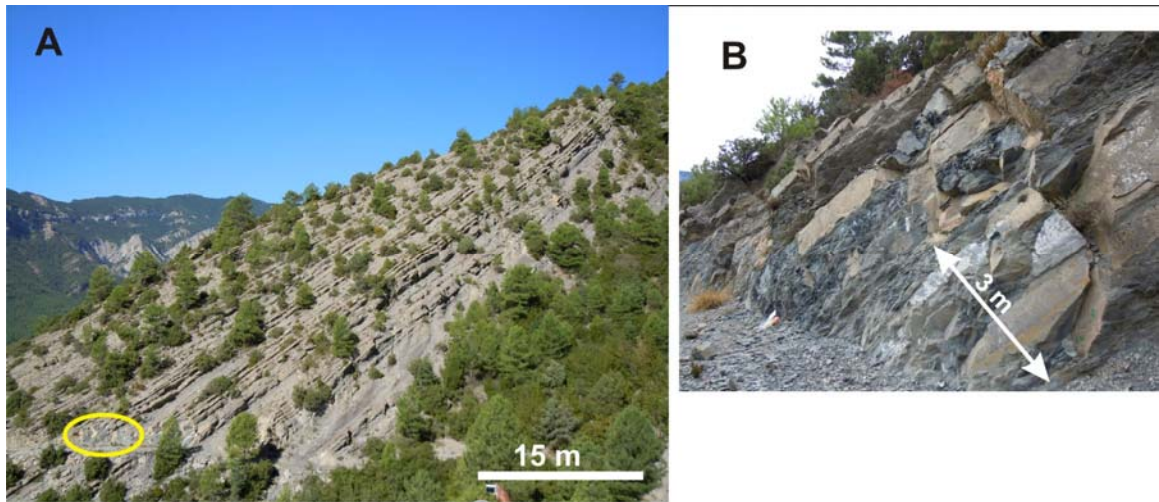


Figure 4-3 El Pui section: A) Panoramic view of the lower 25 m (sediment thickness) of the sampled area showing a continuous succession. B) Close up view of the yellow oval that corresponds to the stratigraphic interval from ~15 m to ~20 m showing the lithology along a road cut to the top of Sierra de Prada; note the well-consolidated dark limestone beds.

4.3 Material and Methods

The multiproxy approach used to assess environmental changes in the basin was achieved as follows:

4.3.1 Petrographic analysis

Two hundred seven (207) samples were collected targeting each apparent bed, giving an average sampling interval of ~40 cm along the 85 m of the studied section. The lowest 87 samples were collected on fresh outcrops along a recently built private dirt-

road leading to the top of the Sierra de Prada. The remaining samples were taken along erosional ridges and valleys, as previously described. In order to ensure lesser influence of weathering, the samples were taken at least 5 cm deep from the surface of the recently exposed rock masses. At least one thin section per sample was made for petrographic analysis. Because of the scarcity of both benthic and planktic foraminifera throughout the section (less than 15 per 10 cm² of thin section) a specific scale was created to define their relative abundance: more than 10 specimens per 10 square centimeters is equivalent to abundant (>10/10 cm² abundant); between 10 and 4 specimens per 10 cm² (10-4/10 cm²), scarce; and less than 4 specimens per 10 cm² (<4/10 cm²), rare. Petrographic and microfacies analyses were carried out on all samples with conventional transmitted light microscopy (Olympus BH-2 microscope). In addition, 55 small cubes (~1 cm³) of rock were cut and semi-polished for Scanning Electron Microscopy (SEM) and Energy Dispersive Spectrometry (EDS) in order to obtain more detailed paleontological and sedimentological information. Sample selection for these analyses was based on three main factors: color of fresh cut specimen, abundance of benthic fauna, and presence of unidentified grains in thin sections. As a complement to field scale observations, the microscopic study also paid special attention to the presence/absence of benthic fauna, bioturbation and early diagenetic minerals indicative of redox conditions. The petrographic analysis of thin sections was also used to determine the bioturbation index, which was assigned a value from 0 to 6, following the description proposed by Taylor and Goldring (1993). These analyses provide information about sedimentary facies, mineral composition, concentration and identification of faunas.

4.3.2 Total carbon/carbonate –TC, TIC, TOC

Total carbon (TC) and total inorganic carbon (TIC) were measured at Florida International University (FIU) for all samples following the standard analytical procedures of our carbonate laboratory facility. The measurements were performed on a LECO CR-412 carbon analyzer, which uses an infrared cell to measure the CO₂ produced by combustion of 0.250 g of powdered sample placed in a furnace at 1450 °C. Calibration of the LECO CR-412 was performed using calcite (C64-500, Fisher Scientific) and dolomite (Dolomitic Limestone NIST 88b) as standard reference materials. The measured carbon was standardized to pure calcite, and the results of TC and TIC are expressed as a percentage by weight of bulk CaCO₃. The analytical precision of the results was of ± 5%.

In preparation for TC measure, every piece of rock was cut using a diamond saw in order to remove the exposed surface. Small pieces (1-2 cm) were cut, dried at 45 °C for 24 h and powdered using a Bell-Art micromill with a tungsten-carbide chamber and hardened blade. Powdered samples were later put in the oven at 60 °C for 2 h and stored in a desiccator until analysis was carried out. TC was determined from 0.250 ± 0.003 g of rock powder. To obtain the TIC (CaCO₃), an aliquot of the same powdered samples was placed into a furnace at 580 °C for 2 h in order to burn off all organic matter, before being processed by the LECO CR-412 analyzer. Given that the instrument provides all results as a CaCO₃ weight percent, the difference (TC-TIC) was divided by 8.33 (molecular weight of CaCO₃ divided by molecular weight of C:100.086/12.011) to obtain total organic carbon (TOC) expressed as a weight percent of carbon. TIC values are used to assign a lithologic classification based on the nomenclature adopted in our sedimentary laboratory. Hence, the relative percentage of total measured CaCO₃ (TIC) indicates:

limestone, > 65% CaCO₃; marly-limestone, 60-65% CaCO₃; marlstone, 30-60% CaCO₃; calcareous mud-rock/shale, 10-30% CaCO₃; and mud-rock/shale, 0-10% CaCO₃.

4.3.3 C-stable isotope on the organic fraction ($\delta^{13}\text{C}_{\text{org}}$)

Carbon isotope analyses on the organic fraction of 147 samples from the El Pui section were conducted on a Finnigan Delta C EA-IRMS (with TC/EA), at the Southeast Environmental Research Center, FIU. The analytical technique uses 0.1-1.0 mg samples of powdered dry rock. The homogenized rock samples require initial dissolution of the inorganic carbon (CaCO₃) in a 1M HCl solution. The carbon isotope ratios are expressed on a per mil (‰) basis relative to the Vienna Pee Dee Belemnite standard (VPDB). Carbon ratios obtained were repeatedly compared with a laboratory reference gas under identical conditions. Precision of isotopic analyses for replicate samples, the international standard IAEA-CH-6 (Sucrose) and our lab standard (glycine) was better than $\pm 0.025\%$.

4.3.4 Major and trace element analyses

The method and calibration applied follow the methodology of Arroyo et al., (2009). Laser Ablation-Inductively Coupled Plasma Mass Spectrometry (LA-ICP-MS) was used in order to determine the concentrations of trace and major elements. ICP-MS analyses were conducted at the FIU Forensic Center using a quadrupole ELAN DRC II (Perkin Elmer LAS, Shelton CT USA), in the standard operation mode. A 266 nm Nd-YAG laser (LSX 500, CETAC, USA) was used for this work. Best ablation results, previously evaluated as the best precision and accuracy for reference standards were obtained using a depth profile ablation mode with a 200 μm spot size and 10 Hz. Ablations were conducted as discrete scans in previously prepared pressed sample pellets, in four different locations in the same pellet die.

We analyzed forty-two (42) samples of small rock fragments selected from areas with no evidence of weathering, and processed as described for TC preparation. Fine powdered samples were weighted between 0.5 and 1.0 g, and a Scandium solution (1000 ppm in 3% HNO₃) added as internal standard, dried at 80 °C overnight, homogenized with a ball-mill for 10 min and converted to pellets using a manual press. As control samples, two sand blanks of known composition were prepared using identical steps and conditions as for the actual samples. Standards and sand blanks were run at the beginning and end of the sample line. Concentrations of Ni, V, Cr, P, Fe, U, Th, and Co, and major elements such as Al, Si and Ti are reported herein (Table 4-1). No significant external contribution from the sample preparation process was identified. Data processing was performed using the Glitter software.

Results of every measurement were averaged for each sample and the relative standard deviation (standard deviation/mean) calculated. Percentages of the relative standard deviation were consistently below 10% for all the elements measured, although accuracy of the measurements for every sample is different and depends on factors as choice of standards and abundance of measured element. The following soil and sediment standards were used for evaluation of the analytical performance of the method: a) marine sediment reference material, PACS-2 (National Research Council of Canada, Ottawa, Canada); b) soil reference material, SRM NIST2710 (Montana Soil), and c) NIST2704 (Buffalo River Sediment), US Department of Commerce, National Institute of Standards and Technology, Gaithersburg, MD, USA).

4.3.5 SEM and EDS analyses

A JEOL JSM 5910LV available at the Florida Center for Analytical Electron Microscopy (FCAEM) at FIU was used to perform SEM analyses on selected samples. SEM images were taken on partially polished fragments of rocks and thin sections. Samples for SEM examination were coated using a Gold/Palladium target in order to improve conductivity and reduce surface charging on the specimen. Both secondary and backscattered electron images were produced. In order to determine the qualitative composition of non-biogenic grains energy dispersive spectroscopy (EDS) was also performed on polished fragments of rock coated with carbon to the orange thickness (150 Å).

4.4 Results

4.4.1 Petrographic analysis

The general variation in lithology and fossil characterization for the El Pui section is summarized in the simplified stratigraphic column (Fig. 4-2B). The bioturbation index varies throughout the sequence between 0 and 3 out of 6 (Taylor and Goldring, 1993), with the smallest values corresponding to intervals impoverished in benthic organisms. SEM micrographs reveal calcareous nanofossil fragments as the main source of carbonate in the rock matrix (Fig. 4-4) with minor contribution from benthic and planktonic foraminifera. Typical microfacies at all levels of the studied sequence are characterized by a matrix of dark, fine micrite with less than 20% allochems (Folks, 1962) that consist of minute echinoderm spine fragments, rare ostracods, and benthic and planktic foraminifera. *Globigerinelloides blowi* (Bolli, 1959; Caron, 1985; Premoli Silva and Verga, 2006), was effectively first identified at about 4 m above the base of the

section, and two well-preserved specimens were obtained at 16 m (Fig. 5A) and 36 m respectively. Thin section studies also revealed the presence of this taxon within the 85 m interval (Fig. 4-5B, C). *G. blowi* has been assigned a relative chronological position within the late Barremian-early Aptian time interval (Caron, 1985; Erba, 1994).

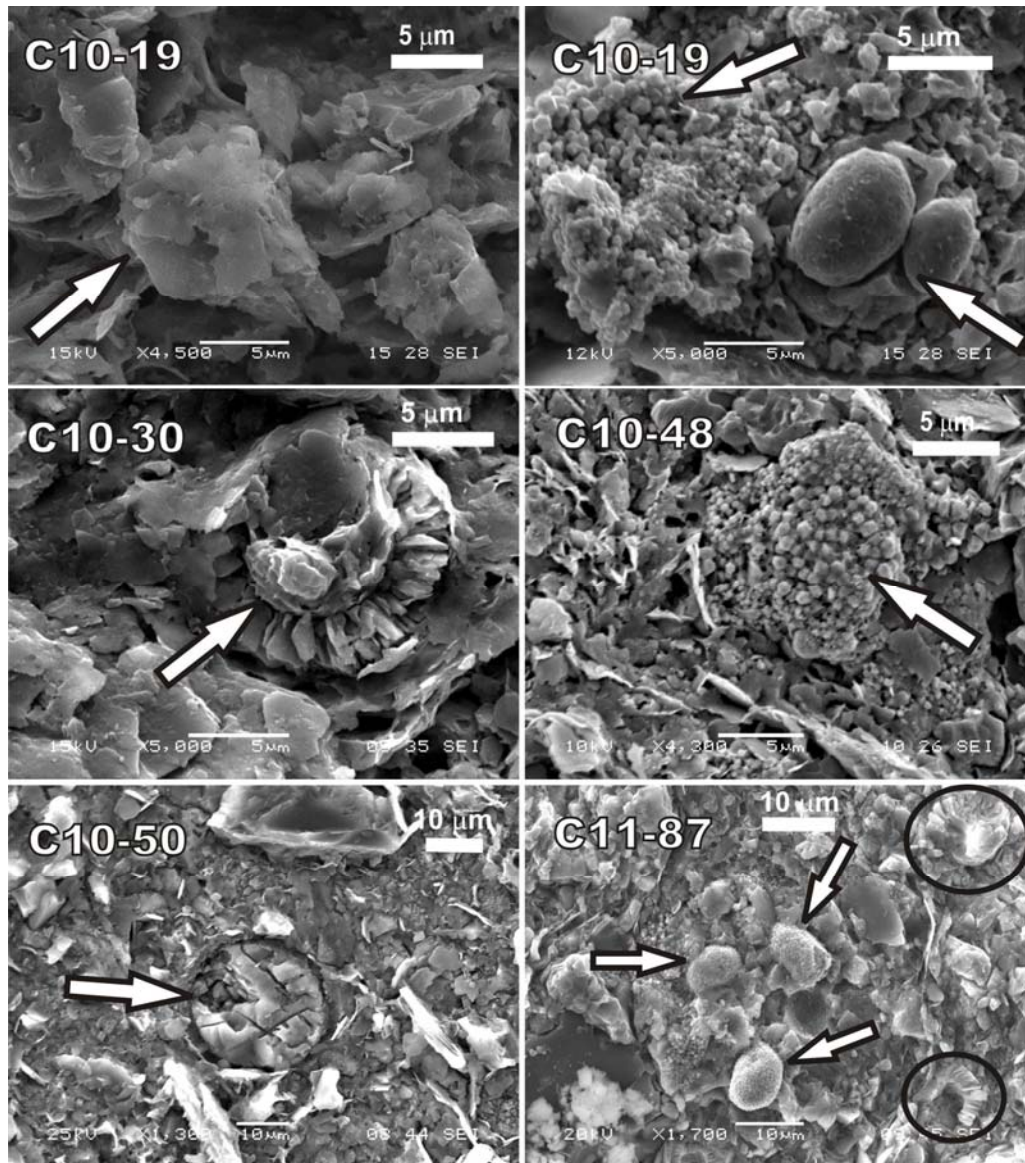


Figure 4-4 SEM micrograph of samples at different levels within the studied section. C10-19 left: Arrow points to coccolith fragments. C10-19 right: Lower arrow points to small calcite spheres, remains of coccoid bacteria; upper arrow indicates dispersive pyrite. C10-30: Arrow points to a relatively well preserved calcareous nannofossil. C10-48: Arrow indicates dispersive pyrite in a carbonate matrix of calcareous nannofossil fragments. C10-50: Cyanobacterial structure. C11-87: Arrows point to abundant framboidal pyrite less than 10 µm in size; black circles enclose calcareous nannofossils.

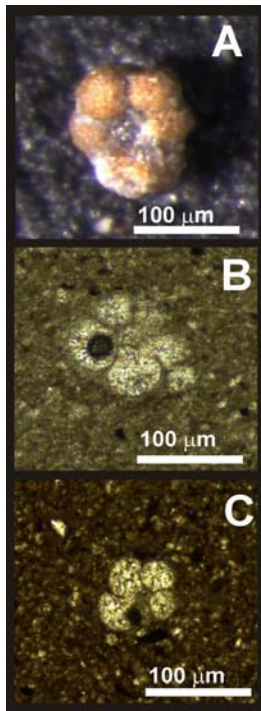


Figure 4-5 Illustrations of *G. blowi*. A: picture taken with a Leica reflected light microscope of a relatively well-preserved whole specimen obtained at ~16 m; B and C: photomicrograph of *G. blowi* in thin section at 12 m and 33 m respectively.

Relative abundance of benthic fauna varies throughout the section, with lesser values (scarce to rare) in the lower part of the studied section as observed in the following stratigraphic segments: 1) 0-1.0 m, and 2) 4.0-6.0 m, two sub-intervals with scarce specimens of small (< 80 μm) uniserials; 3) 10.0-15.5 m, a large sub-interval characterized by rare benthic specimens which become completely absent between 12.0 and 13.0 m; 4) 17.5 to about 19.0 m, sub-interval that encloses rare uniserial taxa; and 5) from about 27.0 to 38.0 m, another large interval (11 m thick) where there are scarce, small benthic foraminifera represented by uniserial as well as

coiled morphotypes. In contrast, the last interval is also marked by higher presence and diversity of planktic foraminifera (up to 10 specimens per 10 cm²), while benthic taxa also vary within the scarce classification (4-10/10 cm²) throughout. SEM secondary and backscattered imaging revealed the presence of dispersive framboidal pyrite (Fig. 4-4, C10-19, C10-48, and C11-87) which

increases significantly from ~27 to 33.0 m; while EDS allowed the identification of small quartz grains, and feldspars (Fig. 4-6).

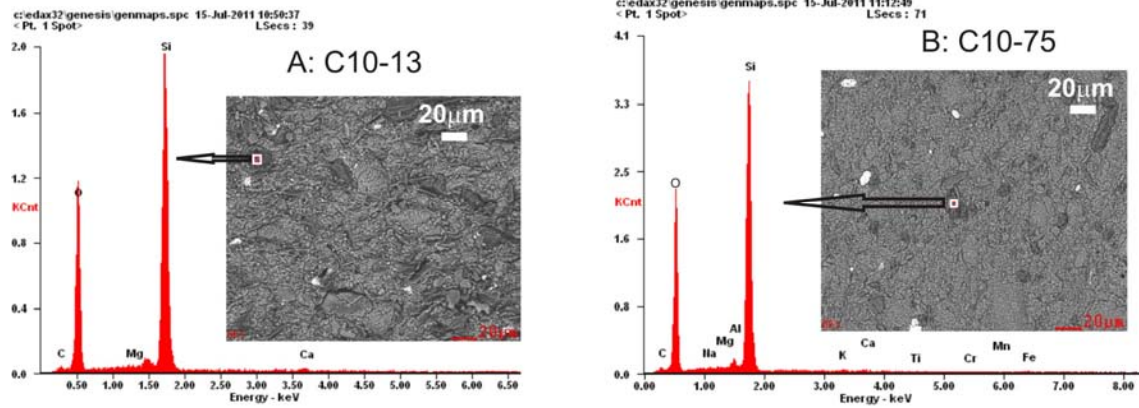


Figure 4-6 Figure 6. SEM with EDS analysis performed on samples showing the presence of siliciclastic material. Diagrams show the qualitative elemental composition of the grains analyzed. Micrographs show the texture of the fine matrix and the random distribution of the grains. Arrows pointing to the elemental diagram originate at small squares where EDS was performed.

4.4.2 TOC, TIC, and $\delta^{13}\text{C}_{\text{org}}$

TOC content measured in 147 samples revealed fluctuating values ranging from ~0 to 1.74%, with most of the samples rich in organic carbon ($\geq 1.0\%$) recorded within the lower 31 m of the section [Appendix 1 (samples C10-01 – C11-207 for current chapter), Fig. 4-7A, B]. Higher TOC values occur within the following levels: at about 1 m, 4.0-7.2 m, 10.0-15.5 m, 18.0-18.7 m, 27.7-31.1 m, and at 41.8 m, respectively. Notably, with the exception of the 41.8 m level, all the high TOC values are coincident with levels included in the previously identified intervals that are characterized by relatively low abundance of benthic foraminifera and correspond to the lowest 31 m (Fig. 4-7A, B).

TIC fluctuates between 43.5 and 87.6% in an indeterminate rhythmic fashion (Appendix 1, Fig. 4-7C). The carbonate content stays consistently above 65% throughout the stratigraphic column, except for five marly intervals in the lower part of the section (0-0.3 m, 1.8-3.0 m, 4.7-6.5 m, 12.0-13.0 m, and 14.8-15.2 m), two upper intervals (52.6-56.9 m and 75.8-84.5 m), and discrete occurrences at 48.7 m and ~62 m where TIC stays

below 65% but mostly higher than 50%. In general, TIC shows poor correlation with the TOC (Fig. 4-7B, C). Abundant calcareous nannofossils confirm the autochthonous biogenic origin of the carbonate fraction in the El Pui sediments.

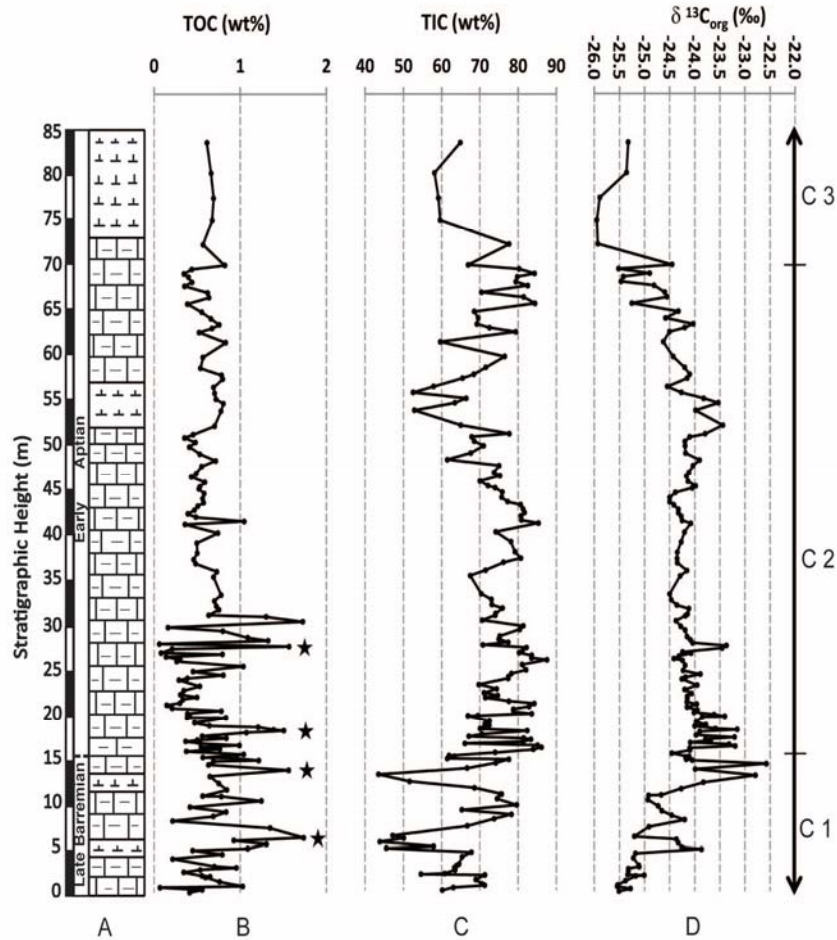


Figure 4-7 Lithostratigraphy and carbon chemostratigraphy: A) Simplified chronostratigraphic column of the studied section. B) Vertical variation in TOC. Star symbols indicate levels of high TOC concurrent with positive excursions in $\delta^{13}\text{C}_{\text{org}}$. C) Vertical variation in TIC. D) Vertical variation in $\delta^{13}\text{C}_{\text{org}}$ including the characteristic late Barremian – lower Aptian carbon isotope segments C1-C3 from Menegatti et al. (1998). The C segments define patterns in the $\delta^{13}\text{C}_{\text{org}}$ curve that are widely used for chemostratigraphic correlation.

$\delta^{13}\text{C}_{\text{org}}$ values measured in the bulk organic fraction vary between -25.95 and -22.57‰ (Appendix 1, Fig. 4-7D). The lowest 4 m show relatively small variations (< 0.5‰) in $\delta^{13}\text{C}_{\text{org}}$, followed by a positive spike with a maximum increase of ~1.3‰ from 4.3 to 4.7 m. Also, characteristically higher $\delta^{13}\text{C}_{\text{org}}$ values occur at intervals 16.4-20.5 m

(>-24.09‰), and 27.5-28.4 m (>-24.09‰), respectively. The succeeding relatively long interval (28.5-51.0 m) yielded comparably low variations (less than 0.5‰ in $\delta^{13}\text{C}_{\text{org}}$), which average -24.23‰, with an overall steady trend lasting up to about 51.3 m (Fig. 4-7A, D). From 51.6 to 55.6 m, $\delta^{13}\text{C}_{\text{org}}$ increases positively by more than 0.75‰ with an average value of -23.71‰. Subsequent $\delta^{13}\text{C}_{\text{org}}$ values fluctuate toward a negative trend, reaching the lowest number of -25.93‰ at the 73 m sampling level. $\delta^{13}\text{C}_{\text{org}}$ values remain low, with hardly any change, within the succeeding 5 m, and then rise again by about 0.5‰ to -25.33‰ at the top of the section.

4.4.3 Major and trace elements analyses

Major and trace element concentrations are reported here as parts per million (ppm) and parts per thousand (ppt), (Appendix 2, samples C10-02 – C11-207 for current chapter). They were measured in 42 selected samples distributed along the stratigraphic column with variable TOC content. In order to have a clearer understanding of the intensity of fluvial fluxes and authigenic enrichment of trace metals, major and trace element concentration are also presented as Aluminum normalized values (Fig. 4-8, Table 4-1) plotted versus depth and compared to the corresponding average shale value (Turekian and Wedepohl, 1961; Wedepohl, 1971, 1991; Brumsack, 2006). Subsequent to the work of Turekian and Wedepohl (1961), and Wedepohl (1971), other studies (Wignall and Myers, 1988; Calvert and Pedersen, 1993; Morford and Emerson, 1999; Rimmer, 2004; Algeo and Maynard, 2004; Tribovillard et al., 2005, 2006; Algeo and Tribovillard, 2009; Algeo and Rowe, 2012) have used lithophile elements (Al, Si, and Ti) and redox sensitive trace elements (RSTE) (U, Ni, V, Cr), and/or their normalized values to reconstruct paleoenvironmental conditions.

Linear plots of Al, Si and Ti show excellent positive correlation between the three elements (Fig. 4-9A, B). The highest values of Si/Al (2.3), and Ti/Al (~0.07) are found at ~15.5 m (Sample C10-37, Table 4-1), and coincide with relative high TOC (>1.0%). The lowest absolute concentrations occur at 41.8 m (sample C10-109) with values of ~6 ppt for Al, ~12 ppt for Si and ~0.2 ppt for Ti (Appendix 2). Phosphorous concentration varies between 107 and 424 ppm, with an average value of 222 ppm (Appendix 2), and shows a good positive correlation with Al (Fig. 4-9C). P/Al values are consistently above the average shale throughout the section (Fig. 4-8). Iron ranges between 3.0 and 21.7 ppt, with an average of ~7.7 ppt (Appendix 2). It shows an excellent correlation with Al (Fig. 4-9D) and the Fe/Al ratio is consistently between 70 and 95% of the average shale Fe/Al ratio with few discrete occurrences as low as 55% (Fig. 4-8).

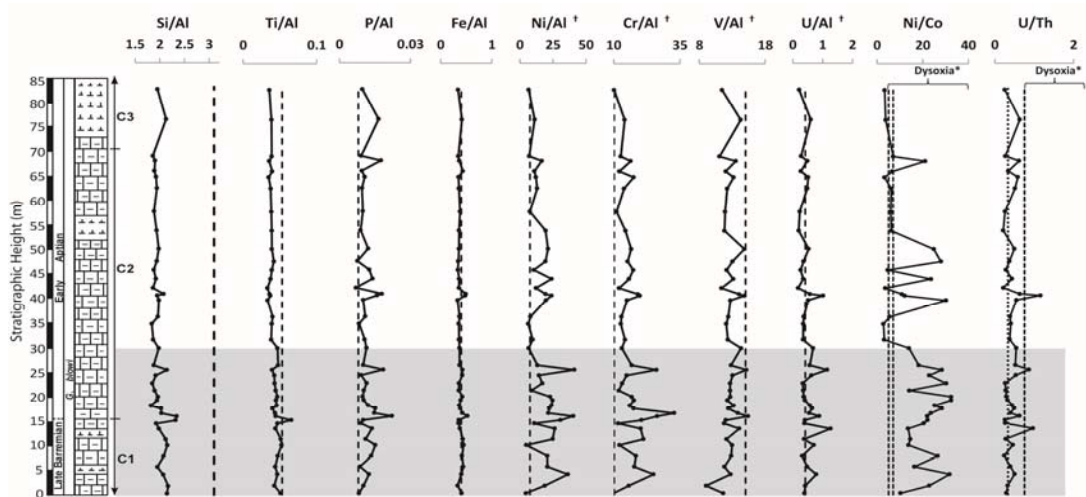


Figure 4-8. Stratigraphic correlation of major and trace elements normalized to Al concentration († represents values $\times 10^{-4}$). C1- C3 corresponds to $\delta^{13}\text{C}_{\text{org}}$ carbon isotope segments in the El Pui section based on the “Cismon” carbon isotope subdivision proposed by Menegatti et al. (1998). The studied 85 m correspond to the *G. blowi* Zone. The two far right columns in the chart show the redox indices Ni/Co and U/Th, and are included for vertical comparison. Dashed lines represent the Al normalized concentration of each corresponding element in the average shale from Wedepohl (1971, 1991). Dashed lines in the Ni/Co and U/Th plots indicate the redox fields proposed by Jones and Manning (1994) (see also Fig. 4-10). Dotted line to the left in the U/Th plot reflects the standard value suggested by Wignall and Myers (1988) for normal mudstones. The asterisks (*) for the redox indices in this figure indicate dysoxia as a general term for oxygen limited conditions as proposed by Wignall and Myers (1988). The shaded interval refers to recurrent oxygen deficient conditions within the lower 31 m of the section.

Ni/Al values are consistently higher than the value for the average shale throughout the section (Fig. 4-8). The highest peaks are located within the lower 27 m with a maximum of 41.2×10^{-4} (Table 4-1). The Ni/Al fraction shows less variation in the upper 58 m where the values are closer to the referenced shale (7.7×10^{-4}) (Fig. 4-8, Table 4-1). Ni shows poor correlation with Al ($R^2 \sim 0.42$) (Fig. 4-9E) suggesting an incorporation pathway different to simply detrital fluxes.

Cr/Al remains higher than 10.2×10^{-4} (average shale) at all levels (except at 0 m, 10.0) and covaries with Ni/Al. The ratio decreases to values very close to the reference line from 27 to 85 m (Fig. 4-8). For values of Al < 25 ppt the linear trend with Cr shows a good fit, whereas for values of Al > 25 ppt the dispersion of the Cr values increases (Fig. 4-9F). The general fit is moderated with an $R^2 \sim 0.67$.

Uranium like Ni shows a poor correlation with Al ($R^2 \sim 0.35$) (Fig. 4-9H), which is consistent with different mechanisms of absorption into the sediment. In the lower 31 m U/Al ratios reach different levels of minor enrichment compared to the average shale (Fig. 4-8). The remaining values are close to the shale line or below (with the exemption of level 41.8 m) suggesting a direct relationship between U and TOC, as the latter also decreases with respect to the lowest 31 m interval. V/Al reflects a relatively small depletion, and in few points, equal values to the average shale (Fig. 4-8). V correlation with Al is excellent ($R^2 \sim 0.94$) (Fig. 4-9G) implying that its presence in the basin has a detrital origin.

Sample Id	Height (m)	Si/Al	Ti/Al	P/Al	Fe/Al	V/Al †	Cr/Al †	Ni/Al †	U/Al †	Ni/Co	U/Th
C-10-02	0.3	2.1	0.05	0.008	0.4	11.6	10.0	4.6	0.4	10.3	0.3
C-10-08	1.9	2.2	0.04	0.010	0.3	9.0	15.7	18.8	0.4	22.8	0.3
C-10-14	4.3	2.1	0.05	0.012	0.4	12.7	25.0	36.3	0.8	31.7	0.5
C-10-18	5.8	2.0	0.04	0.009	0.4	11.8	17.8	20.9	0.5	16.3	0.4
C-10-21	8.0	2.1	0.05	0.013	0.4	12.8	18.4	20.7	0.3	26.5	0.2
C-10-25	10.3	2.2	0.05	0.015	0.4	13.0	12.2	4.9	0.7	13.7	0.5
C-10-28	11.5	2.1	0.05	0.011	0.4	12.1	21.2	24.8	0.4	14.5	0.3
C-10-31	13.7	2.0	0.04	0.014	0.4	14.1	20.2	26.3	1.3	13.6	1.0
C-10-34	14.8	1.9	0.05	0.009	0.4	11.8	11.7	11.0	0.4	20.4	0.3
C-10-37	15.5	2.3	0.07	0.010	0.4	12.0	20.4	30.8	0.4	22.1	0.3
C-10-40	16.4	2.3	0.04	0.022	0.5	15.4	26.4	40.4	0.9	22.0	0.6
C-10-43	17.0	2.0	0.04	0.015	0.4	13.8	32.8	21.6	0.5	23.6	0.4
C-10-47	18.0	2.0	0.04	0.015	0.4	12.4	17.5	22.2	0.6	28.3	0.5
C-10-50	18.6	1.8	0.05	0.012	0.4	13.2	16.1	23.9	0.6	25.2	0.4
C-10-54	19.7	1.9	0.04	0.010	0.4	12.3	17.6	24.8	0.4	32.4	0.3
C-10-57	20.5	2.0	0.05	0.010	0.4	12.7	16.9	22.9	0.4	32.4	0.3
C-10-61	21.8	1.9	0.04	0.010	0.4	12.7	12.0	8.7	0.3	14.1	0.3
C-10-65	23.3	1.8	0.04	0.011	0.4	12.7	13.2	17.0	0.3	30.3	0.3
C-10-69	24.9	1.9	0.04	0.009	0.4	13.0	14.9	14.5	0.6	22.8	0.5
C-10-71	26.1	2.1	0.04	0.018	0.4	15.1	26.2	41.2	1.2	28.3	0.9
C-10-75	27.0	1.9	0.05	0.010	0.4	12.8	16.8	13.3	0.6	18.2	0.5
C-10-83	30.5	2.0	0.05	0.011	0.4	14.3	13.1	6.7	0.7	13.9	0.5
C-11-87	32.3	1.9	0.04	0.011	0.4	12.3	14.3	9.7	0.3	3.1	0.4
C-11-93	35.6	1.8	0.04	0.008	0.4	12.1	12.7	6.3	0.3	2.8	0.4
C-11-97	37.1	2.0	0.04	0.011	0.4	12.4	12.9	8.1	0.4	5.4	0.4
C-11-105	40.5	2.0	0.03	0.010	0.3	12.7	15.0	19.7	0.5	30.1	0.5
C-11-107	41.5	2.0	0.04	0.016	0.5	14.9	19.8	24.0	1.0	12.1	1.2
C-11-109	41.8	2.1	0.04	0.018	0.5	14.0	19.1	19.5	0.6	10.8	0.6
C-11-115	43.1	1.9	0.03	0.007	0.4	11.4	12.0	12.2	0.2	3.5	0.2
C-11-123	45.0	1.9	0.04	0.014	0.4	13.1	15.8	23.9	0.4	23.6	0.4
C-11-131	46.9	1.9	0.04	0.013	0.3	12.1	17.4	10.6	0.3	4.7	0.3
C-11-137	48.7	1.9	0.04	0.008	0.3	13.0	15.3	19.4	0.4	27.9	0.4
C-11-145	51.3	2.0	0.04	0.012	0.4	14.8	16.6	21.3	0.5	24.8	0.5
C-11-153	55.1	1.9	0.04	0.009	0.4	11.8	14.5	19.5	0.2	6.3	0.2
C-11-165	59.1	1.9	0.04	0.010	0.4	11.9	11.1	7.6	0.2	6.0	0.3
C-11-175	64.0	1.9	0.04	0.009	0.4	12.2	13.9	13.1	0.5	6.2	0.5
C-11-181	66.3	1.9	0.03	0.011	0.3	13.2	17.5	12.2	0.5	3.2	0.6
C-11-185	67.6	1.9	0.04	0.009	0.4	12.0	12.1	11.0	0.3	6.7	0.3
C-11-193	69.7	1.9	0.04	0.018	0.4	13.5	16.4	16.5	0.5	21.0	0.6
C-11-197	70.7	1.9	0.04	0.009	0.3	11.1	12.7	7.1	0.3	7.1	0.3
C-11-203	78.3	2.1	0.04	0.017	0.4	14.3	14.1	11.2	0.6	3.7	0.6
C-11-207	84.5	2.0	0.04	0.010	0.3	11.5	10.2	6.7	0.2	3.3	0.2

Table 4-1 Aluminum normalized values of selected major and trace elements measured in the El Pui section and calculated values of the redox indices (Ni/Co, U/Th) used in this study. († = $\times 10^{-4}$).

Elemental ratios of Ni/Co and U/Th were calculated and plotted as an additional supporting proxy to assess redox conditions (Fig. 4-8). Jones and Manning (1994) proposed Ni/Co ratios as a good index to infer oxygenic conditions, suggesting that values less than 5 (<5) correspond to oxic levels, those in the 5-7 interval fit dysoxic conditions, and values greater than 7 (>7) characterize suboxic to anoxic conditions (Fig. 4-10). In the case of the U/Th ratio the same authors suggested a value of 0.75 for the oxic/dysoxic boundary, and >1.25 for the dysoxic/suboxic transition (Fig. 4-10). However, Wignall and Myers (1988) proposed that in normal mudstones the minimum Th/U value in which U is considered detrital is 3 (0.33 for U/Th). This idea implies that at El Pui, sediments with U/Th > 0.33 (Fig. 4-8) could also hold authigenic U because of existent reducing conditions and/or incorporation with OM.

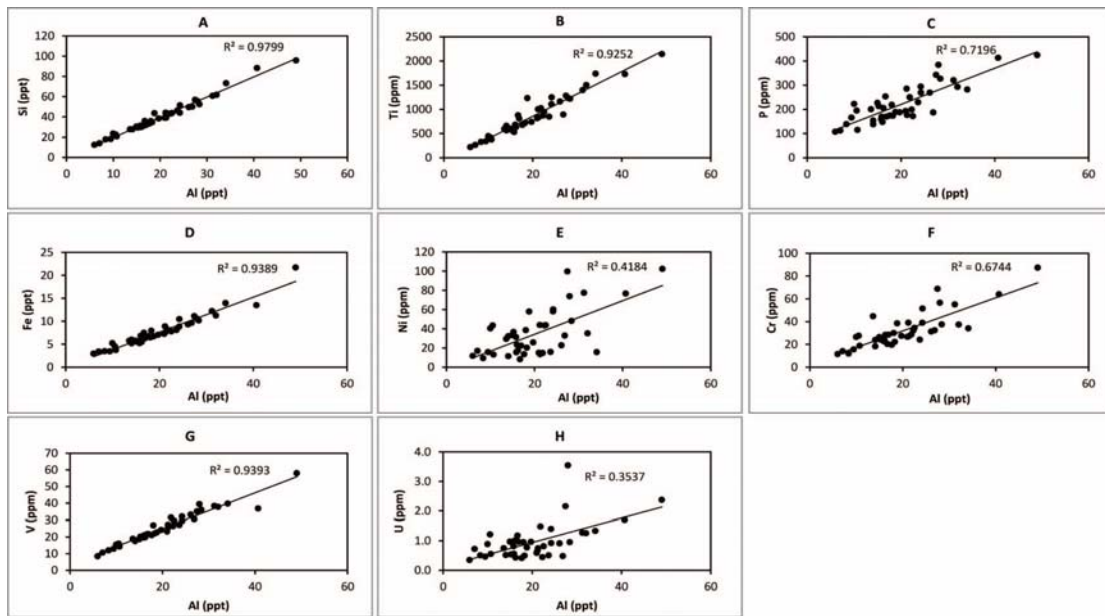


Figure 4-9 Linear plots of selected elements versus Al, showing the correlation coefficient used to support the interpretation on provenance. A) Silicon; B) Titanium; C) Phosphorous; D) Iron ; E) Nickel; F) Chromium ; G) Uranium; H) Vanadium.

Varying factors (e.g., redox potential, pH, sulfur abundance, chemical availability, TOC values and sediment provenance), may induce conflicting results for these paleoredox proxies (Rimmer, 2004; Rimmer et al., 2004; Algeo and Maynard, 2008; Algeo and Rowe, 2012; Xu et al., 2012) thus limiting their applicability in the absence of additional proxies. Because of possible ambiguities, in the present work such redox indices are used as a possible reference of oxic and oxygen deficient conditions regardless of the intensity of the reducing phases and the values shown in Fig. 4-10 are of illustrative purposes only.

	Oxic	Dysoxic	Suboxic	Anoxic
Oxygen concentration (ml O ₂ /l H ₂ O)	> 2.0	0.2 - 2.0	0 - 0.2	0
Ni/Co	< 5.00	5.00 - 7.00	> 7.00	
U/Th	< 0.75	0.75 - 1.25		> 1.25

Figure 4-10 Redox fields classification based on oxygen levels after Tyson and Pearson (1991) and redox indices after Jones and Manning (1994). The suggested limits for the Ni/Co and U/Th are not of strict application in this work.

In general, neither Ni/Co nor U/Th appears to show specific correlation with TOC at El Pui. The Ni/Co ratio is consistently >10.0 in the lower 30.5 m of the section with an average of ~22 (Fig. 4-8, Table 4-1), whereas in the upper 54 m it shows a

value as low as 2.8 and varies up to 30.1. Within this upper part, low values of Ni/Co (<10) occur at intervals 32.3-37.1 m, and 55.1-84.5 m, respectively; with the exception of level 69.7 m (sample C11-193) where the value reaches 21.0. Similar high values occur intermittently at levels 40.5 m (30.14, sample C11-105); 45.0 m (23.57, sample C11-123); 48.7 m (27.9, sample C11-137) and 51.3 m (24.81, sample C11-145) (Table 4-1).

The U/Th index varies independently from Ni/Co and stays regularly below 0.75 in the entire section, but mostly over 0.33 (Fig. 4-8). Nonetheless, peaks > 0.75 occur as

exceptions approximately at 13.7 m (0.97), 26.1 m (0.86) and 41.5 m (1.16) (Table 4-1; Fig. 4-8).

4.5 Discussion

4.5.1 Carbon isotope chemostratigraphy and age correlation

Organic and inorganic carbons produced by living organisms and preserved in marine sediments provide a record that encodes valuable information about environmental conditions (Scholle and Arthur, 1980; Schlanger et al., 1987; Hayes, 1993; Jenkyns, 1995; Meyers, 1997). Assuming minor effects for possible local species-specific fractionation (e.g. Ravelo and Fairbanks, 1995) and despite some degree of chemical transformations (Dean et al., 1986) the isotopic record being ocean-wide allows unambiguous chronological links of the overall ocean isotopic carbon reservoir between different areas. In some cases the preservation state of the OM, the biological fractionation and/or the degree of diagenesis of the carbonate fraction can affect the original isotopic composition leading to discrimination between $\delta^{13}\text{C}_{\text{carb}}$ and $\delta^{13}\text{C}_{\text{Org}}$ to select the most reliable indicator.

In general the $\delta^{13}\text{C}$ curve of carbonates and organic matter show covariation and can be used indistinctively to assess changes in the carbon pool linked to major events (Erba, 1994; Jahren et al., 2002; Leckie et al., 2002; Erba, 2004; Weissert and Erba, 2004; Tejada et al., 2009). For example, the chemostratigraphy of the Cismon section (Weissert, 1989; Menegatti et al., 1998) has been widely used as a standard reference curve for Barremian—Aptian correlation (Erba et al., 1999; Godet et al., 2006; Millán et al., 2009; Huck et al., 2011; Stein et al., 2012; Papp et al., 2013; Gaona-Narvaez et al., 2013a; 2013b) and is characterized by temporal subdivisions of the $\delta^{13}\text{C}_{\text{carb}}$ and $\delta^{13}\text{C}_{\text{Org}}$

values into isotopic segments labeled C1 to C8 (Menegatti et al., 1998). This widely recognized carbon isotopic subdivision as well as the standard pattern registered by the $\delta^{13}\text{C}_{\text{org}}$ and $\delta^{13}\text{C}_{\text{carb}}$ curves have been calibrated with planktonic foraminifera, nannofossils and ammonites biostratigraphy at other Tethyan sections (Menegatti et al., 1998; Moullade et al., 1998; Kuhnt et al., 1998; Erba et al., 1999; De Gea et al., 2003; Erba, 2004; Weissert and Erba, 2004; Godet et al., 2006; Najarro et al., 2010; Stein et al., 2011, 2012; Papp et al., 2013) and is used here to assess temporal correlation at El Pui (Fig. 4-11). In general there is good agreement with the use of microfossils between different sites, although discrepancies may occur with exclusive use of larger taxa such as ammonite (Reboulet et al., 2006; Millán et al., 2009; Moreno-Bedmar, 2010; Reboulet et al., 2012).

At El Pui, in the lowermost part of the section $\delta^{13}\text{C}_{\text{org}}$ values fluctuate following an overall positive trend that reaches a peak of -22.6‰, at ~14.3m (Fig. 4-7D, Fig. 4-11F). The peak is followed by a negative excursion to a value of ~-24.5‰ at ~15.5 m. A very similar trend and values are also identified at the lower part of La Bédoule section (Fig. 4-11B) where it corresponds to the upper level of segment C1. Comparatively, the same pattern is observed in the Cismon section (Fig. 4-11A) where the upper part of segment C1 falls within the latest Barremian correlative with the lower part of the *G. blowi* Zone, and is marked by a positive progression that ends in a peak, followed by a negative trend that defines the limit of C1 and the onset of C2. In the Pădurea Craiului section this transition is less pronounced but shows a very similar shape (Fig. 4-11C). However, at the Igaratza section (Fig. 4-11D) the same pattern was identified in the earliest Aptian, whereas in the reconstruction of geological events from Erba (2004) (Fig.

4-11E) the C1-C2 limit is also located within the late Barremian. Also, in the reference Cismon section segment C2 overlaps the Barremian-Aptian boundary, which is situated in the *G. blowi* Zone and correlates with a negative excursion in $\delta^{13}\text{C}_{\text{carb}}$ preceding the spike followed by declining $\delta^{13}\text{C}$ values harbinger to the sharp negative excursion associated with segment C3 (Menegatti et al., 1998; Erba et al., 1999; Erba, 2004). The boundary correlates with the base of magnetic polarity Chron MO (Channell and Erba, 1992; Erba et al., 1999; Channell et al., 2000; Erba, 2004). El Pui, being part of the Cabó Marls, comprising ~800 m of sediments in ~5 Ma, is an expanded section (Seguret, 1972; Peybernès, 1976; Berástegui et al., 1990; García-Senz, 2002), thus the C2 segment interval is more developed than in the Cismon reference section (Fig. 4-7D), and the position of the comparable inflection point in the $\delta^{13}\text{C}_{\text{org}}$ curve within the *G. blowi* Zone is at 15.5 m (Figs. 7D, 11F). Similarly to the reference section the approximate level of the Barremian- Aptian boundary is placed at that level. Such assignment considers the fact that the inflection that defines the time boundary is followed by a positive recovery (Fig. 4-11A, E). The subsequent decrease of $\delta^{13}\text{C}$ values throughout the C2 interval up to the sudden drop is widely accepted to correlate with segment C3. The El Pui section provides an amplified vertical record of segment C2 similar to the Cassis-La Bédoule section, in contrast with the Cismon section, which is a more condensed sequence (Fig. 4-11A, B, F).

The C3 segment also occurs in the early Aptian within the *G. blowi* Zone (e.g. Erba, 1994; Menegatti et al 1998, Moullade et al., 1998; Najarro et al., 2010; Gaona-Narvaez et al, 2013a; 2013b) and its initiation is defined by a pronounced negative excursion in $\delta^{13}\text{C}$ of ~2‰ followed by a less pronounced positive recovery (Fig. 4-11A,

C, D, E). The same pattern is also identified at El Pui at about 70 m from the base of the section (Figs. 4-7D, Fig. 4-11F) and within the *G. blowi* Zone.

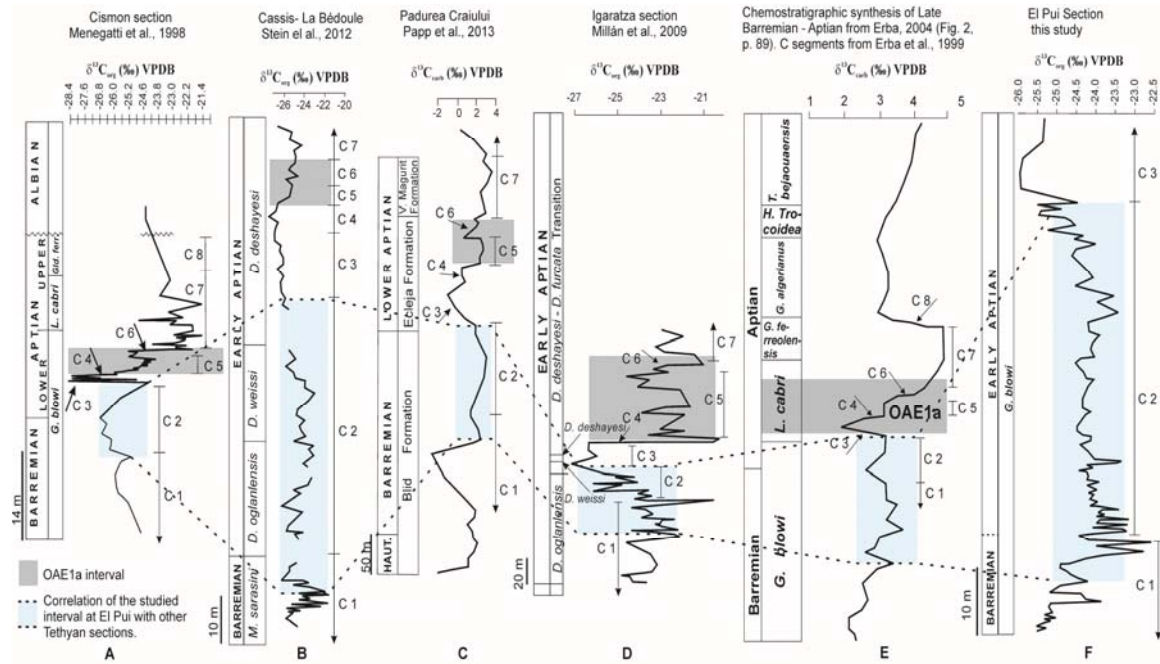


Figure 4-11 Geochemical correlation of $\delta^{13}\text{C}$ for several Tethys sections: A) Cison (Menegatti et al., 1998); B) Cassis-La Bédoule (Stein et al., 2012); C) Pădurea Craiului (Papp et al., 2013); D) Igaratza (Millán et al., 2009); E) chemostratigraphic synthesis of the late Barremian - Aptian from Erba (2004); and F) El Pui, this study. The light blue areas indicate intervals of correlation. Gray shaded rectangles correspond to the interval of OAE1a. The approximate Barremian-Aptian boundary at El Pui is proposed based on geochemical correlation with calibrated sections. C1- C8 segments represent trends in the $\delta^{13}\text{C}_{\text{carb}}$ and $\delta^{13}\text{C}_{\text{org}}$ defined by Menegatti et al. (1998).

The level assigned to the Barremian–Aptian transition zone is in agreement with previous paleontological studies of ammonites and benthic and planktonic foraminifera for the Organyà Basin as follows: 1) Peybernès (1976) and Martínez (1982 a) identified the *Deshayesites forbesi* ammonite zone corresponding to the lower Aptian in the lower part of the Cabó Marls at about 20 m from the top of the Prada Formation (García-Senz, 2002) (Fig. 4-2A), while Bernaus (1995) identified the *G. blowi* Zone at the same level. This stratigraphic position indicated that the base of the Cabó Marls can be confined to the uppermost Barremian–earliest Aptian interval with a time boundary located within

the first 20 m. 2) Recent ammonite biostratigraphic analysis of the Cabó Marls (Moreno-Bedmar, 2010, his Fig. 4-22) identified ammonites of the *Imerites giraudi* Zone belonging to the uppermost Barremian in the lower part of the Cabó Marls. Ammonite taxa identified further up-section reveal assemblages that he referred to the *Deshayesites oglanlensis* Zone, or the first ammonite zone of the lower Aptian. Nonetheless, the distribution of ammonites in the section and their variable preservation did not allow for an exact definition of the Barremian–Aptian boundary, which was presumed to lie within the first 15 to 20 m of the Cabó Marls, and therefore is compatible with our proposed assigned transition zone at approximately 15.5 m.

OAE1a has been reported to occur in the uppermost part of the *G. blowi* and/or within the superjacent *L. cabri* Zone for most Tethyan sections (Erba, 1994; Bellanca et al., 2002; Erba, 2004; Föllmi et al., 2006; Coccioni et al., 2006; Castro et al., 2006), but at El Pui *L. cabri* does not occur in the lower part of the section, its first occurrence is reported at more than 200 m from the base (Schwenke, 1993; Bernaus, 1995). Therefore, the published biochronologic data concur with the present results, which suggest that the occurrence of the event should be about 115 m higher up section. This is compatible with the carbon isotope stratigraphy yielding a positive excursion no greater than 2‰, while OAE1a elsewhere is characterized by a spike of about 4‰ (Erba, 1994; Jenkyns, 1995; Föllmi, 1996; Menegatti et al., 1998; Immenhauser et al., 2005). Thus, the geochemical and paleontological data in the studied 85 m of the El Pui section concur with our assignment of carbon isotope segments C1 to lower part of C3, which occur prior to the onset of OAE1a as described in Menegatti et al. (1998).

4.5.2 Role of basin physiography on nutrient-driven productivity

Enhanced nutrient delivery to the ocean due to intensified runoff in the latest Barremian–early Aptian has been proposed as the cause for increased biological productivity that led to the burial of sediments highly enriched in organic matter (Weissert, 1989; Erba, 1994; Bralower et al., 1994). Global forcing mechanisms related to climates are well recognized as causal factors for wide-scale intensified continental runoff (Dunham et al., 1988; Bralower et al., 1994; Erba, 1994; Föllmi, 1996), but adequate local physiographic conditions can also produce environments that independently replicate similar effects at a regional scale (e.g. Bréhéret, 1988; Föllmi et al., 1994; Papp et al., 2013). Nutrient fluxes from land to epicontinental seas and restricted marine environments may be further enhanced by physiographic conditions and adjacent landmasses (Ponton and Maurrasse, 2006; Föllmi et al., 2012; Föllmi, 2012).

Based on average TOC values of 0.99% in shales from the continental shelf and slope, and 0.33% for carbonates (Durand, 1980), black, TOC-rich (up to 1.74% for this study), hemipelagic facies of the El Pui section suggest enhanced carbon preservation during the late Barremian-early Aptian interval. Moreover, the lowest 31 m of the section shows pronounced positive excursions (up to $\sim 2.00\text{‰}$) in $\delta^{13}\text{C}_{\text{org}}$ that coincide with values of TOC > 1.0% (Fig. 4-7B, D) thus indicating a direct relationship between increased primary productivity and organic carbon sequestration. Similar relationships have been described in several coeval sections from the western Tethys, notably: Cassis-La Bédoule (Stein et al., 2012), Cismon (Menegatti et al., 1998), Igaratza section (Millán et al., 2009), Gorgo a Cerbara (Stein et al., 2011). In agreement with previous evidence indicative of continental runoff provided elsewhere (Brumsack, 2006), the temporal

variation of Al, Si and Ti in the El Pui section allows us to assess the role of continental runoff in productivity. As shown in Fig. 4-9 (C, D) positive correlation of biolimiting elements (P, Fe) with Al implies a direct relationship between OM production in the Organyà Basin and sustained nutrient input from fluvial fluxes.

In the studied section, P is consistently enriched with respect to the average shale (Fig. 4-8). Long-term effects of phosphorus in the global cycle are tectonically driven through time as the terrestrial input to the ocean originates essentially from the weathering of rocks and minerals, particularly apatite [$\text{Ca}_5(\text{PO}_4)_3\text{OH}$] that undergoes carbonation (Föllmi, 1996; Filippelli, 2002). Phosphorous enrichment in sediments is thus interpreted as the result of high nutrient levels in the ocean (Föllmi, 1995; Bodin et al., 2006; Stein et al., 2012). Based on the paleophysiography of the area (Peybernès, 1976; Ábalos et al., 2002; García-Senz, 2002, Masse et al., 2000) we may postulate that enhanced transport of phosphorus to the Organyà Basin from river fluxes not only derived from the result of weathering due to prevailing warm humid conditions (Barron, 1989; Föllmi, 1996), but also because of intensive fresh water collection and rapid down-slope delivery intensified by elevation differences and low permeability of the eroding adjacent Paleozoic crystalline rocks uplifted during the Variscan (Hercynian) Orogeny (Peybernès, 1976; Muñoz et al., 1984; Berástegui et al., 1990; García-Senz, 2002).

Iron is an important biolimiting element in the ocean, as demonstrated for regions far from continental margins as well as deep ocean upwelling areas (Martin, 1992, Jickells et al., 2005). Iron concentration in the El Pui sediments shows an average fluctuation of 70-95% of that of the average shale (Fig. 4-8). Since the lithology at El Pui is predominately calcareous (average TIC > 50%), such concentration of Fe (~3 to 22 ppt,

average ~ 7.7 ppt; Appendix 2) indicates that sufficient Fe was supplied to the basin to support enhanced primary productivity. In Fig. 4-8, Fe covaries with P, thus indicating a commonality of source and transport mechanism for both.

Positive linear correlation of the biolimiting elements with aluminum (Fig. 4-9C, D) supports their steady supply from terrigenous fluxes, thus indicating that sustained surface productivity in the Organyà Basin must have essentially depended on continental runoff. Such condition would be similar to the modern Black Sea that may be taken (to a lesser extent) as a present analog (e.g. Giosan et al., 2012) where ample flux of lighter-density freshwater induces water column stratification that prevents mixing and recycling of bottom nutrients. Unlike normal open ocean conditions characterized by major upward recycling of nutrients that maintains productivity, limited recycling in the Organyà Basin implies that sustained OM productivity occurred in a system such that P gained from surface waters sufficiently balanced losses by export production and burial in the sediment. Furthermore, because P/Al and Fe/Al show moderate covariation with high TOC, the values suggest the existence of enrichment pathways for P different from its biotic incorporation in the sediment.

In fact, covariation between Al-normalized Ti, Si, P and Fe (Fig. 4-8) suggests that an appreciable amount of phosphate may have been adsorbed to particulate inorganic phosphorus or Fe-Mn oxide/oxyhydroxide particles from chemically weathered-phosphorus in river fluxes (Compton et al., 2000). Therefore, we infer that P is not only buried as constituent of organic matter, but it is also present as P-adsorbed to riverine abiotic particulate matters, which may account for its relatively higher enrichment factor compared to Fe. Because that time interval of the early Aptian coincides with the onset of

pronounced oceanic magmatic episodes of the Ontong Java Large Igneous Provinces in the Pacific (Neal et al., 1997; 2008), arguably P scavenging on such particles might have also been related to their abundance from hydrothermal activities, and enhanced productivity (Stinton and Duncan, 1997; Tejada et al., 2009). However, since this interval also coincides with the time of fastest episode of counterclockwise rotation of Iberia with respect to Eurasia (Gong et al., 2009), closest proximity of the Organyà Basin to magmatic effusion related to this tectonic phase may have had more influence on its sedimentation based on the limited circulation pattern that we can infer from paleogeographic reconstruction (Masse et al., 2000).

In summary, the combined effects of sustained riverine P and Fe fluxes, enhanced by basin physiography, may be invoked as causal factors for enduring productivity conducive to eutrophication of the surface waters and accelerated OM flux to the sediment in the restricted Organyà Basin. The prevalence of calcareous nannofossils in the matrix (Fig. 4-4: C10-19, C10-30, C11-87) certainly proves that they contributed to significant OM generation. Nevertheless, high uncommon abundance of these primary producers cannot be considered solely as the cause of high TOC (up to 1.74%), because the OM/CaCO₃ burial ratio of these organisms is too low (1/6, Hay, 2002), therefore the dilution effect will considerably decrease the OC content. Since microbial mats and cyanobacterial blooms have been documented to thrive under similar paleoenvironments (Bralower et al., 2002; Duque-Botero and Maurrasse, 2005), such organisms (including non-calcifying bacteria) may have also been important contributors to the OM production in the Organyà Basin. In fact, microstructures found in the studied samples (Fig. 4-4: C10-50, C11-87) are comparable to cyanobacterial structures described elsewhere

(Tribovillard, 1998; Duque-Botero and Maurrasse, 2005; 2008), thereby confirming bacterial contribution to the OC content of El Pui sediments.

4.5.3 Redox conditions

Alternating levels of TOC > 1.0% in the lowest 31m of the section denotes the existence of a mechanism that limited OM oxidation. It is also conceivable that the TOC values may have been mitigated by abundant supply of CaCO₃ (TIC > 50%) from calcareous nanofossils mixed with terrestrial material from fluvial fluxes. The scarcity of benthic fauna throughout this interval concurrent with a bioturbation index < 3 implies intermittent poorly oxygenated bottom waters (Wignall and Myers, 1988). Since variations of Al, Si and Ti indicate continental runoff as a major factor in productivity, import of terrestrial OM to the basin could have been significant. Nonetheless, given the large negative fractionation of organically-derived carbon compounds from terrestrial environments (Dean et al., 1986; Meyers, 1997), an increase in recycled respired (¹³C depleted) CO₂ would have greatly depleted the isotopic composition of the TOC in the El Pui sediments, and caused a notable negative shift of the $\delta^{13}\text{C}_{\text{org}}$. On the contrary, as shown in Fig. 4-7 (D), $\delta^{13}\text{C}_{\text{org}}$ follows an increasing trend within the lowest 15 m and remains stable with punctuated excursions up to about 31 m. Pronounced positive excursions in $\delta^{13}\text{C}_{\text{org}}$ coincide with levels high in TOC suggesting heightened ¹²C removal due to pulses in primary productivity (Fig. 4-7B, D). In addition, preliminary biomarker analysis has indicated autochthonous origin of the OM (Sanchez-Hernandez and Maurrasse, 2012a; 2012b).

4.5.3.1 Oxygen levels based on morphology and abundance of benthic foraminifera

Benthic foraminiferal assemblages have been extensively used to document variations in oxygen levels (Wignall and Myers, 1988; Moodley and Hess, 1992; Loubere, 1996; Bernhard and Bowser, 1999; Patterson et al., 2000). Morphologic changes, size and wall thickness, as well as variations in diversity and abundance of benthic foraminifera can be used to reliably describe oxygen concentration below 2 ml/l (Murray, 2001), which may be correlated to the classification of oxygen level shown in Fig. 4-10.

Sediments from the El Pui section include scarce to rare benthic foraminifera, most specimens show sizes less than 100 μm , and at some levels less than 80 μm (particularly in the lower 31 m). Diversity is very low throughout, with < 4 species found at the same level. These characteristics attest to existent stressful bottom conditions (Murray, 2001) that prevented benthic foraminifera from effective colonization of the sea floor. Limiting conditions do not appear to be related to availability of food because TOC values are consistently > 0.5% at most levels. In fact, all benthic taxa disappear between 12 and 13 m where TOC values reach a maximum of 1.74%, and recur as few uniserial and rare coiled morphotypes in superjacent levels. Such effects in abundance, diversity and morphology of benthic foraminifera in active populations are characteristic of environments with limited oxygen concentration (Fig. 4-10) (Wignall and Myers 1988; Jorissen et al., 1995; Bernhard and Sen Gupta 1999; Levin et al., 2001).

Concurrence of high TOC values with absence of benthic foraminifera may have been related to intensify export of OM to the sediment and increased oxidation rate within the water column that produced oxygen depletion. The fact that the interval of 12

to 13 m is solely where benthic foraminifera abundance was extremely low indicates that strong oxygen deficiency was short termed and not recurrent in the studied 85 m. From 31 m to 85 m, benthic foraminifera abundance remains less than 15/10 cm², but slightly higher than within the lower interval and with a broader size range.

The occurrence pattern of benthic foraminifera in the lowest 31m of the section is compatible with recurrent dysoxic to suboxic conditions (Fig. 4-10) with possibly oxic stages, whereas in the upper 54 m their abundance suggests more oxygenic conditions with uncommon (if present) weak dysoxic facies (Wignall and Myers, 1988; Tyson and Pearson, 1991, Murray, 2001). Their presence also indicates that anoxic conditions or euxinia (Meyer and Kump, 2008) did not develop in the basin during the studied period.

4.5.3.2 Redox sensitive trace elements (RSTE) and oxygen levels

Studies of modern organic-rich oxygen-depleted marine environments have established the relationship between higher concentrations of certain RSTEs (e.g., U, Mo, Cd, Zn, V, Cu, Co, Ni, and Cr) and reducing states in ocean basins (Berner, 1974; Emerson et al., 1983; Pohl and Hennings, 1999; Kremling, 1983; Wijsman et al., 2001; Anderson and Raiswell, 2004; Brumsack, 2006; Dellwig et al., 2010), thereby providing a firm foundation to interpret paleoredox conditions in ancient sediments.

Hence, RSTEs have been applied to infer paleoredox states in organic-rich deposits associated with oxygen-depleted environments on a variety of time scales (Tuttle et al., 1983; Brumsack, 1989; Arthur et al., 1990; Hatch and Leventhal, 1992; Calvert and Pedersen, 1993; Jones and Manning, 1994; Aksu et al., 1995; Calvert et al., 1996; Nijenhuis et al., 1999; Rimmer, 2004; Rimmer et al., 2004; Algeo and Maynard, 2004; Doveton and Merriam, 2004; Schultz, 2004; Tribovillard et al., 2005; Tribovillard et al.,

2006; Bodin et al., 2006; März et al., 2008; Algeo and Tribovillard, 2009; Hetzel et al., 2009; Sliwinski et al., 2011; Xiong et al., 2012; among others).

The El Pui sediments show a fluctuating abundance of benthic foraminifera and bioturbation index < 3.0 (Fig. 4-2B) that suggest recurrent oxygen-depleted conditions with short-termed re-oxygenation episodes (Rhoads and Morse, 1971; Wignall and Myers, 1988; Tyson and Pearson, 1991). Oxygen-depleted environments favor the fixation of trace elements in the sediment, especially in the presence of strong microbial activity that can use RSTEs in their metabolic pathways (e.g. Anderson et al., 1989, Calvert and Pedersen, 1993). Microbial organisms also contribute to the amount of particulate and dissolved OM in the water column leading to higher oxygen consumption and greater availability of organic compounds for the synthesis of organo-metallic ligands (Anderson et al., 1989; Patterson et al., 1995). Furthermore, in undisturbed reducing sediments trace metals can be strongly fixed into sulfidic minerals (Huerta-Diaz and Morse). However, if re-oxygenation of the bottom waters takes place (enhanced circulation and/or less OM productivity) organic compounds and authigenic minerals can be reoxidized resulting in the release of trace metals (Khalid, et al., 1978; Petersen et al., 1995; Tribovillard et al., 2006). In consequence, the reliability of RSTEs as a redox proxy is more consistent in environments with long-lasting, strong reducing conditions (anoxic/euxinic) and less predictable in intermediate phases of oxygen deficiency (Algeo and Maynard, 2004; Rimmer et al., 2004; Tribovillard et al., 2006; Algeo and Maynard, 2008).

Because RSTEs show significantly less enrichment in weak reducing sedimentary facies with respect to the average shale when compared to anoxic/euxinic environments

(Wedepohl, 1971, Algeo and Maynard, 2004; Tribovillard et al., 2005; Tribovillard et al., 2006), their application in this work together with the redox indices (Ni/Co and U/Th) is coupled with the benthic foraminifera proxy to more reliably address paleoredox depositional environments in the studied sequence. In fact, the application of these proxies at El Pui suggest the absence of a strong development of a sulfidic phase that would have restricted the formation of insoluble sulfidic minerals resulting in limited enrichment of RSTEs.

The Lower 31 m

At El Pui, Ni/Al, Cr/Al and U/Al values fluctuate in the lowest 31 m with constant minor enrichment (Fig. 4-8), a pattern which can be interpreted as indicative of a prolonged phase of recurring limited reducing conditions (Fig. 4-8). These ratios are compatible with the morphology and scarcity of benthic foraminifera throughout that interval, which also suggest pervasive occurrence of intermittent oxygen-deprived episodes, but no anoxia (Rhoads and Morse, 1971; Wignall and Myers, 1988; Tyson and Pearson, 1991). However, the poor correlation of Ni and U with Al (Fig. 4-9E, H) indicates that their presence in the sediment may be associated with a mechanism different from exclusive terrestrial fluxes, instead they could be related to minor sulfides, as corroborated by the presence of dispersive pyrite (Fig. 4-4, C10-48; C11-87). By contrast, V/Al is slightly depleted with respect to the average shale, and its excellent correlation with Al (Fig. 4-9G) thus reveals its terrigenous origin in the sediment.

Perhaps, the difference in the mechanism of absorption of V and Ni under reducing conditions could also be invoked to explain the contrast between low V and relatively high enrichment of Ni within the lowest 31 m of the studied section (Fig. 4-8).

Indeed, under weak reducing conditions and chemical availability of both Ni^{2+} and VO^{2+} , the Vanadyl species may be partially blocked by sulfide complexation (Lewan, 1984; Killops and Killops, 2005) resulting in enhanced absorption of Ni. Therefore, a relatively higher enrichment of Ni with respect to the average shale within the lowest 31 m at El Pui (Fig. 4-8, Appendix 2) could be consistent with Ni absorption into organic compounds under a weak reducing state (Morse and Luther, 1999; Algeo and Maynard, 2004), whereas V depletion within the sequence further confirms that strong reducing phases did not develop within that time interval of the studied section (Breit and Wanty, 1991; Lipinski et al., 2003).

As shown in Fig. 4-7 (B, D) short-duration spikes of $\delta^{13}\text{C}_{\text{org}}$ synchronous with high TOC at 4.7 m, 8.0 m, 13.0 m, 14.3 m, 16.4 m, 17.4 m, 18.2 m, and 19.7 m, also correlate with predominance of calcareous nannofossils in the matrix (Fig. 4-4). These productivity pulses may have induced enhanced Ni intake by plankton and its fixation with OM, hence subsequent incorporation to the sediment (Tribovillard et al., 2006; Akinlua et al., 2010). Nonetheless, the presence of framboidal pyrite with sizes between 5 and 10 μm (Fig. 4-4, C10-19, C10-48, C11-87), supports some degree of Ni incorporation in sulfides, as Wilkin et al. (1996, 1997) suggested that this size range is indicative of a reducing sediment-water interface. In the case of El Pui such conditions may have developed few centimeters below the sediment water interface because the presence of benthic fauna rules out full-scale anoxia. Thus, besides the potential of Ni incorporation in organo-metallic compounds, the presence of pyrite within the lower 31 m of the sequence may account in part for Ni retention in the sediment as insoluble sulfides (Huerta-Diaz and Morse, 1992).

As shown in Fig. 4-8, the lower 31 m interval includes two small spikes in U/Al and U/Th at 13.7 and 26.1 m, which are further compatible with a weak reducing environment (Dypvik and Harris, 2001). Such values of U concentration may be related to incorporation in the sediment by organisms and/or complexation with OM (Anderson et al., 1989). Its limited enrichment, however, may imply that some loss of U may have taken place due to remobilization related to short oxygenic phases in the basin (Morford and Emerson, 1999; Morford et al. 2001, Tribovillard et al., 2006).

Regarding the small relative enrichment of Cr in the lower 31 m, since a combination of high TOC content and terrigenous elements is characteristic of that interval both factors could also account for such Cr/Al values (Algeo and Maynard, 2004; Tribovillard et al., 2006). Because its enrichment is attenuated with respect to that of Ni, the Cr values can be interpreted as the result of limited incorporation of Cr into the pyrite structure (Huerta-Diaz and Morse, 1992) (Fig. 4-8).

The Upper 54m

The upper 54 m of the studied section includes TOC values that remain below 1%, and the $\delta^{13}\text{C}_{\text{org}}$ follows an overall negative progression (Fig. 4-7D, Fig. 4-11F) suggesting remineralization and incorporation of recycled ^{12}C to the reservoir because of OM oxidation. This trend concurs with low level of enrichment of Ni, Cr, and U that simultaneously decreases (in some cases depleted), with less variability than their record in the lower interval (Fig. 4-8). The Ni/Co ratio shows extreme fluctuation between the oxic and dysoxic region from 40 to 50 m, with most of the values in the uppermost 35 m of the section falling into the oxic zone albeit a small digression between 65 and 70 m (Fig. 4-8). Because of the extreme abundance of nanofossils, and the lack of pyrite

throughout the upper 54 m, the spikes in the Ni/Co ratios suggest some degree of Ni retention in the structure of calcareous nannofossil (Calvert and Pedersen, 1993; Whitfield, 2002) rather than any redox mechanism as proposed for the lower 31 m of the section. A similar process may be invoked for the small U/Al and U/Th peaks recorded at 42 m.

4.6 Conclusions

The high-resolution study of the El Pui section in the restricted Organyà Basin, south-central Spanish Pyrenees, reveals that the $\delta^{13}\text{C}_{\text{org}}$ values concur with the $\delta^{13}\text{C}$ signature of the late Barremian carbon record elsewhere in the Tethys Ocean. Chemostratigraphic correlation with other Tethyan sections allowed the identification of the C1-C2 and C2-C3 segments boundary resulting in a more accurate temporal constraint of C2, which falls within the *G. blowi* Zone, thus consistent with a late Barremian-early Aptian age range of the studied section.

$\delta^{13}\text{C}_{\text{org}}$ positive excursions (up to $\sim 2.00\%$) in the lower 31 m coincide with TOC $> 1.0\%$, thus showing a direct relationship between intensified primary productivity and organic carbon preservation. In addition, relative enrichment of P (up to ~ 2.8 times) and Fe (70 - 95%) with respect to the average shale confirms sustained availability of these biolimiting nutrients to support enhanced primary productivity. Positive linear correlation between P and Fe with Al points to continental runoff as the source of nutrients to the basin. The lack of good correlation between P and TOC suggests that productivity in the Organyà Basin may have depended essentially on terrigenous fluxes with very limited upward recycling of P. Paleogeographic reconstruction of the restricted basin combined with existing climatic conditions also support the results that suggest that punctuated low

oxygen conditions are related to intensified OM oxidation in the water column and limited ventilation of bottom waters due to possible density stratification.

Ni/Al values (up to 5.4 times the average shale), and concurrent minor relative enrichment of U and Cr within the lower 31 m indicate incorporation of these elements to the sediments through complexation with OM, and limited bacterially mediated sulfidization. Persistently high Ni/Co values (>7) and low abundance of benthic ($<10/10\text{ cm}^2$) foraminifera support the occurrence of a weak dysoxic phase within the same interval, whereas depletion of V and low U/Th values suggest that anoxia/euxinia did not develop in the basin.

The upper 54 m shows more stable TOC values ($< 1.0\%$), the $\delta^{13}\text{C}_{\text{org}}$ follows and overall negative progression characteristic of carbon isotope segment C2. The pattern suggests remineralization and incorporation of recycled ^{12}C to the reservoir because of OM oxidation and increased level of water column ventilation. Decreased enrichment of Ni, Cr and U, lower Ni/Co ratios and slightly more abundant benthic foraminifera are further indication that oxygen levels increased in the basin.

This study highlights the effects of physiographic conditions in marine restricted basins where sustained nutrient input coupled with enhanced primary productivity leads to higher oxygen consumption in the water column and oxygen-deficient facies, thereby making these regional basins important organic carbon sinks aside from major worldwide forcing mechanisms.

4.7 Acknowledgments

This research benefited from various sources of support, and mainly from the Glenn Goodfriend Memorial Funds. We gratefully acknowledge the invaluable help provided by Diane Pirie and Thomas Beasley with the instruments used at the department facilities. We thank our colleague Josep Moreno-Bedmar for valuable logistical help and discussion about the biochronology of the section, which is presented in another joint paper. We are most grateful to Mr. Ferran who graciously allowed us to work on his private hunting property. Supplies and other laboratory materials were generously provided by the Earth and Environment Department at FIU. We are most grateful also to Bill Anderson and Carrie Rebenack for the carbon isotope analyses, and the FIU Forensic Center, specially Tatiana Trejos and Sarah Jantzy, for their assistance with trace element analyses. Yosmel Sanchez gratefully acknowledges the DEA fellowship from the FIU Graduate School that provided valuable time to do field work and process the samples. We also thank two anonymous reviewers for insightful comments that have significantly improved our manuscript, and Dr. Laurel Collins for inputs on the initial manuscript.

4.8 References

- Ábalos, B., Carreras, J., Druguet, E., Escuder-Viruete, J., Gómez-Pugnaire, M.T., Lorenzo-Alvarez, S., Quesada, C., Rodríguez-Fernández, L.R., Gil-Ibarguchi, J.I., 2002. Variscan and pre-Variscan Tectonics. In: Gibbons, W., and Moreno, M.T. (Eds.), *The Geology of Spain*. Geological Society, London, pp. 155–183.
- Aguado, R., Castro, J.M., Company, M., de Gea, G.A., 1999. Aptian bio-events and integrated biostratigraphic analysis of the Almadich Formation, Inner Prebetic Domain, SE Spain. *Cretaceous Research* 20, 663–683.
- Akinlua, A., Adekola, S.A., Swakamisa, O., Fadipe, O.A., Akinyemi, S.A., 2010. Trace element characterization of Cretaceous Orange Basin hydrocarbon source rocks. *Applied Geochemistry* 25, 1587–1595.
- Aksu, A.E., Yasar, D., Mudie, P.J. 1995. Paleoclimatic and paleoceanographic conditions leading to development of sapropel layer S1 in the Aegean Sea. *Palaeogeography, Palaeoclimatology, Palaeoecology* 116, 71–101.
- Algeo, T.J., Maynard J. B., 2004. Trace element behavior and redox facies in core shales of Upper Pennsylvanian Kansas-type cyclothems, *Chemical Geology* 206, 289–318.
- Algeo, T.J., Maynard J. B., 2008. Trace-metal covariation as a guide to water-mass conditions in ancient anoxic marine environments. *Geosphere* 4 (5), 872–887.
- Algeo, T.J., & Tribovillard, N. (2009). Environmental analysis of paleoceanographic systems based on molybdenum–uranium covariation. *Chemical Geology* 268 (3), 211–225.
- Algeo T.J., Rowe H., 2012. Paleoceanographic applications of trace-metal concentration data. *Chemical Geology* 324–325, 6–18.
- Anderson, R.F., Fleisher, M.Q., Le Huray, A.P., 1989. Concentration, oxidation state and particulate flux of uranium in the Black Sea. *Geochimica et Cosmochimica Acta* 53, 2215–2224.
- Anderson, T.F., Raiswell, R. 2004. Sources and mechanisms for the enrichment of highly reactive iron in euxinic Black Sea sediments. *American Journal of Science* 304, 203–233.
- Ando, A., Kaiho, K., Kawahata, H., Kakegawa, T., 2008. Timing and magnitude of early Aptian extreme warming: Unraveling primary $\delta^{18}\text{O}$ variation in indurated pelagic carbonates at Deep Sea Drilling Project Site 463, central Pacific Ocean: *Palaeogeography Palaeoclimatology Palaeoecology* 260, 463–476.

- Arroyo, L., Trejos, T., Gardinalli, P.R., Almirall, J.R., 2009. Optimization and validation of a Laser Ablation Inductively Coupled Plasma Mass Spectrometry method for the routine analysis of soils and sediments. *Spectrochimica Acta Part B* 64, 16–25.
- Arthur, M., Premoli Silva, I., 1982. Development of widespread organic carbon-rich strata in the Mediterranean Tethys, in Schlanger, S.O. and Cita, M.B., (Eds.) *Nature and origin of Cretaceous carbon-rich facies*: London, Academic Press Inc. pp. 7–54.
- Arthur, M.A., Dean, W.E., Schlanger, S.O., 1985. Variations in the global carbon cycle during the Cretaceous related to climate, volcanism, and changes in atmospheric CO₂: In Sundquist, E.T., and Broecker, W.S. (Eds.), *The Carbon Cycle and Atmospheric CO₂: Natural Variations Archean to Present*, Geophysical Monographs, American Geophysical Union 32, 504–529.
- Arthur, M.A., Brumsack, H.-L., Jenkins, H.C., Schlanger, S.O., 1990. Stratigraphy, geochemistry, and paleoceanography of organic carbon-rich Cretaceous sequences: in Ginsburg, R.N., and Beaudoin, B., (Eds.), *Cretaceous Resources, Events and Rhythms*: Kluwer Academic Publishers, pp. 75–119.
- Bachmann, M., Willems, H., 1996. High-frequency cycles in the upper Aptian carbonates of the Organyà basin, NE Spain. *Geologische Rundschau* 85(3), 586–605.
- Barragan, R., Maurrasse, F.J.-M.R., 2008. Lower Aptian (Lower Cretaceous) ammonites from the basal strata of the La Peña Formation of Nuevo León State, northeast Mexico: biostratigraphic implications. *Revista Mexicana de Ciencias Geológicas* 25 (1), 145–157.
- Barron, E.J., Hay, W.W., Thompson, S., 1989. The hydrologic cycle: A major variable during Earth history, *Palaeogeography Palaeoclimatology Palaeoecology* 75, 157–174.
- Barron, E.J., Fawcett P. J., Peterson, W.H., Pollard, D., Thompson S. L., 1995. A “simulation” of mid-Cretaceous climate, *Paleoceanography* 10, 953–962.
- Bellanca, A., Erba, E., Neri, R., Premoli Silva, I., Sprovieri, M., Tremolada, F., Verga, D. (2002). Palaeoceanographic significance of the Tethyan ‘Livello Selli’ (Early Aptian) from the Hybla Formation, northwestern Sicily: biostratigraphy and high-resolution chemostratigraphic records. *Palaeogeography Palaeoclimatology Palaeoecology* 185 (1), 175–196.
- Berástegui, X., García-Senz, J.M., Losantos, M., 1990. Tectonosedimentary evolution of the Organyà extensional basin (Central South Pyrenean Unit, Spain) during the Lower Cretaceous. *Bulletin de la Société Géologique de France* 8, VI, 2, 251–264.

- Berástegui X., Losantos M., Muñoz J.A., Puig de Fàbregas. C., 1993. Tall geològic del Pirineu central 1:200 000. Map and explanations. Servei Geològic de Catalunya, Barcelona, 58 pp.
- Bernaus, J. M. 1995. L'evolució dels foraminífers com avaluació de la plataforma carbonatada de l'Aptià de la conca d'Organyà (Lleida). MSc thesis, Universitat Autònoma de Barcelona, 99 pp.
- Bernaus, J.M., Arnaud-Vanneau, A., Caus, E., 2002. Stratigraphic distribution of Valanginian Early Aptian shallow-water benthic foraminifera and algae, and depositional sequences of a carbonate platform in a tectonically-controlled basin: the Organyà Basin, Pyrenees, Spain. *Cretaceous Research* 23, 25–36.
- Bernaus, J.M., Arnaud-Vanneau, A., Caus, E., 2003. Carbonate platform sequence stratigraphy in a rapidly subsiding area: the Late Barremian–Early Aptian of the Organyà Basin, Spanish Pyrenees. *Sedimentary Geology* 159 (3–4), 177–201.
- Berner, R.A., 1974. Iron sulfides in Pleistocene deep Black Sea sediments and their paleoceanographic significance. In: E.T. Degens and R.A. Ross (Editors), *The Black Sea-Geology, Chemistry and Biology*. Memoir No. 20. American Association of Petroleum Geologists, Tulsa, 524–531.
- Bernhard, J.M., Bowser, S.S., 1999. Benthic foraminifera of dysoxic sediments: chloroplast sequestration and functional morphology. *Earth-Science Reviews* 46, 149–165.
- Bernhard, J.M., Sen Gupta, B.K., 1999. Foraminifera of oxygen-depleted environments. In: Sen Gupta B.K. (Ed.), *Modern Foraminifera*. Kluwer Academic Press, pp. 201–216.
- Bodin, S., Godet, A., Matera, V., Steinmann, P., Vermeulen, J., Gardin, S., Adatte, T., Coccioni, R., Föllmi, K.B., 2007. Enrichment of redox-sensitive trace metals (U, V, Mo, As) associated with the late Hauterivian Faraoni oceanic anoxic event, *International Journal of Earth Sciences (Geologisches Rundschau)* 96, 327–341.
- Bolli, H., 1959. Planktonic foraminifera from the Cretaceous of Trinidad, B.W.I. *Bulletins of American Paleontology* 39, 257–277.
- Bralower, T.J., Arthur, M.A., Leckie, R.M., Sliter, W.V., Allard, D.J., Schlanger, S.O., 1994. Timing and paleoceanography of oceanic dysoxia/anoxia in the Late Barremian to Early Aptian. *Palaios* 9, 335–369.
- Bralower, T.J., Premoli-Silva, I., Malone, M.J., 2002. New evidence for abrupt climate change in the Cretaceous and Paleogene: An Ocean Drilling Program expedition to Shatsky Rise, northwest Pacific. *GSA Today*, 12, 4–10.

- Bréhéret, J.G. 1988. Episodes de sédimentation riche en matière organique dans les marnes bleues d'age aptien et albien de la partie pélagique du bassin vocontien. *Bulletin de la Société Géologique de France* IV, 2, 349–356.
- Breit, G.N., Wanty, R.B., 1991. Vanadium accumulation in carbonaceous rocks: A review of geochemical controls during deposition and diagenesis. *Chemical Geology* 91, 83–97.
- Brumsack, H.-J., 1989. Geochemistry of recent TOC-rich sediments from the Gulf of California and the Black Sea. *Geologische Rundschau* 78, 851–882.
- Brumsack, H. J., 2006. The trace metal content of recent organic carbon-rich sediments: Implications for Cretaceous black shales formation, *Palaeogeography Palaeoclimatology Paleoecology* 232, 344–361.
- Calvert, S.E., Pedersen, T.F., 1993. Geochemistry of recent oxic and anoxic marine sediments: implications for the geological record. *Marine Geology* 113, 67–88.
- Calvert, S.E., Bustin, R.M., Ingall, E.D., 1996. Influence of water column anoxia and sediment supply in the burial and preservation of organic carbon in marine shales. *Geochimica et Cosmochimica Acta* 60, 1577–1593.
- Caron, M. 1985 Cretaceous Planktic Foraminifera. Chapter 4. In: Bolli, Saunders, and Perch-Nielsen (Eds), *Plankton Stratigraphy*. Cambridge University Press, pp. 17–86.
- Castro, J.M.; Gea, G.A. de; Quijano, M.L. 2006. Record of the oceanic anoxic event OAE1a (Lower Aptian) in a platform setting. Prebetic (Alicante province). *Geogaceta* (40), 251–254.
- Caus, E., García-Senz, J. M., Rodés, D. & Simón, A., 1990. Stratigraphy of the Lower Cretaceous (Berriasian-Barremian) sediments in the Organyà Basin, Pyrenees, Spain. *Cretaceous Research* 11, 313–320.
- Channell, J.E.T., Erba, E., 1992. Early Cretaceous polarity chrons CM0 to CM11 recorded in northern Italian land sections near Brescia, *Earth and Planetary Science Letters* 108 (4), 161–179.
- Channell, J.E.T., Erba, E., Muttoni, G., Tremolada, F., 2000. Early Cretaceous magnetic stratigraphy in the APTICORE drill core and adjacent outcrop at Cismon (Southern Alps, Italy), and the correlation to the proposed Barremian/Aptian boundary stratotype. *Geological Society of America. Bulletin*. 112, 1430–1443.
- Coccioni, R., Luciani, V., Marsili, A. (2006). Cretaceous oceanic anoxic events and radially elongated chambered planktonic foraminifera: paleoecological and paleoceanographic implications. *Palaeogeography, Palaeoclimatology, Palaeoecology* 235 (1), 66–92.

- Compton, J., Mallinson, D., Glenn, C., Filippelli, G., Föllmi, K., Shields, G., Zanin, Y. 2000 Variations in the global phosphorus cycle. In Glenn C, Prévôt-Lucas, L., Lucas, J., (Eds) SEPM Special Publications 66, Marine Authigenesis: From Microbial to Global, 21–34.
- De Gea, G.A., Castro, J.M., Aguado, R., Ruiz-Ortiz, P.A., Company, M., 2003. Lower Aptian carbon isotope stratigraphy from a distal carbonate shelf setting: the Cau section, Prebetic zone, SE Spain. *Palaeogeography, Palaeoclimatology, Palaeoecology* 200 (1–4), 207–219.
- Dean, W.E., Arthur, M. A., and Claypool, G. E., 1986. Depletion of $\delta^{13}\text{C}$ in Cretaceous marine organic matter: Source, diagenetic, or environmental signal? *Marine Geology* 70 (1), 119–157.
- Dellwig, O., Leipe, T., März, C., Glockzin, M., Pollehne, F., Schnetger, B., Yakushev, E. V., Böttcher, M. E., Brumsack, H-J., 2010. A new particulate Mn–Fe–P-shuttle at the redoxcline of anoxic basins. *Geochimica et Cosmochimica Acta* 74, 7100–7115.
- Doveton, J. H. and Merriam, D. F., 2004. Borehole petrophysical chemostratigraphy of Pennsylvanian black shales in the Kansas subsurface. *Chemical Geology* 206, 249–258
- Dunham, K.W., Meyers P.A. and Ho Eileen S., 1988. Organic geochemistry of Cretaceous black shales and adjacent strata from the Galicia Margin. North Atlantic Ocean. In: Boillot, G., Winterer, E. L., et al., *Proceedings of the Ocean Drilling Program, Scientific Results 103*: College Station, Texas (Ocean Drilling Program), 155–169.
- Dunham, R.J., 1962. Classification of carbonate rocks according to depositional texture. In: Ham W.E. (Ed), *Classification of carbonate rocks*. American Association of Petroleum Geologists Memoir 1, 108–121.
- Durand, B., 1980. Sedimentary organic matter and kerogen. Definition and quantitative importance of kerogen. In: Durand, B. (Ed), *Kerogen: insoluble matter from sedimentary rocks*. Editions Technip. Paris, 13—34.
- Duque-Botero, F., Maurrasse, F., 2005. Cyanobacterial productivity, variations in the organic carbon, and facies of the Indidura Formation (Cenomanian-Turonian), Northeastern Mexico. *Journal of Iberian Geology* 31, 85–98.
- Duque-Botero, F., Maurrasse, F., 2008. Role of cyanobacteria in Corg-rich deposits: an example from the Indidura Formation (Cenomanian–Turonian), northeastern Mexico. *Cretaceous Research* 29, 957–964.
- Dypvik, H., Harris, N.B., 2001. Geochemical facies analysis of fine-grained siliciclastics using Th/U, Zr/Rb and (Zr+Rb)/Sr ratios. *Chemical Geology* 181, 131–146.

- Emerson, S., Jacobs, L., Tebo, B., 1983. The behavior of trace metals in marine anoxic waters: Solubilities at the oxygen-hydrogen sulfide interface. In Trace metals in sea water, 579–608. Springer US.
- Erba, E., 1994. Nannofossils and superplumes: the early Aptian “nannoconid crisis”. *Paleoceanography* 9, 483–501.
- Erba, E., Channell, J.E.T., Claps, M., Jones, C., Larson, R., Opdyke, B., Premoli Silva, I., Riva, A., Salvini, G., Torricelli, S., 1999. Integrated stratigraphy of the Cismon APTICORE (Southern Alps, Italy): a “reference section” for the Barremian–Aptian interval at low latitudes. *Journal of Foraminiferal Research* 29, 371–392.
- Erba, E., 2004. Calcareous nannofossils and Mesozoic oceanic events. *Marine Micropaleontology* 52, 85–106.
- Filippelli, G.M., 2002. The global phosphorus cycle. *Reviews in Mineralogy and Geochemistry* 48 (1), 391–425.
- Folk, R.L., 1962. Spectral subdivision of limestone types. In: Ham W.E. (Ed) *Classification of Carbonate Rocks*. American Association of Petroleum Geologists Memoir 1, 62–84.
- Föllmi, K.B., 1996. The phosphorus cycle, phosphogenesis, and marine phosphate-rich deposits. *Earth-Science Reviews* 40, 55–124.
- Föllmi, K.B., 2012. Early Cretaceous life, climate and anoxia. *Cretaceous Research* 35, 230–257.
- Föllmi, K.B., Gainon, F., 2008. Demise of the northern Tethyan Urgonian carbonate platform and subsequent transition towards pelagic conditions: the sedimentary record of the Col de la Plaine Morte area, central Switzerland. *Sedimentary Geology* 205(3), 142–159.
- Föllmi, K.B., Weissert, H., Bisping, M., Funk, H., 1994. Phosphogenesis, carbon-isotope stratigraphy, and carbonate-platform evolution along the Lower Cretaceous northern tethyan margin. *Geological Society of America, Bulletin* 106, 729–746.
- Föllmi, K.B., Godet, A., Bodin, S., Linder, P., 2006. Interactions between environmental change and shallow-water carbonate build-up along the northern Tethyan margin and their impact on the early Cretaceous carbon-isotope record. *Paleoceanography* 21, 4, PA4211.
- Föllmi, K.B., Bôle, M., Jammet, N., Froidevaux, P., Godet, A., Bodin, S., Adatte, T., Mattera, V., Fleitmann, D., Spangenberg, J.E., 2012. Bridging the Faraoni and Selli oceanic anoxic events: late Hauterivian to early Aptian dysaerobic to anaerobic phases in the Tethys. *Climate of the Past* 8, 171–189.

- Gaona-Narvaez, T., Maurrasse, F.J-M.R., and Moreno-Bedmar, J. A., 2013a. Stable Carbon Isotope Stratigraphy and Ammonite Biochronology at Madotz (Navarra, N Spain): Implications for the Timing and Duration of Oxygen Depletion during OAE-1a. *Cretaceous Research* 40, 143–157.
- Gaona-Narvaez, T., Maurrasse, F.J-M.R., Etayo-Serna, F., 2013b. Geochemistry, paleoenvironments and timing of Aptian organic-rich beds of Paja Formation (Curití, Eastern Cordillera, Colombia). In: Bojar, A.V., Melinte-Dobrinescu, M.C., and Smit, J. (Eds.), *Isotopic Studies in Cretaceous Research*. Geological Society of London, Special Publications 382, 31–48.
- García-Senz, J., 2002. Cuencas extensivas del Cretácico Inferior en los Pirineos Centrales: formación y subsecuente inversión. PhD Thesis, University of Barcelona, Barcelona, 310 pp.
- Giosan, L., Coolen, M.J.L., Kaplan, J.O., Constantinescu, S., Filip, F., Filipova-Marinova, M., Kettner, A.J., Thom, N., 2012. Early anthropogenic transformation of the Danube-Black Sea system. *Scientific Reports* 2 (582), 1–6.
- Godet, A., Bodin, S., Föllmi, K., Vermeulen, J., Gardin, S., Fiet, N., Adatte, T., Berner, Z., Stüben, D., van de Schootbrugge, B., 2006. Evolution of the marine stable carbon isotope record during the Early Cretaceous: a focus on the late Hauterivian and Barremian in the Tethyan realm. *Earth and Planetary Sciences Letters* 242, 254 –271.
- Godet, A., Bodin, S., Adatte, T., Föllmi, K.B., 2008. Platform-induced clay-mineral fractionation along a northern Tethyan basin-platform transect: implications for the interpretation of Early Cretaceous climate change (Late Hauterivian-Early Aptian). *Cretaceous Research* 29, 830–847.
- Godet, A., Föllmi, K. B., Spangenberg, J. E., Bodin, S., Vermeulen, J., Adatte, T., Bonvallet, L., Arnaud, H., 2013. Deciphering the message of Early Cretaceous drowning surfaces from the Helvetic Alps: What can be learnt from platform to basin correlations? *Sedimentology* 60(1), 152–173.
- Gong, Z., van Hinsbergen, D. J.J., Vissers R. L.M., Dekkers M. J., 2009. Early Cretaceous syn-rotational extension in the Organyà Basin - New constraints on the palinspastic position of Iberia during its rotation. *Tectonophysics* 473, 312–323.
- Hay, W.W., Deconto R. M., 1999. Comparison of modern and Late Cretaceous meridional energy transport and oceanology, in *Evolution of the Cretaceous Ocean-Climate System*. In: Barrera, E., Johnson, C. C. (Eds), Geological Society of America, Special Papers 332, 283–300.
- Hay, William W., 2002. Carbonate fluxes during earth history. GEOMAR, Kiel, Germany.
http://csdms.colorado.edu/mediawiki/images/Carbonate_Fluxes_n_Earth_History.pdf

- Hayes, J. M. (1993). Factors controlling $\delta^{13}\text{C}$ contents of sedimentary organic compounds: Principles and evidence. *Marine Geology* 113(1), 111-125.
- Hatch, J.R., Leventhal, J.S., 1992. Relationship between inferred redox potential of the depositional environment and geochemistry of the Upper Pennsylvanian (Missourian) Stark Shale Member of the Dennis Limestone, Wabaunsee County, Kansas, U.S.A., *Chemical Geology* 99, 65–82.
- Hetzel, A., Böttcher, M.E., Wortmann, U.G., Brumsack, H.-J., 2009. Paleo-redox conditions during OAE 2 reflected in Demerara Rise sediment geochemistry (ODP Leg 207). *Palaeogeography Palaeoclimatology Palaeoecology* 273, 302–328.
- Huck, S., Heimhofer, U., Rameil, N., Bodin, S., Immenhauser, A., (2011). Strontium and carbon-isotope chronostratigraphy of Barremian–Aptian shoal-water carbonates: Northern Tethyan platform drowning predates OAE 1a. *Earth and Planetary Science Letters* 304(3), 547–558.
- Huerta-Diaz, M.G., Morse, J.W., 1992. Pyritization of trace metals in anoxic marine sediments. *Geochimica et Cosmochimica Acta* 56, 2681–2702.
- Immenhauser, A., Hillgärtner, H., Van Bentum, E., 2005. Microbial-foraminiferal episodes in the Early Aptian of the southern Tethyan margin: ecological significance and possible relation to oceanic anoxic event 1a. *Sedimentology* 52 (1), 77–99.
- Jahren, A. H., Arens, N. C., Sarmiento, G., Guerrero, J., & Amundson, R., 2001. Terrestrial record of methane hydrate dissociation in the Early Cretaceous. *Geology* 29(2), 159-162.
- Jenkyns, H.C., 1980. Cretaceous anoxic events: from continents to oceans. *Journal of the Geological Society of London* 137, 171–188.
- Jenkyns, H.C., 1995. Carbon-isotope stratigraphy and paleoceanographic significance of the lower Cretaceous shallow-water carbonates of resolution Guyot, Mid-Pacific Mountains. *Proceedings of the Ocean Drilling program, Scientific Results*, 143, 99–104.
- Jenkyns, H.C., 2010. Geochemistry of oceanic anoxic events, *Geochemistry, Geophysics and Geosystems* 11(3), 1525 - 2027.
- Jickells, T.D., et al., 2005. Global iron connections between desert dust, ocean biogeochemistry, and climate. *Science* 308, 67–71.
- Jones, B., Manning, D.A.C., 1994. Comparison of geochemical indices used for the interpretation of palaeoredox conditions in ancient mudstones, *Chemical Geology* 111, 111–129.

- Jorissen, F.J., De Stigter H.C., Widmark, J.G.V., 1995. A conceptual model explaining benthic foraminiferal microhabitats. *Marine Micropaleontology* 22, 3–15.
- Khalid, R.A., Patrick Jr., W. H., Gambrell, R. P., 1978. Effect of dissolved oxygen on chemical transformations of heavy metals, phosphorus, and nitrogen in an estuarine sediment. *Estuarine and Coastal Marine Science* 6, 21–35.
- Killops, S.D., Killops, V., 2005. *Introduction to Organic Geochemistry*, second ed., pp. 391. Blackwell Publishing Ltd. MA, USA.
- Kremling, K., 1983. Trace metal fronts in European shelf waters. *Nature* 303, 225–227
- Kuhnt, W., Moullade, M., Masse, J.-P., Erlenkeuser, H., 1998. Carbon-isotope stratigraphy of the lower Aptian historical stratotype at Cassis-La Bédoule (SE France). *Géologie Méditerranéenne* 25 (3–4), 63–79.
- Larson, R.L., Erba, E., 1999. Onset of the mid-Cretaceous greenhouse in the Barremian - Aptian: igneous events and the biological, sedimentary, and geochemical responses. *Paleoceanography* 14, 663–678.
- Leckie, R.M., Bralower, T.J., Cashman, R., 2002. Oceanic anoxic events and plankton evolution: biotic response to tectonic forcing during the mid-Cretaceous. *Paleoceanography*, 17 (3), 1–29.
- Levin, L.A., Etter, R.J., Rex, M.A., Gooday, A.J., Smith, C.R., Pineda, J., Stuart, C.T., Hessler, R.R., Pawson, D., 2001. Environmental influences on regional deep-sea species diversity. *Annual Review of Ecology and Systematics* 132, 51–93.
- Lewan, M.D., 1984. Factors controlling the proportionality of vanadium to nickel in crude oils. *Geochimica et Cosmochimica Acta* 48, 2231–2238.
- Li, Y. X., Bralower, T. J., Montañez, I.P., Osleger, D.A., Arthur, M.A., Bice, D.M., Herbert, T.D., Erba, E., and Premoli Silva, I., 2008, Toward an orbital chronology for the early Aptian Oceanic Anoxic Event (OAE1a, ~120 Ma): *Earth and Planetary Science Letters* 271, 88–100.
- Lipinski, M., Warning, B., Brumsack, H.-J., 2003: Chemistry of Jurassic/Cretaceous black shales. Trace metal signatures of Jurassic/Cretaceous black shales from the Norwegian shelf and the Barents Sea. *Palaeogeography Palaeoclimatology Palaeoecology* 190, 459–475.
- Loubere, P., 1996. The surface ocean productivity and bottom water oxygen signals in deep water benthic foraminiferal assemblages. *Marine Micropaleontology* 28, 247–261.
- Martin, J.H., 1992. Iron as a limiting factor in oceanic productivity (Vol. 137). Plenum Press, New York.

- Martínez, R., 1982. Ammonoideos cretácicos del Prepirineo de la provincia de Lleida. PhD thesis, publicaciones de la Universitat Autònoma de Barcelona, 17, pp. 197.
- März, C., Poulton, S.W., Beckmann, B., Küster, K., Wagner, T., Kasten, S., 2008. Redox sensitivity of P cycling during marine black shale formation: Dynamics of sulfidic and anoxic, non-sulfidic bottom waters. *Geochimica et Cosmochimica Acta* 72 (15), 3703–3717.
- Masse, J.P., Bellion, Y., Benkhelil, J., Boulin, J., Cornee, J.J., Dercourt, J., Guiraud, R., Mascle, G., Poisson, A., Ricou L.E., Sandulescu, M., 2000. Early Aptian (114–112 Ma). In: Dercourt, J., Ricou, L.E., and Vrielynck, B., (Eds), *Atlas Tethys, palaeoenvironmental maps*. CCGM/CGMW, Paris (2000).
- Masse, J.P., Ferneci-Masse, M., 2013. Drowning events, development and demise of carbonate platforms, and controlling factors: The Late Barremian–Early Aptian record of Southeast France. *Sedimentary Geology* 298, 28–52.
- Menegatti, A. P., Weissert, H., Brown, R. S., Tyson, R. V., Farrimond, P., Strasser, A. & Caron, M., 1998. High resolution $\delta^{13}\text{C}$ stratigraphy through the Early Aptian “Livello Selli” of the Alpine Tethys. *Paleoceanography* 13 (5), 530–545.
- Méhay, S., C. E. Keller, S. M. Bernasconi, Weissert, H., Erba, E., Bottini, C., and Huchuli, P. A., 2009. A volcanic CO_2 pulse triggered the Cretaceous oceanic anoxic event 1a and a biocalcification crisis, *Geology* 37, 819–822.
- Meyers, P.A., 1997. Organic geochemical proxies of paleoceanographic, paleolimnologic, and paleoclimatic processes, *Organic Geochemistry* 27, 213–250.
- Meyer, K. M., and Kump, L. R. 2008. Oceanic euxinia in earth history: causes and consequences. *Annual Review, Earth Planetary Sciences* 36, 251–288.
- Millán, M.I., Weissert, H.J., Fernández-Mendiola, P.A., García-Mondéjar, J., 2009. Impact of Early Aptian carbon cycle perturbations on evolution of a marine shelf system in the Basque-Cantabrian Basin (Aralar, N Spain), *Earth and Planetary Science Letters* 287, 3–4, 15, 392–401.
- Moodley, L., Hess, C., 1992. Tolerance of infaunal benthic foraminifera for low and high oxygen concentrations. *Biological Bulletin* 183(1), 94–98.
- Moreno-Bedmar, J.A., 2010. Ammonites de l’Aptià inferior de la península Ibèrica. Biostratigrafia i aportacions a l’estudi del Oceanic Anoxic Event 1a. Universitat de Barcelona, 331 pp.
- Morford, J.L., Emerson, S., 1999. The geochemistry of redox sensitive trace metals in sediments. *Geochimica et Cosmochimica Acta* 63, 1735–1750.

- Morford, J.L., Russell, A.D., Emerson, S., 2001. Trace metal evidence for changes in the redox environment associated with the transition from terrigenous clay to diatomaceous sediments, Saanich Inlet, BC. *Marine Geology* 174, 355–369.
- Morse, J.W., Luther III, G.W., 1999. Chemical influences on trace metal-sulfide interactions in anoxic sediments. *Geochimica et Cosmochimica Acta* 63, 3373–3378.
- Moullade, M., Kuhnt, W., Bergen, J.A., Masse, J.-P., Tronchetti, G., 1998. Correlation of biostratigraphic and stable isotope events in the Aptian historical stratotype of La Bédoule (southeast France). *Comptes Rendus de l'Académie des Sciences - Series IIA - Earth and Planetary Science* 327, 693–698.
- Muñoz, J.A., Puig de Fàbregas, C., Fontboté, J.M., 1984. Orógenos alpinos, in: Ríos, L. J. J. M. (Ed.), *El Pirineo*. Inst. Geol. Min. España. *Geología de España* 2, pp. 161–205.
- Murray, J.W., 2001. The niche of benthic foraminifera, critical thresholds and proxies. *Marine Micropaleontology* 41(1–2), 1–7.
- Mutterlose, J., Böckel, B. 1998. The Barremian–Aptian interval in NW Germany: a review. *Cretaceous Research* 19(5), 539–568.
- Mutterlose, J., Pauly, S., Steuber, T., 2009. Temperature controlled deposition of early Cretaceous (Barremian–early Aptian) black shales in an epicontinental sea. *Palaeogeography, Palaeoclimatology, Palaeoecology* 273(3), 330–345.
- Najarro, M., Rosales, I., Moreno-Bedmar, J.A., de Gea, G.A., Barrón, E., Company, M., Delanoy, G., 2010. High-resolution chemo- and biostratigraphic records of the Early Aptian oceanic anoxic event in Cantabria (N Spain): Palaeoceanographic and palaeoclimatic implications. *Palaeogeography Palaeoclimatology Palaeoecology* 299, (1–2), 137–158.
- Neal, C.L., Mahoney, J.J., Kroenke, L.W., Duncan, R.A., Petterson, M.G., 1997. The Ontong Java Plateau. In, Mahoney, J.J., and Coffin, M. F, Editors, *Large Igneous Provinces. Continental, oceanic, and planetary flood volcanism*, 183 –216.
- Neal, C.R., Coffin, M.F., Arndt, N.T., Duncan, R.A., Eldholm, O., Erba, E., Farnetani, C., Fitton, J.G., Ingle, S.P., Ohkouchi, N., Rampino, M.R., Reichow, M.K., Self, S., Tatsumi, Y., 2008. Investigating large igneous province formation and associated paleoenvironmental events: A white paper for scientific drilling, *Scientific Drilling* 6, 4–18.
- Nijenhuis, I. A., Bosch, H. J., Sinninghe Damsté, J.S., Brumsack, H. J., De Lange G. J., 1999. Organic matter and trace element rich sapropels and black shales: a geochemical comparison. *Earth and Planetary Science Letters* 169, 277–290.
- Papp, D.C., Cociuba, I., Lazăr, D.F., 2013. Carbon and oxygen-isotope stratigraphy of the Early Cretaceous carbonate platform of Pădurea Craiului (Apuseni Mountains,

- Romania): A chemostratigraphic correlation and paleoenvironmental tool. *Applied Geochemistry* 32, 3–16.
- Patterson, R. T., Guilbault, J-P., Thomson, R.E., 2000. Oxygen level control on foraminiferal distribution in Effingham inlet, Vancouver island, British Columbia, Canada. *Journal of foraminiferal Research* 30 (4), 321–335.
- Pauly, S., Mutterlose, J., Wray, D.S., 2013. Palaeoceanography of Lower Cretaceous (Barremian-Lower Aptian) black shales from northwest Germany evidenced by calcareous nannofossils and geochemistry. *Cretaceous Research* 42, 28–43.
- Petersen, W., Wallman, K., Li, P., Schroeder, F., Knauth, H.O., 1995. Exchange of trace elements at the sediment–water interface during early diagenetic processes. *Marine and Freshwater Research* 46, 19–26.
- Peybernès, B. and Souquet, P., 1973. Biostratigraphie des marnes noires de l' Aptien–Albien de la zone sud-pyrénéenne . *Comptes Rendus de l'Académie des Sciences Paris* 276 (2 Mai 1976), Séries D, 2501–2504.
- Peybernès, B., 1976. Le Jurassique et le Crétacé inférieur des Pyrénées franco-espagnoles. Thèse de doctorat, Laboratoire de Géologie, Université Paul Sabatier, Toulouse, 459 pp.
- Pohl, C., and Hennings, U., 1999. The effect of redox processes on the partitioning of Cd, Pb, Cu, and Mn between dissolved and particulate phases in the Baltic Sea. *Marine Chemistry* 65, 41–53.
- Ponton, C., and Maurrasse, F.J-M.R., 2006. Aptian deposits of the Provençal Platform of Southern France: Evidence for low-oxygen conditions and the influence of local physiography. *Geological Society of America Abstract with Programs* 38 (7), 492.
- Premoli Silva, I., Verga, D., 2006. Classification of Early Cretaceous trochospiral and planispiral planktonic foraminifera: An update. *Anuário do Instituto de Geociências—UFRJ*. 209 (1), 361–362.
- Ravelo, A. C. and Fairbanks, R. G. 1995. Carbon isotopic fractionation in multiple species of planktonic foraminifera from core-tops in the tropical Atlantic. *Journal of Foraminiferal Research* 25(1), 53–74.
- Reboulet, S., Hoedemaeker, P.J., (reporters), Aguirre-Urreta, M.B., Alsen, P., Atrops, F., Baraboshkin, E.Y., Company, M., Delanoy, G., Dutour, Y., Klein, J., Latil, J.L., Lukeneder, A., Mitta, V., Mourgues, F.A., Ploch, I., Raisossadat, N., Ropolo, P., Sandoval, J., Tavera, J.M., Vasicek, Z., Vermeulen, J., 2006. Report on the 2nd International Meeting of the IUGS Lower Cretaceous Ammonite Working Group, the "Kilian Group" (Neuchâtel, Switzerland, 8 September 2005). *Cretaceous Research* 27, 712–715.

- Reboulet, S., Rawson, P.F., Moreno-Bedmar, J.A., Aguirre-Urreta, M.B., Barragán, R., Bogomolov, Y., Company, M., González-Arreola, C., Stoyanova, V.I., Lukeneder, A., Matrimon, B., Mitta, V., Randrianaly, H., Vašiček, Z., Baraboshkin, E.J., Bert, D., Bersac, S., Bogdanova, T.N., Bulot, L.G., Latil, J.-L., Mikhailova, I.A., Ropolo, P., Szives, O., 2012. Report on the 4th International Meeting of the IUGS Lower Cretaceous Ammonite Working Group, the “Kilian Group” (Dijon, France, 30th August 2010). *Cretaceous Research* 32, 786–793.
- Rhoads, D. C., Morse, J. W., 1971. Evolutionary and ecologic significance of oxygen-deficient marine basins. *Lethaia* 4 (4), 413-428.
- Rimmer, S.M., 2004. Geochemical paleoredox indicators in Devonian-Mississippian black shales, central Appalachian Basin (U.S.A.). *Chemical Geology* 206, 373-391.
- Rimmer, S.M., Thompson, J.A., Goodnight, S.A., Robl, T.L., 2004. Multiple controls on the preservation of organic matter in Devonian–Mississippian marine black shales: geochemical and petrographic evidence. *Palaeogeography, Palaeoclimatology, Palaeoecology* 215, 125–154.
- Sanchez-Hernandez, Y., Maurrasse, FJ-MR., 2012a. Late Barremian to early Aptian paleoenvironmental conditions recorded in the sedimentological and geochemical records of the El Pui section, NE Spain. GSA Annual Meeting. Abstracts with program 26–5 p. 83.
- Sanchez-Hernandez, Y., Maurrasse, FJ-MR., 2012b. Lithostratigraphic and geochemical characterization of a semi-enclosed basin (Organyà Basin, NE Spain) prior to the occurrence of the early Aptian OAE-1a. AGU Annual Meeting. Abstracts with program: PP31A–2003.
- Schlanger, S.O., Jenkyns, H.C., 1976. Cretaceous oceanic anoxic events: causes and consequences. *Geologie en Mijnbouw* 55, 179–184.
- Schlanger, S. O., Arthur, M. A., Jenkyns, H. C., & Scholle, P. A. (1987). The Cenomanian–Turonian Oceanic Anoxic Event, I. Stratigraphy and distribution of organic carbon-rich beds and the marine $\delta^{13}\text{C}$ excursion. Geological Society, London, Special Publications 26(1), 371–399.
- Scholle, P.A., Arthur, M.A., 1980. Carbon isotope fluctuations in Cretaceous pelagic limestones: potential stratigraphic and petroleum exploration tool. *American Association of Petroleum Geologists* 64 (1).
- Schultz, R.B., 2004. Geochemical relationships of late Paleozoic carbon-rich shales of the Midcontinent, USA; a compendium of results advocating changeable geochemical conditions. *Geochemistry of organic-rich shales; new perspectives. Chemical Geology* 206, 347–372.

- Schwenke, M., 1993. Geologische Kartierung des Westteils des Val Cabó (Provinz Lérida/mittlere Südpirenen/NE Spanien) unter besondere Betrachtung der Sedimentationsentwicklung im Apt/Alb. Diplomkartierung, Univ. Bremen, Bremen Germany, 99 pp.
- Seguret, M., 1972. Étude tectonique des nappes et séries décollées de la partie centrale du versant sud des Pyrénées. Pub. Ustela, Série Géologie Structurale 2, 155 pp.
- Sliwinski, M.G., Whalen, M.T., Newberry, R.J., Payne, J. and Day, J., 2011. Stable isotope ($\delta^{13}\text{C}_{\text{carb}}$ & $\delta^{15}\text{N}_{\text{org}}$) and trace element anomalies during the Late Devonian Punctata Event in the Western Canada sedimentary basin. *Palaeogeography Palaeoclimatology Palaeoecology* 307, 245–271.
- Stein, M., Föllmi, K.B., Westermann, S., Godet, A., Adatte, T., Matera, V., Fleitmann, D., Berner, Z., 2011. Progressive palaeoenvironmental change during the Late Barremian–Early Aptian as prelude to Oceanic Anoxic Event 1a: evidence from the Gorgo a Cerbara section (Umbria-Marche Basin, central Italy). *Palaeogeography Palaeoclimatology Palaeoecology* 302, 396–406.
- Stein, M., Westermann, S., Adatte, T., Matera, V., Fleitmann, D., Spangenberg, J.E. and Föllmi, K.B., 2012. Late Barremian–Early Aptian palaeoenvironmental change: the Cassis-La Bédoule section, southeast France. *Cretaceous Research* 37, 209–222.
- Stinton, C.W. and Duncan, R.A., 1997. Potential links between ocean plateau volcanism and global ocean anoxia at the Cenomanian-Turonian boundary: *Economical Geology* 92, 836–842.
- Taylor, A. M., Goldring, R. 1993. Description and analysis of bioturbation and ichnofabric. *Journal of the Geological Society of London* 150, 141–148.
- Tejada, M. L. G., Suzuki, K., Kuroda, J., Coccioni, R., Mahoney, J. J., Ohkouchi, N., Sakamoto, T., Tatsumi, Y., 2009. Ontong Java Plateau eruption as a trigger for the Early Aptian oceanic anoxic event. *Geology* 37, 855–858.
- Tribovillard, N.P., 1998. Cyanobacterially generated peloids in laminated, organic-matter rich, limestones; an unobtrusive presence. *Terra Nova* 10, 126–130.
- Tribovillard, N., Ramdani, A., Trentesaux, A., 2005. Controls in organic accumulation in upper Jurassic shales of northwestern Europe as inferred from trace-metals geochemistry. In: Harris, N. (Ed.), *The deposition of Organic-Carbon-Rich sediments: Model, Mechanisms, and Consequences*. SEPM Special Publication 82, 145–164.
- Tribovillard, N., Algeo, T.J., Lyons, T., Riboulleau, A., 2006. Trace metals as paleoredox and paleoproductivity proxies: An update. *Chemical Geology* 232 (1–2), 12–32.

- Turekian, K.K., Wedepohl, K.H. 1961. Distribution of the elements in some major units of the Earth's crust. *Geological Society of America Bulletin* 72, 175–192.
- Tuttle, M.L., Dean, W.E., Parduhn, N.L., 1983. Major and trace elements Mahogany zone oil shale in two cores from the Green River formation, Piceance Basin, Colorado. Symposium on geochemistry and chemistry of oil shale. American Chemical Society, Seattle meeting, March 20–25.
- Tyson, R.V., Pearson, T.H., 1991. Modern and ancient continental shelf anoxia: an overview, in Tyson, R.V., Pearson, T.H. (Eds.), *Modern and Ancient Continental Shelf Anoxia*: Geological Society of London, Special Publication 58, 1–24.
- Vergés J., Muñoz, J.A., 1990. Thrust sequences in the southern central Pyrenees. *Bulletin de la Société Géologique de France* 8, VI 2, 265–271.
- Vergés, J., 1993. Estudi tectònic del versant sud del Pirineu oriental i central. Evolució cinemàtica en 3D. Tesis doctoral Universitat de Barcelona, Barcelona, 191 pp.
- Wedepohl, K.H., 1971. Environmental influences on the chemical composition of shales and clays. In: Ahrens, L.H., Press, F., Runcorn, S.K., Urey, H.C. (Eds.), *Physics and Chemistry of the Earth* 8. Pergamon, Oxford, pp. 305–333.
- Wedepohl, K.H., 1991. The composition of the upper earth's crust and the natural cycles of selected metals. Metals in natural raw materials. *Natural Resources*. In: Merian, E. (Ed.), *Metals and Their Compounds in the Environment*. VCH, Weinheim, pp. 3–17.
- Weissert, H., 1989. C-isotope stratigraphy, a monitor of paleoenvironmental changes: a case study from the Early Cretaceous. *Surveys in Geophysics* 10, 1–16.
- Weissert, H., Erba, E., 2004. Volcanism, CO₂ and palaeoclimate: a Late Jurassic–Early Cretaceous carbon oxygen isotope record. *Journal of the Geological Society of London* 161, 1–8.
- Whitfield, M., 2002. Interactions between phytoplankton and trace metals in the ocean. *Marine Biology* 41, 3–120.
- Wignall, P.B., Myers, K.J., 1988. Interpreting benthic oxygen levels in mudrocks: a new approach. *Geology* 16, 452–455.
- Wijnsman, J. W. M., Middelburg, J. J., Heip, C. H. R., 2001, Reactive iron in Black Sea Sediments: implications for iron cycling: *Marine Geology* 172, 167–180.
- Wilkin, R. T., Barnes, H. L., and Brantley, S. L., 1996. The size distribution of framboidal pyrite in modern sediments: An indicator of redox conditions. *Geochimica et Cosmochimica Acta* 60 (20), 3897–3912.

- Wilkin, R. T., Arthur, M. A. and Dean, W. E., 1997. History of water-column anoxia in the Black Sea indicated by pyrite framboid size distributions. *Earth and Planetary Science Letters* 148, 517–525.
- Wissler, L., Funk, H. and Weissert, H., 2003. Response of Early Cretaceous carbonate platforms to changes in atmospheric carbon dioxide levels. *Palaeogeography Palaeoclimatology Palaeoecology* 200, 187–205.
- Xiong, Z., Li, T., Algeo, T., Chang, F., Yin, X., Xu, Z., 2012. Rare earth element geochemistry of laminated diatom mats from tropical West Pacific: Evidence for more reducing bottom waters and higher primary productivity during the Last Glacial Maximum. *Chemical Geology* 296–297, 103–118.
- Xu, G., Hanna, J.L, Bingen, B., Georgiev, S., Stein H.J., 2012. Digestion methods for trace element measurements in shales: Paleoredox proxies examined. *Chemical Geology* 324–325, 132–147.

5 ASSESSING THE FACTORS CONTROLLING HIGH SEDIMENTATION RATES FROM THE LATEST BARREMIAN–EARLIEST APTIAN IN THE HEMIPELAGIC SETTING OF THE RESTRICTED ORGANYÀ BASIN, NE SPAIN

Sanchez-Hernandez, Y., Maurrasse, F. J-M.R., Melinte-Dobrinescu, M.C., He, D., Butler, S.K., 2014. Assessing the factors controlling high sedimentation rates from the latest Barremian–earliest Aptian in the hemipelagic setting of the restricted Organyà Basin, NE Spain. *Cretaceous Research* 51, 1-21.

Abstract

The Organyà Basin, south–central Spanish Pyrenees, developed as a marginal depocenter during a rapid extensional phase of anticlockwise rotation of the Iberian plate. As a result of increased subsidence, an important change in sedimentation occurred from the late Barremian to the Aptian leading to unusually high sediment accumulation rates. Approximately 1000 m of hemipelagic marls and limestones accumulated during this time interval.

Here we studied the basal 85 m of the hemipelagic facies of the El Pui section, Organyà Basin, that are characterized by alternating 15 cm - ~ 3 m thick beds of limestone and marls. Geochemical analyses indicate high total inorganic carbon (TIC) values (average 70%) suggesting enhanced CaCO₃ production and deposition. SEM analyses of the samples indicate a high abundance of calcareous nannofossils, which together with the absence of shallow-water taxa characteristic of the Urgonian carbonate platform of Organyà, and the lack of sedimentary facies attributable to carbonate platform components, point to nannofossils as the main source for the elevated TIC. Organic-rich levels (total organic carbon (TOC) up to 1.74%) concurrent with positive excursions up to 2‰ in $\delta^{13}\text{C}_{\text{org}}$, imply enhanced preservation of organic matter (OM) in the basin. In addition, pronounced peaks of $\delta^{13}\text{C}_{\text{org}}$ higher than the global average suggest

superimposed local factors related to intensified ^{12}C removal due to primary productivity. Biomarker analyses and the $\delta^{13}\text{C}_{\text{org}}$ profile suggest an autochthonous origin of the OM from phytoplankton and possible additional contributions from microbial communities.

X-ray diffraction (XRD) results attest sustained terrestrial fluxes as the source of nutrients to the basin because of a 30% average non-carbonate bulk mineral content in the sediment. The non-carbonate fraction is dominated by quartz (average, 14%) whereas the clay mineral assemblages are characterized by high illite content (> 73 relative%) with minor concentrations of kaolinite (< 5%), illite /smectite mixed layers (< 17%) and chlorite (< 15%), consistent with a provenance from the Paleozoic metamorphic terranes adjacent to the Organyà Basin.

The integrated results suggest a high sediment accumulation rate (5-7.5 cm/ky) and enhanced carbon burial during the latest Barremian – earliest Aptian in the hemipelagic setting of the El Pui section.

5.1 Introduction

The causes of the occurrence of high accumulation rates within the Barremian – Aptian time interval (~125 Ma) [(e.g. Angles section, southern France (Wissler et al., 2002); northern Germany (Mutterlose et al., 2009); La Bédoule section southeast France, (Kuhnt et al., 2011); Sierra del Rosario eastern Durango state Mexico (Núñez-Useche and Barragan, 2012); Blid and Ecleja Formations of the Pădurea Craiului Massif (Papp et al., 2013); see other locations in Bralower et al. (1994)] have been associated with intensified weathering and transport of continental materials to the marine environment, thereby increasing the nutrient load, especially in epicontinental seas and restricted marine settings (Arthur, 1979; Scott, 1992; Larson and Erba, 1999; Duque-Botero and

Maurrasse, 2005; Föllmi and Gainon, 2008; Melinte- Dobrinescu and Roban, 2011; Föllmi, 2012; Masse and Ferneci-Masse, 2013). Such increased terrigenous fluxes within that time interval have been related to greenhouse conditions (Weissert, 1989; Erba, 1994; Weissert et al., 1998; Frakes, 1999; Pucéat et al., 2003). However, reported dry, colder periods in the late Barremian (Ruffell and Batten, 1990; Malkoč and Mutterlose, 2010) suggest that seasonality could have also been a major factor in controlling nutrient supply to restricted marine basins.

In the case of semi-enclosed basins the transport of terrestrial material may be further enhanced by physiographic conditions, as for example the proximity of landmasses and magnitude of elevation differences, as well as the nature of the surrounding terranes. As observed in modern environments (e.g. Grégoire et al., 2004; Oguz, 2006) these factors can be critical in promoting special conditions favorable to unusual sustained blooms of certain groups of organisms, particularly primary producers, and notably opportunistic or eurytopic taxa.

The paleoenvironmental record provides a glance of similar effects on primary producers that benefited from significant nutrient supply associated with sustained terrigenous input (Erba, 1994; Meyers, 1997; Aguado et al., 2013). Furthermore, the lower Cretaceous record provides evidence that in some fertile marginal basins of the Tethys Ocean enhanced productivity may have intensified both the export of carbonate and organic matter (OM) to the sediment (Koutsoukos et al., 1991a, 1991b; Mutterlose and Böckel, 1998; Stein et al., 2011; Sanchez-Hernandez and Maurrasse, 2014). Higher bottom export of OM adversely affects oxygen levels in the water column because of an accelerated respiration rate, and in basins with limited ventilation, OM influx may exceed

rem mineralization. Such process may induce severe dysoxia [oxygen restricted conditions as indicated by Wignall and Myers (1988), Chapter 4], which further enhance preservation of organic carbon (OC) in the sediments (e.g. Black Sea; Grégoire et al., 2004; Oguz, 2006).

In the Organyà Basin, upper Barremian–lower Aptian hemipelagic facies of mostly dark limestones and marls overlying shallow-water carbonate platform deposits of the Prada Formation suggest a deepening depocenter with similar temporal development of oxygen deficient phases (Peybernès and Souquet, 1973; Peybernès, 1976; Martínez, 1982; Caus et al., 1990; Berástegui et al., 1990; Dinarés-Turell and García-Senz, 2000; García-Senz, 2002; Bernaus et al., 2002; 2003). The section was deposited during a period of unusually high sedimentation rates of pelagic carbonate concomitant with terrigenous material. Coeval sites in the Western Tethys are also reported to include hemipelagic sediments with high accumulation rates and oxygen-deficient episodes (e.g. Arthur, 1979; Mutterlose et al., 2009; Melinte- Dobrinescu and Roban, 2011), but unlike the other sites, recent studies have demonstrated that the El Pui sequence of the Organyà Basin is predominantly calcareous (TIC: 49-88%) and to a lesser extent terrigenous (Sanchez-Hernandez and Maurrasse, 2014). So far, this apparent unusual characteristic of the semi-restricted Organyà Basin has not been addressed, and the main source and factors involved in the high carbonate accumulation at El Pui remain to be fully understood.

The present study aims to determine the sedimentation rate and characterize the factors that controlled such mass accumulation rates in the El Pui section (Fig. 5-1) during the latest Barremian – earliest Aptian through a comprehensive analysis of

different criteria: composition of the nannofossil assemblages; geochemical analyses: carbon content and isotopic variation (TOC, TIC, $\delta^{13}\text{C}_{\text{org}}$), biomarker analysis; bulk and clay mineral content; and scanning electron microscope (SEM) with energy dispersive spectrometry (EDS).

5.2 Geological setting and paleoceanography of the study area

The El Pui section is located in the south-central Spanish Pyrenees ($42^{\circ} 14' 44.46''$ N, $1^{\circ} 13' 31.49''$ E, top of the studied 85 m), near the town of Cabó (Fig. 5-1), and is part of the Organyà Basin. The section is named after the adjacent locality of that name ($42^{\circ} 14' 21.94''$ N, $1^{\circ} 13' 36.85''$ E) (Fig. 5-1) situated on the southern limb of the Sierra de Prada where differential erosion of the beds along dip slope facilitated development of subsequent streams that cut deeply into the layers (Fig. 5-2A). These stream valleys form step-like profiles with water gaps that offer excellent spatial and temporal continuity of outcrops.

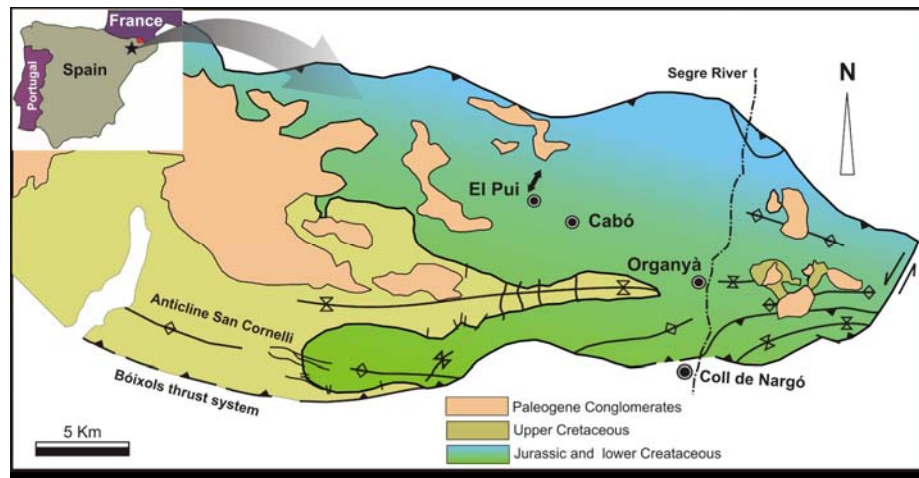


Figure 5-1 General geographic location and simplified geologic map of the Organyà area modified from García-Senz (2002). The arrow next to El Pui represents the approximate location of the studied section.

The Organyà Basin evolved through the breakup of pre-extensional Jurassic platforms (Seguret, 1972; Muñoz, 1991; Caus et al., 1990) concurrent with the opening of

the Atlantic Ocean, and simultaneously with the opening of the Bay of Biscay during Aptian–Albian times (Berástegui et al., 1990; 1993). In such complex paleogeographic setting (Fig. 5-3), a sequence of approximately 1000 m of limestone and marls (Fig. 5-2B, C, Fig. 5-4A) accumulated during the Barremian–Aptian interval (García-Senz, 2002), and the succession often designated as Cabó Marls has been assigned an overall latest Barremian – early Aptian age, (Peybernès and Souquet, 1973; Peybernès, 1976; Martínez, 1982; Bernaus et al., 2002, 2003; Moreno-Bedmar, 2010; Sanchez-Hernandez and Maurrasse, 2014).

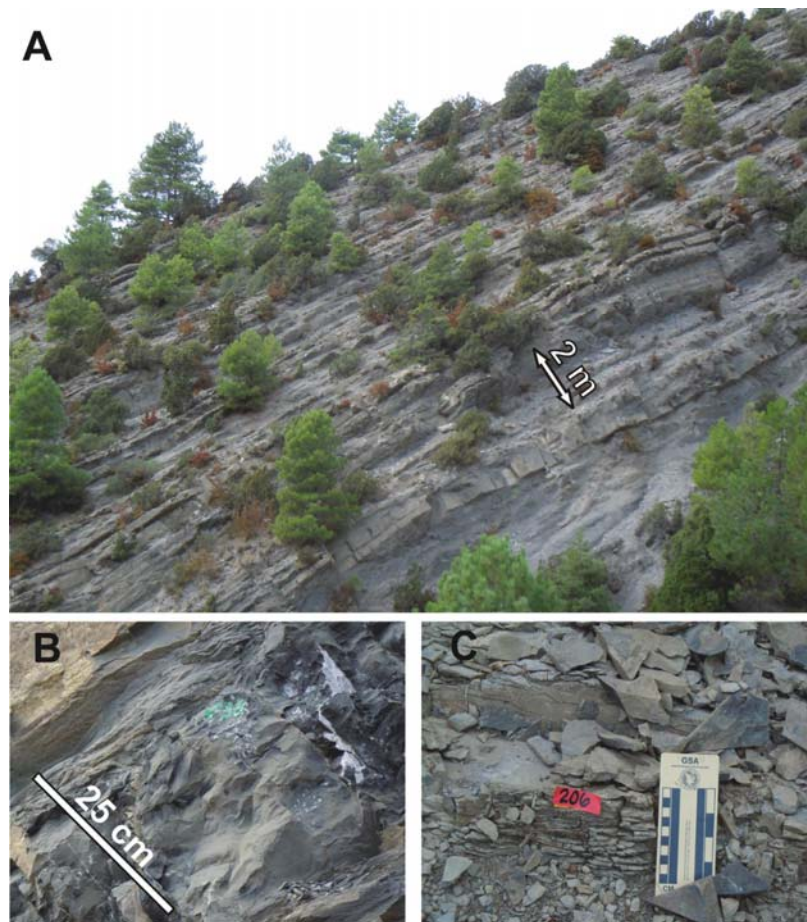


Figure 5-2 (A) Overview of the first ~30 m of the section showing distinct continuous interbeds of limestones and marls characteristic of the entire studied sequence at El Pui. (B) Black limestone facies are more common in the lowest 15 m of the section. (C) Marly facies are more characteristic of the upper 40 m of the section.

The hemipelagic facies of the Organyà Basin accumulated during a Cretaceous extensional phase characterized by high subsidence rates that provided ample accommodation space for deposition. The carbonate-rich facies include intermittent organic-rich layers (TOC: 0.5%-1.74%) throughout (Bernaus et al., 2003) concomitant with an overall positive trend in $\delta^{13}\text{C}_{\text{org}}$ (Figs. 4A-D) but here we focus on hemipelagic facies (Fig. 5-5, 5-6) with a depositional time frame from the latest Barremian – early Aptian, prior to the occurrence of ocean anoxic event 1a (OAE1a).

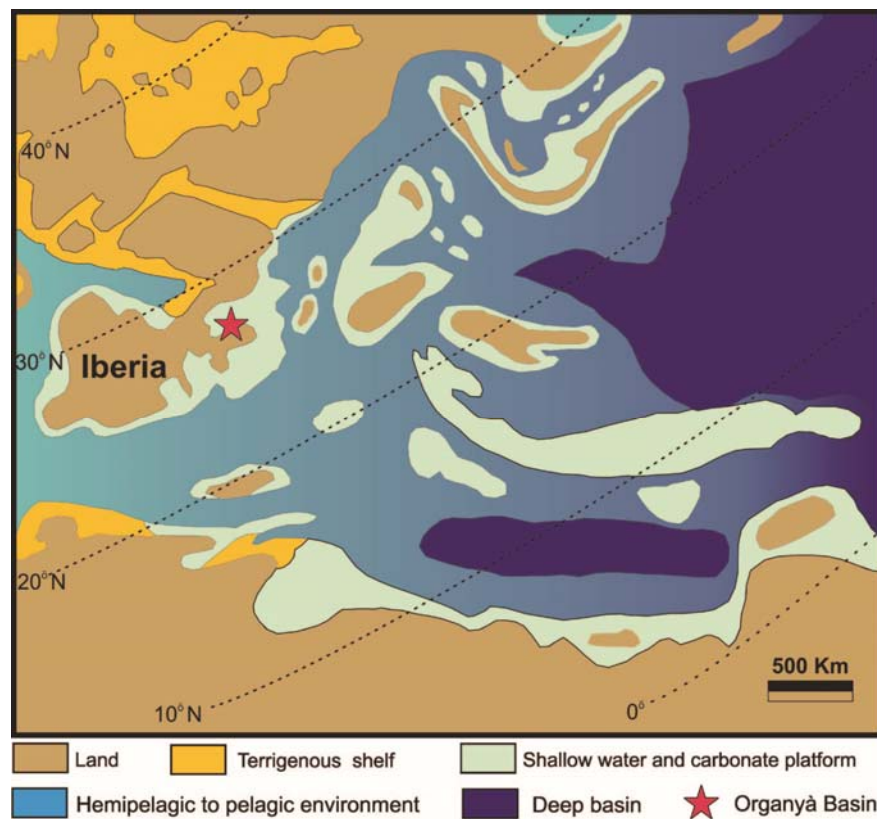


Figure 5-3 Paleoceanographic reconstruction of the western Tethys during the early Aptian modified from Masse et al. (1993). Also, details of bathymetry and paleoenvironments are incorporated from Mancinelli and Chiocchini, (2006), and Godet et al. (2013). Red star shows the relative position of the Organyà Basin in the paleophysiographic context of the Early Cretaceous of Western Tethys.

5.3 Materials and methods

5.3.1 Carbon analysis

Total inorganic carbon (TIC) and total organic carbon (TOC) was determined in 147 samples (Fig. 5-4B, C) of the studied section using standard analytical procedures used at Florida International University (Gaona-Narvaez et al., 2013; Sanchez-Hernandez and Maurrasse, 2014). These authors also described procedures for carbon isotope analyses of the values used herein (Fig. 5-4D). Calculations followed the standard equation $\delta^{13}\text{C}$ (permil, ‰) = $[(^{13}\text{C}/^{12}\text{C})_{\text{sample}} / (^{13}\text{C}/^{12}\text{C})_{\text{std}} - 1] \times 1000$. Also, as adopted in Sanchez-Hernandez and Maurrasse (2014) the lithologic terminology applied herein uses measured CaCO_3 (TIC) values as follows: limestone, > 65% CaCO_3 ; marly-limestone, 60% - 65% CaCO_3 ; marlstone, 30% - 60% CaCO_3 ; calcareous mud-rock/shale, 10% - 30% CaCO_3 ; mud-rock/shale, 0 - 10% CaCO_3 .

5.3.2 Biomarker analysis

In preparation for biomarker determination, small rock slabs corresponding to 24 different samples (Fig. 5-7) were powdered in a Bell-Art micromill. A careful cleaning process, with water, detergent, deionized water and acetone, was completed between samples. Biomarkers were analyzed following the procedures described in Jaffé et al. (2001). Samples were subjected to Soxhlet extraction for 24 hours with 300 ml 100% methylene chloride (Optima, Fisher, USA) as solvent. HCl (10%) activated copper was added during the extraction to eliminate elemental sulfur. Total extract were concentrated by rotary evaporation and saponified with 0.5 N KOH to separate into neutral and acid fractions. The neutral fractions free of elemental sulfur were further fractionated by elution with hexane to obtain saturated hydrocarbon fraction using Pasteur pipette

columns packed with silica gel. A known quantity of squalene was added as internal standard for quantification purpose and the hydrocarbon fraction was run on gas chromatography-mass spectrometry (GC-MS) with a Hewlett-Packard 6890 GC linked to a HP 5973 quadrupole MS system, fitted with Rtx-1MS columns (30 meters long, 0.25 mm ID, 0.25 μm df) from RESTEK, USA. The GC oven was programmed to hold initial temperature of 40°C for 1 min, and then ramped at a rate of 6°C/minute to a final temperature of 300°C held for 20 min. Identification of compounds was performed by comparison of chromatographic retention time, comparison with the mass spectra library and previous mass spectra reported in the literature (Fig. 5-8). The concentration of each biomarker was normalized to organic carbon (OC) as ng/g OC.

5.3.3 Bulk and clay mineral analysis

Mineralogical analyses of 10 samples (Table 5-1, Table 5-2, Fig. 5-9, 5-10) were performed at the Illinois State Geological Survey (ISGS) using X-ray diffraction (XRD) following the methodology described by Moore and Reynolds (1997). For the XRD procedure, the samples were micronized in a McCrone micronizing mill with deionized water for 10 min. Then they were transferred to 50 mL centrifuge tubes, which were placed in the centrifuge for 20 min at 2000 rpm. The clear supernatant was poured off and the remaining material dried overnight at 40°C. When completely dried the material was mixed lightly with a mortar and pestle and then packed into an end-loading sample holder as a random powder bulk-pack. The random powder bulk-pack was analyzed with a Scintag XDS 2000 diffractometer. Step-scanned data was collected from 2° to 60° 2 θ with a fixed time of 5 seconds per 0.05° 2 θ for each sample. All resulting traces were

analyzed using the semi-quantitative data reduction software from Materials Data Inc. (MDI) known as Jade® and a summary presented in Fig. 5-11.

The clay mineral composition was determined using oriented slides of the clay size $< 2 \mu\text{m}$ fraction with semi-quantitative values of the clay mineral assemblage calculated from ethylene glycol (EG) solvated slides (Hughes and Warren, 1989; Hughes et al, 1994; Moore and Reynolds, 1997).

In preparation for XRD 20 g - 30 g of each sample was soaked for about 10 - 12 h in deionized water and protected from external agents. As water interacts with the sample, small clay particles are released into the solution. Further stirring of the solution mechanically induced clay release from the sample. After settling, about 1/3 of the water was removed from the beaker. The beaker was then refilled with deionized water and two drops of sodium hexametaphosphate were added as a dispersant. The mix was stirred and then allowed to settle for 15 min. The generated supernatant was pipetted and several drops were added onto a glass slide and let to dry overnight.

Alternate treatments with EG for 24 hours, and heating to 490°C were also applied in order to establish a better comparison in peak intensity ratios among the expandable clays. Step-scans from $2^{\circ} - 34^{\circ} 2\theta$ with a fixed time of 5 sec per $0.05^{\circ} 2\theta$ were conducted for each sample.

5.3.4 Microscopy

The microscope work on calcareous nanofossils was performed at GEOECOMAR on an Olympus BH-2 petrographic microscope with a magnification of $\times 1500$. Calcareous nanofossils were examined using simple smear slides (Lamolda et al., 1994) and standard light-microscope techniques (Bown and Young, 1998) in 25

samples along the stratigraphic column, following the spatial distribution indicated in Fig. 5-12. The criteria for sample selection followed apparent changes in facies at the field, as well as at the microscopic scale; for samples in the lower 31 m variations in TOC, TIC and $\delta^{13}\text{C}_{\text{org}}$ were also considered. In order to achieve quantitative analyses, at least 300 specimens were counted in each smear-slide, in longitudinal transverses, randomly distributed.

The individual abundance of the observed taxa was considered as follows: P - present: 1 specimen (s) />50 fields of view (FOV); R-rare: 1s/21-50 FOV; F-few: 1s/11-20 FOV; C-common: 1s/2-10 FOV; A-abundant: >1s/FOV. The individual taxonomic abundance, in percentage, was considered from the total counted taxa (Melinte and Lamolda, 2007).

SEM analyses were performed at the Florida Center for Analytical Electron Microscopy (FCAEM) located at FIU using a JEOL JSM 5910LV scanning electron microscope with an EDAX energy dispersive spectroscope. The twenty-five samples selected for calcareous nannofossil analysis were also evaluated in SEM and EDS (Fig. 5-5, 5-12).

SEM images were taken on partially polished fragments following the procedures described in Sanchez-Hernandez and Maurrasse (2014). Energy dispersive spectroscopy (EDS) was also performed to determine the composition of the rock matrix and non-biogenic grains. For the analyses, samples were carbon coated to the orange thickness (150 Å) and processed in Compo mode under backscattered electron imaging detection. Areas of interest were first determined and inspected in secondary electron imaging and later switched to backscatter for qualitative elemental analysis. Relative composition was

determined using the Compo mode and both diffractograms and X-ray maps generated to evaluate the grain size and rock matrix composition.

5.4 Results

5.4.1 Carbon geochemistry

The total carbon (TC) present in the hemipelagic deposits of the El Pui section is distributed between the carbonate (CaCO_3) fraction (TIC) and the preserved organic fraction (TOC) from export production (Fig. 5-4B, C). SEM analyses show that the main carbonate components in the rocks of El Pui are essentially from nannoplankton remains (Fig. 5-5). In this regard the TIC together with the TOC, albeit possible remineralization even under reduced conditions should provide an indication of the magnitude of carbonate productivity.

Total carbon fluctuates between 49% and 92% in the studied 85 m of the section, with 85% of the measured values $> 70\%$ TC (Sanchez-Hernandez and Maurrasse, 2014). The TOC content fluctuates between ~ 0 and 1.74%, with most of the levels rich in organic carbon ($\geq 1.0\%$) recorded within the lower 31 m of the section (Fig. 5-4B). The lower interval also shows high-frequency variability in TOC with alternation between high and low values. The variation in TOC diminishes from 31 m to the 85 m level, including minor shifts of 0.4% and 0.8%, except for a value of 1.1% at ~ 41.8 m (Fig. 5-4B)

The carbonate values measured as TIC fluctuate between 43.5% and 87.6% with no evident correlation with TOC (Fig. 5-4C). TIC stays more consistently above 60%, with only 10% of all the values below 60wt% throughout the stratigraphic column. TIC

values lower than 60% are registered at 1.8 m, 4.7 - 6.1 m, 12.2 -13.0 m, 54.3 m, 56.3 m, 57.0 m, 78.3 m, and 81.1 m, respectively.

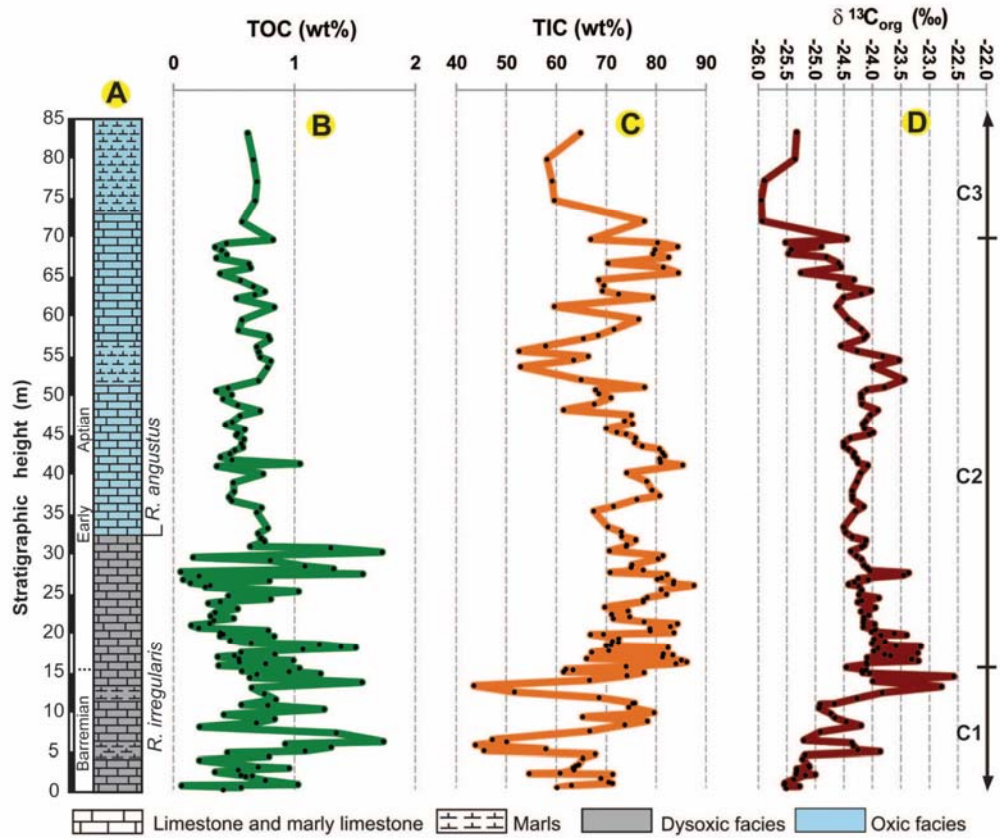


Figure 5-4 Simplified lithological log and geochemical variations in the 85 m El Pui section. (A) Simplified chronostratigraphic column including lithological variations, oxic, dysoxic levels, and relevant nannofossil events. (B) TOC. (C) TIC. (D) $\delta^{13}\text{C}_{\text{org}}$. The “C” Subdivisions correspond to the carbon isotopic segments after Menegatti et al. (1998) that have been proposed for the El Pui section in Sanchez-Hernandez and Maurrasse (2014).

The carbon isotopic ratio of OM ($\delta^{13}\text{C}_{\text{org}}$) is a proxy that allows to evaluate several factors such as: type of organic matter accumulated in the basin, variations in the carbon reservoir associated with productivity pulses, increased OM oxidation rate, and/or input of ^{12}C to the carbon pool (Hunt, 1970; Newman et al., 1973; Gearing et al., 1977; Dean et al., 1986; Dunham et al., 1988; Prahl et al., 1994; Meyers, 1994, 1997). Carbon stable isotope values ($\delta^{13}\text{C}_{\text{org}}$) in the bulk OM fraction vary between -25.95 and -22.57‰

with an average of -24.33‰ (Fig. 5-4D). An overall positive trend defines the lowermost 14.3 m with several negative and positive fluctuations. From ~10.8 m to ~13.0 m a positive excursion of ~ 2‰ indicates important changes in the organic carbon isotopic composition (Fig. 5-4D). From ~ 16.4 m to 26.5 m the $\delta^{13}\text{C}_{\text{org}}$ follows a gentle negative trend that ends at 26.5 m with a positive excursion of ~0.8‰, which coincides with a spike in TOC at 27.7 m, suggesting a link between OM preservation and carbon isotopic changes at that level.

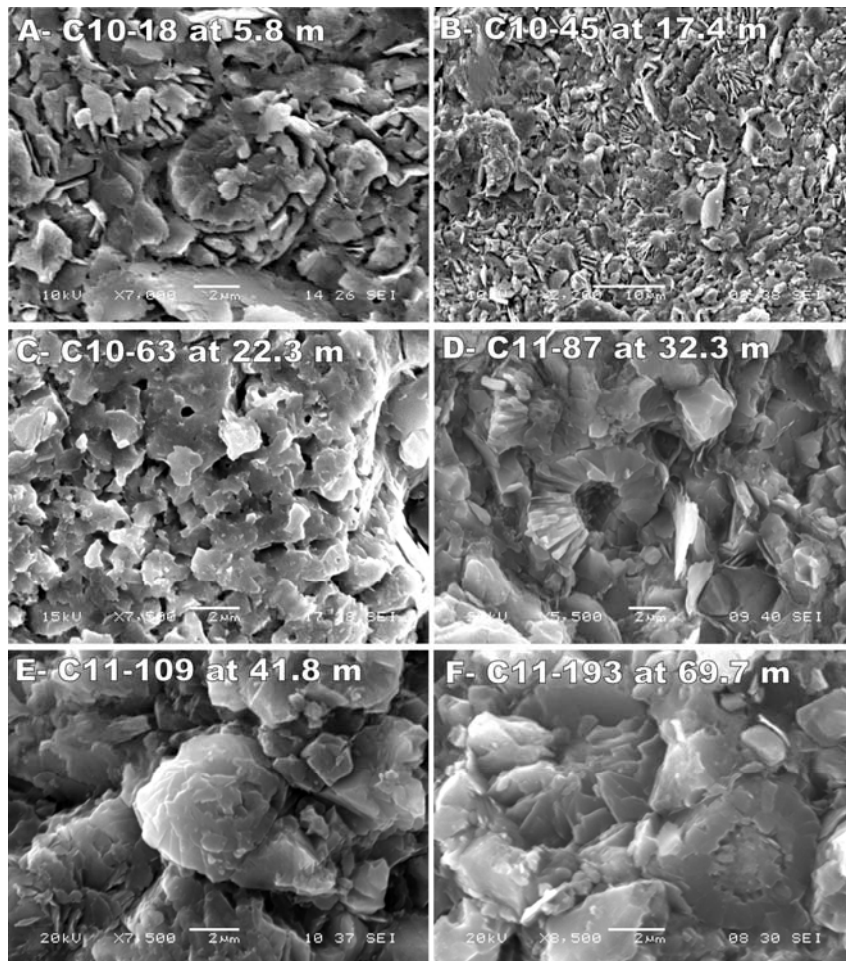


Figure 5-5 SEM micrographs of calcareous nanofossils including the sample code and corresponding stratigraphic position. The carbonate matrix is dominated by disaggregated calcareous nanofossil fragments at any level in the studied section. At higher magnification the fragments surrounding better preserve *Nannoconus* sp. on B resemble those shown in C.

From 28 m to 51 m $\delta^{13}\text{C}_{\text{org}}$ values fluctuate more uniformly between -24.5‰ and -24.0‰ without any major variation. However, from 52.6 m - ~70.0 m a more defined negative trend with intermittent fluctuations of up to 1‰ characterizes the $\delta^{13}\text{C}_{\text{org}}$ record. Continuously a new positive excursion of ~1‰ is immediately followed by a negative spike of ~ 1.5‰ that reaches a section minimum of -26.0‰ at 73.0 m (Fig. 5-4D). The last 12 m of the section yields only minor fluctuations in $\delta^{13}\text{C}_{\text{org}}$ between -26.0‰ and -25.3‰ (Fig. 5-4D).

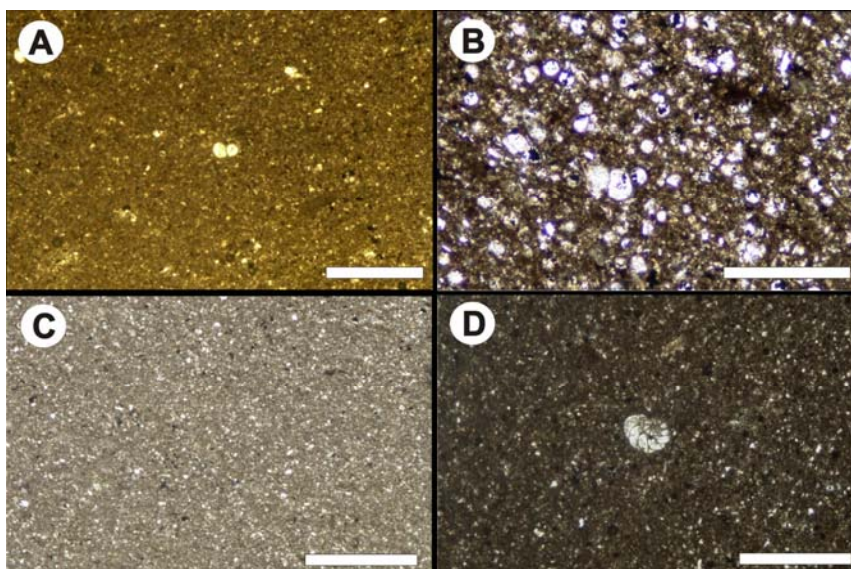


Figure 5-6 Microfacies of selected samples at different levels of the stratigraphic column showing texture and composition characteristic of a hemipelagic setting with dominant calcareous nannofossils shown in Fig. 5. A-) sample C10-05 at ~1.2 m, dark micritic matrix with small planktonic foraminifera in the center; B-) sample C10-16 at ~ 4.9 m, abundant calcispheres and small planktonic foraminifera in a fine, dark carbonate matrix with traces of kerogen; C-) sample C10-42 at ~16.8 m, fine micritic matrix; and D-) sample C10-87 at ~32.3 m, fine micritic matrix with coiled benthic foraminifera in the center. Pictures B, C, and D were taken using a white polarized light source. Scale bar represents 0.5 mm

5.4.2 Biomarkers

Biomarkers are residual complex organic compounds found in rocks and sediments that can preserve the main structural features of the parent molecules from living organisms after deposition (Peters and Moldowan, 1993; Meyers, 1997; Brassell

and Dumitrescu, 2004). Generally, these compounds remain stable during sedimentation and early burial retaining molecular fossils biosignatures that have been used to provide details on the taxonomic origin of the preserved organic matter.

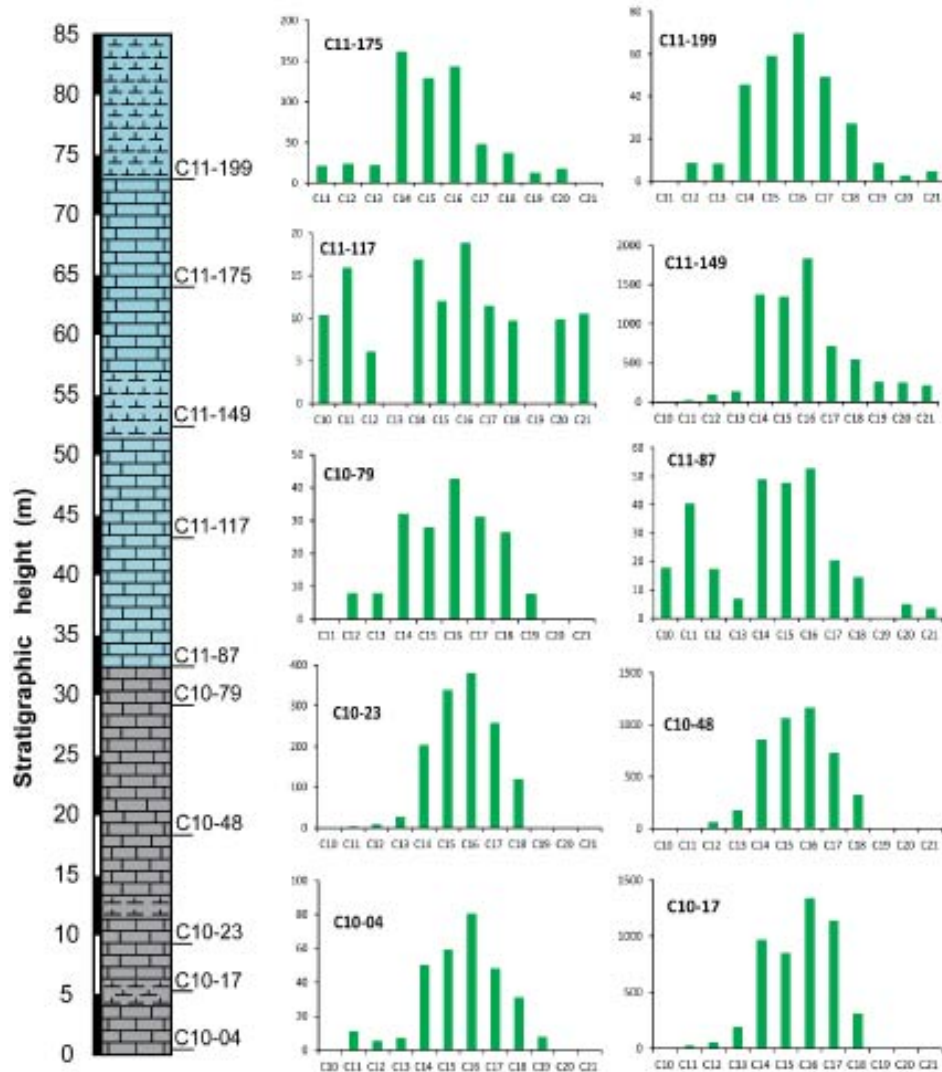


Figure 5-7 Relative stratigraphic position of 10 of the 24 samples analyzed for *n*-alkanes and their corresponding bar diagrams: *n*-alkanes abundance in ng/g (y axis) with respect to the carbon chain length (x axis). Notice the absence of even or odd carbon number preference.

Because marine and terrestrial organisms produce *n*-alkanes with characteristically different carbon chain lengths, *n*-alkanes have been previously used to determine the provenance of the organic matter (Giger et al., 1980; Meyers, 1997;

Dumitrescu and Brassell, 2005, 2006; Peters et al., 2005). Indeed, the presence of *n*-alkanes with chain length longer than C₂₀ (> C₂₀) are commonly thought to be indicative of higher plant OM that is terrestrial in origin, whereas chains shorter than C₁₉ (< C₁₉) are presumed to be mainly derived from marine planktonic organisms and /or microbial communities (Cranwell, 1973; Cranwell et al., 1987; Forster et al., 2004; Peters et al., 2005). However, *n*-alkanes should be used with caution because the abundance of these compounds can be modified by the level of maturity of the organic matter (Quijano et al., 2012). Nonetheless, despite this apparent constraint Jinggui et al., (2002) and Skret and Fabianska, (2009) have successfully assessed the origin of organic matter in overmature samples using *n*-alkanes.

The GC-MS results (ion *m/z* 57 extracted) for 24 samples analyzed in the El Pui section revealed significant enrichment of short chain *n*-alkanes with chain length < C₂₀ and no odd or even carbon chain predominance as shown for ten of the samples (Fig. 5-7, 5-8). Although Bernaus et al. (2003) reported thermally mature OM in the Organyà Basin, the pristane/phytane (Pr/Phy) ratios in the analyzed samples at El Pui (Appendix 4) remain consistently below 2, which suggests that they did not reach an overmature state (ten Haven et al., 1987; 1988; Powell, 1988). Such results are consistent with previous use of *n*-alkanes and may support the assessment of the origin of the OM in the El Pui samples. Hence the detection of only carbon chain lengths < C₂₀ and δ¹³C_{org} values consistent with marine sources (Meyers, 1997) implies a most likely autochthonous origin of the OM (Giger et al., 1980; Cranwell et al., 1987).

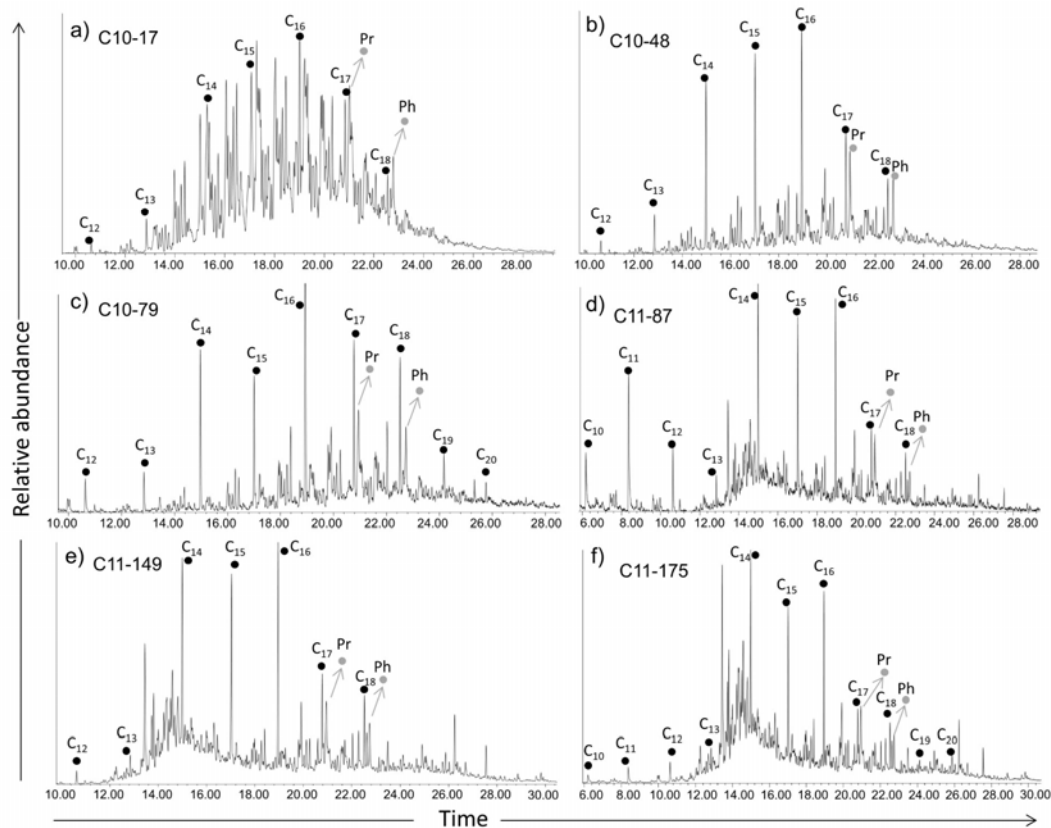


Figure 5-8 Chromatograms of selected samples along the studied section. Notice the absence of *n*-alkanes with carbon chain number > C₂₀. For relative position of the samples, see Figure 5-7.

5.4.3 Clay and bulk mineral assemblages

The clays investigated refer to the fine fraction phyllosilicate minerals (< 2 μm) that include kaolinite, illite, illite/smectite mixed-layer clay, and chlorite. Clay minerals have been used to estimate paleoenvironmental conditions, intensity of weathering and depositional environments at different time scales and in particular during the Mesozoic (Ruffell et al., 2002; Dera et al., 2009; Pauly et al., 2013). The fractionation of clay mineral may be influenced by climatic conditions, tectonic events, diagenetic processes related to pressure and temperature, and geochemical reactions, but commonly clay minerals in sediments are of detrital origin and represent the composition of the source

rock (Burtner and Warner, 1986; Weaver, 1989; Bayhan et al., 2001; Kotel'nikov and Zinchuck, 2008).

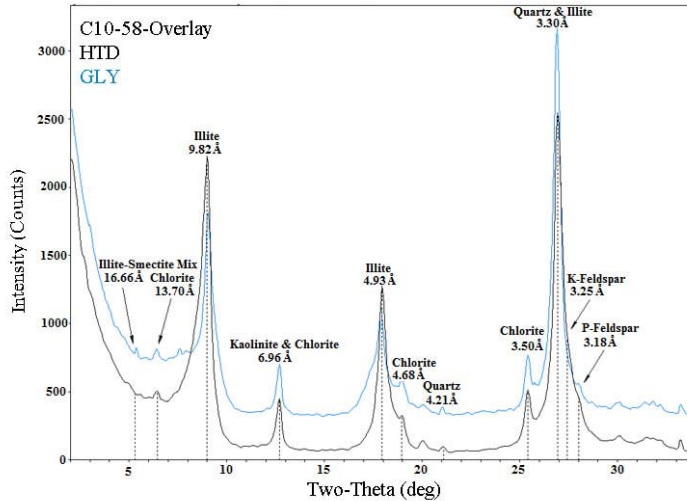


Figure 5-9 Characteristic diffractograms of XRD analyses for sample C10-58 (glycolated (GLY) and heated (HTD)). Qualitative identification of a small amount of mixed-layered clay is represented by the small peak near $5.2^{\circ} 2\theta$ on the EG solvated sample. The broad peak near $17.7^{\circ} 2\theta$ points to a most likely illite/smectite random interlayering. Heating the sample produces a pattern lacking the small peak near $5.2^{\circ} 2\theta$ with an overall resemblance to that of a pure illite pattern with a weakened 003 peak.

El Pui section XRD clay mineral analyses were performed in ten samples distributed along the stratigraphic column (Fig. 5-9, 5-10) in order to assess the origin of the non-carbonate detrital fraction. The diffraction patterns obtained from the EG solvated samples (Fig. 5-9) yielded kaolinite, mixed layer illite/smectite, chlorite and illite (Table 5-1, Fig. 5-9). Relative kaolinite content is small with minor variations (1% - 5%) and an average content of 2%. Mixed layer illite/smectite relative content varies between 6% and 17%, whereas chlorite fluctuates between 3% and 15% with pronounced increases in percentage at ~ 14 m and 62 m with no specific pattern of change. Illite represents most of the clay fraction and its abundance stays relatively stable throughout the section with values fluctuating between 73% and 90% (Table 5-1, Fig. 5-10). Since clay mineral assemblages at all stratigraphic levels analyzed show a strong dominance of

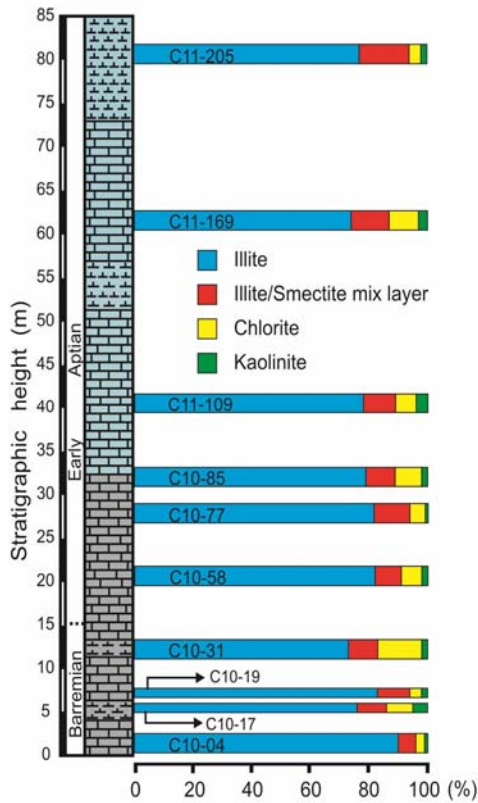


Figure 5-10 Relative percentages of clay minerals at different levels of the studied section. Notice that the assemblages are dominated by illite with minor variations in the concentration of illite/smectite mixed layer, chlorite and kaolinite. Because of the consistency in the concentrations these measurements are considered to represent the general average variation of the 85 m studied.

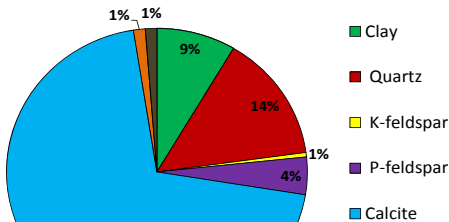


Figure 5-11 Pie diagram of the average mineral composition of limestones and marls in the El Pui section from bulk mineral measurements and EDS analyses.

illite (>73%), while illite/smectite, chlorite and kaolinite remain consistently low, these results are considered to represent the overall clay mineral content of the entire 85 m section.

The bulk mineralogy of the El Pui sediments was also determined for the ten samples analyzed for clay minerals (Table 5-2) with identical purpose. Their composition consists mainly of CaCO₃ (as described in the TIC section, > 50%), quartz (6% - 25%), clay minerals (3% - 15%), plagioclase (P)-feldspar (2% - 7%), minor concentrations of K-feldspar

(0 - 2%, with an average of 0.5%), low presence of dolomite (0 - 3%, with an average of ~ 1.4%) and fluctuating presence of pyrite/marcasite (0- 5%, average ~1.2%). The average bulk mineral composition of the El Pui samples obtained from the XRD and complementing results from EDS analyses is illustrated in Fig. 5-11.

5.4.4 Microscopy: light microscope, SEM and EDS

Microscopic analyses of the samples for nannofloral content and distribution reveal that on the whole the assemblages are characterized by low diversity (number of species) and high abundance (number of specimens). Preservation of nannofloras in all samples ranges from poor to moderate based on classes of preservation established as follows: P (Poor) – between 50% and 75% of specimens show overgrowth and/or recrystallization; M (Moderate) - between 25% and 50% of specimens show overgrowth and/or recrystallization.

In total 35 taxa of calcareous nannofossils were identified throughout the studied sequence. The dominant taxon is represented by *Watznaueria barnesae*, which averages about 44%, but may reach up to 69% (Fig. 5-12) within the 22 m to 28 m interval. This taxon occurs with constantly lower relative percentage in the upper part of the section (Fig. 5-12).

The second most abundant component of the nannofloras is represented by species of the genus *Nannoconus* (Fig. 5-5B, 5-12). The nannoconid narrow-canal group includes *Nannoconus steinmannii*, *N. colomii* and *N. bermudezii* whereas the nannoconid wide-canal group includes *N. bucheri*, *N. vocontiensis*, *N. kamptneri*, *N. truittii* and *N. wassallii*, and shows a clear dominance over the narrow-canal group in all investigated samples. As shown and Fig. 5-12, the lowest part of the section (up to about 11 m) yields about 30% nannoconids, but the overlying interval (15.2 m to 27.7 m) includes a substantial decrease with variations between 7% and 11% coincident with an increase in the percentages of *Watznaueria barnesae*. The nannoconids increase substantially (to over 40% of the total nannofloras) towards the upper part of the section. All taxa

identified in the nannofloral assemblages belong to the NC 6 Biozone, coincident with the *Chiastozygus litterarius* Zone (Roth, 1978).

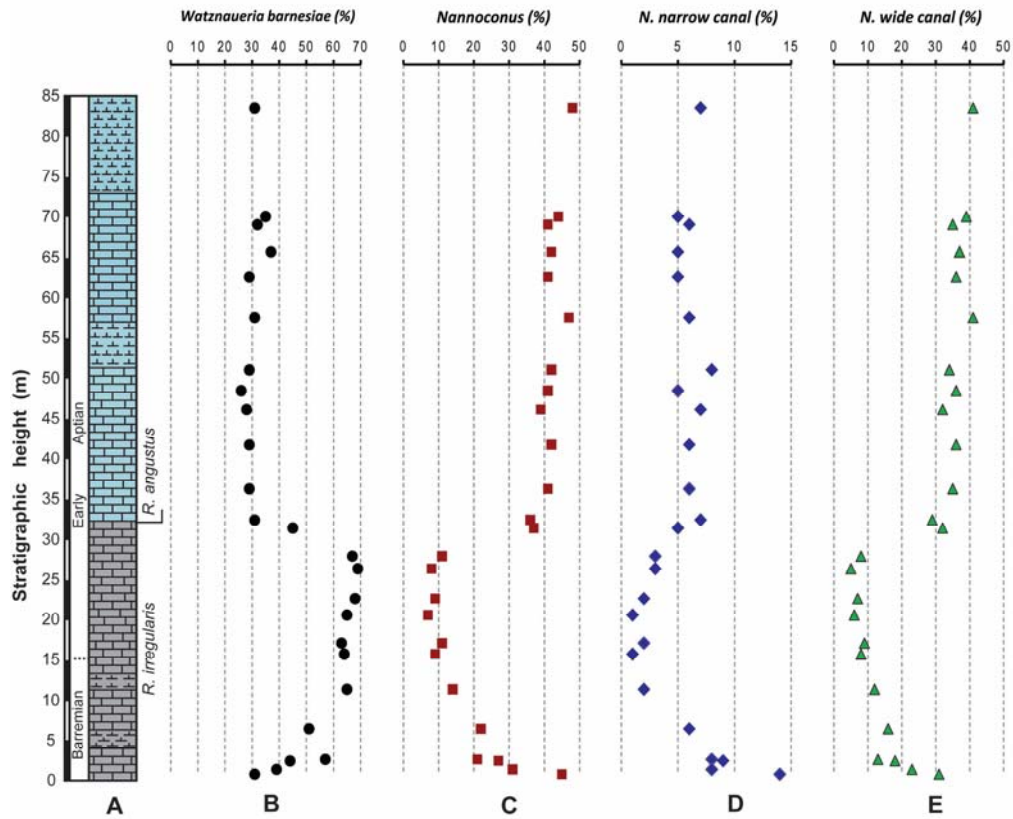


Figure 5-12 (A) Simplified lithological log and nannofossil events in the studied 85 m of El Pui section. Chemostratigraphic correlation and relative position of the Barremian-Aptian boundary discussed in the text suggest that the *R. angustus* appearance at El Pui coincides with its true first occurrence. B, C, D, and E: vertical variation in the relative abundances of *Watznaueria barnesiae*, *Nannoconus* sp., narrow canal *nannoconids*, and wide canal *nannoconids*, respectively. All the samples represented were analyzed using light microscope and SEM with EDS.

SEM micrographs shown in Fig. 5-5 illustrate a significant contribution of nannofossils to the matrix with highly abundant disaggregated nannoconids fragments. Qualitative EDS analyses also indicate CaCO_3 as the main constituent of the rock matrix, a finding that is in agreement with the bulk powder mineral results. The EDS results revealed additional minor presence of siliciclastic material (Sanchez-Hernandez and Maurrasse, 2014). X-ray maps generated on five samples (at 0, 15.2, 27.7, 32.3 and 69.7

m respectively) to monitor the elemental distribution of Ca, C, Al, Ti, Si and K in different areas of the matrix allow for further differentiation of the proportion of CaCO₃ with respect to the detrital fraction represented by Al, Ti and Si. The relative distribution of potassium was jointly monitored as a possible indication of illite and/or K-feldspar distribution, although we recognize that not all illite has K (Moore and Reynolds, 1997).

5.5 Discussion

5.5.1 Biochronology and paleontological significance of calcareous nannofossils in the El Pui section.

Paleontological studies of ammonites, together with benthic and planktonic foraminifera of the Cabó Marls (Peybernès and Souquet, 1973; Peybernès, 1976; Martínez, 1982; Berástegui et al., 1990; Bachmann and Willems, 1996; Bernaus et al., 2002, 2003; Moreno-Bedmar, 2010) assigned an overall upper Barremian- lower Aptian to the lower part of the sequence. That time interval can be estimated with an approximate duration of ~5 Ma (Walker et al., 2012).

The present study provides the first nannofossil data on the Cabò Marls (~800 m) that may allow a useful chronology based on microplankton taxa. For example, relative predominance of wide canal nannoconids from 32 m (Fig. 5-12E) upward concurs with previous studies (Erba, 1994, 2004) that interpreted nannofacies dominated by wide canal nannoconids as indicative of the early Aptian (see also Aguado et al., 1999). As in other hemipelagic to pelagic sections of the Western Tethys (Aguado et al., 1997), applying biostratigraphy to define the exact position of the Barremian - Aptian boundary in the El Pui sequence has proven to be problematic. Recent chemostratigraphic correlation of the El Pui with other Tethyan sections further proposed a Barremian – Aptian boundary at

about 15.5 m from the base of the studied section (Sanchez-Hernandez and Maurrasse, 2014). Even though the preservation state of the assemblages in the studied samples does not allow for a definitive chronologic assignment of the first occurrence (FO) of *Rhagodiscus angustus*, the fact that this taxon occurs elsewhere after the magnetic chron M0, above the Barremian-Aptian boundary (Erba, 1994), makes reasonable the assumption that its first identification in the studied section at 32 m (Fig. 5-12A) corresponds to its true first bioevent.

Microscopic observations show that the preservation of the nannofossils in the lower ~31 m of the El Pui section varies from poor to moderate, and the poorly preserved samples characteristically occur where the highest relative percentages (31% - 69%, Fig. 5-12) of the solution-resistant taxon *Watznaueria barnesae* are recorded. In addition, that part of the sequence contains the smallest relative percentages of nannoconids, as only three samples (out of 13 analyzed in the interval) have relative abundances above 30% (Fig. 5-12C). Such trends in abundance and preservation of nannofossils may indicate some measure of diagenetic overprint that might have affected their concentration. For instance, punctuated lower TIC values that occur at ~5.4 m (43%) and 13.0 m (44.9%) without significant variation in clays and TOC contents could be related to limited partial dissolution in microenvironments with lower pH because of prevailing dysoxic conditions (Sanchez-Hernandez and Maurrasse, 2014).

By contrast, the upper 54 m consistently yield calcareous nannofossils that are moderately preserved with a balanced relative abundance between *Watznaueria barnesae* and nannoconids (Fig. 5-12B, C). Alteration of nannofossil remains in the upper interval appears to be related to increased bioturbation.

In pelagic environments calcareous nannofossil assemblages can be altered because of selective dissolution in the calcium carbonate compensation realm resulting in an increase in the relative proportion of solution resistant taxa (McIntyre and McIntyre, 1971; Schneidermann, 1973; Roth and Coulbourn, 1982). Calcareous nannofossil assemblages dominated by *Watznaueria barnesae* have been reported as indicative of oligotrophic or low fertility environments (Roth, 1989; Roth and Krumbach, 1986; Premoli Silva et al., 1989; Watkins, 1989; Erba, 1992). They have also been considered to indicate heavily altered assemblages with respect to their original composition (Roth and Krumbach, 1986). However, the use of *W. barnesae* as indicative of oligotrophic conditions remains in question because it has been recognized as a strong eurytopic taxon (Mutterlose and Kessels, 2000; Lees et al., 2005; Aguado et al., 2013). Following these findings it has been proposed that percentage abundance of *W. barnesae* may indicate an inverse correlation with the success of other species, but not specific environmental signals (Lees et al., 2005; Aguado et al., 2013). Furthermore, as argued by Scarparo Cunha and Koutsoukos (1998) the trophic level associated with *W. barnesae* may vary as this species is recorded in laminated shales and marls of the Sergipe Basin, Brazil, interpreted as deposits of predominantly inner neritic environments (Koutsoukos et al., 1991a; 1991b).

In the case of the nannoconids, based on further knowledge of their environmental distribution and ecology, their classification as indicators of oligotrophic surface waters remains contentious (Bown, 2005). This uncertainty is further corroborated by their abundance and distribution in organic-rich layers during the late Barremian and the upper Albian (Kennedy et al., 2000; Herrle, 2002). Also, Scarparo Cunha and Koutsoukos

(1998) pointed out that most deposits rich in nannoconids usually yield low-diversity coccolith assemblages, which suggest community dynamics controlled by competitive displacement of very close resource utilization as nutrient levels fluctuated.

Although the preservation state of calcareous nannofossils assemblages in the El Pui section suggest partial alteration from the original composition, geochemical analyses of the sediment together with productivity proxies (TOC, $\delta^{13}\text{C}_{\text{org}}$) are consistent with the findings of Erba (1994), Mutterlose and Kessels (2000), Lees et al. (2005), and Aguado et al. (2013) that support a possible occurrence of assemblages dominated by *W. barnesae* and nannoconids in environments with high nutrient availability (P, Fe,) and enhanced primary productivity (Sanchez-Hernandez and Maurrasse, 2014). In order to better assess sediment provenance and accumulation rate in the El Pui section, we used integrated taxonomic data and chemostratigraphy (Sanchez-Hernandez and Maurrasse, 2014) based on carbon isotope ($\delta^{13}\text{C}_{\text{org}}$) segments defined by Menegatti et al. (1998).

5.5.2 Assessing the provenance of sediment components in the El Pui section

Facies distribution of rock sequences associated with the Organyà Basin is interpreted to indicate a marginal depression affected by adjacent Variscan crystalline rocks and surrounded by shallow-water carbonate platforms (Caus et al., 1990; Berástegui et al., 1990; García-Senz, 2002). In the case of the hemipelagic setting of the El Pui section, which is characterized by an unusually high accumulation rate (García-Senz, 2002), questions therefore arose regarding the provenance of the main contributors, which determined the high sediment accumulation in the restricted marginal basin. As for all sedimentary systems, it ensues three main possibilities: 1) siliciclastic contribution

from adjacent landmasses; 2) shedding of carbonate particles from the adjacent platforms; 3) *in situ* productivity.

5.5.2.1 Siliciclastic

Siliciclastics such as clays can be the major contributor to marginal basins as is known in the present (e.g., Cariaco Trench; Hoering, 1973). In the El Pui section TIC prevails throughout with consistently high values, mostly above 60%, albeit two punctuated short intervals that register ~ 43 and 45 % in the lower 15 m (Fig. 5- 4). The siliciclastic fraction accounts for ~ 30 % of the bulk material in the sediment (Fig. 11) with a clay content dominated by illite (Fig. 5-10). The sequence lacks primary sedimentary structures that can be associated with either proximal or distal turbidite depositional systems that could have enhanced the flux of allochthonous components. Therefore, the proportion of siliciclastic may not explain the high sedimentation rate in the basin.

5.5.2.2 Platform shedding

The transport of significant amounts of platform-derived carbonate bioclasts to deeper marine settings occurs mainly through high energy events (e.g. storms, turbidite currents, slumps) (Ericson et al., 1961; Droxler and Schlager, 1985). These allochthonous small bioclasts reveal characteristics of their original source and include typical neritic taxa (e.g., orbitolinids, annelids, miliolids, dasycladaceans photozoans, bivalves, brachiopods, calcareous algae) (Scholle et al., 1983; Scholle and Ulmer-Scholle, 2003; Flügel, 2010). Hence platform shedding could have been an important factor in the sedimentation system of the Organyà Basin with significant export of CaCO₃ to the pelagic environment. Platform shedding components would have been easily

recognizable as demonstrated elsewhere in basins adjacent to platforms (e.g., off the Great Bahama Bank, Ericson et al., 1961; Betzer et al., 2000; Kroon et al., 2000; Sergipe Basin, Brazil, Koutsoukos et al., 1991a; 1991b; Scarparo Cunha and Koutsoukos, 1998; Valanginian of the Vergol section SE France, Reboulet et al., 2003).

Extensive carbonate platform deposits (Peybernès and Souquet, 1973; Peybernès, 1976; Martínez, 1982; Caus et al., 1990; Berástegui et al., 1990; Dinarés-Turell and García-Senz, 2000; García-Senz, 2002; Bernaus et al., 2002; 2003) are coeval with the hemipelagic sediments of the Organyà Basin at El Pui. Facies analyses of the shallow-water deposits of the Organyà area indicate that the Barremian–Aptian carbonate platforms included biotic communities dominated by calcareous algae, rudists, and orbitolinids (Bernaus et al., 2002; 2003). However, the hemipelagic sediments of the basin show no evidence of shallow-water bioclasts (Fig. 5-6). The thin section analysis of 207 samples of the studied interval reveals a micritic matrix with absence of benthic taxa characteristic of the shallow water platform (Bernaus et al., 2002). Benthic foraminifera (5-6) are consistently very rare, and represent deeper water morphotypes as shown elsewhere in coeval deposits of the Tethys (Neagu and Cîrnaru, 2004). The lack of shallow-water components (Fig. 5-6) thus implies a limited contribution of allochthonous bioclasts to the total carbonate flux in the basin. The absence of sharp contrast between facies and the nearly homogeneous composition of the microfacies throughout the studied interval further suggest that transport of carbonate material by means of storm and marine currents may have been negligible.

Based on recent studies of past and present carbonate platform environments (e.g. Kroon et al., 2000; Wilson and Vecsei, 2005; Westphal et al., 2010) it is conceivable that

the absence of bioclasts from the shallow platforms could have been controlled by the degree of shelter provided by the existent physiography, more likely a flat homogeneous shelf (Caus et al., 1990, García-Senz, 2000). Because sediments of the studied section contain essentially planktonic components as remains of calcareous nannoplankton, they suggest that the inner part of the basin was outside the outer ramp or zone of influence of the platform areas during the latest Barremian – earliest Aptian. Assuming no accommodation control on the depositional system, therefore, accumulation would reflect conditions inherent to autecological factors that favored *in situ* productivity. Whether the absence of platform-derived components is due to the paleophysiography or prevailing low wind systems, this question is difficult to assess. Nonetheless, the sedimentological record of the El Pui section can be inferred to have accumulated away from aggradation of the platform ramp into the basin.

5.5.2.3 In situ carbonate production

Given that neither clastics from the adjacent landmasses, nor platform-derived particles provide sufficient evidence to constitute the bulk of the sediment components that contributed to enhance the accumulation rate of the El Pui sediments, a different controlling mechanism has to be invoked. The third alternative is to assess how *in situ* production of calcifying nannoplankton may account for the unusually thick sequence in that area of the Organyà Basin.

Periods of enhanced marine primary productivity in hemipelagic and pelagic environments may be recorded in sediments as enhanced deposition of biogenic carbonate and/or opal from the test of organisms, and also as higher organic carbon (OC) content (Zachos et al., 1989; Addison et al., 2012). However, these indicators do not

always concur because changes in biogenic carbonate dissolution rate and diagenetic processes can alter the proportion in which the biogenic carbonate is preserved in the sediment (e.g. Roth and Coulbourn, 1982; Aguado et al., 2013). Also, the OC content in sediments may depend on the respiration rate (oxygen availability) in the water column and the dynamic of microbial communities, as these organisms can follow different pathways for OM degradation regarding redox conditions (Valiela, 1984; Meyers, 1994). In the case of El Pui section the occurrence of high TOC values concurrent with high TIC and positive spikes in $\delta^{13}\text{C}_{\text{org}}$ (Fig. 5-4B, C, D) suggest enhanced primary productivity as the governing factor for the high TIC and TOC content in the sediment.

Large variations in the accumulation of biogenically derived calcium carbonate in marine environments related to various physiographic and ecologic factors have been recognized since the “Challenger Expedition” (Murray and Renard, 1891) and subsequent works (e.g., Ericson et al., 1961; Tracey et al., 1971; Ziveri et al., 1995; Beaufort and Heussner, 1999). Since sediment accumulation in the El Pui section took place in the bathyal zone, present knowledge of the marine environment permits to infer that dissolution due to undersaturation with respect to CaCO_3 related to the calcite compensation depth (Berger, 1970; 1976) may not account for much loss of carbonate from calcifying phytoplankton. Therefore, based on modern analogs of proposed relationship between production, transportation, and dissolution of coccoliths in the pelagic domain (Reid, 1962; Hulburt, 1962; Honjo, 1976; Kennett, 1982) we can postulate that at El Pui original assemblages and net production of biogenic carbonate should not be severely affected before accumulation.

Arguably, as the microscopic analysis revealed, some degree of dissolution may have taken place along prevailing oxygen-deficient unit (lower 31 m) because of partial acidification in the bottom waters, associated with enhanced export production of phytoplankton byproducts, partial remineralization and subsequent metabolic accumulation of CO₂ (Mucci et al., 2011). Investigations of comparable modern marine systems on the effects of such conditions on biogenic pelagic carbonate (e.g. Peterson, 1966; Berger, 1970; Colbourn et al., 1980; Roth and Colbourn, 1982; Cullen and Prell, 1984; Zachariasse et al., 1984; Burdige, 1991; Principato et al., 2006; Conley et al., 2009; Kemp et al., 2009) might support such assumption for the Organyà Basin. However, SEM analyses performed in the samples studied show that most of the micro-carbonate fragments in the El Pui could be attributed to calcareous nannofossils remains, coccoliths and nannoconids (Fig. 5-5). The distribution and appearance of the micro-carbonate particles suggest a higher influence of mechanical disaggregation of the nannoconids rather than dissolution (e.g., Lampert et al., 2002). Such indication implies that the applicability of traditional taxonomic methods and statistical analyses of microfaunal abundance and diversity may not provide reliable results (Roth and Colbourn, 1982) to estimate trophic level and true assessment of original assemblages in the studied section. In fact, there is increasing evidence from both modern (McIntyre and Bé, 1967) and past environments that the actual record in the sediment results from multiple environmental (Mutterlose et al., 2005) and preservation factors that influence the composition of nannofossil assemblages observed in the biomass (e.g., Molfino and McIntyre, 1990; Scarparo Cunha and Koutsoukos, 1998; Gaudy and Champalbert, 2003; Sun et al., 2013).

At this stage, we cannot prove exactly what caused such sustained high production of carbonate by the nannoplankton, but studies of modern environments also provide a glance at the complexity of a great number of critical factors that may influence the productivity of calcifying organisms whose records still remain mostly unknown in the Barremian–Aptian time interval studied (e.g., level of Ca^{++} in the ocean, Arp et al., 2001), the ecosystem food web (e.g., relationship between phytoplankton and protozooplankton, grazers and nutrient dynamics (Johnson and Sieburth, 1979; van Beusekom et al., 2009; Stelmakh, 2013) and intraspecific adaptative variability (Yakimov et al., 2007; Bowler and Scanlan, 2014; Kashtan, et al., 2014).

5.5.3 Significance of $\delta^{13}\text{C}$ /TOC/TIC/Biomarkers in assessing productivity rates

In an attempt to empirically assess the magnitude of productivity in the El Pui sequence, geochemical parameters tested to provide clues regarding the relationship between primary production and carbon isotope fractionation are applied. To evaluate such relationships our premise relies on established evidence that photosynthetic fixation of carbon involves an extensive negative fractionation (e.g. Fontugne and Duplessy, 1978; Hayes, 1993; Popp et al., 1997) attested by the fact that primary producers preferentially incorporate ^{12}C and therefore discriminate the ^{13}C . Given such circumstance, as primary productivity and OM decomposition proceed simultaneously in oxic ($\text{O}_2 > 2.0 \text{ ml / lH}_2\text{O}$) environments, the isotopic ratios are maintained in the reservoir because of proportional remineralization and upward recycling. However, in environments with sustained high primary productivity the oxygen demand in the water column increases significantly as the result of OM respiration. Furthermore, in basins with limited ventilation of bottom waters and high productivity these conditions

superimpose to create lasting oxygen depletion, hence heightening OC preservation from export production (Calvert et al., 1996; Paerl, 1997). In such cases, the removal rate of ^{12}C is uncompensated leading to ^{13}C enrichment in the reservoir that will be later reflected in the isotopic composition of the preserved OM. The mechanism associated with significant carbon sequestration hence causes positive excursions of the $\delta^{13}\text{C}$ curve that can be used in paleoenvironmental reconstruction.

In the use of the $\delta^{13}\text{C}_{\text{org}}$ profile it is also recognized that the isotope record is a blend of organic fractions that may be partially altered by the effects of extraneous factors. They can be related either to the ocean carbon reservoir (Arthur et al., 1985), biosynthetic fractionation (e.g. Hayes, 1993; Popp et al., 1997; Bentaleb et al., 1996; Boller et al., 2011) or maturity of the OM. Accordingly, the temporal fluctuations in the OC isotope values may be influenced to different extents by these factors regarding the depositional environment. Nonetheless profiles of $\delta^{13}\text{C}_{\text{org}}$ have been widely regarded to successfully reflect fluctuations in productivity (e.g. Coccioni et al., 1992; Meyers, 1997; Kuypers et al., 2002).

The fluctuating $\delta^{13}\text{C}_{\text{org}}$ pattern observed in the lower 14.3 m of the studied section (Fig. 5-4D) shows peaks of ^{12}C removal more pronounced than for the overall $\delta^{13}\text{C}_{\text{org}}$ global signature reported in the upper part of segment C1 and the onset of C2 (see Dumistrescu and Brassell, 2006, their Fig. 5-6 for a compilation of $\delta^{13}\text{C}_{\text{org}}$ in several sections). Despite assumed partial dissolution, the inverse variation of TIC with respect to TOC found at ~5.4 m, 6.1 m and ~13.0 m within that interval may suggest the occurrence of productivity pulses related to ecosystem variability as perhaps observed in modern

Black Sea (Grégoire, et al., 2004; Oguz, 2006; Boero et al., 2008; Stelmakh, 2013).

Sanchez-Hernandez and Maurrasse (2014) indicated that the phosphorous and iron levels in the El Pui section are comparable or higher than for the average shale (Wedepohl, 1971; 1991). Given that the basin was essentially a carbonate environment, such high values also imply that high availability of biolimiting nutrients was essential to maintain high productivity rate (Paytan and McLaughlin, 2007). In fact, significant enrichment of Ni in sediments from the section is consistent with increased transport to the sediment from particulate matter produced by calcareous nannoplankton.

As shown in Fig. 5-4B, the temporal trend of TOC in the El Pui section defines two different accumulation patterns of carbon sequestration: the earliest pattern straddles the latest Barremian and the earliest Aptian and extends from 0 to 31 m; the subsequent one continues into the early Aptian from 31 to 85 m. The lower trend is characterized by discontinuous TOC spikes ($> 1.0\%$) concurrent with positive excursions of $\delta^{13}\text{C}_{\text{org}}$ together with relatively elevated TIC values (Fig. 5-4C). Synchronous peaks on TOC, TIC and $\delta^{13}\text{C}_{\text{org}}$ suggest that enhanced local phytoplankton productivity in the Organyà Basin simultaneously intensified the oxygen demand in the water column and led to higher burial of organic carbon under oxygen-deficient sub-surface waters.

The predominance of nannofossils, concomitant with high accumulation rates controlled by the TIC, further imply long-term sustained dense phytoplankton blooms in surface waters that may have activated competitive exclusion, which severely limited the survival of other faunal groups (Busson and Noel 1991; Boero et al., 2008). However, the calcareous phytoplankton production alone is unlikely to justify the amount of OM preserved, because the OM/CaCO₃ ratio of these organisms is too low (1/6, Hay 2002;

Sanchez-Hernandez and Maurrasse, 2014). Perhaps, the apparent excess OM preserved in the El Pui sediments originated from a mechanism similar to that documented in modern oceans whereby phytoplankton exude organic compounds or transparent exopolymer particles (Jiao et al., 2010; Van Oostende et al., 2013). Such enrichment of labile compounds in surface waters also stimulates bacterial growth and oxygen demand in the water column.

Concerning the unusual high abundance of biogenically derived carbonate from primary producers, a comparable case is related to calcifying coccoid cyanobacteria in the Cenomanian-Turonian restricted basins of the Indidura Formation at Parras, northeastern Mexico (Duque-Botero and Maurrasse, 2005; 2008; Duque-Botero et al., 2009). In that basin the coccoid cyanobacteria dominated in a dysoxic to anoxic environment and produced between 43.0 to 78.3% carbonate that led to an accumulation rate ranging from 6.2 cm/ky to 10.0 cm/ky. Hence the results from the El Pui sequence may not be exceptional in the geologic record, and they suggest that similar conditions may have persisted in the semi-restricted Organyà Basin with different assemblages that led to high TIC together with elevated TOC as a result of increased biological activity in the photic zone.

Because of sustained terrigenous fluxes (Sanchez-Hernandez and Maurrasse, 2014) it is conceivable that significant OM could have been transported to the Organyà Basin, as demonstrated for other marginal basins (DSDP Site 398, Arthur et al., 1979; modern Cariaco Basin, Edgar et al., 1973a; Hoering, 1973), but the absence of higher *n*-alkanes ($C > 25$) and enriched presence of *n*-alkanes with C number $C < 20$ (Figs. 5-7, 5-8), are indicative of autochthonous OM sources outweighing terrestrial plant input. Thus

the *n*-alkanes data lend support to essentially a primary marine phytoplankton origin of the OM (Cranwell, 1973; Cranwell et al., 1987; Forster et al., 2004; Peters et al., 2005). The carbon isotopes values further corroborate the biomarker data. Indeed, given the very large negative fractionation of organically-derived carbon compounds from terrestrial environments, an increase in recycled respired (¹³C- depleted) CO₂ would have greatly depleted the isotopic composition of the TOC and caused a more negative shift of the δ¹³C_{org}. The results do not concur with such ¹³C_{org}- depleted record in the carbon isotope profile. Instead, a sustained increase is observed in the δ¹³C_{org} from 0 to ~20 m with subsequent stable values that further indicates minimal involvement of terrestrially derived organic matter (Sanchez-Hernandez and Maurrasse, 2014).

5.5.4 Assessing sediment accumulation rate

Since radiometric data are non-existent for the sedimentary sequence of the Organyà Basin, it is assumed that previous time span estimates are valid and coherent with the GSA Time Scale (Walker et al., 2012).

As the present study includes only the basal part of the El Pui sequence and precise biochronology is difficult, to better constrain the sedimentation rate in the studied section the carbon isotope segments are used, which can provide a more reliable time frame based on correlation of known sections (Menegatti et al., 1998; Moullade et al., 1998; Kuhnt et al., 1998; de Gea et al., 2003; Erba, 2004; Stein et al., 2011, 2012; DeBond et al., 2012; Papp et al., 2013). The 85 m studied at El Pui comprise the upper part of δ¹³C_{org} isotope segment C1, the entire segment C2 and possibly the lower part of segment C3 (Menegatti et al., 1998; Sanchez-Hernandez and Maurrasse, 2014). Thus in the present state of the study segment C2 at El Pui extends from 15.5 m to at least about

70.7 m, which amounts to a thickness of ~ 55 m (Fig. 5-4D). In most sections this segment is confined to the upper Barremian - lowermost Aptian time interval. Although the actual duration is yet to be fully constrained, segment C2 has been shown to span between ~800 kyr and 1.2 myr (e.g. Erba et al., 1999; Erba 2004, DeBond et al., 2012). If we assume a similar extent for segment C2 in the El Pui section, the approximate overall dry bulk sediment accumulation rate for the 55 m of segment C2 would be constrained between at least ~5 cm/ky – 7.5 cm/ky, which is certainly high for marine hemipelagic facies.

As compared to El Pui sediments, similar high sediment accumulation rates (~5.0 - 7.5 cm/ky, or up to 10 cm/ky) have been reported for Lower Cretaceous sediments of a marginal basin at DSDP Site 398 (Arthur, 1979). That site also includes a lasting record of oxygen deficient-conditions. Sediments of Site 398 differ significantly from the rocks of the El Pui sequence, because their main components are reported to consist predominantly of siliciclastic materials related to fluxes from large deltas bordering the Proto-Atlantic during the Early Cretaceous (Arthur, 1979). In fact, carbonate values (see Arthur, 1979, Fig. 5-2) for the late Barremian - early Aptian at Site 398 yield a calculated average TIC of ~ 42% compared to an average of 70% recorded within the same time interval in the El Pui sediments. Also, unlike the El Pui sediments, the organic matter at Site 398 is predominately land derived (Arthur, 1979), hence they indicate a stronger steady input of terrestrially derived materials at that location.

For comparison of an approximate modern analog, perhaps the most closely related physiographic condition to the Organyà Basin (Caus et al., 1990; Berástegui et al., 1990) is that of the Cariaco Basin (Edgar et al., 1973a; 1973b). In fact, the Cariaco Basin

is a small pull-apart depression (length ~ 210 Km; width ~ 62 Km, and 82 Km, respectively; depth at the eastern sub-basin being 2550 m and the western 1380 m) in the Venezuelan continental margin (Edgar et al., 1973a; 1973b). The basin has anoxic waters below 360 m, and reveals high wet sediment accumulation rates of 75 cm/ky (Spiker and Simoneit, 1982). Like the inferred reconstruction of the Organyà Basin, the Cariaco marginal depression has restricted circulation, is adjacent to carbonate platforms and proximal to crystalline substrates. Published porosity measurements for the Cariaco Basin sediments obtained from undisturbed individual samples yielded values of 40% - 67%, and more consistently 56%, respectively (Edgar et al., 1973b). The highest values (50 – 75 cm/kyr) of wet accumulation rates (Spiker and Simoneit, 1982), and the average porosity data (56%), thus yield dry bulk accumulation rates of 22 - 33 cm/kyr, respectively.

These extremely high values apparently exceed the estimated values for the El Pui sequence, although they could actually be lessened due to the fact that Cariaco Basin sediments are normally consolidated (Bjørlykke, 2010), whereas the Cabò Marls are over consolidated such that intergranular volume is negligible. Unlike the Cabò Marls, however, the high rates obtained for the Cariaco Basin stem essentially from terrigenous materials in the sediments, as the TIC averages only ~ 25% (Edgar et al., 1973a). Similarly, fatty alcohols and acids with C chain lengths > C₂₀ generally considered to be characteristic of the waxes of higher terrestrial plants define the organic matter in the Cariaco Basin (Hoering, 1973).

For further comparison, other modern basins with different physiographic settings and accumulating hemipelagic sediments show lower wet sedimentation rates,

e.g., 6 cm/ky proposed for slope sediments in the Gulf of Mexico (Aharon and Fu, 2000), and rates > 10 cm/ky reported for areas of the eastern Mediterranean Sea (Mercone et al., 2000). These locations also show a prevalence of terrigenous components.

The most important finding between the sites used for comparison with the El Pui sediments highlights the fact that values for the sedimentation rates of the hemipelagic facies of the Organyà Basin depended primarily on the carbonate production. The non-carbonate fraction remains consistently on average less than 30% (Fig. 5-11). On that basis, the steady pattern of the proportion of the siliciclastic components in the El Pui sequence provides robust evidence to define its singularity and assume that the high sedimentation rate in the El Pui sequence was essentially related to steady high calcareous nannofossil productivity.

5.5.5 Characterization of terrestrial fluxes in the Organyà Basin

The distribution of the non-carbonate fraction in the El Pui sediments (Fig. 5-11) confirms sustained terrestrial fluxes to the basin, and assessing the sources of the mineral components provides a better understanding of the nutrient delivery mechanism and its effect on productivity.

Illite is the most abundant clay mineral in carbonate rocks and shales where its concentration generally represents the source composition rather than diagenetic alterations (Weaver, 1958). Burial diagenesis can also produce alteration of smectite into illite (Hower et al., 1976; Deer et al., 1977; Burtner and Warner, 1986; Eslinger and Pevear, 1988; Scott, 1992), but a high relative percentage of illite compared with the other clay minerals and small variability of its content with depth are evidence of a limited diagenetic effect (Weaver, 1958).

Sample Id	Height (m)	Gycolated			
		Illite-Smec.	Illite	Kaolinite	Chlorite
C10-04	0.7	6%	90%	1%	3%
C10-17	5.4	10%	77%	5%	9%
C10-19	6.1	11%	84%	2%	4%
C10-31	13.7	10%	73%	2%	15%
C10-58	20.8	9%	82%	2%	7%
C10-77	27.7	12%	82%	1%	5%
C10-85	31.3	10%	79%	2%	9%
C11-109	41.8	11%	78%	4%	7%
C11-169	62.0	13%	75%	3%	10%
C11-205	81.1	17%	77%	2%	4%

Table 5-1 Semi-quantitative clay mineral results from diffraction patterns obtained from EG-solvated samples. XRD traces demonstrated the presence of expandable clay. The EG-solvated provide the most diagnostic patterns for analysis of the clay minerals (Moore and Reynolds, 1997)

At El Pui the percentage of illite fluctuates consistently between 73% and 90%, and mixed layer illite/smectite does not surpass 17% (Table 5-1, Fig. 5-10). Such trend in relative concentration indicates similar content with depth, hence providing further

evidence against significant diagenetic transformations in the sediment. The presence of stable mineral phases of chlorite (Fig. 5-9) along with abundant illite indicate a low degree of thermal alteration consistent with provenance from a source related to erosion of previous mudrocks affected by low-grade metamorphism (Weaver, 1958; Ehlers and Blatt, 1999).

Chlorite is a common mineral characteristic of low-grade metamorphism, zeolite to greenschist facies (Deer et al., 1977); increasing lithostatic pressure and temperature can also induce thermal alteration of smectite into chlorite (Ferry et al., 1983). The random and variable occurrence of chlorite in the sequence (Table 5-1) further attributes its origin to terrigenous fluxes instead of *in situ* transformation in the sequence after deposition. The temporal distribution of clay minerals and mineral constituents characteristic of the El Pui sediments (Fig. 5-10) suggests that they derived from adjacent low-grade metamorphic rocks involved in earlier Paleozoic tectonic history (Variscan) of the area (Peybernes, 1976; Muñoz et al., 1984; García-Senz, 2002; Ábalos et al., 2002).

The relative high abundance of quartz with respect to feldspars (Fig. 5-11, Table 5-2) reveals a certain degree of sediment maturation related to the effects of chemical alteration, slow erosion and mechanical breakdown.

Since conceptual reproduction of environmental conditions in the Organyà Basin indicates absence or limited upward recycling of biolimiting nutrients (Sanchez-Hernandez and Maurrasse, 2014), data from the present study permits further inference that steady riverine fluxes carrying phosphorus from watersheds with apatite-bearing Paleozoic bedrocks (García-Alcade et al., 2002; Ábalos et al., 2002) were a governing factor controlling the unusually high calcareous phytoplankton contribution in the basin.

Sample Id	Height (m)	Clay	Quartz	K-feldspar	P-feldspar	Calcite	Dolomite	Pyrite/Marc.
C10-04	0.7	5%	17%	0%	5%	72%	1%	1%
C10-17	5.4	12%	25%	0%	5%	51%	2%	5%
C10-19	6.1	15%	25%	0%	7%	52%	1%	0%
C10-31	13.7	13%	14%	0%	6%	64%	1%	1%
C10-58	20.8	7%	9%	0%	3%	78%	3%	1%
C10-77	27.7	5%	7%	1%	2%	84%	1%	1%
C10-85	31.3	6%	10%	1%	3%	76%	3%	1%
C11-109	41.8	3%	6%	1%	2%	86%	1%	1%
C11-169	62.0	9%	14%	0%	5%	72%	0%	1%
C11-205	81.1	9%	17%	2%	5%	65%	1%	0%

Table 5-2 Semi-quantitative bulk mineral XRD results for the random powder packs of the 10 samples selected along the section. These results were complemented with EDS analyzes to generate an average bulk mineral distribution for the entire section.

Paleoclimatic reconstruction based on the clay mineral distribution was not the focus of the clay mineral analysis in this work, but the distribution of the clay fraction in the El Pui section is consistent with temperate-warm/ humid conditions as proposed by Aguado et al. (2013) despite the limited abundance of kaolinite whose deposition may have been controlled by the basin paleophysiography (Ruffell et al., 2002; Stein et al., 2011). Perhaps, a modern analog can be found along the present western coast of the

Black Sea where phytoplankton development is sustained during the whole year because surface waters are almost continuously enriched in nutrient from constant discharge of the Danube (Grégoire et al., 2004; Oguz, 2006).

5.6 Conclusions

The present study of the basal 85 m of the El Pui section reveals that unusually high accumulation rates (~5 cm/ky – 7.5 cm/ky) from the latest Barremian–earliest Aptian were primarily controlled by high carbonate content (up to 88%). SEM and petrographic analyses suggest high input of carbonate from calcareous nannofossil remains, which is consistent with high phytoplankton productivity as indicated by the geochemical data.

Similar high sediment accumulation rates (5.0 cm/ky - 10 cm/ky) have been reported for Lower Cretaceous sediments from other marginal basins, but unlike the El Pui sequence they primarily contain terrigenous components. In contrast to similar coeval Cretaceous basins (e.g. DSDP Site 398; Moldavids, Carpathians) and modern marginal basins (e.g. Cariaco Basin), the hemipelagic facies of El Pui are distinctive because of the high carbonate content derived from calcareous nannofossils.

Organic-rich levels (TOC: 0.5 - 1.7%) concurrent with positive excursions in $\delta^{13}\text{C}_{\text{org}}$ imply enhanced preservation of OM from export production. In addition, pronounced peaks of $\delta^{13}\text{C}_{\text{org}}$ higher than the global average suggest that local factors related to primary productivity were superimposed to global forcing mechanisms and intensified the ^{12}C removal. Organic geochemical analyses (*n*-alkanes, $\delta^{13}\text{C}_{\text{org}}$) further support an autochthonous origin of the OM.

The average non-carbonate fraction of the sediments at El Pui accounts only for 30% of the components, and consists predominantly of clays (9%) and quartz (14%). The clay mineral assemblages are dominated by illite (> 73%), which is compatible with a source from low-grade metamorphic rocks involved in earlier Paleozoic tectonic history (Variscan) of the area. Ubiquitous presence of the detrital minerals in the section further suggests steady input of nutrients by riverine fluxes carrying phosphorus that sustained high fertility of surface waters inducing high calcareous phytoplankton productivity.

The results provide fundamental evidence that further our understanding on the controlling factors leading to high carbonate production recorded in the hemipelagic sediments of El Pui in the Organyà Basin. This study highlights the critical role that special physiographic conditions in restricted basins can play in creating uncommon environments that stimulate sustained primary productivity and influence the overall sedimentation. Many aspects of calcifying nannoplankton assemblages and ecosystems still remain conjectural, further multiproxy studies of the geological record are required in order to improve our assessment of all the factors involved. We can infer from the uniformity of the facies that accommodation space and sediment supply in the El Pui sequence were roughly balanced within the time interval corresponding to the lower part of the studied section.

5.7 Acknowledgments

This research was financially supported by the Goodfriend Memorial Funds. We are most grateful to Dr. Rudolf Jaffe for providing lab resources for the biomarker analysis. Diane Pirie and Thomas Beasley are kindly acknowledged for their help with instrumentation and materials at FIU. We thank our colleague Josep Moreno-Bedmar for

valuable logistical help and discussion about the section. Mr. Ferran is gratefully acknowledged for his gracious authorization to work on his private hunting property. Supplies and other laboratory materials were generously provided by the Earth and Environment Department at FIU. We are most grateful also to Bill Anderson and John Harris for the carbon isotope analyses. Y. S-H is thankful for the DEA fellowship from the FIU Graduate School that provided valuable time to do field work and process the samples. We thank Relu Dumitru Roban and an anonymous reviewer for constructive criticism that helped to improve the manuscript. We are also thankful to the chief editor Eduardo Koutsoukos for helpful editorial comments.

5.8 References

- Ábalos, B., Gil-Ibarguchi, J.I., et al., 2002. Variscan and pre-Variscan Tectonics, in: Gibbons, W., and Moreno, T. (Eds.), *The Geology of Spain*. The Geological Society of London, pp. 155–183.
- Addison, J.A., Finney, B., Dean, W., Davies, M., Mix, A., Stoner, J., and Jaeger, J., 2012. Productivity and sedimentary $\delta^{15}\text{N}$ variability for the last 17,000 years along the northern Gulf of Alaska continental slope. *Paleoceanography* 27, 1206.
- Aguado, R., Company, M., Sandoval, J. Tavera, J. M., 1997. Biostratigraphic events at the Barremian/Aptian boundary in the Betic Cordillera (southern Spain). *Cretaceous Research* 18, 309–329.
- Aguado, R., Castro, J.M., Company, M., Gea, G.A. de, 1999. Aptian bioevents – an integrated biostratigraphic analysis of the Almadich Formation, Inner Prebetic Domain, SE Spain. *Cretaceous Research* 20, 663–683.
- Aguado, R., de Gea, G.A., Castro, J.M., O’Dogherty, L., Quijano, M.L., Naafs, B.D.A., Pancost, R.D., 2013. Late Barremian–early Aptian dark facies of the Subbetic (Betic Cordillera, southern Spain): Calcareous nannofossil quantitative analyses, chemostratigraphy and palaeoceanographic reconstructions, *Palaeogeography, Palaeoclimatology, Palaeoecology* 395, 198–221.
- Aharon, P., Fu, B., 2000. Microbial sulfate reduction rates and sulfur and oxygen isotope fractionations at oil and gas seeps in deepwater Gulf of Mexico. *Geochimica et Cosmochimica Acta* 64(2), 233–246.

- Arp, G., Reimer, A., Reitner, J., 2001. Photosynthesis-induced biofilm calcification and calcium concentrations in Phanerozoic oceans. *Science* 292, 1701–1704.
- Arthur, M. A., 1979. North Atlantic Cretaceous Black Shales: The Record at Site 398 and a brief comparison with other occurrences. In Sibuet, J.-C, Ryan, W.B.F., et al., *Initial Reports of the Deep Sea Drilling Project*, v. 47, Part 2: Washington (U.S. Government Printing Office), pp. 451–468.
- Arthur, M.A., Dean, W.E., Schlanger, S.O., 1985, Variations in the global carbon cycle during the Cretaceous related to climate, volcanism, and changes in atmospheric CO₂: In Sundquist, E.T., and Broecker, W.S. (Eds.), *The Carbon Cycle and Atmospheric CO₂: Natural Variations Archean to Present*, Geophysical Monographs, American Geophysical Union 32, pp. 504–529.
- Bachmann, M., Willems, H., 1996. High-frequency cycles in the upper Aptian carbonates of the Organyà basin, NE Spain. *Geologische Rundschau* 85(3), 586–605.
- Bayhan, E., Ergin, M., Temel, A., Keskin, Ş., 2001. Sedimentology and mineralogy of surficial bottom deposits from the Aegean–Çanakkale–Marmara transition (Eastern Mediterranean): effects of marine and terrestrial factors. *Marine Geology* 175(1), 297–315.
- Beaufort, L., Heussner, S., 1999. Coccolithophorids on the continental slope of the Bay of Biscay – production, transport and contribution to mass fluxes. *Deep-Sea Research II* 46, 2147– 2174.
- Bentaleb, I., Fontugne, M., Descolas-Gros, C., Girardin, C., Mariotti, A., Pierre, C., Brunet, C., Poisson, A., 1996. Organic carbon isotopic composition of phytoplankton and sea–surface pCO₂ reconstructions in the Southern Indian Ocean during the last 50,000 yr. *Organic Geochemistry* 24(4), 399–410.
- Berástegui, X., García-Senz, J.M., Losantos, M., 1990. Tectonosedimentary evolution of the Organyà extensional basin (Central South Pyrenean Unit, Spain) during the Lower Cretaceous. *Bulletin de la Société Géologique de France* 8 (VI), 251–264.
- Berástegui X., Losantos M., Muñoz J.A., Puig de Fàbregas. C., 1993. Tall geològic del Pirineu central 1:200 000. Map and explanations. *Servei Geològic de Catalunya*, Barcelona, 58 pp.
- Berger, W. H. 1970. Planktonic foraminifera: Selective solution and the lysocline. *Marine Geology* 8(2), 111–138.
- Berger, W. H., 1976. Biogenous deep-sea sediments: Production, preservation, and interpretation. In: Riley, J. P., Chester, R. (Eds.), *Treatise on Chemical Oceanography* 5. New York, Academic Press. pp. 265 – 388

- Bernaus, J.M., Arnaud–Vanneau, A., Caus, E., 2002. Stratigraphic distribution of Valanginian Early Aptian shallow–water benthic foraminifera and algae, and depositional sequences of a carbonate platform in a tectonically–controlled basin: the Organyà Basin, Pyrenees, Spain. *Cretaceous Research* 23, 25–36.
- Bernaus, J.M., Arnaud–Vanneau, A., Caus, E., 2003. Carbonate platform sequence stratigraphy in a rapidly subsiding area: the Late Barremian – Early Aptian of the Organyà Basin, Spanish Pyrenees. *Sedimentary Geology* 159 (3–4), 177–201.
- Betzler, C., Pfeiffer, M., Saxena, S., 2000. Carbonate shedding and sedimentary cyclicities of a distally steepened carbonate ramp (Miocene, Great Bahama Bank). *International Journal of Earth Sciences* 89, 140–153.
- Bjørlykke, K., 2010. *Petroleum Geoscience: From Sedimentary Environments to Rock Physics*. Springer Springer–Verlag Berlin Heidelberg, pp. 509.
- Boero, F., Bouillon, J., Gravili, C., Miglietta, M. P., Parsons, T., Piraino, S., 2008. Gelatinous plankton: irregularities rule the worlds (sometimes). *Marine Ecology Progress Series* 356, 299–310.
- Boller, A. J., Thomas, P. J., Cavanaugh, C. M., Scott, K. M., 2011. Low stable carbon isotope fractionation by coccolithophore *RubisCOco*. *Geochimica et Cosmochimica Acta* 75, 7200 – 7207.
- Bowler, C., Scanlan, D. J., 2014. Being selective in the *Prochlorococcus* collective. *Science*, 344–366.
- Bown, P.R., Young, J.R., 1998. Techniques. In: Bown, P.R. (Ed.), *Calcareous Nannofossil Biostratigraphy*. Chapman and Hall, London, pp. 16–28.
- Bown, P.R., 2005. Early to mid-Cretaceous calcareous nannoplankton from the northwest Pacific Ocean, Leg 198, Shatsky Rise. In Bralower, T.J., Premoli Silva, I., and Malone, M.J. (Eds.), *Proc. ODP, Sci. Results, 198: College Station, TX (Ocean Drilling Program)*, 1–82.
- Bralower, T.J., Arthur, M.A., Leckie, R.M., Sliter, W.V., Allard, D.J., Schlanger, S.O., 1994. Timing and paleoceanography of oceanic dysoxia/anoxia in the Late Barremian to Early Aptian. *Palaios* 9, 335–369.
- Brassell, S.C., Dumitrescu, M., ODP Leg 198 Shipboard Scientific Party, 2004. Recognition of alkenones in a lower Aptian porcellanite from the west–central Pacific. *Organic Geochemistry* 35, 181–188.
- Burdige, D. J., 1991. The kinetics of organic matter mineralization in anoxic marine sediments. *Journal of Marine Research* 49, 727–761.

- Burtner, R. L., Warner, M. A., 1986: Relationship between illite/smectite diagenesis and hydrocarbon generation in lower Cretaceous Mowry and Skull creek shales of the northern rocky mountain area. *Clay and clay minerals* 34(4), 390–402.
- Busson, G., Noël, D., 1991. Les calcaires fins pélagiques des temps liasiques sont primordialement faits d'une seule espèce du nannophytoplancton calcaire: la schizosphère *S. puntulata*. *C. R. Academie de Sciences de Paris* 313, 795–800.
- Calvert, S.E., Bustin, R.M., Ingall, D. E., 1996. Influence of water column anoxia and sediment supply on the burial and preservation of organic carbon in marine shales. *Geochimica et Cosmochimica Acta* 60(9), 1577–1593.
- Caus, E., García-Senz, J. M., Rodés, D., Simón, A., 1990. Stratigraphy of the Lower Cretaceous (Berriasian-Barremian) sediments in the Organyà Basin, Pyrenees, Spain. *Cretaceous Research* 11, 313–320.
- Coccioni, R., Erba, E., Premoli Silva, I., 1992. Barremian-Aptian calcareous plankton biostratigraphy from the Gorgo a Cerbara section (Marche, central Italy), and implications for plankton evolution. *Cretaceous Research* 13, 517–537.
- Colbourn, W.T., Parker, E., Berger, W. H. 1980. Faunal and solution patterns of planktonic Foraminifera in surface sediments of the North Pacific. *Marine Micropaleontology* 5, 329–399.
- Conley, D. J., Björck, S., Bonsdorff, E., Carstensen, J., Destouni, G., Gustafsson, B. G., Hietanen, S., Kortekaas, M., Kuosa, H., Meier, H. E. M., Müller-Karulis, B., Nordberg, K., Norkko, A., Nürnberg, G., Pitkänen, H., Rabalais, N. N., Rosenberg, R., Savchuk, O. P., Slomp, C. P., Voss, M., Wulff, F., and Zillén, L. 2009. Hypoxia-related processes in the Baltic Sea, *Environmental Science Technology* 43, 3412–3420.
- Cranwell, P. A., 1973. Chain-length distribution of n-alkanes from lake sediments in relation to post- glacial environmental change. *Freshwater Biology* 3, 259–265.
- Cranwell, P. A., Eglinton, G., Robinson, N., 1987. Lipids of aquatic organisms as potential contributors to lacustrine sediments II. *Organic Geochemistry* 11, 513–527.
- Cullen, J. L., Prell, W. L., 1984 Planktonic foraminifera of the northern Indian Ocean: Distribution and preservation in surface sediments. *Marine Micropaleontology* 9 (1), 1–52.
- De Gea, G. A., Castro, J. M., Aguado, R., Ruiz-Ortiz, P. A., Company, M., 2003. Lower Aptian carbon isotope stratigraphy from a distal carbonate shelf setting: the Cau section, Prebetic zone, SE Spain. *Palaeogeography, Palaeoclimatology, Palaeoecology* 200(1), 207–219.

- Dean, W. E., Arthur, M.A., Claypool, G.E., 1986. Depletion of ^{13}C in Cretaceous marine organic matter: source, diagenetic, or environmental signal? *Marine Geology* 70, 119–157.
- DeBond, N., Oakes, R.L., Paytan, A., Wortmann, U.G., 2012. Early Aptian carbon and sulphur isotope signatures at ODP Site 765. *Isotopes in environmental and health studies* 48(1), 180–194.
- Deer, W. A., Howie, R.A., Zussman, J., 1977. *An Introduction to the Rock-Forming Minerals*. Longman Publisher, pp. 528.
- Dera, G., Pellenard, P., Neige, P., Deconinck, J. F., Pucéat, E., Dommergues, J. L., 2009. Distribution of clay minerals in Early Jurassic Peritethyan seas: Palaeoclimatic significance inferred from multiproxy comparisons. *Palaeogeography, Palaeoclimatology, Palaeoecology* 271(1), 39–51.
- Dinarès-Turell, J., García-Senz, J., 2000. Remagnetization of Lower Cretaceous limestones from the southern Pyrenees and relation to the Iberian plate geodynamic evolution. *Journal of Geophysical Research* 105 (B8), 19405–19418.
- Droxler, A.W., Schlager, W., 1985. Glacial versus interglacial sedimentation rates and turbidite frequency in the Bahamas. *Geology* 13, 799–802.
- Dumitrescu, M., Brassell, S.C., 2005. Biogeochemical assessment of sources of organic matter and paleoproductivity during the early Aptian Oceanic Anoxic Event at Shatsky Rise, ODP Leg 198, *Organic Geochemistry* 36(7), 1002–1022.
- Dumitrescu, M., Brassell, S. C., 2006. Compositional and isotopic characteristics of organic matter for the early Aptian Oceanic Anoxic Event at Shatsky Rise, ODP Leg 198, *Palaeogeography, Palaeoclimatology, Palaeoecology* 235(1–3), 168–191.
- Dunham, K.W, Meyers, P.A., Ho, E.S., 1988. Organic geochemistry of Cretaceous black shales and adjacent strata from the Galicia Margin, North Atlantic Ocean. *Proceedings of the Ocean Drilling Program, Scientific Results, Vol. 103*.
- Duque-Botero, F., Maurrasse, F., 2005. Cyanobacterial productivity, variations in the organic carbon, and facies of the Indidura Formation (Cenomanian-Turonian), Northeastern Mexico. *Journal of Iberian Geology* 31, 85–98.
- Duque-Botero, F., Maurrasse, F., 2008. Role of cyanobacteria in C_{org} -rich deposits: an example from the Indidura Formation (Cenomanian-Turonian), northeastern Mexico. *Cretaceous Research* 29, 957-964.
- Duque-Botero, F., Maurrasse, F.J-M-R., Hickey-Vargas, R., Melinte, M., Jaffe, R., and Lopez-Oliva, J. G., *Microspheroids accumulation and geochemistry of an anoxic basin of the Cenomanian/Turonian: The record of the Indidura Formation, NE Mexico*. 2009. (SEPM Special Publication) *Geologic Problem Solving with*

- Microfossils: A Volume in Honor of Garry D. Jones. Society for Sedimentary Geology. SEPM Special Publication 93, 171–186.
- Edgar, N. T., Saunders, J.B., Bolli, H. M., Boyce, R. E., Broecker, W. S., Donnelly, T. W., Gieskes, J.M., Hay, W.W., Horowitz, R. M., Maurrasse, F., Perez Nieto, H., Prell, W., Premoli-Silva, I., Riedel, W.R., Schneidermann, N., Waterman, L., 1973a. Initial Reports of the Deep Sea Drilling Project, v. 15 (U.S. Government Printing Office), pp. 1137.
- Edgar, N. T., Saunders, J. B., et al., 1973b. Site 147. In Edgar, N. T., Saunders, J. B., et al., Initial reports. DSDP, 15: Washington (U.S. Govt. Printing Office), 169–178.
- Ehlers, E. G., Blatt, H. 1999. Petrology Igneous, Sedimentary, and Metamorphic. W. H. Freeman & Co. Publisher, pp. 732.
- Erba, E., 1992. Calcareous Nannofossils distribution in pelagic rhythmic sediments (Aptian–Albian Piobbico Core, Central Italy). *Rivista Italiana di Paleontologia y Stratigrafia* 97, 455–484.
- Erba, E., 1994. Nannofossils and superplumes: The early Aptian “nannoconid crisis”. *Paleoceanography* 9(3), 483–501.
- Erba, E., 2004. Calcareous nannofossils and Mesozoic oceanic events. *Marine micropaleontology* 52, 85–106.
- Erba, E., Channell, J.E.T., Claps, M., Jones, C., Larson, R., Opdyke, B., Premoli Silva, I., Riva, A., Salvini, G., Torricelli, S., 1999. Integrated stratigraphy of the Cismon APTICORE (Southern Alps, Italy): a “reference section” for the Barremian–Aptian interval at low latitudes. *Journal of Foraminiferal Research* 29, 371–392.
- Ericson, D. B., Ewing, M., Wollin, G., Heezen, B. C., 1961. Atlantic deep-sea sediments cores. *Geological Society of America Bulletin*, 72 (2), 193–286.
- Eslinger, E., Pevear, D., 1988. Clay Minerals for Petroleum Geologists and Engineers. SEPM Short Course Notes no. 22, pp. 405 Tulsa: Society of Economic Paleontologists and Mineralogists.
- Ferry, S., Cotillon, P., Rio, M., 1983. Diagenèse croissante des argiles dans des niveaux isochrones de l’alternance calcaire-marne valanginienne du bassin vocontien. Zonation géographique. *Comptes Rendus de l’Académie des Sciences de Paris Série II* 297, 51–56.
- Flügel, E., 2010. Microfacies of Carbonate Rocks: Analysis, Interpretation and Application. Springer-Verlag, Berlin Heidelberg, Germany, Second ed. pp 984.

- Föllmi, K. B., 2012. Early Cretaceous life, climate and anoxia. *Cretaceous Research* 35, 230–257.
- Föllmi, K.B., Gainon, F., 2008. Demise of the northern Tethyan Urgonian carbonate platform and subsequent transition towards pelagic conditions: the sedimentary record of the Col de la Plaine Morte area, central Switzerland. *Sedimentary Geology* 205(3), 142–159.
- Fontugne, M., Duplessy, J.C., 1978. Carbon Isotope Ratio of Marine Phytoplankton related to surface water masses. *Earth and Planetary Science Letters* 41, 365–371.
- Forster, A., Sturt, H., Meyers, P.A., and the Leg 207 Shipboard Scientific Party, 2004. Molecular biogeochemistry of Cretaceous black shales from the Demerara Rise; preliminary shipboard results from Sites 1257 and 1258, ODP Leg 207, In: Erbacher, J., Mosher, D.C., Malone, M.J., et al. (eds.), *Proceedings of the Ocean Drilling Program, Initial Results 207*, 1–22.
- Frakes, L.A., 1999. Estimating the global thermal state from Cretaceous sea surface and continental temperature data. *Geological Society of America, Special Paper* 332, 49–57.
- Gaona-Narvaez, T., Maurrasse, F.J.-M.R., and Moreno-Bedmar, J. A., 2013a. Stable Carbon Isotope Stratigraphy and Ammonite Biochronology at Madotz (Navarra, N Spain): Implications for the Timing and Duration of Oxygen Depletion during OAE-1a. *Cretaceous Research* 40, 143–157.
- García-Alcáde J.L., Carls, P., Pardo Alonso, M.V., Sanz Lopez, J., Soto, F., Truyols-Massoni, M., and Valenzuela-Ríos, J.I., 2002. Devonian in: Gibbons, W., and Moreno, T. (Eds.), *The Geology of Spain*. The Geological Society of London, pp. 67–91.
- García-Senz, J., 2002. Cuencas extensivas del Cretácico Inferior en los Pirineos Centrales: formación y subsecuente inversión. PhD Thesis, University of Barcelona, Barcelona, 310 pp.
- Gaudy, R., Champalbert, G., 2003. Feeding and metabolism of mesozooplankton in the equatorial Pacific high-nutrient, low-chlorophyll zone along 180°. *Journal of Geophysical Research* 108 (C12), 1–12.
- Gearing, P. J., Plucker, F. E. Parker, P. L., 1977. Organic carbon stable isotope ratios of continental margin sediments. *Marine Chemistry* 5, 251–266.
- Giger, W., Schaffner, C., Wakeham, S. G., 1980. Aliphatic and olefinic hydrocarbons in recent sediments of Greifensee, Switzerland. *Geochimica et Cosmochimica Acta* 44, 119–129.

- Godet, A., Föllmi, K.B., Spangenberg, J.E., Bodin, S., Vermeulen, J., Adatte, T., Bonvallet, L., Arnaud, H., 2013. Deciphering the message of Early Cretaceous drowning surfaces from the Helvetic Alps: what can be learnt from platform-to-basin correlations? *Sedimentology* 60 (1), 152–173.
- Grégoire, M., Soetaert, K., Nezlin, N. P., Kostianoy, A. G., 2004. Modeling the nitrogen cycling and plankton productivity in the Black Sea using a three dimensional interdisciplinary model. *Journal of Geophysical Research* 109, 28.
- Hay, W., 2002. Carbonate fluxes during earth history. GEOMAR, Kiel, Germany. http://csdms.colorado.edu/mediawiki/images/CarbonateFluxes_in_Earth_History.pdf
- Hayes, J.M., 1993. Factors controlling ^{13}C contents of sedimentary organic compounds: Principles and evidence. In: R.J. Parkes, P. Westbroek and J.W. de Leeuw (Editors), *Marine Sediments, Burial, Pore Water Chemistry, Microbiology and Diagenesis*. *Marine Geology* 113, 111–125.
- Herrle, J.O., 2002. Paleooceanographic and paleoclimatic implications on mid-Cretaceous black shale formation in the Vocontian Basin and the Atlantic: evidence from calcareous nannofossils and stable isotopes. Ph.D. dissertattion. Univ. Tübingen, Federal Republic of Germany, pp. 114.
- Hoering, T. C., 1973. Characterization of the organic matter in a Site 147 Core from the Cariaco Trench. In Edgar, N. T., Saunders, J. B., et al., 1973. Site 147. In Edgar, N. T., Saunders, J. B., et al., *Init. Repts. DSDP, 15: Washington (U.S. Govt. Printing Office)*, 937– 939.
- Honjo, S., 1976. Coccoliths: Production, transportation, and sedimentation. *Marine Micropaleontology* 1, 65–79.
- Hower, J., Eslinger, E.V., Hower, M.E., Perry, E.A., 1976. Mechanism of burial metamorphism of argillaceous sediments: *Geological Society of America* 87, 725–37.
- Hughes, R. E.; Warren, R., 1989. Evaluation of the Economic Usefulness of Earth Materials by X-ray Diffraction, 23rd Forum Geology Industrial Minerals; Hughes, R. E.; Bradbury, L. C., Eds. Illinois State Geological Survey.
- Hughes, R. E., Moore, D. M., Glass, H. D., 1994. Qualitative and quantitative analysis of clay minerals in soils: in Amonette, J. E., and Zelazny, L. W., editors, *Quantitative Methods in Soil Mineralogy*, SSSA Miscell. Pub., 330–59.
- Hulburt, E. M., 1962. Phytoplankton in the southwestern Sargasso Sea and South Equatorial Current, February 1961. *Limnology and Oceanography*, 7 (3) 307–315.
- Hunt, J. M., 1970. The significance of carbon isotope variations in marine sediments. In *Advances in Organic Geochemistry, 1966*, eds. Hobson, G.D., and Spears G.C., Pergamon, Oxford, pp. 27–35.

- Jaffe, R., Mead, R., Hernandez, M.E., Peralba, M.C., DiGuida, O.A., 2001. Origin and transport of sedimentary organic matter in two subtropical estuaries: a comparative, biomarker-based study. *Organic Geochemistry* 32, 507–526.
- Jiao, N., Herndl, G.J., Hansell, D.A., Benner, R., Kattner, G., Wilhelm, S.W., Kirchman, D.L., Weinbauer, T. L., Chen, F., Azam, F., 2010. Microbial production of recalcitrant dissolved organic matter: long-term carbon storage in the global ocean. *Nature Reviews Microbiology* 88, 593–599.
- Jinggui, L., Philp, R.P., Mingzhong, C., 2002. Unusual N-alkane distributions in extracts from marine carbonate rocks at high levels of maturity and overmaturity. *Chinese Journal of Geochemistry* 21(4), 322–333.
- Johnson, P. W., Sieburth, J. M., 1979. Chroococcoid cyanobacteria in the sea: a ubiquitous and diverse phototrophic biomass. *Limnology and Oceanography* 24(5), 928–935.
- Kashtan, N., Roggensack, S. E., Rodrigue, S., Thompson, J. W., Biller, S.J., Coe, A., Ding, H., Marttinen, P., Malmstrom, R. R., Stocker, R., Follows, M. J., Stepanauskas, R., Chisholm, S. W., 2014. Single-cell genomics reveals hundreds of coexisting subpopulations in wild *Prochlorococcus*. *Science* 344, 416–420.
- Kemp, W. M., Testa, J. M., Conley, D. J., Gilbert, D., Hagy, J. D., 2009. Temporal responses of coastal hypoxia to nutrient loading and physical controls. *Biogeosciences* 6(12), 2985–3008.
- Kennedy, W.J., Gale, A.S., Bown, P.R., Caron, M., Davey, R.J., Gröcke, D., Wray, D.S., 2000. Integrated stratigraphy across the Aptian-Albian boundary in the Marnes Bleues, at the Col de Pré-Guiterd, Arnayon (Drôme), and at Tortonne (Alpes-de-Haute-Provence), France: a candidate global boundary stratotype section and boundary point for the base of the Albian Stage. *Cretaceous Research* 21, 591–720.
- Kennett, J., 1982. *Marine Geology*. Prentice Hall, Inc., Englewood Cliffs, NJ 07632, pp. 813.
- Kotel'nikov, D.D., Zinchuk, N. N., 2008. Comparative analysis of clay mineral evolution under the conditions of humid and arid lithogenesis. *Russian geology and geophysics* 49, 727–737.
- Koutsoukos, E.A.M., Mello, M.R., Azambuja Filho, N.C., Hart, M.B., Maxwell, J.R., 1991a. The upper Aptian–Albian succession of the Sergipe Basin, Brazil: paleoenvironmental assessment. *Bull. Am. Assoc. Pet. Geol.* 75, 475–498.
- Koutsoukos, E.A.M., Mello, M.R., Azambuja Filho, N.C., 1991b. Micropalaeontological and geochemical evidence of mid-Cretaceous dysoxic–anoxic palaeoenvironments in

- the Sergipe Basin, northeastern Brazil. In: Tyson, R.V., Pearson, T.H. Geological Society London Special Publication 58, 427–447
- Kroon, D., Williams, T., Pirmez, C., Spezzaferri, S., Sato, T., Wright, J. D., 2000. Coupled Early Pliocene-Middle Miocene Bio-cyclostratigraphy of site 1006 reveals orbitally induced cyclicity patterns of Great Bahama Bank carbonate production. In: Swart, P.K., Eberli, G.P., Malone, M.J., and Sarg, J.F. (Eds.), 2000. Proceedings of the Ocean Drilling Program, Scientific Results 166, 155–166.
- Kuhnt, W., Moullade, M., Masse, J.P., Erlenkeuser, H., 1998. Carbon isotope stratigraphy of the lower Aptian historical stratotype at Cassis– La Bédoule (SE France): *Géologie Méditerranéenne* 25(3), 63–79.
- Kuhnt, W., Holbourn, A., Moullade, M., 2011. Transient global cooling at the onset of early Aptian oceanic anoxic event (OAE) 1a. *Geology* 39(4), 323–326.
- Kuypers, M. M. M., Pancost, R. D., Nijenhuis, I. A., Sinninghe-Damsté, J. S., 2002. Enhanced productivity led to increased organic carbon burial in the euxinic North Atlantic basin during the late Cenomanian oceanic anoxic event. *Paleoceanography* 17(4), 1051–1064.
- Lamolda, M. A., Gorostidi, A., Paul, C. R. C., 1994. Quantitative estimates of calcareous nannofossil changes across the Plenius Marls (latest Cenomanian), Dover, England: implications for the generation of the Cenomanian-Turonian Boundary Event. *Cretaceous Research* 14, 143–164.
- Lampert, L., Quéguiner, B., Labasque, T., Pichon, A., Lebreton, N., 2002. Spatial variability of phytoplankton composition and biomass on the eastern continental shelf of the Bay of Biscay (north-east Atlantic Ocean). Evidence for a bloom of *Emiliana huxleyi* (Prymnesiophyceae) in spring 1998. *Continental Shelf Research*, 22(8), 1225–1247.
- Larson, R. L., Erba, E., 1999. Onset of the Mid-Cretaceous greenhouse in the Barremian-Aptian: Igneous events and the biological, sedimentary, and geochemical responses. *Paleoceanography*, 14(6), 663–678.
- Lees, J.A., Bown, P.R., Mattioli, E., 2005. Problems with proxies? Cautionary tales of calcareous nannofossils paleoenvironmental indicators. *Micropaleontology* 51, 333–343.
- Malkoč, M., Mutterlose, J., 2010. The early Barremian warm pulse and the late Barremian cooling: a high-resolution geochemical record of the Boreal Realm. *Palaios* 25, 14–23.

- Mancinelli, A., Chiocchini, M., 2006. Cretaceous benthic foraminifers and calcareous algae from Monte Cairo (southern Latium, Italy). *Bolletino della Società Paleontologica Italiana* 45(1), 91–113.
- Martínez, R., 1982. Ammonoideos cretácicos del Prepirineo de la provincia de Lleida. PhD thesis, publicaciones de la Universitat Autònoma de Barcelona, 17, pp. 197.
- Masse, J.-P., Bellion, Y., Benkhelil, J., Dercourt, J., Guiraud, R., Ricou, L.E., 1993. Lower Aptian Palaeoenvironments (114 to 112 Ma). In: Dercourt, J., Ricou, L.E., Vrielynck, B. (Eds.), *Atlas Tethys Palaeoenvironmental Maps* Gauthier-Villars, Paris, pp. Maps. BEICIP-FRANLAB, Rueil-Malmaison.
- Masse, J.-P., Fenerci-Masse, M., 2013. Drowning events, development and demise of carbonate platforms, and controlling factors: The Late Barremian-Early Aptian record of Southeast France, *Sedimentary Geology* 298, 28–52.
- McIntyre, A., Bé, A. W. H., 1967. Modern Coccolithophoridae of the Atlantic Ocean. Placoliths and Cyrtoliths. *Deep-Sea Research* 14, 561–597.
- McIntyre, A., McIntyre, R., 1971. Coccolith concentrations and differential solution in oceanic sediments. In: Funnel, B. B., Riedel, W. R. (Eds.), *The Micropaleontology of Oceans*, p. 253–261. Cambridge University Press.
- Melinte, M.C., Lamolda, M.A., 2007. Calcareous nannofossil biostratigraphy of the Coniacian/Santonian boundary interval in Romania and comparison with other European regions. *Cretaceous Research* 28(1), 119–127.
- Melinte-Dobrinescu, M.C., Roban, R.D., 2011. Cretaceous anoxic–oxic changes in the Moldavids (Carpathians, Romania). *Sedimentary Geology* 235(1–2), 79–90.
- Menegatti, A. P., Weissert, H., Brown, R. S., Tyson, R. V., Farrimond, P., Strasser, A., Caron, M., 1998. High resolution $\delta^{13}\text{C}$ stratigraphy through the Early Aptian “Livello Selli” of the Alpine Tethys. *Paleoceanography* 13(5), 530–545.
- Mercone, D., Thomson, J., Croudace, I. W., Siani G., Paterne, M., Troelstra, S., 2000. Duration of S1, the most recent sapropel in the eastern Mediterranean Sea, as indicated by accelerator mass spectrometry radiocarbon and geochemical evidence. *Paleoceanography* 15(3), 336–347.
- Meyers, P.A., 1994. Preservation of elemental and isotopic source identification of sedimentary organic matter. *Chemical Geology* 144, 289–302.
- Meyers, P.A., 1997. Organic geochemical proxies of paleoceanographic, paleolimnologic, and paleoclimatic processes. *Organic Geochemistry* 27(5–6), 213–250.

- Molfino, B., McIntyre, A., 1990. Precessional Forcing of Nutricline in the Equatorial Atlantic. *Science* 249, 766–769.
- Moore, D.M., Reynolds, R.C.Jr., 1997. X-Ray diffraction and the Identification and Analysis of Clay Minerals. Oxford University Press, New York, second ed. pp. 378.
- Moreno-Bedmar, J.A., 2010. Ammonits de l’Aptià inferior de la península Ibèrica. Biostratigrafia i aportacions a l’estudi del Oceanic Anoxic Event 1a. Universitat de Barcelona, 331 pp.
- Moullade, M., Tronchetti, G., Busnardo, R., and Masse, J-P., 1998, Description lithologique des coupes types du stratotype historique de l’Aptien inferieur dans la région de Cassis–La Bédoule (SE France): *Géologie Méditerranéenne* 25, 15–29.
- Mucci, A., Starr, M., Gilbert, D., Sundby, B., 2011. Acidification of lower St. Lawrence Estuary bottom waters. *Atmosphere-Ocean* 49(3), 206–218.
- Muñoz, J.A., 1991. Evolution of a continental collision belt: ECORS-Pyrenees crustal balanced cross-section, In *Thrust Tectonics* Ed. K.R. McClay. Chapman and Hall, New York, pp.235-247.
- Muñoz, J.A., Puigdefàbregas, C., Fontboté, J.M., 1984. Orógenos alpinos III.4.1. In: Ríos, L.J.J.M. (Ed.), *El Pirineo*. Inst. Geol. Min. España. *Geología de España* 2, pp. 161–205.
- Murray, J., Renard, A. F., 1891. Deep Sea deposits: Challenger Expedition Report (1873–1876), London, 525 pp.
- Mutterlose, J., Bockel, B., 1998. The Barremian - Aptian interval in NW Germany: a review. *Cretaceous Research* 19, 539–568.
- Mutterlose, J., Kessels, K., 2000. Early Cretaceous calcareous nannofossils from high latitudes: implications for paleogeography and paleoclimate. *Palaeogeography, Palaeoclimatology, Palaeoecology* 160, 347–372.
- Mutterlose, J., Bornemann, A., Herrle, J. O., 2005, Mesozoic calcareous nannofossils–state of the art. *Paläontologische Zeitschrift* 79(1), 113–133.
- Mutterlose, J., Pauly, S., Steuber, T., 2009. Temperature controlled deposition of early Cretaceous (Barremian–early Aptian) black shales in an epicontinental sea. *Palaeogeography, Palaeoclimatology, Palaeoecology* 273(3), 330–345.
- Neagu, T., Cîrnaru, P., 2004. Lower Aptian agglutinated foraminifera from the southern Dobrogea and SE part of the Moesian Platform. *Acta Paleontologica Romaniaae* 4, 277–297.

- Newman, J. W., Parker, P. L., Behrens, E. W., 1973. Organic carbon isotope ratios in Quaternary cores from the Gulf of Mexico. *Geochimica et Cosmochimica Acta* 37, 225–238.
- Núñez-Useche, F., Barragán, R., 2012. Microfacies analysis and paleoenvironmental dynamic of the Barremian-Albian interval in Sierra del Rosario, eastern Durango State, Mexico. *Revista Mexicana de Ciencias Geológicas* 29(1), 204–218.
- Oguz, T., 2006. Regime shifts at multiple trophic levels of the Black Sea pelagic ecosystem. European Geosciences Union, Geophysical Research Abstracts 8.
- Paerl, H. W., 1997. Coastal eutrophication and harmful algal blooms: Importance of atmospheric deposition and groundwater as "new" nitrogen and other nutrient sources. *Limnology and Oceanography* 42(5), 1154–1165.
- Papp, D.C., Cociuba, I., Lazăr, D.F., 2013. Carbon and oxygen-isotope stratigraphy of the Early Cretaceous carbonate platform of Pădurea Craiului (Apuseni Mountains, Romania): A chemostratigraphic correlation and paleoenvironmental tool. *Applied Geochemistry* 32, 3–16.
- Pauly, S., Mutterlose, J., Wray, D.S., 2013. Palaeoceanography of Lower Cretaceous (Barremian-Lower Aptian) black shales from northwest Germany evidenced by calcareous nannofossils and geochemistry. *Cretaceous Research* 42, 28–43.
- Paytan, A., McLaughlin, K., 2007. The oceanic phosphorous cycle. *Chemical Reviews* 107, 563-576.
- Peters, K. E., Moldowan, J. M., 1993. *The Biomarker Guide. Interpreting Molecular Fossils in Petroleum and Ancient Sediment*, (Prentice-Hall), Englewood Cliffs, NJ. 1993.
- Peters, K.E., Walters, C.C., Moldowan, J.M., 2005. *The biomarker guide: II, Biomarkers and isotopes in petroleum systems and Earth history*, Cambridge, UK, Cambridge University Press, pp. 475–1155.
- Peterson, M.N.A., 1966. Calcite: Rates of dissolution in a vertical profile in the central Pacific: *Science* 154, 1542–1544.
- Peybernès, B., 1976. *Le Jurassique et le Crétacé inférieur des Pyrénées franco-espagnoles*. Thèse de doctorat, Laboratoire de Géologie, Université Paul Sabatier, Toulouse, 459 pp.
- Peybernès, B., Souquet, P., 1973. Biostratigraphie des marnes noires de l' Aptien-Albien de la zone sud-pyrénéenne . *Comptes Rendus de l'Académie des Sciences Paris* 276 (2 Mai 1976), Séries D, 2501–2504.

- Popp, B. N., Parekh, P., Tilbrook, B., Bidigare, R. R., Laws, E. A., 1997. Organic carbon $\delta^{13}\text{C}$ variations in sedimentary rocks as chemostratigraphic and paleoenvironmental tools. *Palaeogeography, Palaeoclimatology, Palaeoecology* 132, 119–132.
- Powell, T. G., 1988. Pristane/phytane ratio as environmental indicator. *Nature* 333, 604.
- Prahl, F. G., Ertel, J. R., Goñi, M. A., Sparrow, M.A., Eversmeyer, B., 1994. Terrestrial organic carbon contributions to sediments on the Washington margin. *Geochimica et Cosmochimica Acta* 58, 3048–3055.
- Premoli Silva, I., Erba, E., Tornaghi, M. E., 1989. Paleoenvironmental signals and changes in surface fertility in mid-Cretaceous Corg-rich pelagic facies of the Fucoid Marls (central Italy), *Geobios, Mémoire Spécial* 11, 225–236.
- Principato, M.S., Crudeli, D., Ziveri, P., Slomp, C. P., Corselli, C., Erba, E., de Lange, G.J., 2006. Phyto- and zooplankton paleofluxes during the deposition of sapropel S1 (eastern Mediterranean): Biogenic carbonate preservation and paleoecological implications. *Palaeogeography, Palaeoclimatology, Palaeoecology* 235, 8–27.
- Pucéat, E., Lecuyer, C., Sheppard, S.M.F., Dromart, G., Reboulet, S., Grandjean, P., 2003. Thermal evolution of Cretaceous Tethyan marine waters inferred from oxygen isotope composition of fish tooth enamels. *Paleoceanography* 18, 1–12.
- Quijano, M. L., Castro, J. M., Pancost, R. D., de Gea, G. A., Najarro, M., Aguado, Rosales, I., Martín-Chivelet, J., 2012. Organic geochemistry, stable isotopes, and facies analysis of the Early Aptian OAE– New records from Spain (Western Tethys). *Palaeogeography, Palaeoclimatology, Palaeoecology* 365–366, 276–293.
- Reboulet, S., Mattioli, E., Pittet, B., Baudin, F., Olivero, D., Proux, O. 2003. Ammonoid and nannoplankton abundance in Valanginian (early Cretaceous) limestone - marl successions from the southeast France Basin: carbonate dilution or productivity? *Palaeogeography, Palaeoclimatology, Palaeoecology* 201, 113–139.
- Reid, J. L., 1962. On circulation, phosphate-phosphorus content, and zooplankton volumes in the upper part of the Pacific Ocean. *Limnology and Ocean* 7 (3), 287–306.
- Roth, P.H., 1978. Cretaceous nannoplankton biostratigraphy and oceanography of the northwestern Atlantic Ocean. *Initial Reports of the Deep Sea Drilling Project* 44, 731–759.
- Roth, P.H., 1989. Ocean circulation and calcareous nannoplankton evolution during the Jurassic and Cretaceous. *Palaeogeography, Palaeoclimatology and Palaeoecology* 74, 111–126
- Roth, P. H., Coulbourn, W. T., 1982. Floral and solution patterns of coccoliths in surface sediments of the North Pacific. *Marine Micropaleontology* 7(1), 1–52.

- Roth, P.H., Krumbach, K.R., 1986. Middle Cretaceous calcareous nannofossil biogeography and preservation in the Atlantic and Indian oceans; implications for paleoceanography. *Marine Micropaleontology* 10, 235–266.
- Ruffell, A.H., Batten, D.J., 1990. The Barremian-Aptian arid phase in Western Europe. *Palaeogeography, Palaeoclimatology, Palaeoecology* 80, 197–212.
- Ruffell, A., McKinley, J. M., Worden, R. H., 2002. Comparison of clay mineral stratigraphy to other proxy palaeoclimate indicators in the Mesozoic of NW Europe. *Philosophical Transactions of the Royal Society of London. Series A: Mathematical, Physical and Engineering Sciences* 360(1793), 675–693.
- Sanchez-Hernandez, Y., Maurrasse, F.J-M.R., 2014. Geochemical characterization and redox signals from the latest Barremian to the earliest Aptian in a restricted marine basin: El Pui section, Organyà Basin, south-central Pyrenees. *Chemical Geology* 372, 12–31.
- Scarpato Cunha, A. A., Koutsoukos, E.A.M., 1998. Calcareous nannofossils and planktonic foraminifers in the upper Aptian of Sergipe Basin, northeastern Brazil: palaeoecological inferences. *Palaeogeography, Palaeoclimatology, Palaeoecology* 142, 175–184.
- Schneidermann, N., 1973. Deposition of coccoliths in the Compensation Zone of the Atlantic Ocean. In: L. E. Smith, L. E., Hardenbol, J. (Eds.), *Proceedings of a symposium on calcareous nannofossils*, Gulf Coast Section Society of Economic Paleontologists and Mineralogists, pp. 140–151.
- Scholle, P.A., Bebout, D.G, Moore, C.H., eds., 1983. *Carbonate Depositional Environments*, AAPG Memoir 33(33), pp. 708.
- Scholle, P., Ulmer-Scholle, D.S., 2003. A color guide to the petrography of carbonate rocks: grains, textures, porosity, diagenesis, AAPG Memoir 77 (77), pp. 474.
- Scott, C.C.H., 1992. Clay mineralogy of the Upper Cretaceous Mancos Shale near Mesa Verde National Park, Southwestern Colorado: Clues to the paleoceanography of the Western Interior Seaway, Thesis, University of Massachusetts, pp. 191.
- Seguret, M., 1972. Étude tectonique des nappes et séries décollées de la partie centrale du versant sud des Pyrénées Pub. Ustela, Série Géologie Structurale 2, pp.155
- Skreń, U., Fabiańska, M., 2009. Geochemical characteristics of organic matter in the Lower Paleozoic rocks of the Peribaltic Syncline (Poland). *Geochemical Journal* 43, 343–369.
- Spiker, E. C. Simoneit, B. R. T., 1982. Appendix III. Radiocarbon dating of sediments from the Cariaco Trench, Deep Sea Drilling Project Site 147 (data supplementary to DSDP Leg 15, Site 147) Initial Reports of the Deep Sea Drilling Project 66, 863–864.

- Stein, M., Föllmi, K.B., Westermann, S., Godet, A., Adatte, T., Matera, V., Fleitmann, D., Berner, Z., 2011. Progressive palaeoenvironmental change during the Late Barremian–Early Aptian as prelude to Oceanic Anoxic Event 1a: evidence from the Gorgo a Cerbara section (Umbria-Marche Basin, central Italy). *Palaeogeography, Palaeoclimatology, Palaeoecology* 302, 396–406.
- Stein, M., Westermann, S., Adatte, T., Matera, V., Fleitmann, D., Spangenberg, J.E. and Föllmi, K.B., 2012. Late Barremian –Early Aptian palaeoenvironmental change: the Cassis-La Bédoule section, southeast France. *Cretaceous Research* 37, 209–222.
- Stelmakh, L. V., 2013, Microzooplankton Grazing Impact on Phytoplankton Blooms in the Coastal Seawater of the Southern Crimea (Black Sea). *International Journal of Marine Science*, 3 (15), 121–127.
- Sun, J., Feng, Y., Zhou, F., Song, S., Jiang, Y., Ding, C., 2013. Top-down control of spring surface phytoplankton blooms by microzooplankton in the central Yellow Sea, China. *Deep-Sea Research II*, 97, 51–60.
- ten Haven, H.L., de Leeuw, J.W., Rullkotter, J., Sinninghe-Damsté, J., 1987. Restricted utility of the pristane/phytane ratio as a palaeoenvironmental indicator. *Nature* 330, 641–643.
- ten Haven, H.L., de Leeuw, J.W., Rullkotter, J., Sinninghe-Damsté, J., 1988. Pristane/phytane ratio as environmental indicator. *Scientific correspondence. Nature* 333, 604.
- Tracey, J.I., et al., 1971, Initial Reports of the Deep Sea Drilling Project, volume VIII, Washington (U.S. Government Printing Office), pp. 1035.
- Valiela, I., 1984. *Marine Ecological Processes*, second ed. Springer, New York, pp. 686.
- van Beusekom, J. E. E., Mendedoht, D., Augustin, C. B., Schilling, M., Boersma, M., 2009. Phytoplankton, protozooplankton and nutrient dynamics in the Bornholm Basin (Baltic Sea) in 2002–2003 during the German GLOBEC Project. *International Journal of Earth Sciences* 98 (2), 251–260.
- van Oostende, N., Moerdijk-Poortvliet, T. C. W., Boschker, H. T. S., Vyverman, W. Sabbe, K., 2013. Release of dissolved carbohydrates by *Emiliana huxleyi* and formation of transparent exopolymer particles depend on algal life cycle and bacterial activity. *Environmental Microbiology* 15, 1514–1531.
- Walker, J.D., Geissman, J.W., Bowring, S.A., Babcock, L.E., compilers, 2012. *Geologic Time Scale v. 4.0*: Geological Society of America.
- Watkins, D., 1989. Nannoplankton productivity fluctuations and rhythmically-bedded pelagic carbonates of the Greenhorn Limestone (Upper Cretaceous). *Palaeogeography Palaeoclimatology, Palaeoecology* 74, 75–86.

- Weaver, C. E., 1958. A discussion on the origin of clay minerals in sedimentary rocks. *Clays and clay minerals* 5, 159–173.
- Weaver, C.E., 1989. *Clays, muds, and shales, Developments in Sedimentology* 44. Elsevier, Amsterdam, pp. 819.
- Wedepohl, K.H., 1991. The composition of the upper earth's crust and the natural cycles of selected metals. *Metals in natural raw materials. Natural Resources*. In: Merian, E. (Ed.), *Metals and Their Compounds in the Environment*. VCH, Weinheim, pp. 3–17.
- Weissert, H., 1989. C-isotope stratigraphy, a monitor of paleoenvironmental changes: a case study from the Early Cretaceous. *Surveys in Geophysics* 10, 1–16.
- Weissert, H., Lini, A., Föllmi, K. B., Kuhn, O., 1998. Correlation of Early Cretaceous carbon isotope stratigraphy and platform drowning events: a possible link? *Palaeogeography, Palaeoclimatology, Palaeoecology*, 137(3), 189–203.
- Westphal, H., Halfar, J., Freiwald, A., 2010. Heterozoan carbonates in subtropical to tropical settings in the present and past. *International Journal of Earth Sciences* 99(1), 153–169.
- Wilson, M.E.J., Vecsei, A., 2005. The apparent paradox of abundant foramol facies in low latitudes: their environmental significance and effect on platform development. *Earth Sciences Reviews* 69(1), 133–168.
- Wissler, L., Weissert, H., Masse, J.P., Bulot, L., 2002. Chemostratigraphic correlation of Barremian and lower Aptian ammonite zones and magnetic reversals. *International Journal of Earth Sciences*, 91, 272–279.
- Yakimov, M. M., La Cono, V., Denaro, R., D'Auria, G., Decembrini, F., Timmis, K. N., Golyshin, P. N., Giuliano, L., 2007. Primary producing prokaryotic communities of brine, interface and seawater above the halocline of deep anoxic lake L'Atalante, Eastern Mediterranean Sea. *International Society of Microbial Ecology (ISME) Journal* 1, 743–755.
- Zachariasse, J., Schmidt, R. R., Van Leeuwen, R. J. W., 1984. Distribution of foraminifera and calcareous nannoplankton in Quaternary sediments of the Eastern Angola Basin in response to climatic and oceanic fluctuations. *Netherlands Journal of Sea Research* 17, 250–275.
- Zachos, J. C., Arthur, M. A., Dean, W. E., 1989. Geochemical evidence for suppression of pelagic marine productivity at the Cretaceous/Tertiary boundary. *Nature*, 337.
- Ziveri, P., Thunnell, R. C., Rio, D., 1995. Export production of coccolithophores in an upwelling region: Results from San Pedro Basin, Southern California borderlands. *Marine Micropaleontology* 24, 335–358.

6 MICROFACIES CHARACTERIZATION AND FAUNAL VARIATIONS IN THE UPPER BARREMIAN–LOWER APTIAN HEMIPELAGIC SEDIMENTS OF THE ORGANYÀ BASIN: PALEOENVIRONMENTAL IMPLICATIONS

Sanchez-Hernandez, Y., Maurrasse F.J-M.R., (Submitted for publication to the Journal Facies, Springer) Microfacies characterization and faunal variations in the upper Barremian–lower Aptian hemipelagic sediments of the Organyà Basin: paleoenvironmental implications. (The format follows the guidelines of the Journal: <http://www.springer.com/earth+sciences+and+geography/geology/journal/10347>)

Abstract

The Early Cretaceous sedimentary record of different geologic sections of the Tethys Ocean reveals varying depositional conditions that often fluctuated rapidly within the same basin, mostly related to eustatic sea level changes coupled with tectonic reconfiguration linked to the opening of the Atlantic Ocean. Here we present a high-resolution microfacies analysis of the basal 85 meters of the El Pui section that includes a continuous Barremian/Aptian hemipelagic sequence corresponding to the Cabó Formation of the Organyà Basin, south-central Pyrenees.

The succession of facies consists essentially of a series of interbedded sparsely fossiliferous marlstones, marly limestones and limestones with scarce to rare benthic and planktonic foraminifera, small ostracods, and echinoderm and ammonite microfragments. The dominant fabric of the microfacies is isotropic, but may become mildly isotropic at certain levels that display alternate low bioturbation index and enhanced preservation of OM indicative of an environment with varying oxygen levels. Continued enhanced surface productivity concomitant with stagnation of bottom waters, related to physiography, can best explain the main controlling factors that maintained special conditions of dysoxia and enhanced organic carbon burial in the basin.

The present study documents the first recurrent record of roveacrinids in the Barremian/Aptian interval of the Organyà Basin where their constant abundance indicates that these pelagic microcrinoids were a significant element of the food web, which benefited from heightened primary productivity under special conditions in the semi-restricted Organyà Basin during that time. The results also reveal that the sedimentary succession recorded in the El Pui accumulated continuously without the effects of tectonism throughout the latest Barremian to the earliest Aptian phase of basin development.

6.1 Introduction

The geologic record provides significant examples of deposits that indicate severe oxygen-deficient environments in ocean basins as far back as the early Paleozoic era [e.g., in Eastern North America, Middle Cambrian Burgess Shale, ~505 Ma (Powell et al. 2003); Middle Devonian epoch, Marcellus Shale ~ 384–390 Ma (Sageman et al. 2003); Pennsylvanian Kansas-type cyclothems ~ 311–290 Ma (Caldwell 1983; Algeo and Maynard, 2004)]. Nevertheless, the Cretaceous Period is most characteristic for recurrent organic-rich sediments that accumulated under widespread conditions of oxygen deficiency, or even culminated into anoxia known as oceanic anoxic events (OAEs) (Schlanger and Jenkyns 1976; Jenkyns 1980; Arthur and Premoli-Silva 1982; Arthur et al. 1985, 1990). OAEs are of major significance in the Cretaceous because their incidence had a remarkable impact on the sedimentary record (e.g., wide accumulation of black shales associated with large amounts of organic matter) and represent unusual biogeochemical changes in the ocean both prior to and after their occurrences (Jenkyns 2010; Wang et al. 2011).

Complex conceptual models based on biogeochemical, stratigraphic and sedimentological studies have proposed a sequence of factors triggered by concurrent intensified volcanic and hydrothermal activities (Stinton and Duncan 1997; Weissert et al. 1998; Larson and Erba 1999; Tejada et al. 2009), and possible episodes of methane hydrate dissociation (Jahren et al. 2001, Méhay et al. 2009) as the causes for the vast deposition of organic-rich sediments during the Cretaceous OAEs. Such organic-rich deposits are not only characteristic of the pelagic environment, but also developed in various foreland basins, epeiric seas, and marginal basins that grew by rifting subsequent to the breakup of Pangaea in the Triassic Epoch (Olsen 1997; Masse et al. 2000).

Marginal basins of the Tethys Ocean include a complex spatio-temporal record of organic carbon (OC) preservation because active tectonic reconfiguration (e.g., rotating microplates, extensional processes) and climate variability activated mechanisms that induced varying degrees of high marine productivity indicative of readjustments of the nutricline, and differential oxygenation at the basin scale that became recurrent starting in the Early Jurassic, Pliensbachian stage (Borrego et al. 1996; van de Schootbrugge et al. 2005). These conditions recurred intermittently through the Lower Cretaceous (e.g., Mutterlose et al. 2009; Föllmi 2012; Gaona-Narvaez et al. 2013; Pauly et al. 2013; Aguado et al. 2013), and regional physiographic factors and/or zonal climatic forcing mechanisms led to sediments in restricted basins that may include short episodes of enhanced OC sequestration with irregularity in duration and intensity in part decoupled from the tempo of major global forcing factors (e.g., Arthur 1979; Kuss and Schlagintweit 1988; Aguado et al. 1997; Masse 1998; Masse and Machhour 1998; Moullade et al. 1998; Scarparo-Cunha and Koutsoukos 1998; Bersezio et al. 2002;

Maurrasse and Ponton 2005; Abu-Zied 2007; Barragan and Maurrasse 2008; Michalik et al. 2008; Raisossadat and Shokri 2011; Föllmi et al. 2011; Leonide et al. 2012; Hu et al. 2012; Husinec et al. 2012; Roban and Melinte-Dobrinescu 2012; Elkhazri et al. 2013). The complex factors controlling regional episodes of enhanced carbon sequestration in semi-enclosed basins and their relationship to global mechanisms are still not fully understood. The present analysis of facies complements a multiproxy study (Sanchez Hernandez and Maurrasse 2014; Sanchez-Hernandez et al. 2014) that characterized the geochemical and sedimentary conditions from the uppermost Barremian to the earliest Aptian (Fig. 6-1) in the hemipelagic sediments of the El Pui section. The present objective is to further our understanding of the temporal changes revealed by the microfacies that reflect the paleoenvironmental conditions in the Organyà Basin prior to OAE1a.

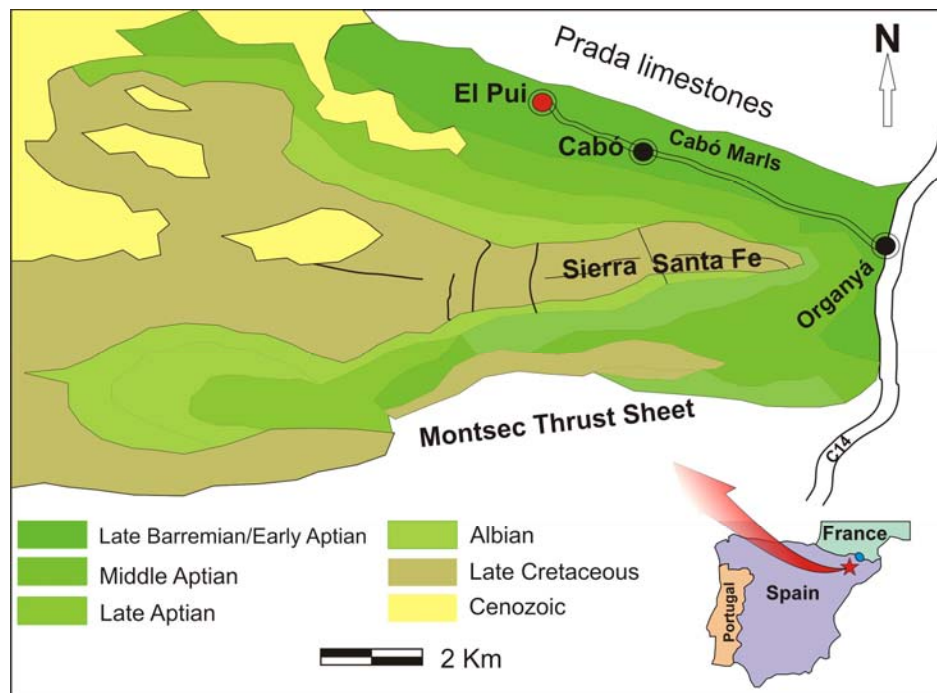


Figure 6-1 Geologic map of the Organyà area showing the relative position of the El Pui section (Adapted from Bachmann and Willens, 1996).

6.2 Physiographic and geologic settings

The El Pui section (Figs. 6-1, 6-2) is located on the southern flank of the Sierra de Prada in the South Central Pyrenees, Catalunya, Spain. The sequence of strata that comprises the Prada Mountain west of the town of Cabó (Fig. 6-1) is incorporated in the predominantly E-W trending, folded structure of the Bóixols thrust sheet (Muñoz 1991; Bond and McClay 1995). Previous works (Berástegui et al. 1990; Bernaus et al. 2002, 2003) described in detail the series of well-exposed tightly imbricated sequences immediately north of the town of Organyà along the west side of the road cut on C-14 (Fig. 6-1) following Riu Segre canyon, which cuts through the Cretaceous deposits.



Figure 6-2 Distant view of the basal ~40 m of the El Pui section. Yellow arrows point to geologists seen on the site for scale. Note the well-defined, continuous interbeds of limestones and marlstones characteristic of the lower 85 m studied.

The El Pui section is about 7 Km west of Organyà, and 1.5 Km west of the nearby village of Cabò (42° 14' 44.46" N, 1° 13' 31.49" E, top of the studied 85 m). The sequence is exposed along an easily accessible road cut starting at El Pui and follows a ridge adjacent to Llau de la Casa Vella del Pui (shown in Fig. 1 of Sanchez-Hernandez and Maurrasse 2014). The road goes toward the summit of Prada Mountain and provides

an exceptional spatio-temporal exposure of Cretaceous sediments. In the study area the stacked succession of the well-bedded sequence displays a unique Lower Cretaceous series (Figs. 6-2 – 6-6) that is laterally continuous and shows no clear evidence of significant syn- or post-depositional deformations. The absence of apparent subaqueous gravity flow or intraformational deformation within the studied sequence implies basin stability, and no syntectonic effects involving folding and thrusting during sedimentation in this part of the Organyà Basin, thus ensuring a normal continuous succession.

Estimates of the Cretaceous series of the Organyà Basin give a thickness of ~4500 m of marine sediments, and approximately 1000 m would correspond to the Barremian–Early Aptian interval (Berástegui et al. 1990; 1993; García-Senz 2002; Bernaus et al. 2003).

The apparent undisturbed succession in the El Pui area (Fig. 6-2) should therefore provide a detailed continuous record of the paleoenvironmental conditions of that time in the Organyà Basin. The long period of passive evolution under relative tectonic quiescence in that part of the Basin correlates with the time of the extensional/trans-tensional regime associated with the opening of the Bay of Biscay.

The base of the studied section begins with dark-colored carbonate rocks referred to in the literature as the “Cabó Marls” (Garrido-Mejías 1973; Peybernès and Souquet 1973; Peybernès 1976; Berástegui et al. 1990; García-Senz 2002; subsequently used as Cabó Formation) superjacent to the biocalcarenites and calcirudites with rudists and annelids of the Prada Formation (Caus et al. 1990; García-Senz, 2002). The term “Formation” as an informal name applied to the sequence of marly rocks including the earliest Aptian was first used by Peybernès and Souquet (1973): “ In the series of black marls in the southern Pyrenees, where two formations are distinguished: the *Cabó marls*

(Bedoulian - Gargasian) and the *Bóixols marls* (lower Albian)”. Peybernès (1976) further applied the term “Formation” as an informal name using both lithologic and faunal content as distinctive characteristic features, as he exemplified with the units he designated as “Marnes noires à Hypacanthoplites”, or by a local name, or a combination of both. Subsequently García-Senz (2002) formally assigned the name Cabó Formation to the sequence, using international standards for stratigraphic nomenclature (AAPG-NACSN, 1982). The type section is near the town of Cabó, namesake of the Formation.

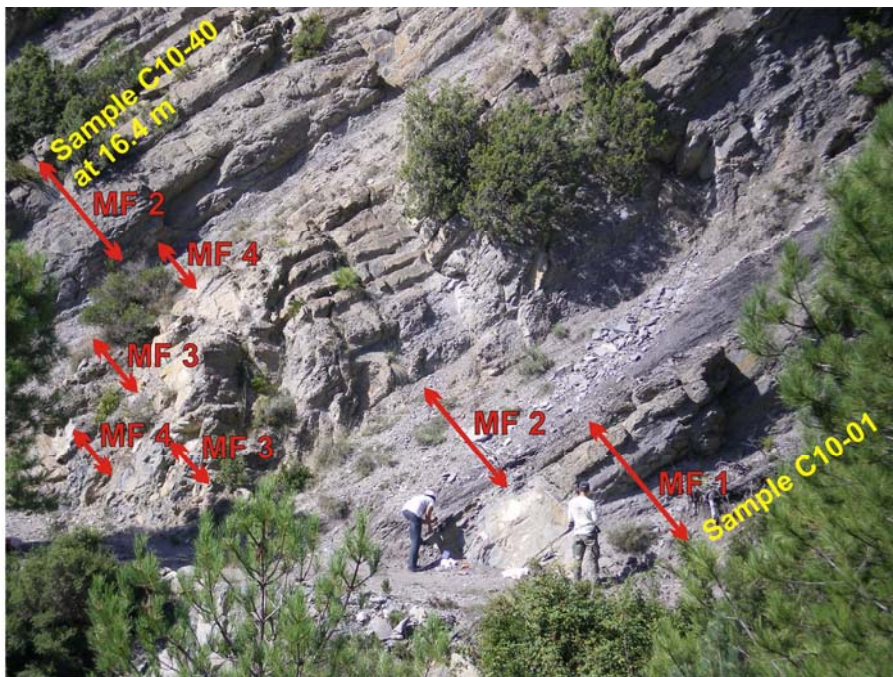


Figure 6-3 Near field view of the lower ~17 m of the stacked limestones and marlstones of the El Pui section. Note facies intervals as described in the text.

Because neither the composition, nor the hardness often used to designate these rocks as Cabó marls (*sensu lato*) can be uniformly applied to the lithologic succession in the Organyà Basin, we use the more appropriate nomenclature of Cabó Formation (García-Senz 2002). Despite some differences with the lithologies that define the type section (García-Senz 2002, p 51–59), the sequence defined at El Pui is now its equivalent

with lithologic names based on objective values of their actual content in total inorganic carbon (TIC) (Sanchez-Hernandez and Maurrasse 2014).

6.3 Materials and Methods

The study includes 207 samples of the lower 85 meters of the outcrop at El Pui. At the field scale we recorded variations in bed thickness, color, primary sedimentary structures presence or absence of visible faunal components, and bioturbation.

For initial lithologic designation in the field we made use of the different visual parameters such as bed thickness, apparent dominant coarse constituents, fissility (Ingram 1953), and whether the rocks could be categorized as different types of limestones (Pettijohn 1957; Folk 1959; 1962), marlstones or mudrock. Final lithologic names were assigned after carbonate content analysis and are based on TIC content.

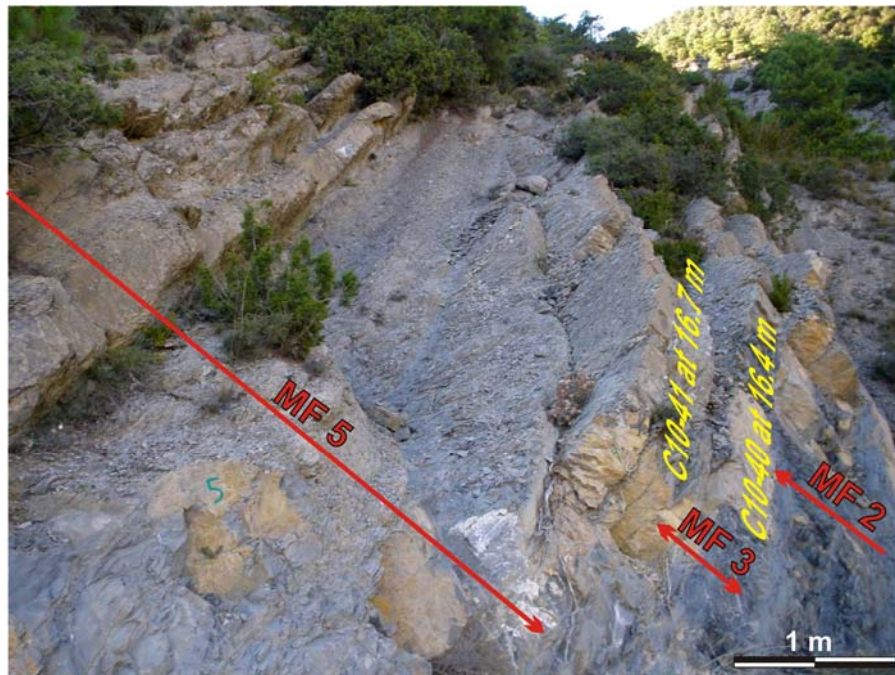


Figure 6-4 Close-up view of part of the succession shown in Fig. 6-3 and immediately above. Note the Dark yellowish orange (10YR 6/6) of the weathered surface in contrast to the true Bluish gray (5B 6/1) of the unaltered rock.

In order to obtain an objective assessment of dry rock colors that may be indicative of the organic carbon content we used the “Rock-color chart” distributed by the Geological Society of America (GSA, Goddard et al. 1963), which is designed as a modified Munsell color system. The number and range on the chart were developed based on studies of more than 1300 rock specimens, and the chart is a simple booklet that can be used in the field as well as in the laboratory. It provides an objective representation of colors that permits the same visual correlation by different observers. It defines *color* with a combined letter and numerical designation and uses three simple variables: its *hue* (actual color), *value* (indicates lightness or tone, measures how light or dark a color is, as it will depend on whether the rock is dry, damp, or wet), and *chroma* (intensity). The system uses a grading scale so that *value* ranges from white (absolute white, highest number 10) to dark (absolute black, lowest number 0). A color of *value* “5” is midway between the two end colors. The symbol for hue is the letter abbreviation of the color of the rainbow. The *Chroma* increases from somber (lower number) to the most vivid colors (higher number). The color notation uses the order: *hue*, *value* and *Chroma*, with a space between the *hue* letter and the succeeding value number, and a slash between the two numbers for *value* (left) and *Chroma* (right), as for example in the color designation for Olive Gray (5Y 4/1). The N section of the chart represents the gray hues from absolute black (N1) to white (N9). Colors of the El Pui sequence were evaluated on freshly cut samples on dry outcrops, or individual air dry samples because wetting usually decreases the *value* number, thus making the rock specimen darker, although the *Chroma* may not change.

Microscopic analyses were carried out using a Wild-M5 binocular microscope for initial examination of cut samples, as well as washed residues, and an Olympus BH-2 petrographic microscope equipped with conventional transmitted and/or polarized light for microfacies analysis.

Semi-quantitative analyses using Scanning Electron Microscopy (SEM) and Energy Dispersive Spectroscopy (EDS) were obtained on selected samples representative of facies intervals to identify the components of the matrix and evaluate dominant constituents (Sanchez-Hernandez and Maurrasse, 2014). Selected samples were polished and acid etched based on the technique described by Folk (1993), and used in our laboratory (Duque-Botero and Maurrasse 2005) for imaging and semi-quantitative chemical analyses with a JEOL JSM 5910LV available at the Electron Microscopy facility of the Earth and Environment Department at FIU.



Figure 6-5 Close-up view higher up the sequence showing part of the outcrop of microfacies MF5.

The nomenclature selected to describe and characterize microfacies is mostly after Folk (1980) modified from Folk (1962) classification scheme. Occasionally, we also refer to Dunham (1962) scheme, when convenient and for simplicity. At the microscopic scale we also consider fabric, primary microstructures including burrowing, presence or absence of planktonic and benthic organisms, as well as all other identifiable bioclasts (e.g. ostracod, ammonoid and echinoderm fragments), mineral content, and miscellaneous components indicative of conditions of sedimentation and diagenesis (pyrite).

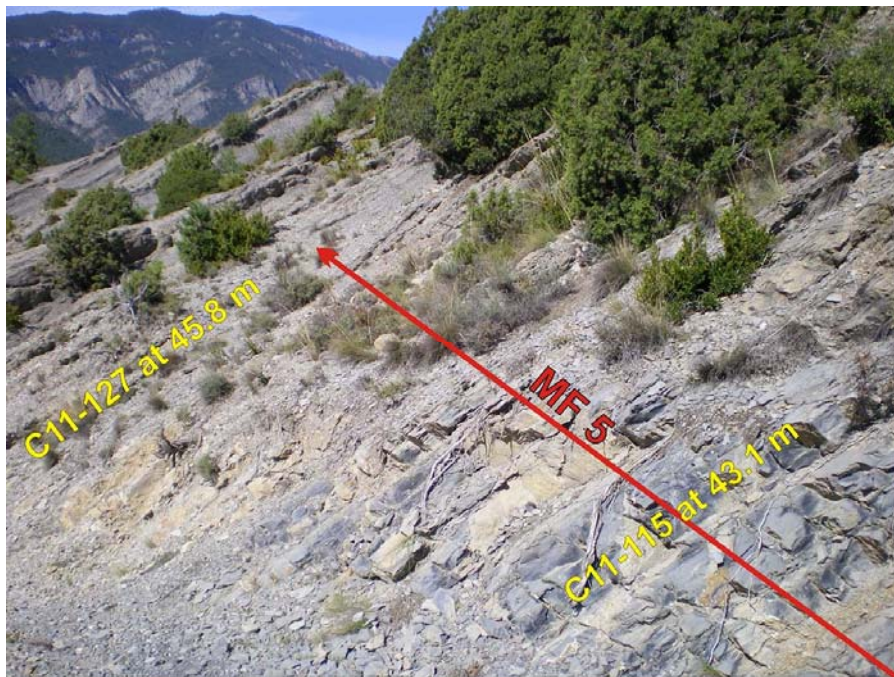


Figure 6-6 Close-up view of the outcrop comprising microfacies MF5 showing the transition from massive well consolidated limestones to marlstones.

Textural terms used in the petrographic analyses are after Folk (1962), Dunham (1962), Friedman and Sanders (1978); Flügel (1982), and Scholle and Holmer-Scholle (2003). Estimate of grain size distribution was made in 20 fields of view at $\times 40$ and $\times 100$ magnifications per thin section. Relative abundance of fossil components is given as

per 10 cm² of a thin section, where abundant is considered for more than 10 specimens/10 cm²; scarce = 10-4/10 cm²; rare = < 4/10 cm² (Sanchez-Hernandez and Maurrasse, 2014). Concerning lithologic terms of the carbonate rocks, there is no definitive agreement in the literature on the range of appropriate carbonate values to define the different lithologies. Pettijohn (1957) suggested a detailed subdivision, including 35 to 65 percent carbonate for marls. Here we use the values adopted in Sanchez-Hernandez and Maurrasse (2014) based on measured CaCO₃ (TIC) as follows: limestone, > 65% CaCO₃; marly-limestone, 60% - 65% CaCO₃; marlstone, 30% - 60% CaCO₃; calcareous mud-rock/shale, 10% - 30% CaCO₃; and mud-rock/shale, 0 - 10% CaCO₃.

Concerning foraminiferal nomenclature for the index taxon identified in the studied section we apply the taxonomic name *Globigerinelloides* for the species *G. blowi* (also commonly referred to in the literature as *Blowiella blowi*). The choice of this taxonomic name is based on the work of Verga and Premoli-Silva (2002, 2003) that clearly established the validity of the genus *Globigerinelloides* as applied to this taxon. Because the samples were well indurated, normal disaggregation method using a detergent was unsuccessful therefore we attempted the liquid nitrogen [LN₂] method for foraminifera (Remin et al. 2012), which enabled extraction of a few loose specimens of *G. blowi* (Sanchez-Hernandez and Maurrasse 2014). However, the LN₂ method did not yield loose specimens of the co-occurring species such as *Globigerinelloides maridalensis* and *Globigerinelloides paragottisi*, or any other planktonic foraminifera. Thin section analysis of sample C11-113 at the 43 m level (Fig. 6-7A) yielded morphotypes that could be conferred to *G. maridalensis*, which is in agreement with both the stratigraphic range assigned to this taxon in the earliest Aptian (Verga and Premoli-

Silva 2002, 2003), and the chronology based on chemostratigraphy (Sanchez-Hernandez and Maurrasse 2014).

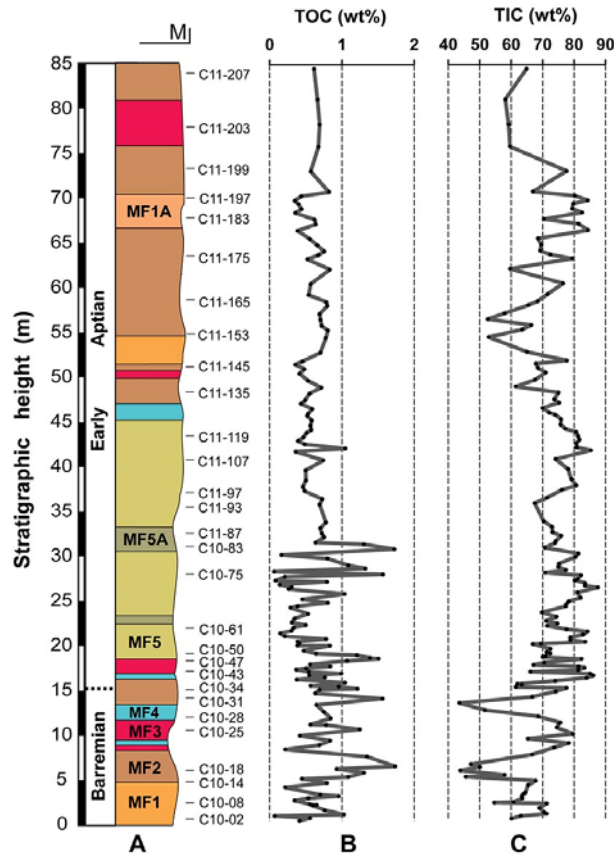


Figure 6-7 A) Simplified lithologic column of the lower 85 m of the El Pui section with partial sample location and microfacies distribution. Color assignment to microfacies follows the same pattern throughout the column. B) Total organic carbon curve (TOC), and C) total inorganic carbon (TIC) as wt % CaCO₃.

Leupoldina (Bolli 1957; Caron 1985; emended Verga and Premoli Silva 2002) is also a characteristic genus reported from the late Barremian to the early Aptian (Premoli Silva et al. 1999; Verga and Premoli Silva 2002; Elkhazri et al. 2013) with variations in levels of occurrences that may be due to their rarity and susceptibility to diagenetic dissolution (Premoli Silva et al. 1999). In the El Pui section very rare morphotypes that could be attributed to leupoldinids were recorded starting at ~51m (sample C11-145, Fig. 6-7A). However, none of the forms inferred to this genus could be conferred to a species

because of the complex shell type. As discussed and illustrated in Verga and Premoli Silva (2002), *Leupoldina* has tridimensional morphological features that are extremely complex. The forms vary from pseudosplanispiral to very slight trochospiral coiling, and chambers may be branching out (bi-tri or quadrifurcated) in various degrees with terminations that may include ampullae (e.g. Verga and Premoli Silva 2002). In addition, the *Leupoldina* shell shows such pronounced disaxial growth that results in an asymmetry of the last whorl with one side slightly convex and the other side slightly concave, or the last chamber completely shifted towards one of the sides (Verga and Premoli Silva 2002). Hence, *Leupoldina* morphotypes display such a great disparity of asymmetry that the main criterion that distinguishes the different species being the degree of involution cannot be unequivocally identified in thin sections. Since the rocks at El Pui were too lithified to extract whole specimens that might provide unmistakable morphological characteristics of distinct *Leupoldina* species, the assignments here remain at the genus level.

6.4 Results and discussion

6.4.1 Overall lithology and macrofacies

At the field scale the lower 85 m of the El Pui section consists of an interbedded sequence of essentially carbonate rocks that can be referred to as calcilitites (Folk 1962). The beds are essentially tabular, well indurated, and vary in thickness between 15 cm and 3 m (Figs. 6-2 – 6-5) with scattered ammonites at intermittent levels (Moreno-Bedmar 2010; Sanchez-Hernandez and Maurrasse 2014). The lithologic succession is characteristically dark in color, displaying various shades of grays (N7 – N6) to light olive gray (5Y6/1) on weathered surfaces, and medium dark gray (N4) to grayish black

(N2) on fresh cuts. Although color variation shows no relationship to rock texture, previous studies suggested that they might be related to fluctuations in OC and mineral content (Sanchez-Hernandez et al. in press). The rocks may show apparent fissility thus appearing shaly on weathered surfaces, but the flaky appearance (Ingram 1953) often dissipates at depth as the unaltered rock is well lithified. The cleavages that developed parallel to bedding plane are actually related to discrete shears due to tectonic stresses and strains, and in some cases the rocks appear softer due to shearing and partial weathering (Figs. 6-2 – 6-6).

Owing to their dark color and the apparent weathered shaly structures rocks of the Cabó Formation are often associated with black shales, but TOC fluctuates up to 1.7% (Fig. 6-7B), and the measured TIC values remain above the threshold limit of 30% CaCO₃ for shales. In fact, the minimum recorded value is 43.5% at about 13 m (Fig. 6-7C) from the base of the studied section, which is part of the series of thickly bedded units that can be assigned to marlstones (Sanchez-Hernandez and Maurrasse, 2014).

6.4.2 Microfacies description, intervals of occurrence and interpretation

The most important lithologic characteristic of the Barremian–Aptian transition in the El Pui section is a significant change in microfacies character from the calcarenites and calcirudites (Urgonian type facies) of the Prada Formation (García-Senz 2002) to the calcilitites of the Cabó Formation. The shallow-water limestone facies of the Prada Formation are biocalcirudites, or packstones, commonly crowded with annelids, mollusk and echinoid fragments, and other bioclasts in a micritic matrix (Garrido-Mejías 1973; Berástegui et al. 1990; García-Senz 2002). In contrast, the basal part of the Cabó marlstones represents a sudden shift from shallow-water platform deposits to deeper

hemipelagic mudstone facies interpreted by Berástegui et al. (1990) as an offshore/slope and basinal deposit with very limited contribution from shallow platforms (García-Senz 2002). This sharp contrast in sedimentation regime, bio-production and material sources has been related to tectonic reconfiguration of the area as the rifting episode of the Iberian and European plates accelerated during the early Aptian (Gong et al. 2009) thus producing numerous basins with complex bathymetries associated with differential flexural movement. During this interval the development of an E-W trending graben (Dinarès-Turell and García-Senz 2000) characterizes a deepening phase of the Organyà Basin that underwent increased subsidence (García-Senz 2002). A coeval transgressive system (Bernaus et al. 2002) may have also contributed to rapid differentiation of the depositional conditions.

The overall typical microfacies at all levels of the studied sequence are characterized by a matrix of dark yellowish brown (10YR 4/2 to 10YR 5/4) in plane-polarized light, and consist of a fine mud (clay to fine silt sizes: 4 - ~30 μ m) composed of mix carbonate (70%), OM (~ 1.0%), and siliciclastic: fine quartz (14%), clays (9%) and other minerals (6%). Both microscopic and SEM analyses reveal that sparry calcite is extremely rare while the major carbonate constituents in the micritic matrix are calcareous nannofossil remains (Fig. 6-8A–D) (Sanchez-Hernandez and Maurrasse 2014; Sanchez-Hernandez et al. in press), which account for most of the fine fraction. The allochemical fraction fluctuates between 5 and 35% and is mainly composed of comminuted echinoderm (roveacrinids) and ammonite shell microfragments, together with varying amount of calcispheres. All other microfossils are rare to very rare, consisting of ostracods, benthic and planktonic foraminifera (Figs. 6-9 – 6-16).

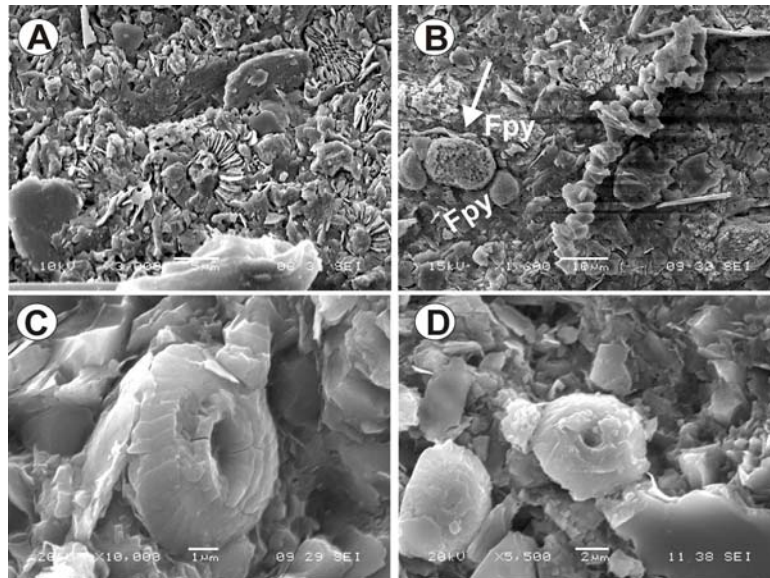


Figure 6-8 SEM micrographs of samples showing characteristic components of the matrix in the 85m section studied. A) C10-52, 19 m; B) C10-77, 28 m; C) C11-87, 32 m); and D) C11-137, 49 m. Calcareous nanofossil remains are consistently abundant and are the main components of the calcareous matrix throughout the studied sequence. Note framboidal pyrite (FP) in micrograph B.

Microscopic compositional and textural changes allow for the identification and characterization of various hemipelagic microfacies (MF) of the El Pui section as follows:

MF1: Sparsely fossiliferous micrite type 1

MF1 occurs within the lowest 4.8 m of the studied section, and recurs between 51.6-54.3 m (Figs. 6-3, 6-7A, 6-9A–G). This microfacies is characterized by a fine micritic matrix with 25-35% allochems that consists of small carbonate debris with fragment sizes between 10 μm and 1 mm. Approximately 99% of the coarser components have size $<50 \mu\text{m}$ (silt size ranges). Larger skeletal grains account for only $\sim 1\%$ of the allochems and consist of thin shelled ammonite ($< 60 \mu\text{m}$), and roveacrinid fragments (Fig. 6-9D, E, G). Planktonic and benthic foraminifera (Fig. 6-9C, F) are rare throughout and consistently of very small sizes $<150 \mu\text{m}$, ostracods are rare and intermittent. The

microfabric is isotropic with a low bioturbation index ranging from 0 to 2 (Taylor and Goldring 1993). Interparticle pores in burrows and intraparticle pores are partially filled with kerogen, which may account for an average TOC of 0.5% (Fig. 6-7B). Calcspheres and pyrite (framboidal and dispersive) are common.

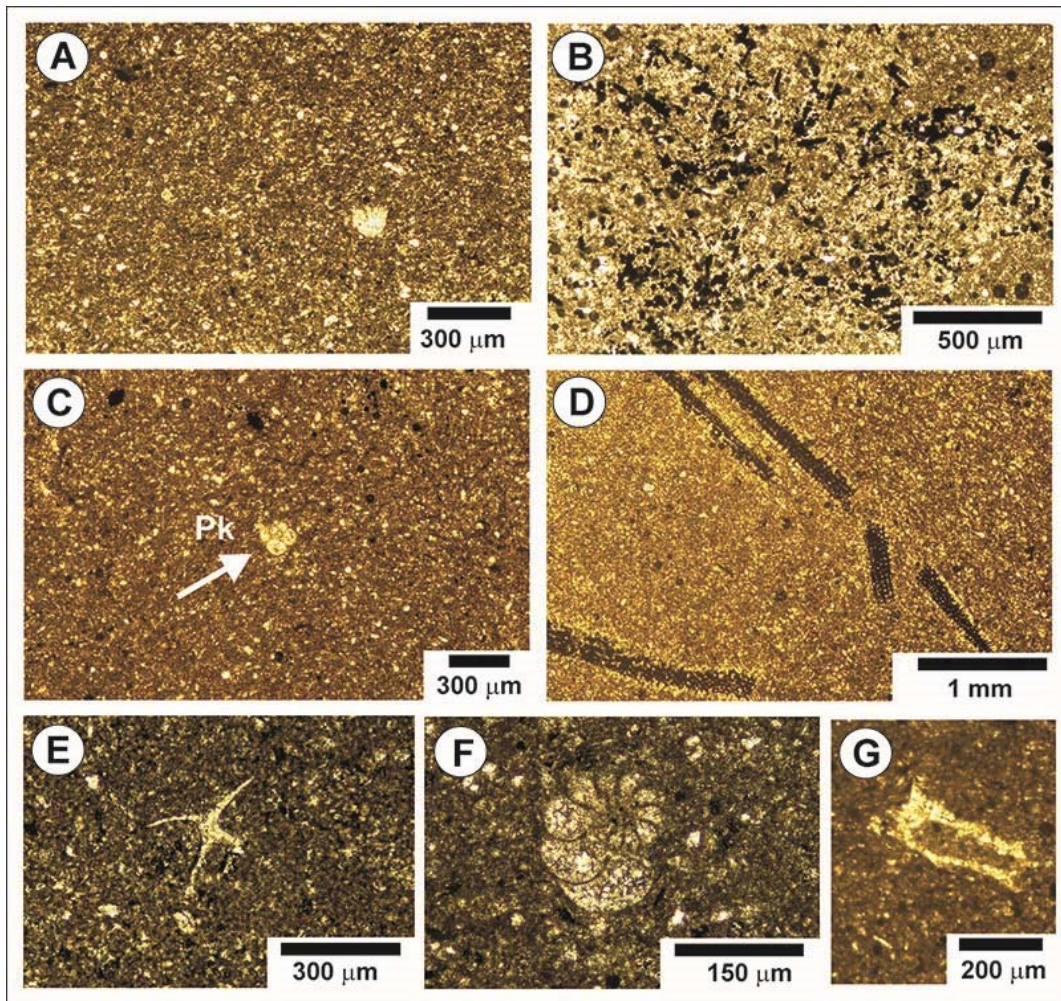


Figure 6-9 Photomicrographs illustrating microfacies MF1. A) Sample C10-01, micritic matrix with a larger unidentified skeletal grain. B) Sample C10-04, bioturbated matrix with kerogen filling in interparticle pore spaces. C) Sample C10-05, very fine micritic matrix with a small planktonic foraminifera (Pk) (cf. *G. blowi*?). D) Sample C10-06, very fine micritic matrix with roveacrinid fragments. E) Sample C10-06, undetermined roveacrinid fragment in a fine carbonate mud. F) Sample C10-09, with well-preserved coiled benthic foraminifera in a carbonate mud with additional carbonate microfragments. G) Sample C10-09, undetermined roveacrinid fragment.

Interpretation

In MF1 the primary sedimentary structures include essentially bioturbation, thus the lack of patterns indicative of hydrodynamic processes implies a calm environment, most likely within bathyal depth or deeper. The preserved biomass indicates that productive surface waters were apparently dominated by calcifying nannoplankton (Fig. 6-8), with fewer calcispheres (Sanchez-Hernandez et al., 2014), and shelled heterotrophs including mostly roveacrinids and small thin-shelled ammonites. Planktonic foraminifera were rare suggesting that they played a minor role of the extant food web. Such scarcity or absence of planktonic foraminifera in environments with roveacrinids is also reported elsewhere (Peck 1943; 1955; Cros et al. 1991; Ferré and Berthou 1994; Ferré 1997; Ferré and Granier 2001).

The absence of shallow-water components in the El Pui sediments suggests retrogradation of the surrounding carbonate platforms, and possibly the effect of sediment traps associated with the complex flexural architecture of the subsiding margin (Gabrielsen 2010). Since increased subsidence rates have been reported for the Organyà Basin in the early Aptian (Berástegui et al. 1990; García-Senz 2002) and paleophysiographic reconstructions suggest a most likely flat configuration of the platform (Caus et al. 1990), we favor a combination of subsidence and a natural barrier that blocked the input of carbonate debris into the hemipelagic domain.

The appearance of rare small (<150µm) benthic foraminifera in MF1 corroborates oxygen-deficient conditions (Wignall and Myers 1988) in bottom waters, as their scarcity cannot be attributed to lack of food supply because of extensive OM in burrows, intergranular and in intragranular pores (Fig. 9B, D), TOC averages 0.5%.

Although anoxia was not achieved, framboidal and dispersive pyrite (similar to Fig. 6-8B) further suggest redox conditions favorable for OM preservation. The relatively high TOC, together with significant carbonate content (45.5 - 71.3%) within MF1 intervals are consistent with enhanced *in situ* surface productivity as indicated by the dominant calcareous nannofossil remains and skeletal detritus from higher pelagic heterotrophs (mesoplankton secondary consumers) (Fig. 6-9D, G) not characteristic of carbonate platform debris (García-Senz 2002).

MF1A: Sparsely fossiliferous micrite

MF1A is a variant of microfacies MF1 occurs only between 67.6 and 70.2 m (Figs. 6-7A, 6-10A–F). Its main characteristic is a relative decrease in the allochem content (<10%) with respect to MF1. Benthic foraminifera remain rare and include only elongated uniserial and biserial morphotypes (Fig. 6-10A, E). Planktonic foraminifera are rare (Fig. 6-10D). MF1A shows some degree of anisotropic fabric, with low bioturbation index (0-1), which may explain the fabric closest to the original orientation of the bioclasts. The allochems >50 µm are <1% of the total content and include also echinoid spines (Fig. 10B), small roveacrinid fragments (Fig. 6-10C), and possibly ostracods (Fig. 6-10F).

Interpretation

Subfacies MF1A showing texture and fabric similar to MF1 with limited bioturbation and biserial benthic foraminifera points to a possible short episode of heightened oxygen depletion close to the water sediment interface that increased OM accumulation, possibly coupled with a surge in intensified plankton productivity

(Sanchez-Hernandez et al., in press). Oxygen depletion may have worsened, but the presence of the benthic foraminifera implies that anoxia was not fully achieved.

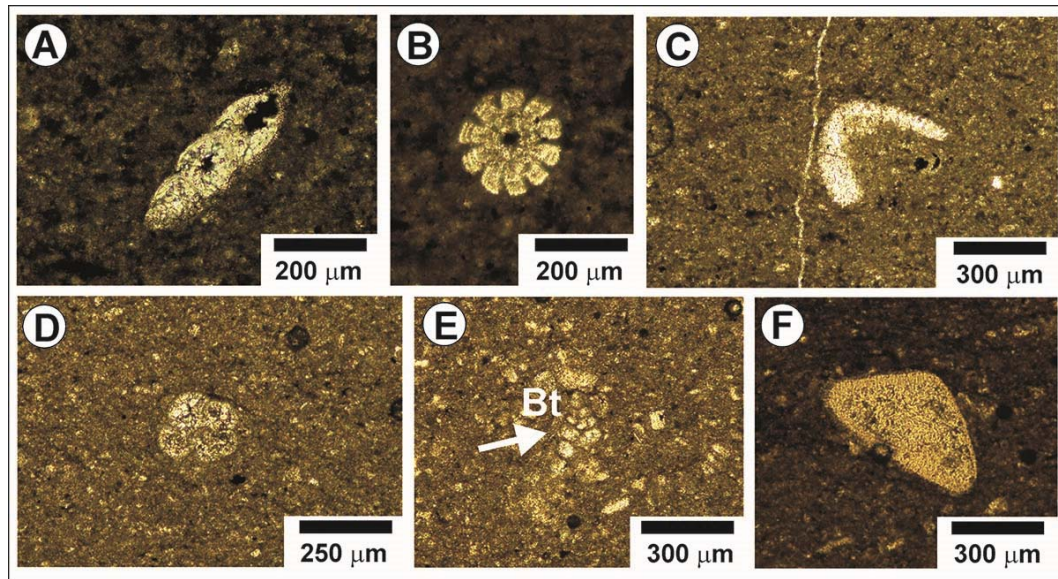


Figure 6-10 Photomicrographs illustrating microfacies MF1A. A) Sample C10-64, benthic foraminifera in a very fine carbonate mud with dispersive amorphous OM. B) Sample C10-65, cross section of a small echinoid spine in a very fine carbonate mud with dispersive amorphous OM. C) Sample C11-19, roveacrinid fragment next to a microfracture in a fine matrix. D) Sample C11-191, planktonic foraminifera *G. blowi*. E) Sample C11-193, biserial benthic foraminifera (Bt) and microcarbonate fragments floating in a micritic matrix. F) Sample C11-189, undetermined bioclast, possibly an ostracod?

MF2: Fossiliferous micrite

MF2 is prevalent within the 85 m-studied interval of the El Pui section. It occurs intermittently within the following levels: 4.8-7.2 m, 13.5-16.4 m, 47-50 m, 51-51.6 m, 54.3-67.6 m, 70.2-76 m and 81-85 m, respectively (Figs. 6-3, 6-4, 6-7A, 6-11A–H, 6-12A–K). The textural appearance of microfacies MF2 is characteristically coarser, with a predominately isotropic microfabric (bioturbation index of 1-3), more diversified skeletal grains (20-35%), and rare larger-sized biserial benthic foraminifera than in MF1 (Figs. 6-11E, 6-12D, K). Planktonic foraminifera vary between abundant (at ~5 m) and scarce in the other intervals, but are consistently very small (80-120 μm) (Figs. 6-11B, 12C). SEM analysis reveals essentially calcareous nannofossils in the matrix similar to MF1.

The average TOC value (Fig. 6-7B) at levels coincident with MF-2 fluctuates between 0.5 and 0.9% and is recorded throughout in the texture as traces of dispersive kerogen, or as small accumulation in the inter- and intraparticle pores, as well as filling skeletal molds (Figs. 6-11E, G, 6-12D, G). The average TIC varies from ~51 to ~73% indicating strong carbonate dominance in the sediment (Fig. 6-7C). Bioclasts range in size from 10 μm to 2 mm (Figs. 6-11, 12) with 80% of fragments < 60 μm in size, ~15% between 60 and 200 μm , and ~ 5% > 200 μm . Elongated acicular particles < 50 μm in size are also common (Fig. 6-11F).

Interpretation

MF2 includes significant amount of acicular carbonate particles together with millimeter scale tabular pieces that suggest active disintegration of ammonite shells nacreous layers (Birkelund and Hansen 1968; Kulicki 1979; 1996; Velásquez-Castillo et al. 2006) presumably from abundant very small pelagic species, because larger molds are very rare in the beds. Larger skeletal grains (Figs. 6-11D, 12E–G, I) have morphological and textural characteristics of roveacrinids (Peck, 1943; 1955; Cros et al. 1991; Ferré and Berthou 1994; Ferré 1997; Ferré and Granier 1997; 2001). Clearly the abundance of ammonite and roveacrinid debris suggests a trophic pyramid in the pelagic domain of the basin where these organisms might have been the primary or secondary consumers benefiting from the intricate food web sustained by high primary productivity (Scarparo Cunha and Shimabukuro 1997; Kruta et al. 2011). The proximity of landmasses and existing physiographic differences between the basin and surrounding terranes (Berástegui et al. 1990) permit to infer that constant fluxes of the most critical biolimiting element in the biological cycle (i.e. phosphorus) to the basin (Sanchez-Hernandez and

Maurrasse 2014) resulted in sustained high primary productivity, and an accelerated food chain in which roveacrinids and ammonites played an active role (Cecca 1998; Kruta et al. 2011).

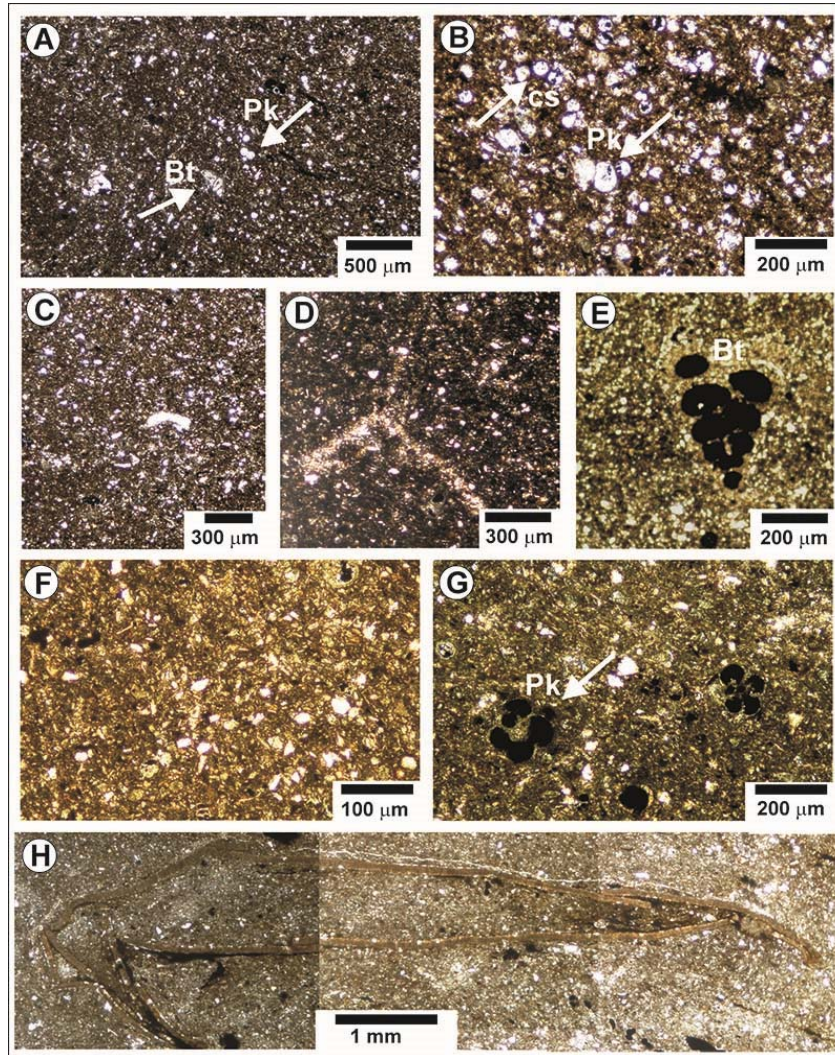


Figure 6-11 Photomicrographs illustrating microfacies MF2. A) Sample C10-16, fine carbonaceous matrix with benthic (Bt) slightly below center, planktonic (Pk) foraminifera, and abundant calcispheres (cs). B) Magnified view of part of photomicrograph shown previously in A. C) Sample C10-17, abundant microcarbonate fragments and skeletal components in a fine matrix. D) Sample C10-18, inferred section of a radial plate of an undetermined roveacrinid. The microcarbonate particles are thought to be from disintegration of these planktonic micro-echinoderms. E) Sample C10-20, biserial benthic (Bt) foraminifera. F) Sample C10-18, slightly bioturbated carbonate matrix with abundant comminuted skeletal debris. G) Sample C10-20, molds of planktonic (Pk) foraminifera replaced with kerogen in a micritic matrix. H) Sample C10-19, undetermined fossil remain embedded in a fine carbonate matrix (copepod ?, loricifera ? van der Wielen et al. 2005, Yakimov et al. 2007).

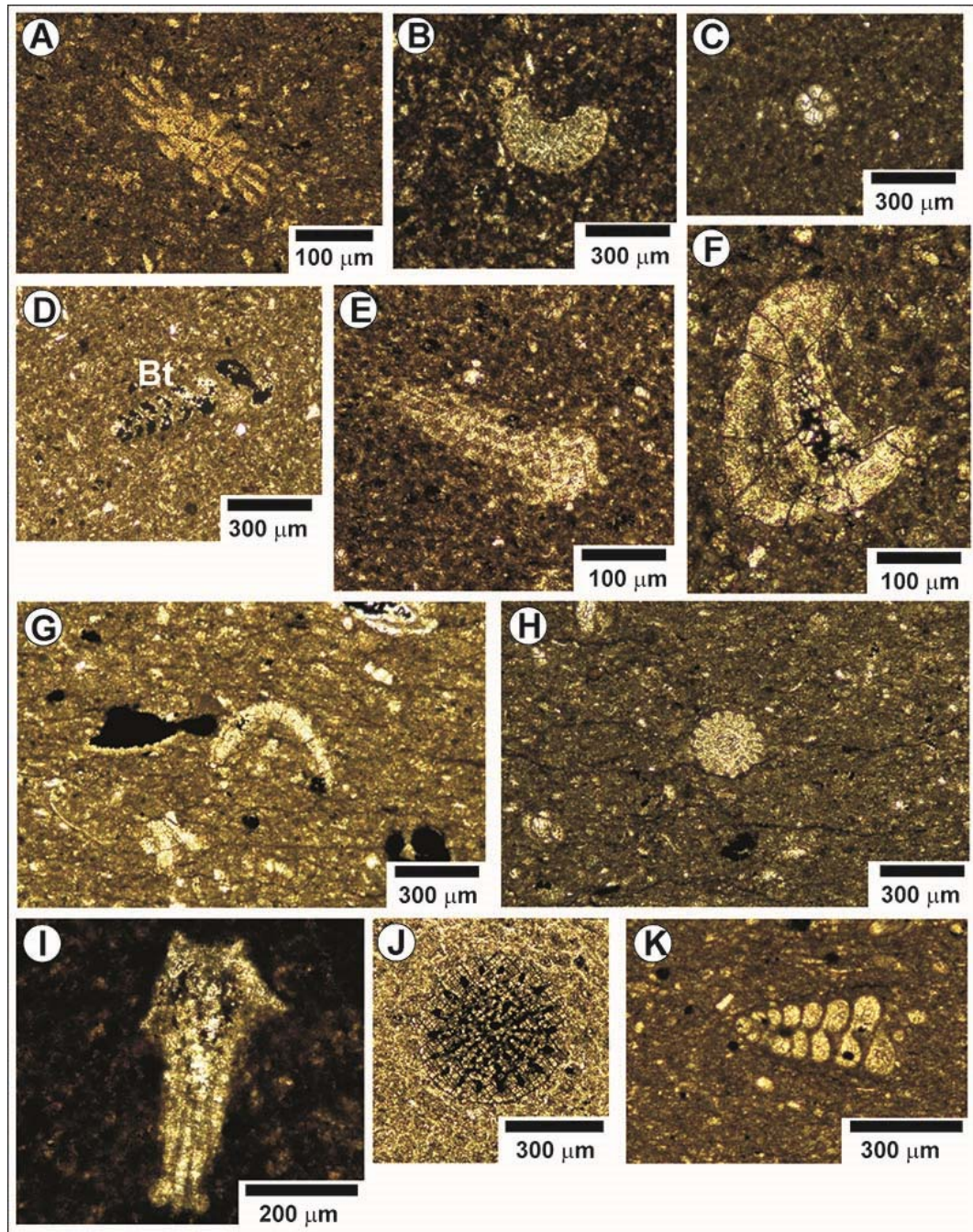


Figure 6-12 Photomicrographs illustrating microfacies type MF2, continued. A) Sample C10-31, oblique section of small echinoderm spine. B) Sample C10-31, undetermined roveacrinid fragment in a fine, dark carbonate mud. C) Sample C10-32, planktonic foraminifera. D) Sample C10-32, biserial benthic foraminifera (Bt) with chambers filled with OM. E, F) Sample C10-39, undetermined roveacrinid fragments in a fine micrite. G) Sample C11-153, comminuted ammonite shells. H) Sample C11-155, cross section of a small echinoid spine in a fine carbonate matrix with occasional subparallel fabric. I) Sample C11-161, undetermined roveacrinid fragment in a dark carbonate mud with dispersive amorphous OM. J) sample C11-165, echinoderm fragment. K) Sample C11-173, biserial benthic foraminifera in a micritic matrix.

By analogy with modern environments (Stelmakh 2013; Sun et al. 2013), which offer viable conceptual models of the complexity of marine ecosystems in the past, various organisms that might have been key participants of the heterotrophic planktonic communities (ciliates, copepods, tintinids, dinoflagellates, chaetognaths, salps), were not preserved in the sediments. Hence, our knowledge of the exact relationships between these various organisms, the roveacrinids and ammonoids in the food web, will remain imperfect. Nonetheless, the assumption based on the present is that the biomass of small ammonites and roveacrinids indicate that they were major components of the food chain in the pelagic domain of the Organyà Basin.

A relatively high organic carbon content (average TOC >0.5%) suggests a chemically reducing phase for MF2, but the bioturbation index (1-3), and the presence of benthic foraminifera indicate that, if present, dysoxic conditions were weak (Sanchez-Hernandez and Maurrasse, 2014; Chapter 4). Fig. 6-11H shows a unique specimen of an apparent soft-bodied organism reminiscent of either copepods? or loricifera? (Yakimov et al. 2007; Danovaro et al. 2010), which could withstand limited oxygenic conditions.

Microfacies MF2 is consistent with stable synrift conditions in basin geometry and depositional energy as the matrix is still dominated by pelagic components.

MF3: Sparsely fossiliferous micrite type 2

MF3 (Fig. 6-13A–J) occurs in relatively short and intermittent episodes that characterize intervals 8.0-8.3 m, 9.6-11.5 m, 16.7-17.4 m, 50-51 m, and 76-81 m, respectively (Figs. 6-3, 4, 6-7A) The typical features of MF3 is a decrease in the allochemical content to ~10% as compared with MF1 and MF2. Planktonic foraminifera are rare with sizes ~100 µm or less (Fig. 6-13A). Benthic foraminifera are scarce and

small, but increase in size (150 - 300 μm) at certain levels (Fig. 6-13B, E, I). Scattered larger ammonoid fragments (Fig. 6-13J), roveacrinid (Fig. 6-13C, F, H) and other unidentified echinoids, still occur in the fine carbonate matrix and may account for <10% of the skeletal grains. The average TIC is \sim 78%, while TOC averages \sim 0.5%. Primary and secondary intraparticle pores are filled with organic matter (Fig. 6-13E– G).

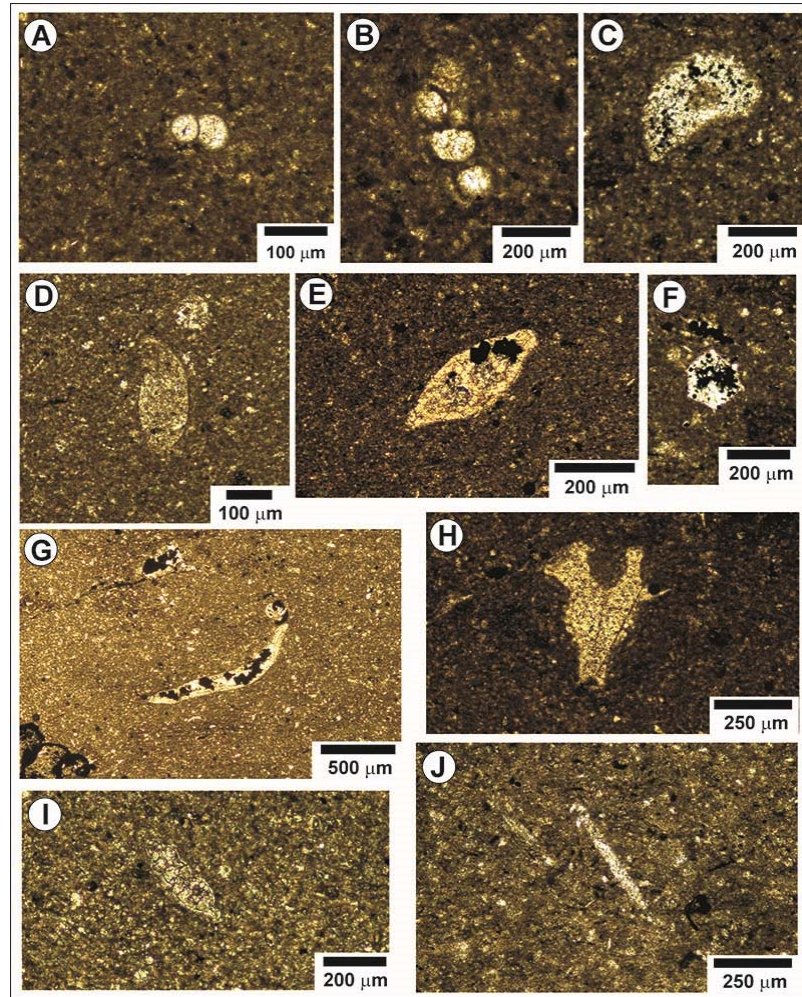


Figure 6-13 Photomicrographs illustrating microfacies MF3. A) Sample C10-21, lateral cut of a small planktonic foraminifera in a very fine, dark carbonate mud. B) Sample C10-24, partial view of a biserial benthic foraminifera in the same type of matrix as C10-21. C) Sample C10-25, roveacrinid skeletal fragment. D, E) sample C10-42, benthic foraminifera in a dark carbonate matrix. F, G, H) Sample C10-43, (F) transversal section of a roveacrinid cup; (G) undetermined bioclast; (H) oblique to transverse section of an undetermined roveacrinid. I) Sample C10-44, benthic foraminifera in a fine carbonate mud. J) Sample C11-203, ammonoid skeletal fragment in a fine carbonate mud (field of view is rotated relative to the normal bedding plane).

Interpretation

The relative decrease in the allochemical content in MF3 appears to coincide with declining terrestrial input (Sanchez-Hernandez and Maurrasse, 2014), which might have affected the nutrient load, thereby negatively impacting the marine food web in the pelagic realm of the basin. Perhaps, a reduction of clastic fluxes contributed to maintain relatively high TIC values while TOC was not greatly affected because of continuously high primary productivity. Bioclasts appear intermittently oriented parallel to bedding plane (Fig. 6-13J), which suggests limited effects of bioturbation. We infer fluctuating dysoxic to oxic bottom waters based on the inconsistent pattern of the size and abundance of benthic foraminifera. Such variation in deposition in the Organyà Basin could be related to climate variability (Bachmann and Willems, 1996). MF3 is consistent with a basinal depositional environment that remained stable.

MF4: Sparsely fossiliferous micrite type 3

MF4 characterizes the following intervals: 8.5-9.0 m, 12.2-13.5 m, 16.5-16.7 m, and 46-47 m, respectively (Figs. 6-3, 6-7A, 6-14A–H). MF4 is texturally closely related to MF2, from which it differs in allochemical content that ranges from 25-35% with ~90% of fragments <50µm, ~7% between 50 µm and 250 µm, and ~3% within the 250 µm and 700 µm range (Fig. 6-14). Planktonic foraminifera are more common than in previous microfacies, and their sizes are typically ~120 µm (Fig. 6-14C). Benthic foraminifera (Fig. 6-14E) are rare to absent, particularly between 12-13 m. Fragments of disintegrated roveacrinids, unidentified echinoderm spines predominate among bioclasts with size >250 µm, although bits of ammonoid, and calcispheres are also present (Fig. 6-

14D, F, G). The bioturbation index fluctuates 0-2, and burrowed areas may show irregular sub-parallel alignment of elongated micro components (Fig. 6-14G, H).

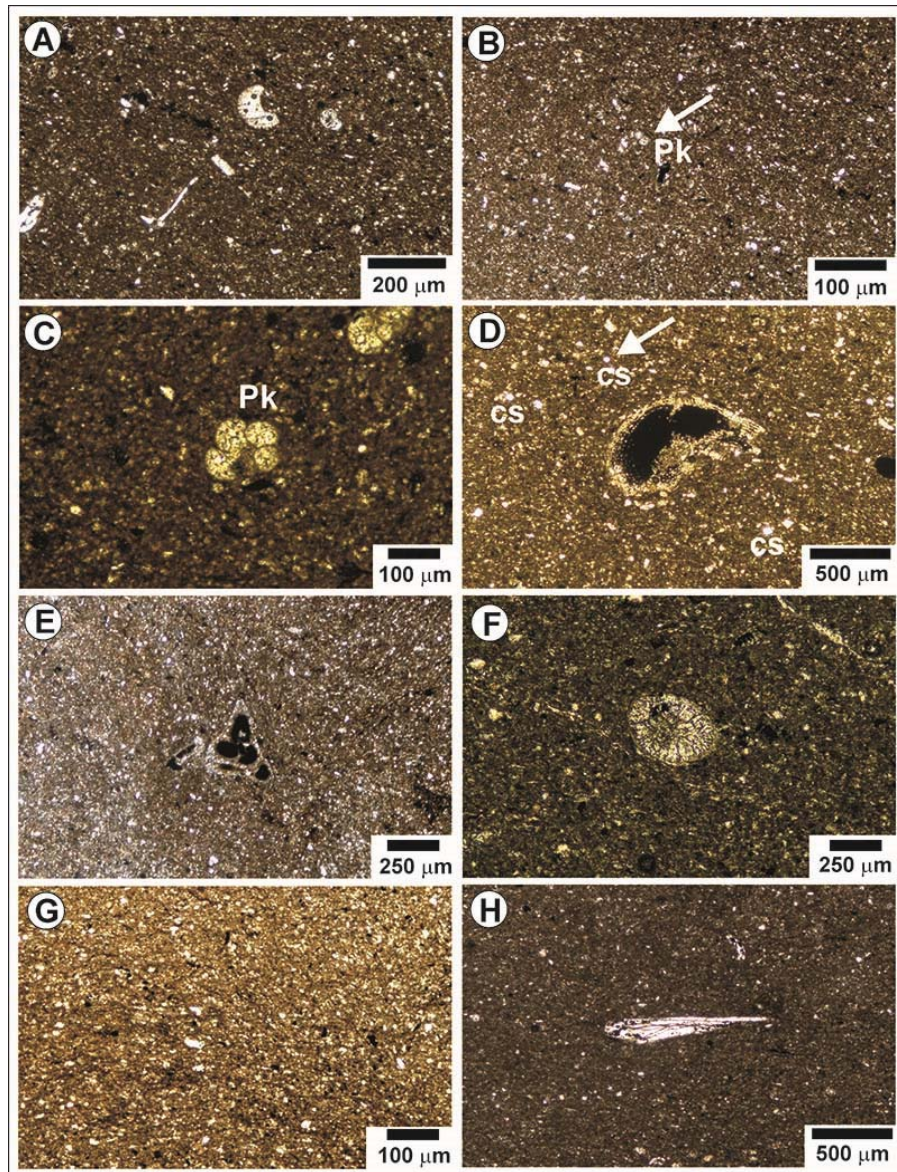


Figure 6-14 Photomicrographs illustrating microfacies MF4. A, B, C, D) sample C10-22, (A, B) abundant acicular to microtabular carbonate particles in a fine-dark matrix; (C) planktonic foraminifera *G. blowi*; (D) unidentified bioclast (? possibly a fragment of the brachial plate of a roveacrinid). E) Sample C10-23, benthic foraminifera in a very fine matrix, chambers filled with kerogen. F) Sample C10-29, unidentified bioclast in a dark matrix with traces of kerogen. G) Sample C11-129, fine micrite with sub-anisotropic fabric. H) Sample C11-131, unidentified bioclast in a dark matrix with traces of OM. Arrows point to calcispheres (cs) and planktonic foraminifera (Pk).

Interpretation

MF4 is consistent with basinal conditions in which the sediment source is dominated by calcifying primary producers and pulses of fine siliciclastics (Sanchez-Hernandez and Maurrasse 2014). Abundance of comminuted skeletal material together with larger fragments in the matrix suggests that higher abundance of heterotrophs is conceivable as the result of increased primary productivity. Slight variations in mineral composition also characterize levels corresponding to MF4 with a small decrease in quartz content, minor changes in clay minerals that might reflect either effects of climatic processes or sporadic flexural subsidence (García-Senz 2002) that affected the physiography and entrapment of coarser detrital materials in more proximal areas. Because the percentages of illite, illite/smectite, and kaolinite show almost no change (Sanchez-Hernandez et al. in press) it supports basinal depositional conditions with limited influence of coarser terrestrial material.

MF5: Sparsely roveacrinidal biomicrite

MF5 is the second most dominant type of facies, which occurs at the following intervals: 17.4-22.5 m, 23.3-30.5 m and 33.5-46 m (Figs. 6-4–6-7A, 6-15A–Q). The general groundmass distribution of MF5 consists of a fine micritic matrix and varying proportion of allochems (~ 5% - 15%) (Fig. 6-15). Coarse skeletal components >200 µm make up ~1% of the total allochemical fraction. The continuous presence of roveacrinid fragments gives MF5 a distinctive character (Fig. 6-15B–D, G, I, O). Fragments of apparent micro-ammonite shells are also present, but are less common (Fig. 6-15P). Interval 17.4-22.5 m contains few intermittent molds of specimens between 2-4cm. Acicular particles interpreted as comminuted ammonite nacreous layer are common (Fig.

6-15N) (Kulicki 1979; 1996). OM and pyrite filling in microfossil molds are common, particularly in the interval 17.4-22.5 m (Fig. 6-15A). Planktonic foraminifera are generally common with average size of ~150 μm (Fig. 6-15F, H), whereas benthic foraminifera fluctuates but remain scarce with various sizes (up to 500 μm ; Fig. 6-15K). The bioturbation index is between 1 and 2 whereas TOC fluctuates from ~0.1-1.7% (Fig. 6-7B).

Interpretation

MF5 is predominant within the lowest 31m of the section characterized by fluctuating dysoxic conditions (Sanchez-Hernandez and Maurrasse, 2014). The presence of amorphous OM together with occasional pyrite replacement in molds and as individual framboids (Fig. 6-8B), and subparallel alignment of allochems (Fig. 6-15H) are consistent with reducing conditions in the MF5 intervals. However scarce to rare benthic foraminifera indicates that anoxic conditions were not achieved within these intervals (Tyson and Pearson 1981; Wignall and Myers 1988). Pervasive bituminous OM suggests enhanced export production from intensified surface productivity, which concurs with the abundance of roveacrinids that have been associated with conditions of higher productivity and oxygen-limited environments (e.g. Santos Basin, southeastern Brazil, Dias-Brito and Ferré 2001). It is plausible that the trophic pyramid of the basin followed gradients similar to modern communities, which would imply that such low-diversity assemblages with high dominance of a few taxa are consistent with an ecological system that fostered high productivity of limited groups (e.g. Gaudy and Champalbert 2003; Grégoire and Lacroix 2001; Grégoire et al. 2004; Meier et al. 2004; Oguz 2006; Bison et al. 2009) either due to competitive exclusion, or that enhanced freshwater and nutrient

input at that time triggered surface conditions favorable mainly to euryhaline primary producers, as suggest the high sedimentation rate dominated by nannoplankton remains.

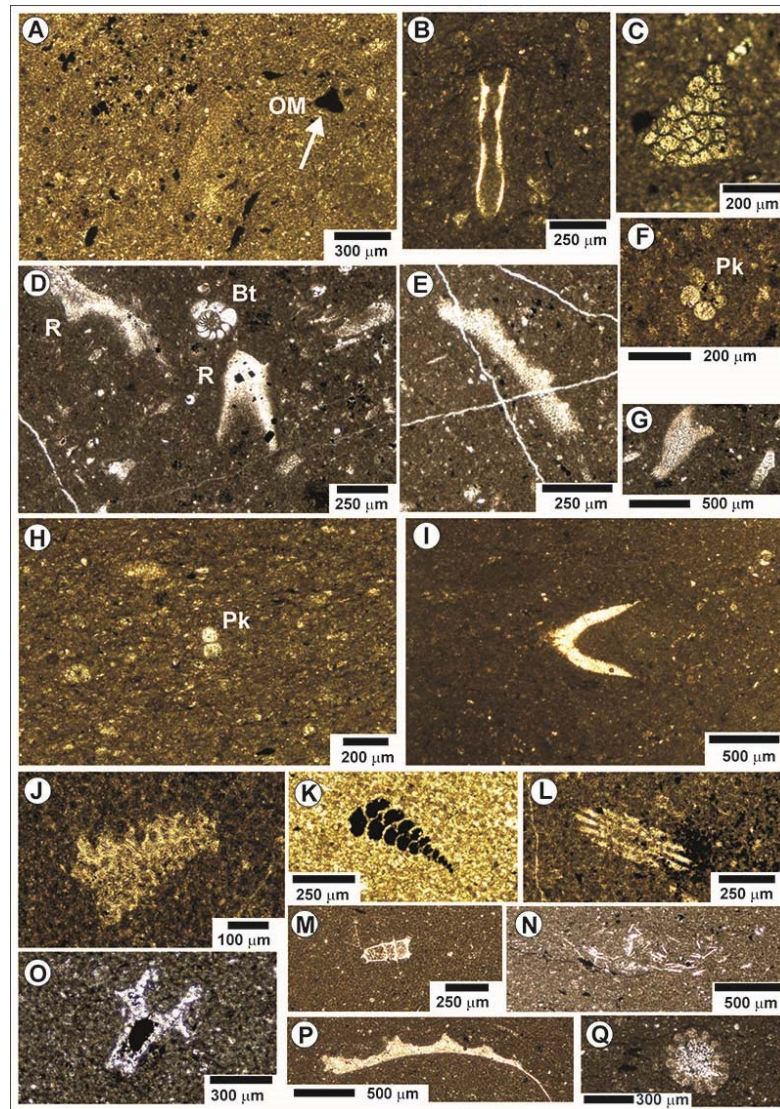


Figure 6-15 Photomicrographs illustrating microfacies MF5. A, B, C) Sample C10-46, (A) micritic matrix with interparticle pores filled with OM; (B) longitudinal section of the brachial plate of an undetermined roveacrinid; (C) roveacrinid fragment. D, E, F, G) Sample C10-47, D) R in the center: transversal section of a brachial plate of a roveacrinid (?), center and above: coiled benthic foraminifera (Bt), left upper corner: roveacrinid fragment; (E) ammonoid shell fragment (?); (F) planktonic foraminifera *G. blowi* ? (G) bioclast. H, I) Sample C10-50, (H) planktonic foraminifera in a dark micritic matrix with subparallel alignment; (I) roveacrinid fragment. J) Sample C10-55, tangential thecal section of a roveacrinid. K) Sample C10-56, relatively large biserial benthic foraminifera. L) Sample C10-59, oblique section of small echinoid spine in a matrix with abundant dispersive OM and pyrite. M) Sample C10-69, unidentified bioclast. N) Sample C10-74, abundant acicular fragments from disintegration of ammonite nacreous layer. O, P) Sample C10-75, (O) brachial fragment of roveacrinid, (P) section of a small ammonite shell. Q) Sample C10-83, small echinoid spine.

MF5A: Sparsely fossiliferous biomicrite

MF5A is a variant of MF5 occurring in two narrow intervals: 22.5-23.3 m and 30.5-33.5 m, respectively (Figs. 7A, 16A–D). It is also a sparsely fossiliferous micrite with foraminifera and lesser abundance of roveacrinids. The matrix is very similar to MF5, but its distinguishing characteristic is a relative increase in planktonic foraminifera concurrent with a relative decrease in roveacrinid fragments.

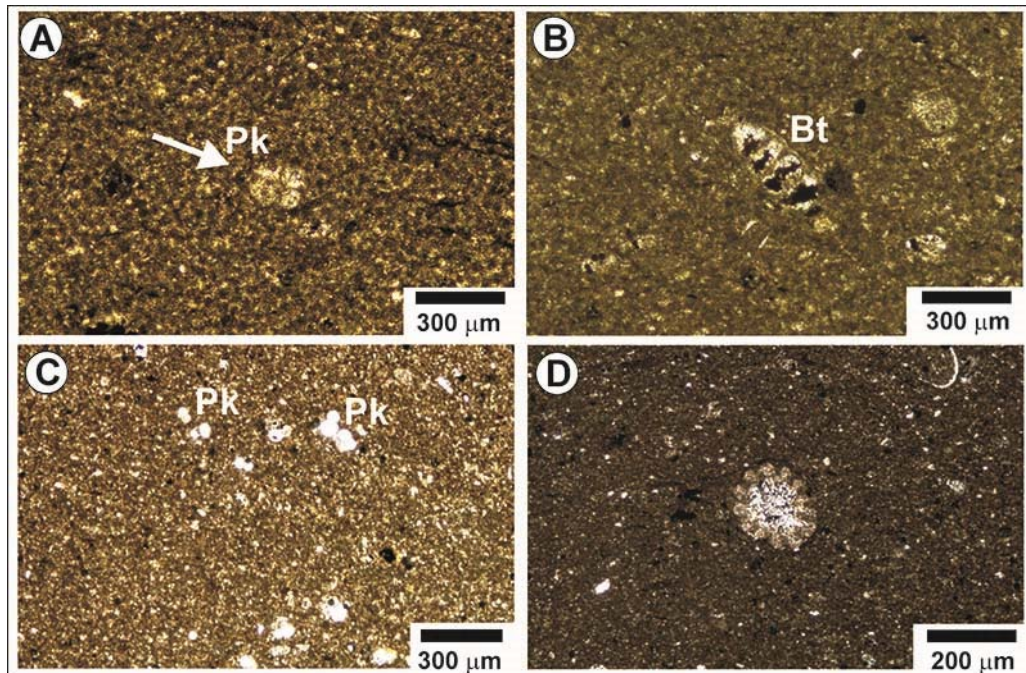


Figure 6-16 Photomicrographs illustrating microfacies MF5A. A) Sample C10-64, planktonic foraminifera in a fine micritic matrix with dispersive OM. B) Sample C10-65, uniserial benthic foraminifera in a very fine carbonate mud rich in OM. C) Sample C10-84, comminuted skeletal fragments in a fine micrite with small planktonic foraminifera (Pk) and calcispheres. D) Sample C10-85, small echinoid spine in a dark matrix of carbonate mud rich in OM and very fine skeletal grains.

Interpretation

The nearly inverse correlation in the proportion of planktonic foraminifera and roveacrinid fragments recorded in MF5A further points to a possible competitive exclusion relationship, as these pelagic microcrinoids might have played a pivotal role in the marine ecosystem as primary grazers of the restricted Organyà Basin, perhaps much

like the present day copepods. They might have relied on abundant primary producers as well as microplankton heterotrophs such as foraminifera for food resources, as suggest their remarkable presence in stressful as well as various eutrophic environments (Dias-Brito and Ferré 2001; Ferré and Granier 2001, Ferré et al. 2005). MF5A suggests a stable basin with short intervals when conditions were less favorable to the roveacrinids.

6.4.3 Paleoecologic significance of micro-ammonoids and roveacrinids in the El Pui sediments

6.4.3.1 Ammonoids

Visible and microscopic skeletal grains attributed to disaggregated small planktonic ammonite shells occur very sparsely in the sediments (Fig. 6-15P). As discussed with the various facies, in addition to the calcareous nannoplankton remains that constitute the dominant fraction of the micritic groundmass, comminuted shells as microtablets probably originated from the nacreous layer of phragmocones (Birkelund and Hansen 1968; Kulicki 1979; 1996), contribute up to 15 percent of the bioclasts below 10 to 20 microns (Fig. 6-15N). Because of the unusually thin shells observed in thin sections (e.g. Fig. 6-15P) we presume that preservation of whole shells of the pelagic ammonoids in the Organyà Basin was limited, they disaggregated quickly upon death contributing to the marine snow. In fact, most cross sections show shell thicknesses less than 500 μm , predominately within the range of 120 - 200 μm , even in large bioclasts > 2 cm across the thin sections. Based on the high proportion of bioclasts in the groundmass, it is evident that small pelagic ammonites must have been in great abundance in the upper water column of the basin of that time, and might have been important members of the secondary consumers in the food web. Whether such small ammonoids represent neanic

or dwarf taxa remains an open question because large specimens have also been found intermittently in the sequence where there are more comminuted ammonoid remains. Kruta et al (2011) suggested that different species of ammonoids may live at different depth levels in the water column, but the similarity in their buccal apparatus implies comparable feeding habit, which consisted of small organisms in the water column, including planktotrophic larvae. The abundance of roveacrinid fragments concomitant with comminuted small ammonite shells also permit to hypothesize a similar relationship may have existed between these two groups in the pelagic food web of the Organya Basin. As observed in modern marine ecosystems unusual blooms of the primary producers could have fueled exceptional production of a complex trophic pyramid whereby roveacrinids belonged in the group of primary consumers while the larger sizes micro-ammonoids were part of the secondary consumers.

6.4.3.2 Roveacrinids

Roveacrinids are pelagic microcrinoids of the Roveacrinidae family (Peck 1943; 1955; Cros et al. 1991; Ferré and Berthou 1994; Ferré 1997; Ferré and Granier 1997; 2001; Farinacci and Manni 2003). The oldest roveacrinid occurrence in the western Tethys corresponds to the early Hauterivian of Busot (Alicante, Spain) where they have been reported by Ferré and Granier (1997); however roveacrinids are most commonly identified in sections from the Albian to the Maastrichtian in other areas of the Tethys Ocean.

Consistent gaps in the presence of roveacrinids in the sedimentary record suggest that these microcrinoids were possibly r-strategists with special abilities to colonize stressful environments (Dias-Brito and Ferré 2001). The occurrence of roveacrinids in the

Albian of the Santos Basin, southeastern Brazil, interpreted as neritic to shallow bathyal with hypoxic conditions is in agreement with such hypothesis (Dias-Brito and Ferré, 2001).

At El Pui roveacrinids remains occur consistently in sediments from the latest Barremian to the earliest Aptian, but mainly within microfacies MF5 (Figs. 6-7A, 6-17) Although their occurrences are not confined exclusively to MF5, higher abundance concurrent with TOC-rich intervals associated with intensified primary productivity and reducing bottom conditions (Sanchez-Hernandez and Maurrasse 2014) provide further evidence to relate their presence with such environments.

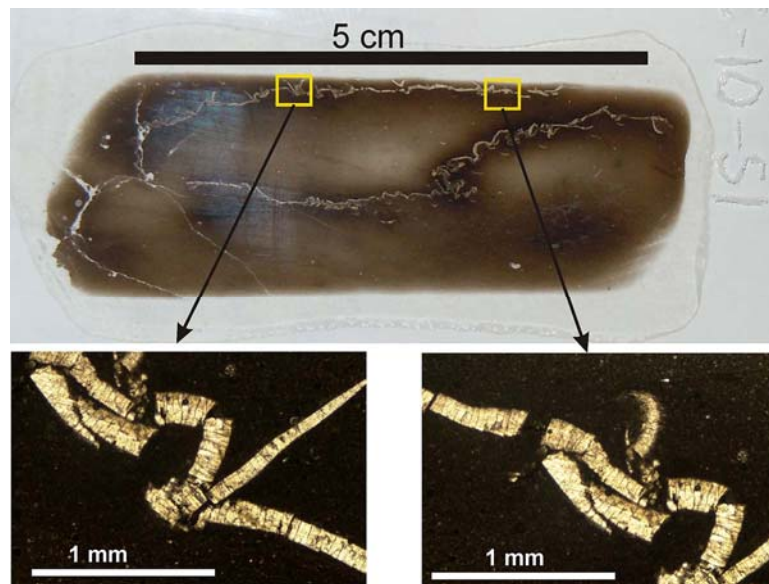


Figure 6-17 Thin section of sample C10-51 at 18.8 m (MF5) showing a dislocated roveacrinid arm with pinnules. Magnified views shown below were taken at the point indicated by the arrows. Note the microtabular structure of the shell, which may account for at least 10% of the allochemical constituents.

The roveacrinids in the El Pui sediments are the first reported for the Barremian–Aptian of the marginal basins in the south-central Pyrenees, which was probably comparable to restricted basins elsewhere in the early phase of the Atlantic (Cros et al. 1991; Dias-Brito and Ferré 2001; Ferré and Granier 2001; Farinacci and Manni 2003).

Fragments observed in thin sections point to their very small sizes, perhaps smaller than those found in sections elsewhere in the Tethys, although fragments of theca and occasionally pinnules can be observed (Fig. 6-17) (Ferré and Berthou 1994; Ferré 1997; Ferré and Granier 1997; 2001; Farinacci and Manni 2003). Since they were epipelagic, they might have been more efficient consumers of the phytoplankton than their competitors, and oxygen deficiency in the lower part of the water column did not affect their survival.

6.5 Conclusions

Hemipelagic sediments in the El Pui section of the Organyà Basin include a continuous record from the late Barremian to the early Aptian that indicates a deepening depocenter which developed over a rapidly subsiding carbonate platform. Flexural interactions associated with rifting accelerated subsidence of the rifted basin and provided adequate accommodation space for rapid accumulation of a distinctive set of hemipelagic marlstones and limestones with predominant contribution from nannofossil remains. Skeletal grains consist essentially of comminuted roveacrinids and ammonoids that contributed up to 15% of the allochems at certain levels.

The continuous 85m sequence studied implies no significant architectural changes affecting the extensional basin during that time interval. High-resolution record of the temporal evolution of the basin reveals five main microfacies and two subfacies that mirror paleoenvironmental changes in the basin mainly related to enhance primary productivity and the ensuing active trophic levels that influenced oxygen level, and favored organic matter preservation.

Roveacrinids are reported for the first time in Barremian–Aptian sediments along the northern margin of Iberia, and their presence in the periodically dysoxic environment of the Organyà Basin concurs with previous indication that these taxa are associated with stressful environments. Low diversity of all forms of organisms in El Pui sediments concur with such interpretation because phototrophs represented by calcareous nannoplankton together with heterotrophic microscopic planktonic roveacrinids and minuscule ammonoids dominated the ecosystem of the Organyà Basin at that time.

6.6 Acknowledgments

The Goodfriend Memorial Funds supported this research. We are most grateful to Diane Pirie and Thomas Beasley for their help with instrumentation and materials at FIU. We thank our colleague Josep Moreno-Bedmar for valuable logistical help and discussion about the section. Y. S-H is thankful for the DEA fellowship from the FIU Graduate School.

6.7 References

- Abu-Zied RH (2007) Palaeoenvironmental significance of Early Cretaceous foraminifera from northern Sinai, Egypt. *Cretac Res* 28:765–784
- Aguado R, Company M, Sandoval J, Tavera JM (1997) Biostratigraphic events at the Barremian/Aptian boundary in the Betic Cordillera (southern Spain). *Cretac Res* 18:309–329
- Aguado R, de Gea GA, Castro JM, O’Dogherty L, Quijano, ML, Naafs BDA, Pancost RD (2013) Late Barremian–early Aptian dark facies of the Subbetic (Betic Cordillera, southern Spain): Calcareous nannofossil quantitative analyses, chemostratigraphy and palaeoceanographic reconstructions. *Palaeogeogr Palaeoclimatol Palaeoecol* 395:198–221
- Algeo TJ, Maynard JB (2004) Trace-element behavior and redox facies in core shales of Upper Pennsylvanian Kansas-type cyclothems. *Cheml Geol* 206(3):289–318

- American Association of Petroleum Geologists, 1982. North American Commission on Stratigraphic Nomenclature North American Stratigraphic Code. AAPG Bull 67(5):841–875
- Arthur MA (1979) North Atlantic Cretaceous Black Shales: The Record at Site 398 and a brief comparison with other occurrences. In: Sibuet JC, Ryan WBF et al Initial Reports of the Deep Sea Drilling Project 47 (2) Washington (U.S. Government Printing Office), pp 451–468
- Arthur M, Premoli Silva I (1982) Development of widespread organic carbon-rich strata in the Mediterranean Tethys. In: Schlanger SO, Cita MB (eds) Nature and origin of Cretaceous carbon-rich facies, London Academic Press Inc., pp 7–54
- Arthur MA, Dean WE, Schlanger SO (1985) Variations in the global carbon cycle during the Cretaceous related to climate, volcanism, and changes in atmospheric CO₂. In: Sundquist ET, Broecker WS (Eds) The Carbon Cycle and Atmospheric CO₂: Natural Variations Archean to Present, Geophysical Monographs, American Geophysical Union 32, pp 504–529
- Arthur MA, Brumsack HJ, Jenkyns HC, Schlanger SO (1990) Stratigraphy, geochemistry, and paleoceanography of organic carbon-rich Cretaceous sequences. In: Ginsburg RN, Beaudoin B (eds) Cretaceous resources, events, and rhythms: Kluwer Academic Publishers, pp 75–119
- Bachmann M, Willems H (1996) High-frequency cycles in the upper Aptian carbonates of the Organyà basin, NE Spain. Geol Rundsch 85(3):586–605.
- Barragan R, Maurrasse FJ-MR (2008) Lower Aptian (Lower Cretaceous) ammonites from the basal strata of the La Peña Formation of Nuevo León State, northeast Mexico: biochronostratigraphic implications. Revista Mexicana de Ciencias Geológicas 25(1):45–157
- Berástegui X, García-Senz JM, Losantos M (1990) Tectonosedimentary evolution of the Organyà extensional basin (Central South Pyrenean Unit, Spain) during the Lower Cretaceous. Bull. Soc. Geol. France 8(2):251– 264
- Berástegui X, Losantos M, Muños JA, Puigdefàbregas C (1993) Tall geològic del Pirineu central 1 :200 000. Map and explanations. Servei Geològic de Catalunya, Barcelona
- Bernaus JM, Arnaud–Vanneau A, Caus E (2002) Stratigraphic distribution of Valanginian Early Aptian shallow–water benthic foraminifera and algae, and depositional sequences of a carbonate platform in a tectonically–controlled basin: the Organyà Basin, Pyrenees, Spain. Cretac Res 23:25–36

- Bernaus JM, Arnaud-Vanneau A, Caus E (2003) Carbonate platform sequence stratigraphy in a rapidly subsiding area: the Late Barremian-Early Aptian of the Organyà Basin, Spanish Pyrenees. *Sediment Geol* 159:177–201
- Bersezio R, Erba E, Gorza M, Riva A (2002) Berriasian -Aptian black shales of the Maiolica formation (Lombardian Basin, Southern Alps, Northern Italy): local to global events. *Palaeogeogr Palaeoclimatol Palaeoecol* 180:253–275
- Birkelund T, Hansen HJ (1968) Early shell growth and structures of the septa and the siphuncular tube in some Maastrichtian ammonites. *Meddelelser fra Dansk Geologisk Forening København* 18:71–78
- Bison KM, Versteegh GJM, Orszag-Sperber F, Rouchy JM, Willems H (2009) Palaeoenvironmental changes of the early Pliocene (Zanclean) in the eastern Mediterranean Pissouri Basin (Cyprus) evidenced from calcareous dinoflagellate cyst assemblages. *Mar Micropaleontol* 73:49–56
- Bolli HM (1957) The foraminiferal genera *Schackoina* Thalmann, emended and *Leupoldina*, n. gen., in the Cretaceous of Trinidad, BWI *Eclogae Geol Helv* 59:271–281.
- Bond RMG, McClay KR (1995) Inversion of a Lower Cretaceous extensional basin, south central Pyrenees, Spain. *Geol Soc Sp* 88:415–431
- Borrego AG, Hagemann HW, Blanco CG, Suarez M, Suarez de Centi C (1996) The Pliensbachian (Early Jurassic) “anoxic event in Asturias, northern Spain: Santa Mera Member, Rodiles Formation. *Org Geochem* 25(5-7):295–309
- Caldwell CD (1983) Kansas-type cyclothems and porosity development in the Middle Pennsylvanian Marmaton Group, Dirks field, Logan County, Kansas. *Kansas Geological Survey, Subsurface Geology* 6:74–101
- Caron M (1985) Cretaceous planktic foraminifera. In: Bolli HM, Saunders JB, Perch-Nielsen K (eds) *Plankton Stratigraphy*. Cambridge University Press, pp 17–86
- Caus E, García-Senz JM, Rodés D, Simón A (1990) Stratigraphy of the Lower Cretaceous (Berriasian-Barremian) sediments in the Organyà Basin, Pyrenees, Spain. *Cretac Res* 11:313–320
- Cecca F (1998) Early Cretaceous (pre-Aptian) ammonites of the Mediterranean Tethys: Palaeoecology and palaeobiogeography. *Palaeogeogr Palaeoclimatol Palaeoecol* 138:305–323
- Cros P, Dercourt J, Gunay Y, Fourcade E, Bellier J-P, Lauer J-P, Manivit H, Kozlu H (1991) La plateforme arabe en Turquie du sud: une rampe carbonatée albo-turonienne effondrée au Sénonien. *Bull Cent Rech Explor Prod Elf-Aquitaine* 15(1):215–237

- Danovaro R, Dell'Anno A, Pusceddu A, Gambi A, Heiner I, Kristensen RM (2010) The first metazoan living in permanently anoxic conditions. *BMC Biol* 8:30
- Dias-Brito D, Ferré B (2001) Roveacrinids (stemless crinoids) in the Albian carbonates of the offshore Santos Basin, southeastern Brazil: stratigraphic, paleobiogeographic and paleoceanographic significance. *J S Am Earth Sci* 14:203–218
- Dinarès-Turell J, García-Senz J (2000) Remagnetization of Lower Cretaceous limestones from the southern Pyrenees and relation to the Iberian plate geodynamic evolution. *J Geophys Res* 105(B8):19405–19418.
- Dunham RJ (1962) Classification of carbonate rocks according to depositional textures. In: Ham WE (ed) *Classification of carbonate rocks: AAPG Memoir* 1:108-121
- Duque-Botero F, Maurrasse FJ-MR (2005) Cyanobacterial productivity, variations in the organic carbon, and facies of the Indidura Formation (Cenomanian-Turonian), Northeastern Mexico: *J Iber Geol* 31(1):85–98
- Elkhazri A, Abdallah H, Razgallah S, Moullade M, Kuhnt W (2013) Carbon-isotope and microfaunal stratigraphy bounding the Lower Aptian Oceanic Anoxic Event 1a in northeastern Tunisia. *Cretac Res* 39:133–148
- Farinacci A, Manni R (2003) Roveacrinids from the Northern Arabian Plate in SE Turkey. *Turkish J Earth Sci*, 12:209–214
- Ferré B (1997) Lombardia-facies and saccomid-like sections in Cretaceous sediments: Whose pieces? [Final Meeting of IGCP Project 362: Tethyan/Boreal Cretaceous Correlation (Stara Lesna)]. *Miner Slov (Bratislava)* 29:336–337
- Ferré B, Berthou PY (1994) Roveacrinid remains from the Cottinguiba formation (Cenomanian-Turonian) off the Sergipe Basin (NE-Brazil). *Acta Geol Leopold* 17:299–313
- Ferré B, Granier B (1997) *Roveacrinus berthouii*, nov. sp., the earliest representative of the family Roveacrinidae (Roveacrinida, Crinoidea) in the lower Hauterivian of Busot (Alicante, Spain). *Miner Slov* 29:338–339
- Ferré B, Granier B (2001) Albian Roveacrinids from the southern Congo Basin off Angola. *J S Am Earth Sci* 14: 219–235
- Ferré B, Walter S, Bengtson P (2005) Roveacrinids in mid-Cretaceous biostratigraphy of the Sergipe Basin, northeastern Brazil. *J S Am Earth Sci* 19:259–272
- Flügel E (1982) *Microfacies analysis of limestones*. Springer-Verlag, Berlin
- Folk RL (1959) Practical petrographic classification of limestones. *AAPG Bull* 43:1–38

- Folk RL (1962) Spectral subdivision of limestone types. In: Ham WE (ed) Classification of carbonate rocks: AAPG Memoir 1:62–84
- Folk RL (1980) Petrology of sedimentary rocks. Hemphill Publishing Company, Austin Texas
- Folk RL (1993) SEM imaging of bacteria and nanobacteria in carbonate sediments and rocks. *J Sediment Petrol* 63:990–999
- Föllmi KB (2012) Early Cretaceous life, climate and anoxia. *Cretac Res* 35:230–257
- Föllmi KB, Bole M, Jammet N, Froidevaux P, Godet A, Bodin S, Adatte T, Matera V, Fleitmann D, Spangenberg JE (2011) Bridging the Faraoni and Selli oceanic anoxic events: late Hauterivian to early Aptian dysaerobic to anaerobic phases in the Tethys. *Clim Past* 8:171–189
- Friedman GM, Sanders JE (1978) Principles of sedimentology. John Wiley & Sons, New York
- Gabrielsen RH (2010) The Structure and Hydrocarbon Traps of Sedimentary Basins. In: K. Bjørlykke (ed) Petroleum Geoscience: From Sedimentary Environments to Rock Physics Springer-Verlag Berlin Heidelberg, pp 299–327
- Gaona-Narvaez T, Maurrasse FJ-MR, Moreno-Bedmar JA (2013) Stable Carbon Isotope Stratigraphy and Ammonite Biochronology at Madotz (Navarra, N Spain): Implications for the Timing and Duration of Oxygen Depletion during OAE-1a. *Cretac Res* 40:143–157
- García-Senz J (2002) Cuencas extensivas del Cretácico Inferior en los Pirineos Centrales -formación y subsecuente inversión. Dissertation, University of Barcelona
- Garrido-Mejías A (1973) Estudio geológico y relación entre tectónica y sedimentación del Secundario y Terciario de la vertiente meridional pirenaica en su zona central (provincias de Huesca y Lérida). Dissertation, Universidad de Granada
- Gaudy R, Champalbert G (2003) Feeding and metabolism of mesozooplankton in the equatorial Pacific high-nutrient, low-chlorophyll zone along 180°. *J Geophys Res-Oceans* 108:C12
- Goddard EN, Trask PD, De Ford RK, Rove ON, Singewald JT, Overbeck RM (1963) Rock-Color Chart. Geol Soc America, Colorado
- Gong Z, van Hinsbergen DJJ, Vissers RLM, Dekkers MJ (2009) Early Cretaceous syn-rotational extension in the Organyà Basin - New constraints on the palinspastic position of Iberia during its rotation. *Tectonophysics* 473:312–323.

- Greenberg J, Madin K, Lippsett L (2010) Salps catch the ocean's tiniest organisms. *Oceanus* 48(2)
- Grégoire M, Lacroix G (2001) Study of the oxygen budget of the Black Sea waters using a 3D coupled hydrodynamical–biogeochemical model. *J Marine Syst* 31:175–202
- Grégoire M, Soetaert K, Nezlin NP, Kostianoy AG (2004) Modeling the nitrogen cycling and plankton productivity in the Black Sea using a three dimensional interdisciplinary model. *J Geophys Res-Oceans* 109:C5
- Hu X, Zhao K, Omer Yilmaz I, Li Y (2012) Stratigraphic transition and palaeoenvironmental changes from the Aptian oceanic anoxic event 1a (OAE1a) to the oceanic red bed 1 (ORB1) in the Yenicesihlar section, central Turkey. *Cretac Res* 38:40–51
- Husinec A, Harman CA, Regan SP, Mosher DA, Sweeney RJ, Read JF (2012) Sequence development influenced by intermittent cooling events in the Cretaceous Aptian greenhouse, Adriatic platform, Croatia. *AAPG Bull* 96(12):2215–2244
- Ingram RL (1953) Fissility of mudrocks. *Geol Soc Am Bull* 64:569–578
- Jahren AH, Arens NC, Sarmiento G, Guerrero J, Amundson R (2001) Terrestrial record of methane hydrate dissociation in the Early Cretaceous. *Geology* 29:159–162
- Jenkyns HC (1980) Cretaceous anoxic events: From continents to oceans. *J Geol Soc London* 137:171–188
- Jenkyns HC (2010) Geochemistry of oceanic anoxic events. *Geochem Geophys Geosy* 11(3):1525–2027
- Kruta I, Landman N, Rouget I, Cecca F, Tafforeau P (2011) The Role of Ammonites in the Mesozoic Marine Food Web Revealed by Jaw Preservation. *Science* 331:70–72
- Kulicki C (1979) The ammonite shell: its structure, development and biological significance. *Acta Palaeontol Pol* 39:97–168
- Kulicki C (1996) Ammonoid shell microstructure, in Landman, NH, et al. (eds) *Ammonoid paleobiology*, New York, Plenum Press, pp 65–101
- Kuss J, Schlagintweit F (1988) Facies and Stratigraphy of Early to Middle Cretaceous (Late Aptian– Early Cenomanian) Strata from the Northern Rim of the African Craton (Gebel Maghara - Sinai, Egypt). *Facies* 19:77–96
- Larson RL, Erba E (1999) Onset of the Mid-Cretaceous greenhouse in the Barremian–Aptian: Igneous events and the biological, sedimentary, and geochemical responses. *Paleoceanography* 14(6):663–678

- Leonide P, Borgomano J, Masse J-P, Doublet S (2012) Relation between stratigraphic architecture and multi-scale heterogeneities in carbonate platforms: The Barremian–lower Aptian of the Monts de Vaucluse, SE France. *Sediment Geol* 265:87–109
- Masse J-P (1998) Sédimentologie du stratotype historique de l’Aptien inférieur dans la région de Cassis-La Bédoule (S.E. France). *Geol Mediterr* 15(3-4):31–41
- Masse J-P, Machhour L (1998) La matière organique de la série du stratotype historique de l’Aptien inférieur de Cassis-La Bédoule (SE, France). *Geol Mediterr* 15(3-4):55–63
- Masse J-P et al. (2000) Early Aptian. In: Dercourt J, Gaetani M et al. (eds). *Atlas Peritethys, Palaeogeographical Maps*. CCGM/CGMW, Paris, Map
- Maurrasse FJ-MR, Ponton C (2005) Aptian deposits in southeastern France and northeastern Mexico: Implications concerning paleoclimatic conditions: Scientific Program and Abstracts, 7th International Symposium on the Cretaceous, pp 137.
- Méhay S, Keller CE, Bernasconi SM, Weissert H, Erba E, Bottini C, Huchuli PA (2009) A volcanic CO₂ pulse triggered the Cretaceous oceanic anoxic event 1a and a biocalcification crisis. *Geology* 37:819–822
- Meier KJS, Zonneveld KAF, Kasten S, Willems H (2004) Different nutrient sources forcing increased productivity during eastern Mediterranean S1 sapropel formation as reflected by calcareous dinoflagellate cysts. *Paleoceanography* 19:1–12
- Michalík J, Soták J, Lintnerová O, Halásová E, Bak M, Skupien P, Boorová D (2008) The stratigraphic and paleoenvironmental setting of Aptian OAE black shale deposits in the Pieniny klippen belt, Slovak Western Carpathians. *Cretac Res* 29:871–892
- Moullade M, Kuhnt W, Bergen JA, Masse J-P, Tronchetti G (1998) Correlation of biostratigraphic and stable isotope events in the Aptian historical stratotype of La Bédoule (Southeast France). *C R Acad Sci Paris* 327:693–698
- Moreno-Bedmar JA (2010) Ammonites de l’Aptià inferior de la península Ibèrica. Biostratigrafia i aportacions a l’estudi del Oceanic Anoxic Event 1a. Dissertation Universitat de Barcelona
- Muñoz JA (1991) Evolution of a continental collision belt: ECORS-Pyrenees crustal balanced cross-section. In: *Thrust Tectonics* (ed) MacClay KK, Chapman and Hall, New York, pp 235–247
- Muñoz JA, Puigdefàbregas C, Fontboté JM (1984) Orógenos alpinos In: Ríos LJJM (ed) *El Pirineo*. Inst Geol Min España Geología de España pp 161–205

- Mutterlose J, Pauly S, Steuber T (2009) Temperature controlled deposition of early Cretaceous (Barremian–early Aptian) black shales in an epicontinental sea. *Palaeogeogr Palaeoclimatol Palaeoecol* 273(3):330–345
- North American Commission on Stratigraphic Nomenclature (NACSN) (1983) North American Stratigraphic Code. *AAPG Bull* 67(5):841–875
- Oguz T (2006) Regime shifts at multiple trophic levels of the Black Sea pelagic ecosystem. European Geosciences Union, *Geophys Res Abstr* 8
- Olsen PE (1997) Stratigraphic record of the Early Mesozoic breakup of Pangea in the Laurasia-Gondwana rift system. *Ann Rev Earth Planet Sc* 25:337– 401
- Pauly S, Mutterlose J, Wray DS (2013) Palaeoceanography of Lower Cretaceous (Barremian-Lower Aptian) black shales from northwest Germany evidenced by calcareous nannofossils and geochemistry. *Cretac Res* 42:28–43
- Peck, RE (1943) Lower Cretaceous crinoids from Texas. *J Paleontol* 22(5):451–475
- Peck, RE (1955) Cretaceous microcrinoids from England. *J Paleontol* 29(9):1019–1029
- Pettijohn FJ (1957) *Sedimentary Rocks*. Harper and Row, Publishers, New York
- Peybernès B (1976) *Le Jurassique et le Crétacé inférieur des Pyrénées franco-espagnoles, entre la Garonne et la Méditerranée*. Thèse de Doctorat ès Sciences Naturelles, Université Paul-Sabatier de Toulouse
- Peybernès B, Souquet P (1973) Biostratigraphie des marnes noires de l'Aptien-Albien de la zone sud-Pyrénéenne . *Comptes Rendus de l'Académie des Sciences Paris* 276:2501–2504
- Powell WG, Johnston PA, Collom CJ (2003) Geochemical evidence for oxygenated bottom waters during deposition of fossiliferous strata of the Burgess Shale Formation. *Palaeogeogr Palaeoclimatol Palaeoecol* 201(3):249–268
- Premoli Silva I, Erba E, Salvini G, Locatelli C, Verga D (1999) Biotic changes in Cretaceous oceanic anoxic events of the Tethys. *J. Foraminiferal Res* 29:352–370
- Raisossadat SN, Shokri MH (2011) Biostratigraphic studies of the lower cretaceous (Upper Barremian–lower Aptian) Sarcheshmeh and Sanganeh Formations in the Kopet Dagh basin, NE Iran: An integration of calcareous nannofossil and ammonite stratigraphies. *Stratigraphy and Geological Correlation* 19(2):188–204
- Remin Z, Dubicka Z, Kozłowska A, Kuchta B (2012) A new method of rock disintegration and foraminiferal extraction with the use of liquid nitrogen [LN₂]. Do conventional methods lead to biased paleoecological and paleoenvironmental interpretations? *Mar Micropaleontol* 86–87:11–14

- Roban R-D, Melinte-Dobrinescu MC (2012) Lower Cretaceous lithofacies of the black shales rich Audia Formation, Tarcau Nappe, Eastern Carpathians: Genetic significance and sedimentary palaeoenvironments. *Cretac Res* 38:52–67
- Sageman BB, Murphy AE, Werne JP, Ver Straeten CA, Hollander DJ, Lyons TW (2003) A tale of shales: The relative roles of production, decomposition, and dilution in the accumulation of organic-rich strata, Middle-Upper Devonian, Appalachian basin. *Chem Geol* 195:229–273
- Sanchez-Hernandez Y, Maurrasse FJ-MR (2014) Geochemical characterization and redox signals from the latest Barremian to the earliest Aptian in a restricted marine basin: El Pui section, Organyà Basin. *Chem Geol* 372:12–31
- Scarparo Cunha AA, Shimabukuro S (1997) *Braarudosphaera* blooms and anomalous enrichments of *Nannoconus*: evidence from the Turonian South Atlantic, Santo Basin, Brazil. *Journal of Nannoplankton Research* 19:51–55
- Scarparo Cunha AA, Koutsoukos EAM (1998) Calcareous nannofossils and planktonic foraminifers in the upper Aptian of Sergipe Basin, northeastern Brazil: palaeoecological inferences. *Palaeogeogr Palaeoclimatol Palaeoecol* 142:175–184
- Schlanger SO, Jenkyns HC (1976) Cretaceous oceanic anoxic events: causes and consequences. *Geol Mijnbouw* 55(3-4):179–184
- Scholle PA, Holmer-Scholle D (2003) A Colour Guide to the Petrography of Carbonate Rocks: grains, textures, porosity, diagenesis. AAPG Memoir 77
- Stelmakh LV (2013) Microzooplankton Grazing Impact on Phytoplankton Blooms in the Coastal Seawater of the Southern Crimea (Black Sea). *International Journal of Marine Science* 3(15)
- Stinton CW, Duncan RA (1997) Potential links between ocean plateau volcanism and global ocean anoxia at the Cenomanian-Turonian boundary. *Econ Geol* 92, 836–842
- Sun J, Feng Y, Zhou F, Song S, Jiang Y, Ding C (2013) Top-down control of spring surface phytoplankton blooms by microzooplankton in the central Yellow Sea, China. *Deep Sea Res PT II* 97:51–60
- Taylor AM, Goldring R (1993) Description and analysis of bioturbation and ichnofabric. *J Geol Soc London* 150:141–148
- Tejada ML, Suzuki GK, Kuroda J, Coccioni R, Mahoney JJ, Ohkouchi N, Sakamoto T, Tatsumi Y (2009) Ontong Java Plateau eruption as a trigger for the Early Aptian oceanic anoxic event. *Geology* 37:855–858

- Tyson RV, Pearson TH (1991) Modern and ancient continental shelf anoxia: an overview. In: Tyson RV, Pearson TH (eds) *Modern and ancient continental shelf anoxia*. Geol Soc Spec Publ 58:1–24
- Van de Schootbrugge B, McArthur JM, Bailey TR, Rosenthal Y, Wright JD, Miller KG, (2005) Toarcian oceanic anoxic event: an assessment of global causes using belemnite C isotope records. *Paleoceanography* 20:PA3008
- van der Wielen PWJJ, Bolhuis H, Borin S, Daffonchio D, Corselli C, Giuliano L, D'Auria G, de Lange GJ, Huebner A, Varnavas SP, Thomson J, Tamburini C, Marty D, McGenity TJ, Timmis KN, BioDeep Scientific Party (2005) The Enigma of Prokaryotic Life in Deep Hypersaline Anoxic Basins. *Science* 307:121–123
- Velásquez-Castillo RF, Reyes-Gasga JR, García-Gutierrez DI, Jose-Yacama M (2006) Crystal structure characterization of nautilus shell at different length scales. *Biomaterials* 27:4508–4517
- Verga D, Premoli Silva I (2002) Early Cretaceous planktonic foraminifera from the Tethys. The genus *Leupoldina*. *Cretac Res* 23:189–212
- Verga D, Premoli Silva I (2003) Early Cretaceous planktonic foraminifera from the Tethys. The small-sized representatives of the genus *Globigerinelloides*. *Cretac Res* 24:305–334
- Wang C, Hu X, Huang Y, Wagreich M, Scott R, Hay W (2011) Cretaceous oceanic red beds as possible consequence of oceanic anoxic events. *Sed Geol* 235:27–37
- Weissert H, Lini A, Föllmi KB, Kuhn O (1998) Correlation of Early Cretaceous carbon isotope stratigraphy and platform drowning events: a possible link? *Palaeogeogr Palaeoclimatol Palaeoecol* 137(3):189–203
- Wignall PB, Myers KJ (1988). Interpreting benthic oxygen levels in mudrocks: A new approach. *Geology* 16:452–45.
- Yakimov MM, La Cono V, Denaro R, D'Auria G, Decembrini F, Timmis KN, Golyshin PN, Giuliano L (2007). Primary producing prokaryotic communities of brine, interface and seawater above the halocline of deep anoxic lake L'Atalante, Eastern Mediterranean Sea. *ISME J* 1:743–755

7 THE RECORD OF OCEANIC ANOXIC EVENT 1a (OAE1a) IN THE SEMI-RESTRICTED ORGANYÀ BASIN: IMPLICATIONS FOR UNDERSTANDING THE INFLUENCE OF REGIONAL FACTORS IN THE EXPRESSION OF OAE1a

Abstract

The early Aptian is characterized by the global occurrence of oxygen-deprived conditions in the oceans, and the hallmark of that time interval is the accumulation of organic-rich sediments during an episode of severe oxygen deficiency that led to anoxia, hence the term oceanic anoxic event 1a (OAE1a). The high-resolution, multi-proxy study (petrographic, TIC, TOC, carbon isotope, clay mineralogy, biomarkers) of the upper 155m of El Pui section of the Organyà Basin reveals that low oxygen conditions prevailed throughout with varying degrees of depletion, as supported by elevated TOC values (>1%), but petrographic observations, molecular biomarkers, and redox sensitive trace elements (RSTEs) indicate that full anoxic conditions were not achieved, even at the corresponding level of OAE1a. As seen elsewhere, an overall facies change marked by increased terrigenous material characterizes the lower Aptian in the study area, but the nature of the lithologies associated with the organic carbon-rich deposits are expressed differently. This comparison indicates that significant spatial heterogeneity occurred in sub-Tethyan basins during the same global oceanic conditions. The recurrent appearance of facies characteristic of more oxic conditions imply that in certain areas local physiographic factors controlled sediment type, and overprinted global forcing mechanisms that depleted oxygen level elsewhere.

The results provide the first high-resolution $\delta^{13}\text{C}_{\text{org}}$ profile for El Pui that replicates the carbon isotopic signature reported elsewhere in the Tethys Ocean. This

improved high-resolution chemostratigraphic curve offers an exceptionally detailed tool for precise worldwide chronostratigraphic correlation. The upper part of the El Pui section includes expanded and well-defined carbon isotope segments C2 (upper part), C3, C4, C5, and C6 (partial), which correlate with other Tethyan sections and allow for recognition of the lower Aptian OAE1a in at least 35 m of the section.

7.1 Introduction

The occurrence and impact of global climatic forcing events (e.g., intense volcanism, meteorite impact, and astronomical cycles) in the earth system can often be traced by analyzing depositional and compositional patterns in the sedimentary record. However the marine expression of such events is linked to the nature of the sedimentary environment (physiography, circulation patterns, water chemistry, biological composition on the biogeochemical cycle, and terrestrial fluxes), which may induce different specific responses locally as compared to global events at the regional scale.

For instance, the environmental response of the oceanic system to greenhouse conditions and significant perturbations of the carbon cycle during the lower Aptian oceanic anoxic event 1a (OAE1a, 125 Ma) is well recognized for the deposition of organic carbon-rich sediments in pelagic and hemipelagic settings on a global scale (Schangler and Jenkins, 1976; Arthur and Schlanger, 1979; Scholle and Arthur, 1980; Br  h  ret, 1988; Coccioni et al., 1989; Arthur et al., 1990; Bralower et al., 1999; Ando et al., 2002; Puc  at et al., 2003; Li et al., 2008). Besides the global extent of anoxia at that time, there is increasing evidence of coeval deposits in marginal basins that responded differently, and certain may lack the hallmark of organic-rich black shale (TOC > 0.5) characteristic of OAE1a (Kuhnt et al., 1998; Mill  n et al., 2009; Najarro et al., 2011;

Stein et al., 2012; Gaona-Narvaez, 2013). The different responses further suggest dominance of local conditions in the depositional expression of the event.

Similar variations have also been documented in shallow-water deposits coeval with OAE1a, as the effects of differential drowning of carbonate platforms along the northern Tethyan margin (Föllmi et al., 1994; Wissler et al., 2003; Burla et al., 2008; Föllmi and Gainon, 2008, Gaona-Narvaez et al., 2013; Godet et al., 2013; Masse and Ferneci-Masse, 2013) contrast significantly with carbonate growing episodes in the southern Tethys (Immenhauser et al., 2004; 2005; Huck et al., 2010). Nonetheless, regardless of the sedimentary responses to the global perturbation, all the sites carry the same characteristic geochemical pattern that allows meaningful chemostratigraphic correlations and assess paleodepositional conditions for that time (Menegatti et al., 1998; Larson and Erba, 1999; Price, 2003; Kujau et al., 2012; Godet et al., 2014). Indeed, the carbon isotope stratigraphy ($\delta^{13}\text{C}_{\text{carb}}$ and $\delta^{13}\text{C}_{\text{org}}$) (Menegatti et al., 1998) defines eight chemostratigraphic segments (C1-C8) that characterize the late Barremian– middle Aptian time interval that has proven useful for stratigraphic correlation and relative chronology (e.g. Herrle et al., 2004; Moreno-Bedmar et al., 2009; Stein et al., 2012; Gaona-Narvaez, 2013; Papp et al., 2013; Sanchez-Hernandez and Maurrasse, 2014).

Previous studies of the sedimentary deposits of the Organyà Basin (south central Pyrenees, Catalunya, Spain) (Peybernès and Souquet, 1973; Peybernès, 1976; Berástegui et al., 1990; Garcia Senz, 2000; Bernaus et al., 2003) have shown sequences associated with the basin that comprise shallow water, as well as hemipelagic deposits with exceptional continuous record from the late Barremian to the Albian (Berástegui et al., 1990). The series of ~1100 m of limestones and marlstones accumulated during that time

(Bernaus et al., 2003) thus provides an expanded record of the basin suitable for high resolution studies that may unravel how that marginal basin responded to fluctuating environmental conditions associated with OAE1a.

Here we apply a multiproxy approach that includes TIC, TOC, carbon isotope, biomarkers, clay mineralogy, fossil content and petrography to investigate earliest to middle Aptian hemipelagic facies of the El Pui section that may reveal temporal changes correlative with the basin response to changing paleoenvironments in relation to OAE1a (Sanchez-Hernandez and Maurrasse, 2014). The present work focuses on the upper 155 m of the El Pui section in complement to previous studies of the lower 85 m (Sanchez-Hernandez and Maurrasse, 2014; Sanchez-Hernandez et al., 2014).

7.2 Geological setting

The evolution of the Pyrenean basins from the Triassic to the Cretaceous was marked by two important rifting episodes: the first occurred in the Triassic, and the second in the lower Cretaceous (Choukronne et al., 1973; Berástegui et al., 1990). During the Cretaceous an intensified phase of spreading associated with the opening of the Atlantic Ocean was concurrent with the evolution of the Bay of Biscay that led to the development of marginal basins along the European and Iberian Plates (García-Senz, 2002; Gong et al., 2009). Because of prevailing extensional tectonism at that time a system of E-W trending depocenters and irregular margins developed along the northern Iberian plate (Puigdefàbregas and Souquet, 1986) resulting in the accumulation of shallow-marine carbonates and their lateral equivalent of hemipelagic-pelagic sediments with marked facies contrasts (Caus et al., 1990). The Organyá Basin was one of these depocenters (Fig. 7-1A) that recorded the Early Cretaceous sedimentary history and

became exposed during a Late Cretaceous inversion (Berástegui et al., 1990; Mencos et al., 2010).

The Alpine Orogeny caused inversion of the basin as a result of compressional tectonic that led to the development of the Bóixols thrust sheet containing Mesozoic rocks (Garrido-Mejías, 1973; Bond and McClay, 1995). The geometric structure of the depositional framework of the Organyà Basin is comparable to a graben with estimated dimensions of ~ 80 km along the extensional axis and up to 15 km wide (Dinarès-Turell and García-Senz, 2000). During the Mesozoic the basin filled with ~ 4500-5000 m of mostly Lower Cretaceous sediments (Bachmann and Willens, 1996) at the time when subsidence increased providing ample accommodation space for the high sedimentation rate (up to ~20 cm/ky) (García-Senz, 2002; Gong, 2008).

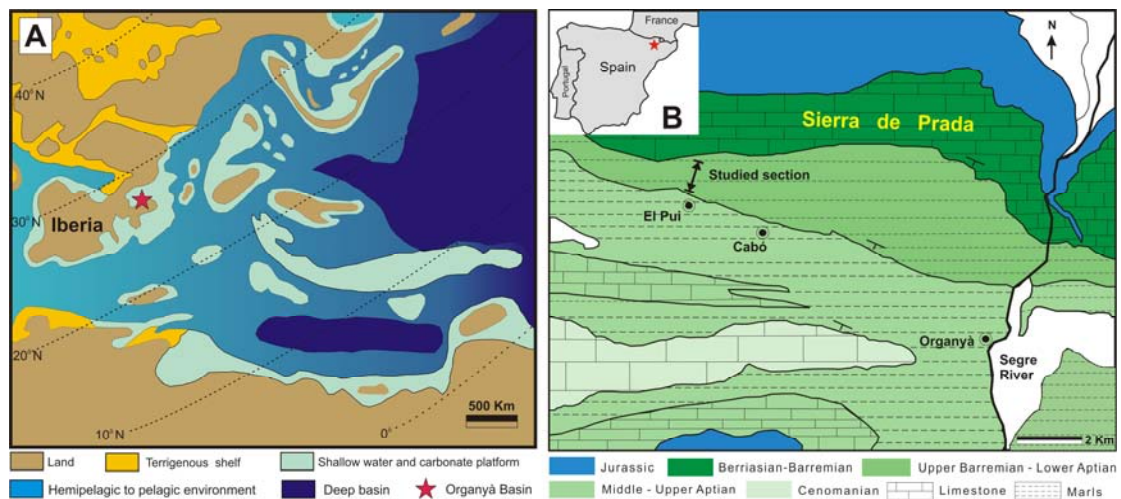


Figure 7-1 A) Paleogeographic map of the lower Aptian with the location of the Organyà Basin and the relative position of Iberia in the Western Tethys (after Masse et al., 1993; 2000). B) Simplified geologic map of the Organyà area with the relative position of the studied section (modified from Bernaus et al., 2003; Sanchez-Hernandez and Maurrasse, 2014)

The El Pui section of the Organyà Basin (Fig. 7-1B) (Sanchez-Hernandez and Maurrasse, 2014) is part of the Cabó Formation (García-Senz, 2002) and comprises a continuous and expanded sequence of hemipelagic sediments from the late Barremian to

the middle Aptian (~240 m). The excellent accessibility of the section is also complemented by an exceptional exposure of the beds along stream valleys with water gaps profiles. Here we focus on the upper part of the El Pui section that includes ~155 m of limestones and marlstones with beds varying in thickness from ~5 cm to 1 m, which Bernaus et al. (2003) suggested might include the record of the early Aptian OAE1a.

7.3 Materials and Methods

7.3.1 Sampling and petrographic analysis

Two field campaigns were conducted and 273 samples collected in the upper 155 m (85 -240 m) of the El Pui section, with sampling resolution averaging ~1 sample per 50 cm. Samples were collected at closer intervals (up to 1 sample/10cm) where beds were thinner (e.g., 180-216 m). The sampling process targeted all the apparent beds as well as the lower and upper transition between beds. All samples were taken along erosional ridges and valleys of subsequent streams that clearly exposed bedding arrangement within the continuous sequence. Sample collection included digging into at least 5 cm of the exposed rock surface to provide access to fresh rocks.

Petrographic and microfacies analyses were carried out on 273 thin sections of ~6×2.5 cm. The sedimentological characterization was performed using a conventional transmitted light microscope (Olympus BH-2 microscope). As a complement to field scale observations, the microscopic study also paid special attention to the presence/absence of benthic fauna, bioturbation and early diagenetic minerals indicative of redox conditions.

7.3.2 Carbon analyses (TOC, TIC, $\delta^{13}\text{C}_{\text{org}}$)

Total inorganic carbon (TIC) and total organic carbon (TOC) were determined for all samples (273) in the 85-240 m interval following standard analytical procedures used at Florida International University (Gaona-Narvaez et al., 2013; Sanchez-Hernandez and Maurrasse, 2014). The measurements were carried out with a LECO CR-412 and the calibration was performed using calcite (C64-500, Fisher Scientific) and dolomite (Dolomitic Limestone NIST 88b) as standard reference materials. The measured carbon was standardized to pure calcite, and the results of TC and TIC are expressed as a percentage by weight of bulk CaCO_3 . TOC was determined from the subtraction of TIC for TC and divided by 8.33 (molecular weight of CaCO_3). Analytical precision of the results was of $\pm 5\%$ based on comparison with the standards true values.

The lithologic nomenclature used for the sequence of 155 m of carbonate rocks is after Sanchez-Hernandez and Maurrasse (2014; Chapter 4) whereby measured CaCO_3 (TIC) values indicate: limestone, $> 65\% \text{CaCO}_3$; marly-limestone, $60\% - 65\% \text{CaCO}_3$; marlstone, $30\% - 60\% \text{CaCO}_3$; calcareous mud-rock/shale, $10\% - 30\% \text{CaCO}_3$; mud-rock/shale, $0 - 10\% \text{CaCO}_3$.

Similarly, procedures for carbon isotope analyses follow the description in Sanchez-Hernandez and Maurrasse (2014; Chapter 4), and calculations are based on the standard equation $\delta^{13}\text{C} (\text{permil,}\text{‰}) = [({}^{13}\text{C}/{}^{12}\text{C})_{\text{sample}} / ({}^{13}\text{C}/{}^{12}\text{C})_{\text{std}} - 1] \times 1000$. Carbon ratios obtained were repeatedly compared with a laboratory reference gas under identical conditions. Precision of isotopic analyses for replicate samples, the international standard IAEA-CH-6 (Sucrose) and our lab standard (glycine) was better than $\pm 0.025\text{‰}$.

7.3.3 Bulk and clay mineral analyses

Mineralogical analyses of 20 samples at different levels of the stratigraphic column were performed at the Illinois State Geological Survey (ISGS) using X-ray diffraction (XRD) following the methodology described by Moore and Reynolds (1997). For the XRD procedure, the samples were micronized in a McCrone micronizing mill with deionized water for 10 minutes. Then they were transferred to 50 mL centrifuge tubes, which were placed in the centrifuge for 20 minutes at 2000 rpm. The clear supernatant was poured off and the remaining material dried overnight at 40°C. When completely dried the material was mixed lightly with a mortar and pestle, and then packed into an end-loading sample holder as a random powder bulk-pack. The random powder bulk-pack was analyzed with a Scintag XDS 2000 diffractometer. Step-scanned data was collected from 2° to 60° 2 θ with a fixed time of 5 seconds per 0.05° 2 θ for each sample. All resulting traces were analyzed using the semi-quantitative data reduction software from Materials Data Inc. (MDI) known as Jade®.

The clay mineral composition was determined using oriented slides of the clay size < 2 μm fraction with semi-quantitative values of the clay mineral assemblage calculated from ethylene glycol (EG) solvated slides (Hughes and Warren, 1989; Hughes et al, 1994; Moore and Reynolds, 1997).

In preparation for XRD, 20 g - 30 g of each sample was soaked for about 10 - 12 hours in deionized water and protected from external agents. As water interacts with the sample, small clay particles are released into the solution. Further stirring of the solution mechanically induced clay release from the sample. After settling, about 1/3 of the water was removed from the beaker. The beaker was then refilled with deionized water and two

drops of sodium hexametaphosphate were added as a dispersant. The mix was stirred and then allowed to settle for 15 minutes. The generated supernatant was pipetted and several drops were added onto a glass slide and let to dry overnight.

Alternate treatments of air dried samples, EG for 24 hours, and heating to 490°C were also applied in order to establish a better comparison in peak intensity ratios among the expandable clays. Step-scans from 2° - 34° 2θ with a fixed time of 5 seconds per 0.05° 2θ were conducted for each sample.

7.3.4 Major and trace element analysis

Major and trace element (TE) concentrations were obtained using the methodology described in Sanchez-Hernandez and Maurrasse (2014; Chapter 4), applying calibration and detailed procedures developed at the FIU Forensic Center (Arroyo et al., 2009). The method combines Laser Ablation and Inductively Coupled Plasma Mass Spectrometry (LA-ICP-MS) using a 266 nm Nd-YAG laser (LSX 500, CETAC, USA) and a quadrupole ELAN DRC II (Perkin Elmer LAS, Shelton CT USA), in the standard operation mode. Ablations were conducted as discrete scans in previously prepared pressed sample pellets, in four different locations in the same pellet die.

The following soil and sediment standards were used for evaluation of the analytical performance of the method: a) marine sediment reference material, PACS-2 (National Research Council of Canada, Ottawa, Canada); b) soil reference material, SRM NIST2710 (Montana Soil), and c) NIST2704 (Buffalo River Sediment), US Department of Commerce, National Institute of Standards and Technology, Gaithersburg, MD, USA).

Elemental analyses were conducted on 80 selected samples along the 155 m interval based on apparent facies changes and marked shifts in TOC and TIC.

Concentrations of Ni, V, Cr, P, Fe, U, Th, and Co, and major elements such as Al, Si and Ti were measured using NIST 2704 as the main reference standard. Since there is no concentration of Mo reported for NIST 2704 its elemental distribution was established using PACS2 as the main reference standard material following identical procedure as for the other elements. The analytical precision for all concentrations was verified to remain better than $\pm 10\%$. No evidence of external contribution from the sample preparation process was identified.

7.3.5 Biomarker analysis

In preparation for biomarker determination, small rock slabs corresponding to 24 different samples were powdered in a Bell-Art micromill. A careful cleaning process, with water, detergent, deionized water and acetone, was completed between samples. Biomarkers were analyzed following the procedures described in Jaffé et al. (2001). Samples were subjected to Soxhlet extraction for 24 hours with 300 ml 100% methylene chloride (Optima, Fisher, USA) as solvent. HCl (10%) activated copper was added during the extraction to eliminate elemental sulfur. Total extracts were concentrated by rotary evaporation and saponified with 0.5 N KOH to separate into neutral and acid fractions. The neutral fractions free of elemental sulfur were further fractionated by elution with hexane to obtain saturated hydrocarbon fraction using Pasteur pipette columns packed with silica gel. A known quantity of squalene was added as internal standard for quantification purpose, and the hydrocarbon fraction was run on gas chromatography-mass spectrometry (GC-MS) with a Hewlett-Packard 6890 GC linked to a HP 5973 quadrupole MS system, fitted with Rtx-1MS columns (30 meters long, 0.25 mm ID, 0.25 μm df) from RESTEK, USA. The GC oven was programmed to hold initial temperature

of 40°C for 1 minute, and then ramped at a rate of 6°C/minute to a final temperature of 300°C held for 20 minutes.

The analysis focused on the aliphatic fraction, more specifically on *n*-alkanes, which have been previously used to determine the provenance of the organic matter (Giger et al., 1980; Meyers, 1997; Dumitrescu and Brassell, 2005; Peters et al., 2005). Identification of compounds was performed by comparison of chromatographic retention time, comparison with the mass spectra library and previous mass spectra reported in the literature. The concentration of each biomarker was normalized to organic carbon (OC) as ng/g OC.

7.4 Results

7.4.1 Lithostratigraphy, and petrographic analysis

At the field scale the upper 155 m of the El Pui section consists of interbedded limestones and marlstones (Fig. 7-2A) with the exposed surface varying in color from light gray (N7) to medium dark gray (N4) but, on fresh-dry samples the color variation ranges from medium dark gray (N4) to grayish black (N2).

The interval between 85 ~150 m includes a monotonous sequence of marlstones and limestones that may appear flaky (Ingram, 1953) due to surficial weathering, but show excellent preserved conditions below. This interval shows an intermittent pseudo-nodular aspect that becomes evident at ~125 m, and more accentuated at ~150 m where the rocks are well lithified (Fig. 7-3). Less indurated beds with coarser texture alternate with hard, finer-textured beds between ~185 and ~215 m, a succession that suggests the influence of high frequency astronomical cycles (Bachman and Willems, 1996). This interval is also characterized by the occurrence of relatively well-preserved sea urchins

(Fig. 7-4). Ammonites increase in abundance and size (2-3 cm to 10cm) upward in the studied interval and coincide with higher amount of iron oxide nodules and pyrite. Scarce belemnites are also present.

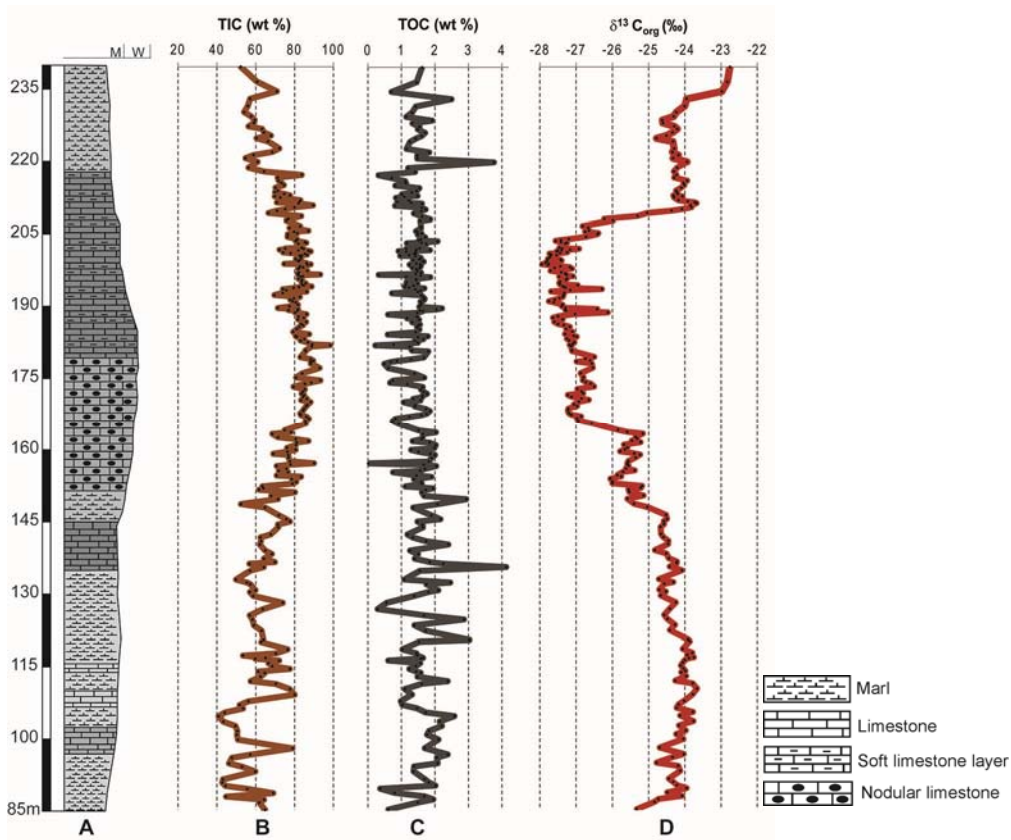


Figure 7-2 A) Simplified stratigraphic log of the upper 155 m of the El Pui section (85-240 m) showing the relative lithological variations. The M and W on top of the column refer to the mudstone and wackestone classification of Dunham (1962). B) TIC profile along the studied interval. C) Temporal variation in the TOC correlated with the stratigraphic log and TIC. D) $\delta^{13}\text{C}_{\text{org}}$ profile along the stratigraphic column.

Microscopically the interval between 85 and 150 m reveals a slight change in facies characterized by a fine micritic matrix (Fig. 7-5A, B) with less than 20% allochems, frequent sub-parallel microfabric and dispersive kerogen. In general abundance of benthic foraminifera is limited (<10 specimens/10 cm²) within this interval, and includes essentially scarce small uniserial and biserial morphotypes. A relatively sharp change in facies takes place at ~152 m with a transition from fossiliferous micrite

in the lower part to packed biomicrite (Fig. 7-5C) with skeletal components consisting mainly of echinoid fragments, and less benthic and planktonic foraminifera. However, the most contrasting change appears at ~182 m where the allochems reach ~60-70% (Fig. 7-5D) , and remain prevalent up to ~199 m where they decline drastically to ~40% in a carbonate mud matrix (Fig. 7-5E) . Proportion and size of allochems decrease gradually upward and at the 213 m level reverted to a predominantly micritic matrix as found at the 85 – 150 m interval.



Figure 7-3 Field view of part of the studied section at about the 186 m level showing well-stratified pseudo-nodular limestone.



Figure 7-4 Fossil echinoid found at level 187.5 m (sample C12-360). These echinoids are common in the 180 – ~200 m interval.

The change in allochemical content is also characterized by recurrence of dominant planktonic foraminifera and small calcispheres. The microfabric within that interval displays subparallel fabric, and these characteristics remain consistent up to the top of the studied

section at 240 m. That uppermost level shows a fine matrix containing only small allochems (<5%), and the rocks can be classified as fossiliferous micrites (Fig. 7-5F) (Folk, 1962).

7.4.2 Inorganic, organic and isotopic carbon analyses (TIC, TOC and $\delta^{13}\text{C}_{\text{org}}$)

Fig. 7-2B, shows the total inorganic carbon (TIC) fluctuating between 40.9 and 98.3% which is relatively high throughout the 155 m of the studied section, particularly between 160 and ~210 m with values mostly above 80%. This interval also coincides with an increase in the allochems and microcarbonate particles (Fig. 7-5D, E).

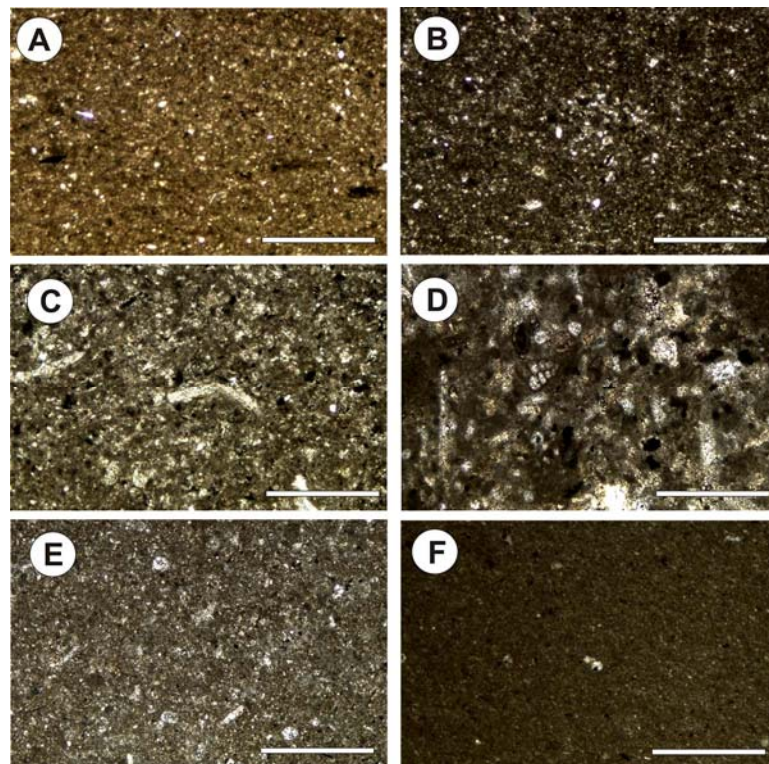


Figure 7-5 Sedimentary microfacies prior to, during and after OAE1a in the El Pui section showing paleodepositional changes. A) Sample C12-216 at 92.5 m; fine carbonate matrix with kerogen content showing subparallel microfabric with low bioturbation. B) Sample C12-280 at 149 m; this level is characterized by an increase in the microcarbonate content and size in a dark carbonate mud. C) Sample C12-286 at ~153 m; showing increase abundance and size in a dark carbonate mud. D) Sample C12-345 at ~182 m; showing a sharp change in microfacies with abundant benthic foraminifera, echinoid and roveacrinid fragments, and other bioclasts. E) Sample C12-418 at ~202 m; a new change in microfacies type takes place at the onset of the positive excursion in $\delta^{13}\text{C}_{\text{org}}$ (Fig. 2D). F) Sample C12-480 at 240 m; a very dark fossiliferous micrite. Scale bar = 500 μm

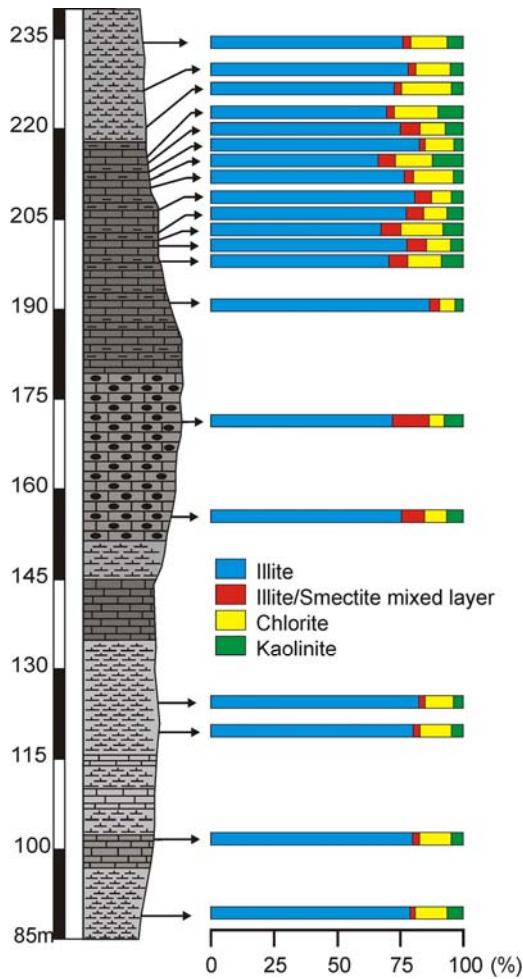
Total organic carbon (TOC) fluctuates from ~0 to 4.1% (Fig. 7-2C) but stays mostly in the range of 1- 2% with an average value of 1.5%. Most of the section shows a moderate enrichment in OC relative to the first part previously studied (Chapter 4: Sanchez-Hernandez and Maurrasse, 2014), as only ~10% of the samples yield values <1%. The high-resolution TOC curve does not follow an apparent specific repetitive pattern correlative with variations in TIC.

As shown in Fig. 7-2D, $\delta^{13}\text{C}_{\text{org}}$ values fluctuate between -22.8 and -28.0‰. The interval between ~85 and ~145 m shows relatively minor variations around -25 to -24‰ with a maximum shift of <1‰. The superjacent level yields values that define a minor negative inflection of ~1‰ that ends at ~163 m. This short interval is characterized by a relative stable trend as $\delta^{13}\text{C}_{\text{org}}$ varies between -26 and -25‰. From 163 m upward in the sequence a distinct negative spike of ~2‰ occurs between 167m and 201m with the lowest values of -27.95‰ at 199 m. That interval (167-201 m) characterizes a negative episode with moderate variation in $\delta^{13}\text{C}_{\text{org}}$ punctuated with two slightly more positive shifts of <1‰ at the 188 m, 189 m and 193 m levels, respectively. This negative episode is succeeded by a sharp positive excursion of ~4‰ beginning immediately above 201m, and rising sharply to a peak of -23.68‰ at 211.4m. The positive spike is followed by a stable trend around -24‰ up to ~228.8 m where a new positive excursion of ~1.5‰ ends at the 240 m level.

7.4.3 Bulk and clay mineral analyses

The bulk mineral content of 20 samples from selected intervals with apparent changes in facies (Fig. 7-6) was determined in order to assess the nature of the non-

carbonate fraction, and as a possible proxy for terrestrial fluxes. The bulk XRD analysis results (Fig. 7-7, Appendix 3) further confirmed CaCO₃ as the dominant constituent, and



revealed the presence of quartz (5-22%), clay minerals (2-13%), K- and plagioclase (P) feldspars (2-9%), pyrite/ marcasite (0-3%), as well as dolomite (<2%) as accessory constituents of the matrix (Fig. 7-7).

The clays investigated refer to the fine fraction phyllosilicate minerals (< 2 μm) that include kaolinite, illite, illite/smectite mixed-layer clay, and chlorite. Clay minerals constitute a potential proxy to evaluate paleoenvironmental conditions, intensity of weathering and depositional environments (Burtner and Warner, 1986; Weaver, 1989; Ruffell et al., 2002; Dera et al., 2009; Pauly et al., 2013). The

results shown in Fig. 7-6 indicate that illite (44-72%) is the dominant component of the

clay fraction followed by illite/smectite mix

layer (12-39%), chlorite (7-18%) and the

lowest is kaolinite (1-8%). This upper part of

the sequence contains a more even distribution

between illite and the poorly crystallized smectite or smectoid minerals (illite/smectite

mix layered) in contrast with the lower 85 m of the section where illite is predominant

(Sanchez-Hernandez et al., 2014). Chlorite also shows a consistent relative increase whereas kaolinite remains low.

7.4.4 Major and trace elements

Concentrations of major and trace elements were measured in order to estimate the intensity of the terrestrial fluxes, availability of nutrients, and the magnitude of the authigenic enrichment as a proxy for redox conditions (Wignall and Myers, 1988; Calvert and Pedersen, 1993; Morford and Emerson, 1999; Rimmer, 2004; Algeo and Maynard, 2004; Tribovillard et al., 2005; Sanchez-Hernandez and Maurrasse, 2014).

Elemental concentrations are expressed as normalized values with respect to Al (Fig. 7-8) in order to compensate for the dilution effect. Normalized concentrations are compared to the average shale value (ASV) (Turekian and Wedepohl, 1961; Wedepohl, 1971, 1991; Brumsack, 2006) to estimate level of enrichment or depletion of the studied elements. The element/Al ratios are plotted versus height in order to generate a comparative vertical profile. The absolute concentrations are included in Appendix 2.

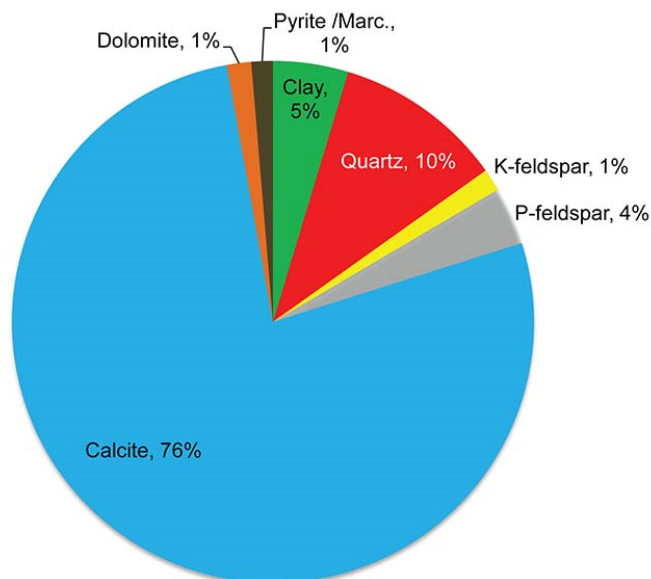


Figure 7-7 Average mineralogical composition of sediments of the 85-240 m interval of the El Pui section.

In order to make an integrated assessment of the paleoenvironmental conditions of the Organyà Basin we also focus on three sets of elements and their respective trend along the studied interval:

1- Al, Si and Ti are derived from crustal rocks, thus their presence provides useful information about terrestrial input (Brumsack, 2006). As presented in Appendix 2 (interval 85 – 240 m), Al fluctuates between 7179 and 55646 ppm with an average value of 22785 ppm. The Si/Al ratio stays mostly below the ASV (Fig. 7-8) with discrete higher values at 146 m and 168-172 m, respectively. Ti values show a relative small variation and two peaks that surpass the ASV identified at ~195 and ~199 m (Fig. 7-8).

2- P and Fe are essential micronutrients incorporated in organic matter; hence they have been used as proxies for nutrient availability (Filippelli, 2002). As a major biolimiting element in the marine environment P/Al values in this part of the El Pui

section fluctuate (Fig. 7-8) mainly above the ASV, with higher abundance between 150 and ~203 m, with more pronounced peaks at 180 m and 198 m, respectively.

Contrariwise, Fe values (Fig. 7-8) remain below the ASV, but higher availability is recorded from 199 to ~210 m.

3- V, Ni, Co, U, Cr, Cu, and Mo are redox sensitive trace elements (RSTEs) that become enriched in sediments under reducing conditions (e.g. Algeo and Maynard, 2008; Sliwinski et al., 2011). Detail variations in the relative concentration of RSTEs shown in (Fig. 7-8). The segment within the 150-200 m interval is of special interest because most elements (Cr, Co, Ni, U and Mo) exhibit TE/Al ratios above the ASV. This interval also coincides with important changes in the $\delta^{13}\text{C}_{\text{org}}$ profile (Fig. 7-2D).

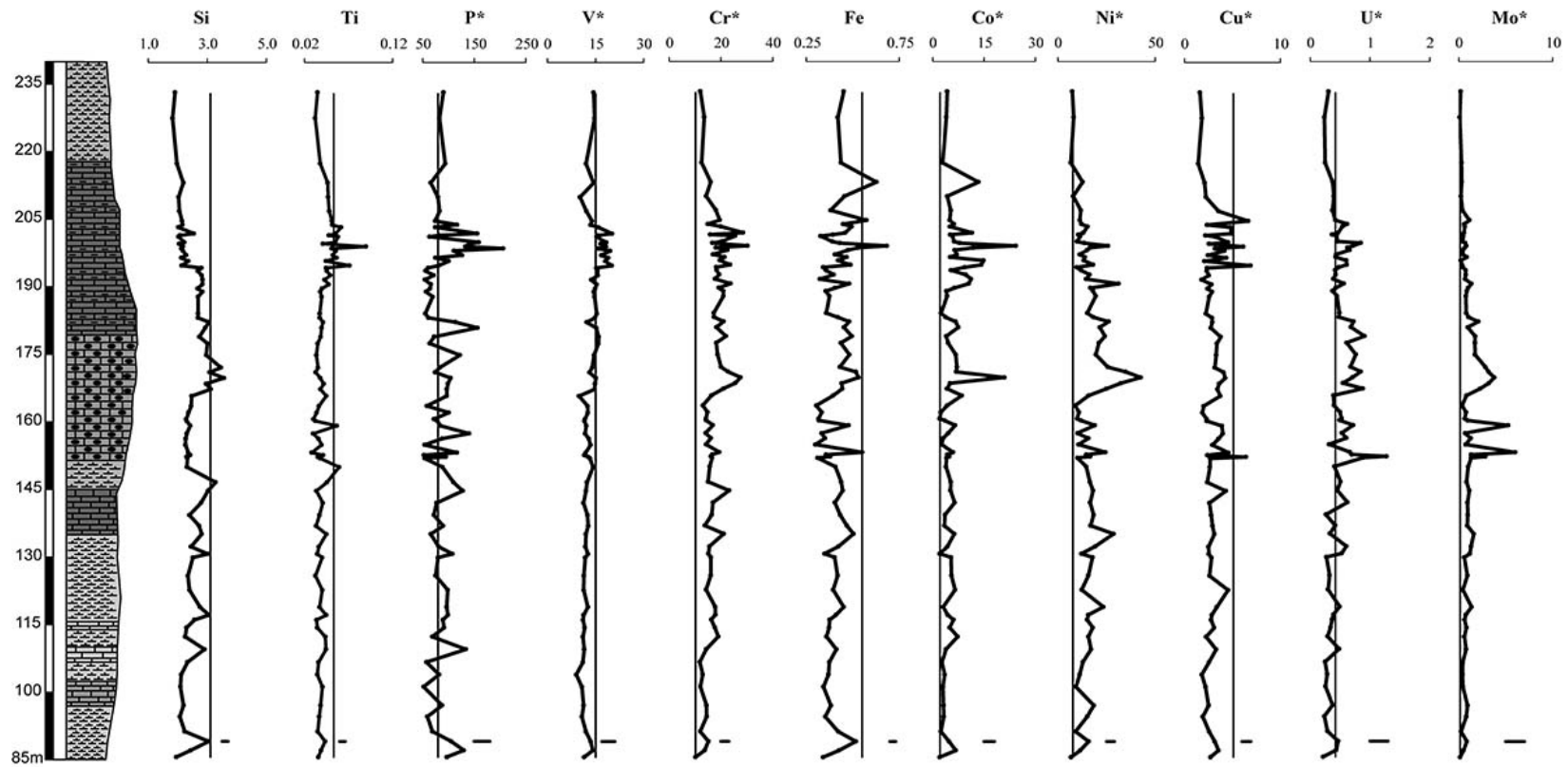


Figure 7-8 Major elements and redox sensitive trace elements concentration normalized with respect to Al. The values are compared to the ASV (fine straight line) of Wedephol (1971; 1991) to assess partial enrichment indicative of chemically reducing depositional conditions. The small horizontal lines at ~88 m correspond to the average calculated error for each element reported in the plots. ($\delta\text{Al}/\text{Mean Al} + \delta\text{Element}/\text{Mean Element}$). * values $\times 10^{-4}$.

7.4.5 Biomarker analysis

Assessing the origin of OM in the sediments of the Organyà Basin is a key component to understand the paleoenvironmental evolution of the basin. Given the physiographic complexity of the depositional environment (Berástegui et al., 1990) several sources of organic compounds are plausible to explain the OC enrichment of the El Pui sediments (e.g., terrestrial input, *in situ* organisms constituting the food web of surface waters, microbial or bacterial population in the water column under oxygen-depleted conditions, and/or phytoplankton). Since *n*-alkanes have been previously used to estimate the provenance of the organic matter in different ancient marine environments (Giger et al., 1980, Meyers, 1997; Dumitrescu and Brassell, 2005; Peters et al., 2005) the analysis of the temporal distribution of such biomarkers has been carried out in 12 samples of the upper 155 m of the El Pui section in order to assess the source of the carbon enrichment.

Sample	Height (m)	Pr/Phy	
C12-470	227.0	1.6	<p>The presence of <i>n</i>-alkanes with chain length longer than C₂₀ (> C₂₀) are commonly thought to be indicative of higher plant OM thus from terrestrial origin, whereas chains shorter than C₁₉ (< C₁₉) are presumed to be mainly derived from marine planktonic organisms and /or microbial communities (Cranwell, 1973; Cranwell et al., 1987; Forster et al., 2004; Peters et al., 2005). However it has been argued that in overmature OM the original <i>n</i>-alkane composition can be altered leading to conflictive results (Quijano et al., 2012). Since Bernaus et al. (2003) reported thermally mature OM in the Organyà Basin;</p>
C12-460	218.9	1.8	
C12-405	199.5	0.8	
C12-349	183.2	0.7	
C12-337	178.0	1.1	
C12-314	166.4	1.1	
C12-287	153.0	1.4	
C12-263	135.2	1.3	
C12-261	132.6	1.3	
C12-252	124.2	1.1	
C12-249	120.0	1.3	
C12-227	104.1	1.2	

Table 7-1 Pristane/phytane ratio of selected samples at different levels of the studied section.

here we use the pristane/phytane (Pr/Phy) ratio (Table 7-1) as a proxy to possibly rule out overmaturation. In fact, in organic-rich marine sediments the Pr/Phy is expected to increase with increasing maturity (ten Haven et al., 1987; Powell, 1988) and Pr/Phy ratios >2.5 may represent an overmature state of the OM in the absence of predominant terrestrial OM. Thus, high abundance of planktonic organisms (Sanchez-Hernandez et al., 2014), TOC levels consistently $>1\%$, and Pr/Phy ratios consistently <1.7 indicate that the OM in the El Pui was most likely preserved with *n*-alkanes distribution that characterizes the original composition.

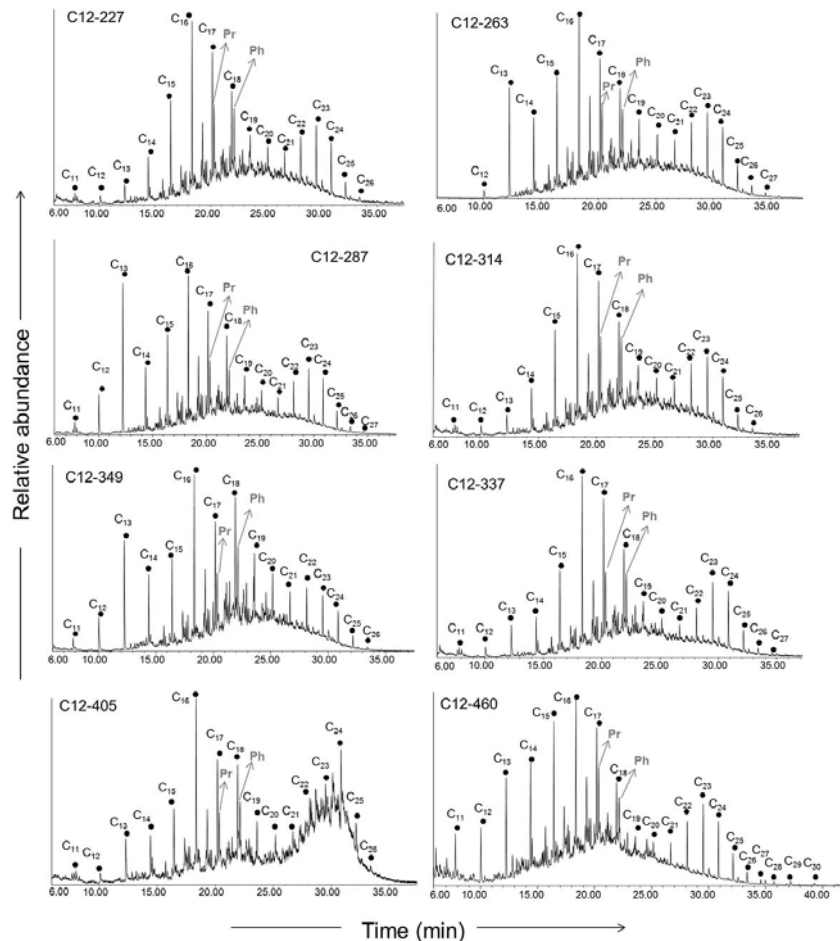


Figure 7-9 *N*-alkane distribution measured in 8 samples corresponding to different levels of the stratigraphic column. The presence of organic compounds with carbon chain lengths >20 indicates contribution of OM from terrestrial sources to the basin.

The *n*-alkane results (Fig. 7-9) reveal a mixed origin of the OM between autochthonous primary producers and terrestrial organic matter. However, the abundance of low molecular weight *n*-alkanes ($C < 19$) and the lack of odd over even carbon-number dominance suggest a more significant contribution from autochthonous sources. Values of Pr/Phy ratio (Table 7-1) in the El Pui samples < 1.7 are in agreement with this hypothesis because it has been suggested that most OM of mainly marine source has values of Pr/Phy < 2.5 (Didyk et al., 1978; Powell, 1988).

7.5 Discussion

7.5.1 Constraints from the integrated $\delta^{13}C_{org}$ record of the El Pui section

As the study of paleoenvironmental records incorporate new techniques that provide a more integrated set of data, a more robust and precise record of paleoenvironmental events can also be constructed. In the case of the El Pui section of the Organyà Basin new available geochemical and stratigraphic data permit to establish improved chemostratigraphic correlations and identification of paleoenvironmental events. The $\delta^{13}C_{org}$ results from the upper 155 m show a distinct and more pronounced negative excursion (2 ‰) at ~163 m than the one recorded in the lower part of the section (Sanchez-Hernandez and Maurrasse, 2014; Chapter 4) at the 70.6 m level that showed a decrease of ~1.5‰. Because this was the lowest inflection of the $\delta^{13}C_{org}$ curve it was assigned to the segment C3 of Menegatti et al. (1998) (Sanchez-Hernandez and Maurrasse, 2014; Chapter 4). In fact, without further $\delta^{13}C_{org}$ data at that time the 70.6 m shift simulates the pattern defined for C3, as both negative excursions are followed by positive spikes (2‰ and 4‰ for the lower and upper occurrences respectively). Both carbon isotopic indicators also imply periods of increased ^{12}C burial that is one the

geochemical signatures of OAE-1a. The present study of the $\delta^{13}\text{C}_{\text{org}}$ of the expanded section further reveals that the negative shift at 70.7 m is similar to, but lesser than, C3. The El Pui section thus reveals for the first time a clear illustration of this lesser event that could not be defined in more condensed sections (e.g., Menegatti et al., 1998; Wissler et al., 2003). In absence of reliable paleontological markers, as often is the case in black shales associated with OAE1a, the newly refined time constraint provided by the chemostratigraphic data offers a higher temporal resolution of events for global correlation. Considering that in the El Pui section both negative excursions (at 70.7 m and 163.1 m respectively) occur within the *Globigerinelloides blowi* planktonic foraminiferal Zone and above the first occurrence of the nannofossil *Rhagodiscus angustus* the lack of an integrated record of $\delta^{13}\text{C}_{\text{org}}$ has proven to be problematic in order to precisely identify the occurrence of segment C3 (Menegatti et al., 1998). The new high-resolution $\delta^{13}\text{C}_{\text{org}}$ data from the El Pui section thus improve our understanding of the occurrence of segment C2, which now spans from the originally defined starting position at 15.5 m (Sanchez-Hernandez and Maurrasse, 2014) up to the 163.1 m level, and includes a characteristic lesser negative inflection preceding the true onset of the more pronounced negative excursion distinguishing C3. Hence, in the El Pui section C3 is distinctly defined by a pronounced negative trend extending from 161.3 m to 203.7 m (Fig. 7-10).

It is the general consensus that the major geochemical signature of the onset of OAE1a consists of a rapid and an extended positive excursion of $\sim 4\text{-}5\text{‰}$ subsequent to C3, and is identified as segment C4 (Menegatti et al., 1998) (Fig. 7-10). At El Pui C4 has a maximum positive excursion of $\sim 4\text{‰}$ and extends within interval 203.7 m – 211.4 m. The peak of this positive shift (C4) is followed by a relatively stable trend with low

$\delta^{13}\text{C}_{\text{Org}}$ variability between -24.5 and -24‰ assigned to C5, which continues up to 228.8m. A subsequent positive spike of ~2‰ is assigned to C6 from 228.8 m up to the end of the studied section at 240 m) (Fig. 7-10).

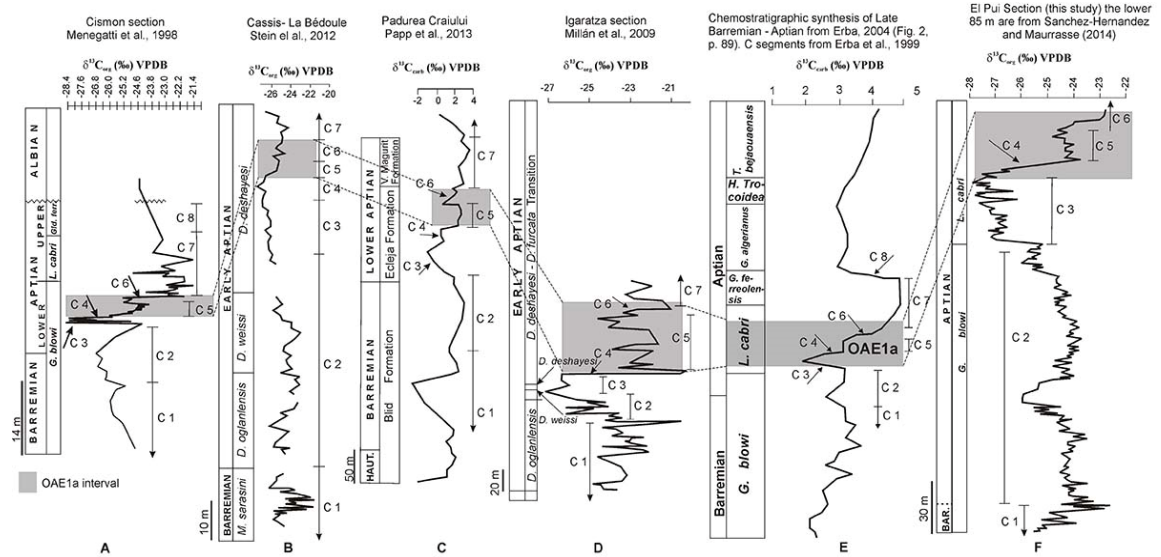


Figure 7-10 Chemostratigraphic correlation based on $\delta^{13}\text{C}$ of the El Pui section with other Tethyan sections. The C segments correspond to the $\delta^{13}\text{C}$ subdivision as proposed by Menegatti et al. (1998) for the lower Aptian. Shaded intervals correspond to the occurrence of the OAE1a. Note that the expanded character of the sedimentary sequence at El Pui allows for a detail description of the C segments.

7.5.2 Facies variability and geochemical proxies as paleoenvironmental indicators

From 85 m to 145 m the sedimentation pattern and components of the matrix display minor changes relative to the lower 85 m. A fine micritic matrix with frequent dispersive kerogen and occasional subparallel fabric suggesting little burrowing activity in the sediment characterizes the facies (Fig. 7-5A, B). Benthic foraminifera remain scarce (< 5 specimens/10 cm²) with the presence of mainly uniserial and biserial morphotypes. Planktonic foraminifera also remain scarce with sizes between (100-150 μm). Microcarbonate particles increase gradually from ~115 m upward.

The type of facies that developed over this 60 m interval is consistent with higher subsidence rates of the basin during the early Aptian (García- Senz, 2002; Gong 2008). As the sediments imply, restricted conditions of the Organyà Basin persisted throughout that interval and sustained poor vertical mixing of the water column, hence limiting oxygenation of the deeper water masses. Lower bioturbation index (0 - 1) is consistent with limited abundance of benthic life. However a fully reducing phase was not achieved within that 60 m-interval because the trace elements distribution (Fig.7- 8) shows no apparent enrichment compared to the background values and the ASV. In addition, the Pr/Phy ratio yield values >1 that are consistent with oxic conditions (Powell, 1988) (Table 7-1).

Since the sedimentation rate increased in the basin during the lower Aptian (García- Senz, 2002; Bernaus et al., 2003; Gong, 2008) the important question arose concerning the origin of the contributing particulate matters. The geochemical results show very low variability of the $\delta^{13}\text{C}_{\text{org}}$ which together with Ni/Al ratios close to the background value within that interval suggests the absence of favorable biogeochemical conditions associated with enhanced organic matter productivity and/or oxygen depletion (Figs. 7-2D, 7-8). Therefore, they do not support high primary productivity as the plausible source of the increased carbonate content (Fig. 7-2B). Because the high TIC concurs with high abundance of microcarbonate particles, their correspondence suggests a possible contribution from surrounding carbonate platforms. Results of the bulk mineral content in the 85 ~150 m interval indicate that the non-carbonate fraction reaches values up to 48% (Appendix 3), which gives evidence of intensified terrestrial fluxes as indicated by peaks in the Si/Al ratio (up to 1.5 times the values in the lower 85

m) close to the average shale value (Fig. 7-8). Depending on existing physiography and climatic conditions, such terrigenous fluxes would have also brought land-derived organic matter into the basin. In fact, the *n*-alkanes results for samples C12-227 and C12-263 (Fig. 7-9) at 104 m and 135 m, respectively, confirm a mixed origin for the OM including contribution from terrestrial plants. The apparent discrepancy between the non-reducing condition revealed by the RSTE results and continuous OM burial can thus be explained by the high terrigenous input, which might have favored OM preservation. Actually, in a depositional setting with a high sedimentation rate, rapid export of OM matter bound to inorganic particles (Edenborn et al., 1987; Allen and Allen, 2013) decreases the exposure time to oxidation in the water column leading to enhanced preservation. Concerning the low abundance of benthic and planktonic foraminifera, high terrigenous fluxes can also be invoked as a factor causing a dilution effect.

At ~150 m the matrix starts to become consistently coarser with intermittent evidence of allochthonous bioclasts (Fig. 7-5C, D) concomitant with further sustained increase in TIC (average ~80%) that continues up to ~200 m (Fig. 7-2B). Benthic and planktonic foraminifera, as well as echinoderm fragments fluctuate in abundance until ~180 m where there appears an abrupt change from sparse-fossiliferous biomicrite to packed biomicrite. The packed biomicrite has a mean allochemical value of ~50-60% with abundant benthic foraminifera (coiled, uniserial, biserial), and skeletal debris of mainly echinoderm and mollusk, and lesser amount of sponge spicules.

The dominant facies in the 150-200 m interval are interpreted as indicative of an environment of deposition affected by allochthonous contribution from the adjacent

outer platform. The sustained high carbonate values, abundant coarse bioclasts, and the maximum value of the Si/Al ratio of the whole section at ~170 m indicate mix sources for the particles that contributed to the high mass accumulation rate. Although this interval may be coincident with the onset of higher eustatic sea level, its chronostratigraphic position preceding the acute positive $\delta^{13}\text{C}_{\text{org}}$ excursion (Figs. 7-2D, 7-10) characteristic of carbon isotope segment C4, suggests that maximum drowning was not yet attained (Föllmi et al., 2006; Föllmi and Gainon, 2008). Assuming a high sedimentation rate of up to 20 cm/ky for the platform carbonates (Gong, 2008) a progradation of the ramp could have intensified the carbonate supply to the basin, hence accelerating partial filling of the basin (Masse and Ferneci-Masse, 2013).

Concerning basin response to global forcing factors, field scale occurrence of alternating cm- to dm-thick, less consolidated, and hard well-lithified pseudo-nodular limestone layers (Fig. 7-3), between 150 and 180 m interval could possibly be representative of high frequency cycles controlled by precession (21 ka) and eccentricity (ca. 100 ka) (Bachmann and Willens, 1996). If this postulate is correct, the fluctuating pattern of the facies observed within that interval could be assigned to climatic cycles.

Furthermore the abundance of biolimiting elements (P, Fe) within the 150-200 m interval points to a nutrient rich environment where P and Fe concentrations reach several maxima (Fig. 7-8). In the case of the high Ni/Al index, the positive correlation with a peak in Si/Al implies that in addition to the autochthonous organic matter, enhanced incorporation of terrigenous OM increased Ni absorption in organometallic compounds that heightened Ni concentration in the sediments (Nijenhuis et al., 1999;

Akinlua et al., 2010; Sanchez-Hernandez and Maurrasse, 2014; Chapter 4).

Nonetheless, the *n*-alkanes for samples C12-287, C12-314, C12-337 and C12-349 (Fig. 7-9), and additional evidence from Pr/Phy ratios <1.4 for the same samples (Table 7-1), reveal that marine organic matter still predominates.

Concerning oxygen levels, this interval did not develop anoxia because under strong reducing conditions and chemical availability of both Ni²⁺ and VO²⁺, the vanadyl species is preferentially incorporated into the organo-metallic ligands (Killops and Killops, 2005), which explains why Ni enrichment is related to terrestrial OM input rather than from anoxic conditions. Since V is not substantially enriched in the 150-200 m interval, and only discrete peaks in U and Mo are present, a strong anoxic/sulphidic episode can be ruled out. Nevertheless, the temporal distribution of trace elements showing partial enrichment of Co, Ni, Cr, U and Mo (Fig. 7-8) concurrent with values of Pr/Phy < 1 at 183 m and 199 m (samples C12-349 and C12-405, respectively) and relatively high TOC values (Fig. 7-2C) support periodic dysoxic episodes.

Variations in the relative abundance of non-carbonate minerals suggest a dilution effect by high carbonate input, whereas high relative percentages of illite, smectoid minerals, and chlorite (Fig. 7-6) coincident with pulses in the Si/Al ratio attest for active weathering of the surrounding metamorphic terranes (Sanchez-Hernandez et al., 2014)

The uppermost interval of the El Pui section (200-240 m) shows an overall slow and gradual decrease in the abundance of carbonate bioclasts. From ~ 200 - 210 m the fine carbonate matrix contains 30-40 % allochems, mainly benthic foraminifera, echinoderm fragments and unidentified bioclasts. The type of facies corresponding to

this level can be described as a bioturbated packed biomicrite. The succeeding level above 210 m shows a significant decrease (<10%) of the allochemical content, and the matrix is dominated by fine microcarbonate particles. Subparallel microfabric is common in thin sections with pervasive kerogen in inter- and intraparticle pores.

Facies characteristics of the uppermost part of the studied section suggest a transition from a depocenter under the influence of materials supplied from the outer ramp, as indicated by high allochthonous skeletal grains, to subsequent semi-restricted depositional conditions with calcilutites rich in OM. Such changes may indicate further drowning of the adjacent carbonate platforms, probably corresponding with the second period of anoxia at the OR-4 sequence type of Bernaus et al. (2003). Combined tectonic movements, as proposed for the Provencal Platform during the early Aptian (Godet et al., 2013), and eustatic sea level rise (Haq et al., 1987; Skelton, 2003; Bernaus et al., 2003) have been invoked as causal factors for maximum flooding of carbonate platforms at that time. In the northern Tethys the major drowning episode of carbonate platforms during the lower-middle Aptian has been associated with rising sea level shown to be correlative with the abrupt $\delta^{13}\text{C}_{\text{org}}$ positive excursion (C4) (Figs. 7-2D, 7-10) that characterizes the onset of OAE1a (Föllmi et al., 2006; Föllmi, 2008; Föllmi and Gainon, 2008). At El Pui the change in facies occurs toward the end of the $\delta^{13}\text{C}_{\text{org}}$ positive excursion (Figs. 7-2D, 7-10) hence we favored a transgressive sea level track for the modification of the depositional conditions. Considering that the sedimentation rate of the studied section was uncommonly high (Bachmann and Willens, 1996), flooding of the shallow-water environment may have been slower compared with coeval sections with lower mass accumulation rate (e.g., Pratt and Smewing, 1993).

During the phase of sedimentation when higher TOC values concur with a decreasing trend in the TIC, this inverse relationship probably reflects the demise of the carbonate platform and reduced export of CaCO₃ to the basin. A simultaneous decline in the siliciclastic input is revealed by a decreasing trend in the Si/Al and Ti/Al fractions (Fig. 7- 8) and other non-carbonate components, which might have also lessened the influx of terrestrial OM to the basin. The high OC content and high accumulation rate registered within the 200 - 240 m interval could therefore be related to *in situ* high productivity, as the availability of biolimiting nutrients (P, Fe) remained stable (Fig. 7-8). Because enrichment levels of the redox sensitive trace elements remain low, and in some cases depleted with respect to the average shale (Fig. 7- 8), anoxic conditions did not develop within that interval. Values of the Pr/Phy ratio >1.4 also support such a conclusion.

7.5.3 Main Controlling factors on the expression of OAE1a in the El Pui section

The hallmark of the lower Aptian anoxic event 1a (OAE1a) has been recognized to include deposition of organic-rich black shales and a pronounced positive excursion of the $\delta^{13}\text{C}$ curve. In most cases there is relative enrichment of redox-sensitive trace elements concomitant with absence of benthic organisms as indicative of oxygen-depleted depositional conditions (Bellanca et al., 2002; Tribovillard et al., 2004; Trindade et al., 2006; Stein et al., 2011; 2012). Different mechanisms have been proposed to interpret the deposition of OM- rich sediments: enhanced primary productivity and/or sustained supply of OM from allochthonous sources, fast export of OM to the sediment, and severe water column anoxia (Bralower et al., 1994; Weissert et al., 1998; Larson and Erba, 1999; Leckie et al., 2002). Certainly a combination of these factors most likely

caused the widespread occurrence of OAE1a in the pelagic domain; however, in marginal basins the influence of local factors can produce an exceptional record of the paleoceanographic and paleoclimatic conditions during major anoxic events (Kuhnt et al., 1998; Luciani et al., 2006).

In the El Pui section the relatively high TOC content of the upper 155 m is compatible with an environment depleted in oxygen, but the overall distribution of the redox sensitive trace elements in the interval corresponding to OAE1a (C4-C5) reveals limited enrichment that cannot be ascribed to anoxic depositional conditions. Furthermore, the presence of benthic foraminifera throughout the studied interval also suggests that bottom conditions did not reach a permanent anoxic phase, although their fluctuating abundance could indicate intermittent dysoxia (Wignall and Myers, 1988; Taylor and Goldring, 1993).

In summary, relatively high content in OM in the upper 155 m of the studied section seems to have been controlled by a combination of concurrent factors that included high primary productivity and intensified accumulation rate enhanced by contribution of terrestrial organic material, as indicated by the *n*-alkanes results. The sediments in the interval from 150 - 200 m indicate that deeper basinal environments generated by higher flexural subsidence induced conditions that exacerbated oxygen depletion of bottom waters through oxidation of OM in the water column prior to OAE1a in the time interval from 150-200 m. The productivity proxies (TOC, P/Al, Ni/Al) support increased autochthonous productivity and partial import of OM. In addition, higher partial enrichment of RSTEs (U, Mo, Co) together with Pr/Phy ratios <1 point to reducing conditions.

Worldwide precursory signals of OAE1a in the sediment record suggest progressive environmental shifts towards higher trophic levels and accentuated oxygen deficiency concomitant with global forcing factors (e.g., outgassing of volcanic CO₂, elevated average temperature (Tejada et al., 2009) that triggered anoxia. However, the effects of global factors coupled with basin physiography led to different responses in semi-enclosed basins where partial preservation of OM became accentuated without the development of anoxia, as is the case for the Organyà Basin.

7.6 Conclusions

High-resolution petrographic and geochemical analyses of the upper 155 m of the El Pui section in the semi-enclosed Organyà Basin, south-central Spanish Pyrenees, reveal that during the early Aptian depositional conditions favored partial preservation of OM mainly through increased sedimentation and shorter OM transit time in the water column because of increased sedimentation rate. The results also show limited enrichment and/or partial depletion of RSTEs, and the presence of benthic foraminifera, which implies that development of anoxic conditions in the basin can be ruled out.

The $\delta^{13}\text{C}_{\text{org}}$ profile for El Pui replicates the carbon isotopic signature reported elsewhere in the Tethys Ocean, and further provides an improved high-resolution chemostratigraphic means for precise worldwide chronostratigraphic correlation for the latest Barremian–middle Aptian. The upper part of the El Pui section includes well-defined carbon isotope segments C2 (upper part), C3, C4, C5, and C6 (partial), which correlate with other Tethyan sections and allow for recognition of the lower Aptian OAE1a in the uppermost 35 m of the section. A change in microfacies indicative of more pronounced hemipelagic conditions concurrent with the onset of the distinct positive

excursion (C4) in $\delta^{13}\text{C}_{\text{org}}$ points to an accentuated platform drowning event as reported for other Tethyan sections related to higher eustatic elevations at that time.

The integrated results of the study (upper 155 m of the El Pui section) highlight the effects of local physiographic conditions in the local sedimentary response of marine restricted basins to global environmental changes. In contrast to the general trend recorded elsewhere, in the Organyà Basin enhanced organic carbon sequestration during OAE1a developed in the absence of strong anoxic conditions. Enhanced burial of organic matter was the result of a combined system of intensified primary productivity, oxygen deficiency in the water column, and a higher mass accumulation rate, which led to rapid burial and preservation of the OM.

7.7 Acknowledgments

The Goodfriend Memorial Funds financially supported this research. Diane Pirie and Thomas Beasley are kindly acknowledged for their help with instrumentation and materials at FIU. We are most grateful to Dr. Rudolf Jaffe and Ding He for providing critical support with the biomarker analyses. Bill Anderson and John Harris provided valuable assistance with the carbon isotope analyses. We are thankful to Tatiana Trejos from the FIU forensic center for technical support with the elemental analyses. Our colleague Josep Moreno-Bedmar is also kindly acknowledged for valuable logistical help and discussion about the section and the OAE1a. We thank Mr. Ferran who graciously allowed us to work on his private property. The Earth and Environment Department at FIU generously provided supplies and other laboratory materials.

7.8 References

- Akinlua, A., Adekola, S.A., Swakamisa, O., Fadipe, O.A., Akinyemi, S.A., 2010. Trace element characterization of Cretaceous Orange Basin hydrocarbon source rocks. Elsevier, Applied Geochemistry 25, 1587–1595.
- Allen, P.A., Allen, J.R., 2013. Basin analysis: principles and applications. Blackwell publishing Ltd, 2nd ed. MA, USA. pp. 560.
- Algeo, T. J., Maynard J. B., 2004. Trace element behavior and redox facies in core shales of Upper Pennsylvanian Kansas-type cyclothems, Chemical Geology 206, 289–318.
- Algeo, T. J., Maynard J. B., 2008. Trace-metal covariation as a guide to water-mass conditions in ancient anoxic marine environments. *Geosphere* 4 (5), 872-887.
- Ando, A., Kaiho, K., Kawahata, H., Kakegawa, T., 2008. Timing and magnitude of early Aptian extreme warming: Unraveling primary $\delta^{18}\text{O}$ variation in indurated pelagic carbonates at Deep Sea Drilling Project Site 463, central Pacific Ocean: Palaeogeography, Palaeoclimatology, Palaeoecology 260, 463-476.
- Arroyo, L., Trejos, T., Gardinalli, P.R., Almirall, J.R., 2009. Optimization and validation of a Laser Ablation Inductively Coupled Plasma Mass Spectrometry method for the routine analysis of soils and sediments. Spectrochimica Acta Part B 64, 16-25.
- Arthur, M.A., Schlanger, S.O., 1979. Cretaceous “Oceanic Anoxic Events” as causal factors in development of reef-reservoired giant oil fields. American Association of Petroleum Geologists Bulletin 63(6), 870–885.
- Arthur, M.A., Brumsack, H.-J., Jenkyns, H.C., Schlanger, S.O., 1990, Stratigraphy, geochemistry, and paleoceanography of organic carbon-rich Cretaceous sequences, in Ginsburg, R.N., and Beaudoin, B., eds., Cretaceous resources, events, and rhythms: Kluwer Academic Publishers, p. 75–119.
- Bachmann, M., Willems, H., 1996. High-frequency cycles in the upper Aptian carbonates of the Organyà basin, NE Spain. Geologische Rundschau 85(3), 586–605.
- Bellanca, A., Erba, E., Neri, R., Premoli Silva, I., Sprovieri, M., Tremolada, F., Verga, D., 2002. Paleooceanographic significance of the Tethyan “Livello Selli” (Early Aptian) from the Hybla Formation, northwestern Sicily: biostratigraphy and high-resolution chemostratigraphic records. Palaeogeography, Palaeoclimatology, Palaeoecology 185, 175–196.
- Berástegui, X., García-Senz, J.M., Losantos, M., 1990. Tectonosedimentary evolution of the Organyà extensional basin (Central South Pyrenean Unit, Spain) during the Lower Cretaceous. Bulletin de la Société Géologique de France 8(2), 251–264.

- Bernaus, J.M., Arnaud-Vanneau, A., Caus, E., 2003. Carbonate platform sequence stratigraphy in a rapidly subsiding area: the Late Barremian - Early Aptian of the Organyà Basin, Spanish Pyrenees. *Sedimentary Geology* 159 (3-4), 177–201.
- Bond, R.M.G., McClay, K.R., 1995. Inversion of a lower Cretaceous extensional basin, south central Pyrenees, Spain. In: Buchanan and Buchanan (eds): *Basin Inversion*. Geological Society Special Publications 88, 415–431.
- Bralower, T. J., Arthur, M. A., Leckie, R. M., Sliter, W. V., Allard, D. J., Schlanger, S. O., 1994. Timing and paleoceanography of oceanic dysoxia/anoxia in the Late Barremian to Early Aptian (Early Cretaceous). *Palaios*, 9(4), 335–369.
- Bralower, T.J., CoBabe, E., Clement, B., Sliter, W.V., Osburn, C.L., Longoria, J., 1999. The record of global change in mid-Cretaceous (Barremian–Albian) sections from the Sierra Madre, northeastern Mexico. *Journal of Foraminiferal Research* 29, 418–437.
- Bréhéret, J.-G., 1988. Episodes de sédimentation riche en matière organique dans les marnes bleues d'âge aptien et albien de la partie pélagique du bassin vocontien. *Bulletin de la Société Géologique de France* 4, 349– 356.
- Brumsack, H. J., 2006. The trace metal content of recent organic carbon-rich sediments: Implications for Cretaceous black shales formation. *Palaeogeography, Palaeoclimatology, Palaeoecology* 232, 344-361.
- Burtner, R. L., Warner, M. A., 1986: Relationship between illite/smectite diagenesis and hydrocarbon generation in lower Cretaceous Mowry and Skull creek shales of the northern rocky mountain area. *Clay and clay minerals* 34(4), 390–402.
- Burla, S., Heimhofer, U., Hochuli, P.A., Weissert, H., Skelton, P., 2008. Changes in sedimentary patterns of coastal and deep-sea successions from the North Atlantic (Portugal) linked to Early Cretaceous environmental change. *Palaeogeography, Palaeoclimatology, Palaeoecology* 257, 38–57.
- Calvert, S.E., Pedersen, T.F., 1993. Geochemistry of recent oxic and anoxic marine sediments: implications for the geological record. *Marine Geology* 113, 67– 88.
- Caus, E., García-Senz, J. M., Rodés, D., Simó, A. 1990. Stratigraphy of the Lower Cretaceous (Berriasian–Barremian) sediments in the Organyà Basin, Pyrenees, Spain. *Cretaceous Research* 11, 313–320.
- Choukroune, P., Le Pichon, X., Séguet, M., Sibuet, J.C., 1973. Bay of Biscay and Pyrenees. *Earth and Planetary Science Letters* 18, 109–118.
- Coccioni, R., Franchi, R., Nesci, O., Wezel, C.F., Battistini, F., Pallecchi, P., 1989. Stratigraphy and mineralogy of the Selli Level (early Aptian) at the base of the Marne a Fucoidi in the Umbrian-Marchean Apennines (Italy). In: Wiedmann, J.

- (Ed.). Cretaceous of the Western Tethys. Third International Symposium, Tübingen, 1987, pp. 563–584.
- Cranwell, P. A., 1973. Chain-length distribution of n-alkanes from lake sediments in relation to post-glacial environmental change. *Freshwater Biology* 3, 259–265.
- Cranwell, P. A., Eglinton, G. and Robinson, N., 1987. Lipids of aquatic organisms as potential contributors to lacustrine sediments II. *Organic Geochemistry* 11, 513–527.
- Dera, G., Pellenard, P., Neige, P., Deconinck, J. F., Pucéat, E., Dommergues, J. L., 2009. Distribution of clay minerals in Early Jurassic Peritethyan seas: Palaeoclimatic significance inferred from multiproxy comparisons. *Palaeogeography, Palaeoclimatology, Palaeoecology* 271(1), 39–51.
- Dinarès-Turell, J., García-Senz, J., 2000. Remagnetization of Lower Cretaceous limestones from the southern Pyrenees and relation to the Iberian plate geodynamic evolution. *Journal of Geophysical Research* 105 (B8), 19405–19418.
- Didyk, B.M., Simoneit, B.R.T., Brassell, S.C., Eglinton, G., 1978. Organic geochemical indicators of palaeoenvironmental conditions of sedimentation. *Nature* 272, 216–222.
- Dumitrescu, M., Brassell, S.C., 2005. Biogeochemical assessment of sources of organic matter and paleoproductivity during the early Aptian Oceanic Anoxic Event at Shatsky Rise, ODP Leg 198, *Organic Geochemistry* 36 (7), 1002–1022.
- Edenborn H. M., Silverberg N., Mucci A., Sundby B., 1987. Sulfate reduction in deep coastal marine sediments. *Marine Chemistry* 21, 329–345.
- Erba, E., 2004. Calcareous nannofossils and Mesozoic oceanic events. *Marine micropaleontology* 52, 85–106.
- Filippelli, G.M. 2002. The Global Phosphorus Cycle. *Reviews in Mineralogy and geochemistry* 48, 391 – 425.
- Föllmi, K.B. (2008) A synchronous, middle Early Aptian age for the demise of the Helvetic Urganian platform related to the unfolding oceanic anoxic event 1a (« Selli event »). *Revue de Paléobiologie*, 27, 461-468.
- Föllmi, K.B., Weissert, H., Bisping, M., Funk, H., 1994. Phosphogenesis, carbon-isotope stratigraphy, and carbonate-platform evolution along the Lower Cretaceous northern tethyan margin. *Geological Society of America, Bulletin* 106, 729–746.
- Föllmi, K. B., Gainon, F., 2008. Demise of the northern Tethyan Urganian carbonate platform and subsequent transition towards pelagic conditions: the sedimentary

- record of the Col de la Plaine Morte area, central Switzerland. *Sedimentary Geology* 205(3), 142-159.
- Föllmi, K.B., Godet, A., Bodin, S., Linder, P., 2006. Interactions between environmental change and shallow-water carbonate build-up along the northern Tethyan margin and their impact on the Early Cretaceous carbon-isotope record. *Paleoceanography* 21.
- Forster, A., Sturt, H., Meyers, P.A., and the Leg 207 Shipboard Scientific Party, 2004. Molecular biogeochemistry of Cretaceous black shales from the Demerara Rise; preliminary shipboard results from Sites 1257 and 1258, ODP Leg 207, In: Erbacher, J., Mosher, D.C., Malone, M.J., et al. (eds.), *Proceedings of the Ocean Drilling Program, Initial Results 207*, 1–22.
- Gaona-Narvaez, T., 2013. Lower Aptian comparative stratigraphy of the Basco-Cantabrian region (Spain) and Eastern Cordillera (Colombia): implications for local factors in the depositional record of oceanic anoxic event 1a (OAE-1A). PhD dissertation, Florida International University, Miami, Florida USA, pp. 276.
- Gaona-Narvaez, T., Maurrasse, F.J.-M.R., Moreno-Bedmar, J. A., 2013. Stable Carbon Isotope Stratigraphy and Ammonite Biochronology at Madotz (Navarra, N Spain): Implications for the Timing and Duration of Oxygen Depletion during OAE-1a. *Cretaceous Research* 40, 143–157.
- García-Senz, J., 2002. Cuencas extensivas del Cretácico Inferior en los Pirineos Centrales -formación y subsecuente inversión. PhD Dissertation, University of Barcelona, Barcelona, 310 pp.
- Garrido Mejias, A., 1973. Estudio geológico y relación entre tectónica y sedimentación del Secundario y Terciario de la vertiente meridional pirenaica en su zona central (provincias de Huesca y Lérida). PhD dissertation, Universidad de Granada, 320 pp.
- Giger, W., Schaffner, C., Wakeham, S. G., 1980. Aliphatic and olefinic hydrocarbons in recent sediments of Greifensee, Switzerland. *Geochimica et Cosmochimica Acta* 44, 119–129.
- Godet, A., Hfaiedh, R., Arnaud-Vanneau, A., Zghal, I., Arnaud, H., Ouali, J., 2014. Aptian palaeoclimates and identification of an OAE 1a equivalent in shallow marine environments of the southern Tethyan margin: Evidence from Southern Tunisia (Bir Oum Ali section, Northern Chott Chain). *Cretaceous Research*, 48, 110–129.
- Gong, Z., 2008. The rotation of Iberia during the Aptian and consequences for pervasive Cretaceous remagnetization. PhD Dissertation, University of Utrecht, Budapestlaan, The Netherlands, 103 pp.

- Gong, Z., van Hinsbergen, D.J.J., Vissers, R.L.M., Dekkers, M.J., 2009. Early Cretaceous syn-rotational extension in the Organyà basin—new constraints on the palinspastic position of Iberia during its rotation. *Tectonophysics*, 473, 312–323.
- Haq, B.U., Hardenbol, J., Vail, P.R., 1987. Chronology of fluctuating sea levels since the Triassic. *Science* 235, 1156–1167.
- Heimhofer, U., Hochuli, P.A., Herrle, J.O., Weissert, H., 2006. Contrasting origins of Early Cretaceous black shales in the Vocontian basin: evidence from palynological calcareous nannofossil records. *Palaeogeography, Palaeoclimatology, Palaeoecology* 235, 93–109.
- Herrle, J.O., Köbler, P., Friedrich, O., Erlenkeuser, H., Hemleben, C., 2004. High-resolution carbon isotope records of the Aptian to Lower Albian from SE France and the Mazagan Plateau (DSDP Site 545): a stratigraphic tool for paleoceanographic and paleobiologic reconstruction. *Earth and Planetary Science Letters* 218, 149–161.
- Huck, S., Rameil, N., Korbar, T., Heimhofer, U., Wieczorek, T.D., Immenhauser, A., 2010. Latitudinally different responses of Tethyan shoal-water carbonate systems to the Early Aptian oceanic anoxic event (OAE 1a). *Sedimentology* 57, 1585–1614.
- Hughes, R. E.; Warren, R., 1989. Evaluation of the Economic Usefulness of Earth Materials by X-ray Diffraction, 23rd Forum Geology Industrial Minerals; Hughes, R. E.; Bradbury, L. C., Eds. Illinois State Geological Survey.
- Hughes, R. E., Moore, D. M., and Glass, H. D., 1994. Qualitative and quantitative analysis of clay minerals in soils: in Amonette, J. E., and Zelazny, L. W., editors, *Quantitative Methods in Soil Mineralogy*, SSSA Miscell. Pub., 330–59.
- Immenhauser, A., Hillgärtner, H., Sattler, U., Bertotti, G., Schoepfer, P., Homewood, P., Vahrenkamp, V., Steuber, T., Masse, J.P., Droste, H., Taal-van Koppen, J., van der Kooij, B., van Bentum, E., Verwer, K., Hoogerduijn Strating, E., Swinkels, W., Peters, J., Immenhauser-Potthast, I., Al Maskery, S., 2004. Barremian–lower Aptian Qishn Formation, Haushi–Hufq area, Oman: a new outcrop analogue for the Kharai/Shu'aiba reservoirs. *GeoArabia* 9, 153–194.
- Immenhauser, A., Hillgartner, H., Van Bentum, E., 2005. Microbialforaminiferal episodes in the Early Aptian of the southern Tethyan margin: ecological significance and possible relation to oceanic anoxic event 1a. *Sedimentology* 52 (1), 77–99.
- Ingram, R. L., 1953. Fissility of mudrocks. *Bulletin, Geological Society of America* 64, 569–578.

- Jaffe, R., Mead, R., Hernandez, M.E., Peralba, M.C., DiGuida, O.A., 2001. Origin and transport of sedimentary organic matter in two subtropical estuaries: a comparative, biomarker-based study. *Organic Geochemistry* 32, 507–526.
- Kuhnt, W., Moullade, M., Masse, J.-P., Erlenkeuser, H., 1998. Carbon-isotope stratigraphy of the lower Aptian historical stratotype at Cassis-La Bédoule (SE France). *Géologie Méditerranéenne* 25 (3–4), 63–79.
- Kujau, A., Heimhofer, U., Ostertag-Henning, C., Gréselle, B., Mutterlose, J., 2012. No evidence for anoxia during the Valanginian carbon isotope event—An organic-geochemical study from the Vocontian Basin, SE France. *Global and Planetary Change* 92, 92–104.
- Larson, R.L., Erba, E., 1999. Onset of the mid-Cretaceous greenhouse in the Barremian - Aptian: igneous events and the biological, sedimentary, and geochemical responses. *Paleoceanography* 14, 663–678.
- Luciani, V., Cobianchi, M., Lupi, C., 2006. Regional record of a global oceanic anoxic event: OAE1a on the Apulia platform margin, Gargano Promontory, southern Italy. *Cretaceous Research* 27 (6), 754–772.
- Masse, J.-P., Bellion, Y., Benkhelil, J., Dercourt, J., Guiraud, R., Ricou, L.E., 1993. Lower Aptian Palaeoenvironments (114 to 112 Ma). In: Dercourt, J., Ricou, L.E., Vrielynck, B. (Eds.), *Atlas Tethys Palaeoenvironmental Maps*, Gauthier-Villars, Paris, pp. Maps. BEICIP-FRANLAB, Rueil-Malmaison.
- Masse, J.P., Ferneci-Masse, M., 2013. Drowning events, development and demise of carbonate platforms, and controlling factors: The Late Barremian-Early Aptian record of Southeast France. *Sedimentary Geology* 298, 28–52.
- Mencos, J., Muñoz, J.A., Hardy, S., 2010. 3D kinematics of the Sant Corneli anticline: insights from structural reconstruction and forward modeling. *Trabalos de Geología, Universidad de Oviedo* 30, 75–80.
- Menegatti, A. P., Weissert, H., Brown, R. S., Tyson, R. V., Farrimond, P., Strasser, A. & Caron, M., 1998. High resolution $\delta^{13}\text{C}$ stratigraphy through the Early Aptian “Livello Selli” of the Alpine Tethys. *Paleoceanography* 13 (5), 530–545.
- Meyers, P.A., 1997. Organic geochemical proxies of paleoceanographic, paleolimnologic, and paleoclimatic processes. *Organic Geochemistry* 27 (5–6), 213–250.
- Millán, M.I., Weissert, H.J., Fernandez-Mendiola, P.A., Garcia-Mondejar, J., 2009. Impact of Early Aptian carbon cycle perturbations on evolution of a marine shelf system in the Basque-Cantabrian Basin (Aralar, N Spain). *Earth and Planetary Science Letters* 287, 392–401.

- Moore, D.M., Reynolds, R. C. Jr., 1997. X-Ray diffraction and the Identification and Analysis of Clay Minerals. Oxford University Press, New York, second ed. pp. 378.
- Moreno-Bedmar, J. A. Company M, Bover-Arnal T, Salas R, Delanoy G, Martínez R, Grauges A., 2009. Biostratigraphic characterization by means of ammonoids of the lower Aptian Oceanic Anoxic Event (OAE1a) in the eastern Iberian Chain (Maestrat Basin, eastern Spain). *Cretaceous Research*, 30, 864-872.
- Morford, J.L., Russell, A.D., Emerson, S., 2001. Trace metal evidence for changes in the redox environment associated with the transition from terrigenous clay to diatomaceous sediments, Saanich Inlet, BC. *Marine Geology* 174, 355–369.
- Najarro, M., Rosales, I., Moreno-Bedmar, J.A., de Gea, G.A., Barrón, E., Company, M., Delanoy, G., 2010. High-resolution chemo- and biostratigraphic records of the Early Aptian oceanic anoxic event in Cantabria (N Spain): Palaeoceanographic and palaeoclimatic implications. *Palaeogeography Palaeoclimatology Palaeoecology* 299, (1–2), 137-158.
- Papp, D.C., Cociuba, I., Lazăr, D.F., 2013. Carbon and oxygen-isotope stratigraphy of the Early Cretaceous carbonate platform of Pădurea Craiului (Apuseni Mountains, Romania): A chemostratigraphic correlation and paleoenvironmental tool. *Applied Geochemistry* 32, 3-16.
- Pauly, S., Mutterlose, J., Wray, D.S., 2013. Palaeoceanography of Lower Cretaceous (Barremian-Lower Aptian) black shales from northwest Germany evidenced by calcareous nannofossils and geochemistry. *Cretaceous Research* 42, 28–43.
- Perkins, R.B., Piper, D.Z., Mason, C.E., 2008. Trace-element budgets in the Ohio/Sunbury shales of Kentucky: Constraints on ocean circulation and primary productivity in the Devonian-Mississippian Appalachian Basin. *Palaeogeography Palaeoclimatology Palaeoecology* 265, 14–29.
- Peters, K.E., Walters, C.C., Moldowan, J.M., 2005. *The biomarker guide: II, Biomarkers and isotopes in petroleum systems and Earth history*, Cambridge, UK, Cambridge University Press, pp. 475–1155.
- Peybernès, B. and Souquet, P., 1973. Biostratigraphie des marnes noires de l' Aptien-Albien de la zone sud-pyrénéenne . *Comptes Rendus Acad. Sciences Paris*, T. 276 (2 Mai 1976), Séries D, 2501-2504.
- Peybernès, B., 1976. *Le Jurassique et le Crétacé inférieur des Pyrénées franco-espagnoles*. Thèse de doctorat, Laboratoire de Géologie, Université Paul Sabatier, Toulouse, 459 pp.
- Powell, T.G., 1988. Pristane/phytane ratio as environmental indicator. *Nature* 333, 604.

- Pratt, B.R., Smewing, J.D., 1993. Early Cretaceous platform-margin configurations and evolution in the Central Oman Mountains, Arabian Peninsula. *American Association Petroleum Geologists* 77, 225–244.
- Price, G.D., 2003. New constraints upon isotope variation during the early Cretaceous (Barremian–Cenomanian) from the Pacific Ocean. *Geological Magazine* 140 (5), 513–522.
- Pucéat, E., Lecuyer, C., Sheppard, S.M.F., Dromart, G., Reboulet, S., Grandjean, P., 2003. Thermal evolution of Cretaceous Tethyan marine waters inferred from oxygen isotope composition of fish tooth enamels. *Paleoceanography* 18, 1–12.
- Puigdefàbregas, C., Souquet, P., 1986. Tecto-sedimentary cycles and depositional sequences of the Mesozoic and Tertiary from the Pyrenees. *Tectonophysics* 129, 173–203.
- Quijano, M. L., Castro, J. M., Pancost, R. D., de Gea, G. A., Najarro, M., Aguado, Rosales, I., Martín-Chivelet, J., 2012. Organic geochemistry, stable isotopes, and facies analysis of the Early Aptian OAE– New records from Spain (Western Tethys). *Palaeogeography, Palaeoclimatology, Palaeoecology* 365–366, 276–293.
- Rimmer, S.M., 2004. Geochemical paleoredox indicators in Devonian-Mississippian black shales, central Appalachian Basin (U.S.A.). *Chemical Geology* 206, 373–391.
- Ruffell, A., McKinley, J. M., Worden, R. H., 2002. Comparison of clay mineral stratigraphy to other proxy palaeoclimate indicators in the Mesozoic of NW Europe. *Philosophical Transactions of the Royal Society of London. Series A: Mathematical, Physical and Engineering Sciences* 360(1793), 675–693.
- Sanchez-Hernandez, Y., Maurrasse, F.J-M.R., 2014. Geochemical characterization and redox signals from the latest Barremian to the earliest Aptian in a restricted marine basin: El Pui section, Organyà Basin, south-central Pyrenees. *Chemical Geology* 372, 12–31.
- Schlanger, S.O., Jenkyns, H.C., 1976. Cretaceous oceanic anoxic events: causes and consequences. *Geologie en Mijnbouw* 55, 179–184.
- Scholle, P.A., Arthur, M.A., 1980. Carbon isotope fluctuations in Cretaceous pelagic limestones- potential stratigraphic and petroleum-exploration tool. *AAPG Bulletin- American Association of Petroleum Geologists* 64 (1), 67–87.
- Schröder, S., Grotzinger, J.P., 2007. Evidence for anoxia at the Ediacaran-Cambrian boundary: the record of redox-sensitive trace elements and rare earth elements in Oman. *Geological Society of London* 164, 175–187.

- Skelton, P., 2003. Fluctuating sea-level. In: Skelton, P. (Ed.), *The Cretaceous World*. The Open University and Cambridge University Press, Milton Keynes and Cambridge, pp. 67–83.
- Sliwinski, M.G., Whalen, M.T., Newberry, R.J., Payne, J., Day, J., 2011. Stable isotope ($\delta^{13}\text{C}_{\text{carb}}$ & $\delta^{15}\text{N}_{\text{org}}$) and trace element anomalies during the Late Devonian Punctata Event in the Western Canada sedimentary basin. *Palaeogeography, Palaeoclimatology, Palaeoecology* 307, 245-271.
- Stein, M., Föllmi, K.B., Westermann, S., Godet, A., Adatte, T., Matera, V., Fleitmann, D., Berner, Z., 2011. Progressive palaeoenvironmental change during the Late Barremian–Early Aptian as prelude to Oceanic Anoxic Event 1a: evidence from the Gorgo a Cerbara section (Umbria-Marche Basin, central Italy). *Palaeogeography, Palaeoclimatology, Palaeoecology* 302, 396–406.
- Stein, M., Westermann, S., Adatte, T., Matera, V., Fleitmann, D., Spangenberg, J.E. and Föllmi, K.B., 2012. Late Barremian –Early Aptian palaeoenvironmental change: the Cassis-La Bédoule section, southeast France. *Cretaceous Research* 37, 209–222.
- Taylor, A. M., Goldring, R. 1993. Description and analysis of bioturbation and ichnofabric. *Journal of the Geological Society of London* 150, 141-148.
- ten Haven, H.L., de Leeuw, J.W., Rullkotter, J., Sinnighe-Damsté, J., 1987. Restricted utility of the pristane/phytane ratio as a palaeoenvironmental indicator. *Nature* 330, 641–643.
- Tribovillard, N., Riboulleau, A., Lyons, T., Baudin, F., 2004. Enhanced trapping of molybdenum by sulfurized marine organic matter of marine origin in Mesozoic limestones and shales. *Chemical Geology* 213, 385–401.
- Tribovillard, N., Ramdani, A., Trentesaux, A., 2005. Controls in organic accumulation in upper Jurassic shales of northwestern Europe as inferred from trace-metals geochemistry. *SEPM Special Publication* 82, 145-164.
- Tribovillard, N., Algeo, T.J., Lyons, T., Riboulleau, A., 2006. Trace metals as paleoredox and paleoproductivity proxies: An update. *Chemical Geology* 232(1-2), 12-32.
- Trindade, M.J., Rocha, F., Dias, M.I., 2006. Geochemical and mineralogical characterization of a Lower Cretaceous sedimentary profile from central Algarve (Portugal). *Journal of geochemical exploration* 88, 450-453.
- Weaver, C.E., 1989. Clays, muds, and shales, *Developments in Sedimentology* 44. Elsevier, Amsterdam, pp. 819.
- Wedepohl, K.H., 1971. Environmental influences on the chemical composition of shales and clays. In: Ahrens, L.H., Press, F.,

Runcorn, S.K., Urey, H.C. (Eds.), *Physics and Chemistry of the Earth* 8. Pergamon, Oxford, pp. 305–333.

Weissert, H., Lini, A., Föllmi, K.B., Kuhn, O., 1998. Correlation of Early Cretaceous carbon isotope stratigraphy and platform drowning events: a possible link? *Palaeogeography, Palaeoclimatology, Palaeoecology* 137, 189–203.

Wignall, P.B., Myers, K.J., 1988. Interpreting benthic oxygen levels in mudrocks: a new approach. *Geology* 16, 452–455.

Wissler, L., Funk, H. and Weissert, H., 2003. Response of Early Cretaceous carbonate platforms to changes in atmospheric carbon dioxide levels. *Palaeogeography Palaeoclimatology Palaeoecology* 200, 187-205.

8 GENERAL CONCLUSIONS

The major objective of my research was to identify and further our understanding of the factors involved in the sedimentary response, and particularly in enhanced organic carbon sequestration, of the semi-restricted Organyà Basin to changing paleoenvironmental conditions prior to and during oceanic anoxic event 1a (OAE1a) from the Late Barremian to the Middle Aptian.

To achieve the objectives an integrated methodology that include: organic and inorganic geochemistry, petrographic analyses, and sedimentology was developed. The results tested the proposed hypotheses and support the following conclusions:

- 1) From the latest Barremian to the lowest Aptian paleoenvironmental conditions in the deeper hemipelagic domain of the Organyà Basin were mainly controlled by local factors related to increased subsidence rate, intensified primary productivity fueled by sustained terrestrial fluxes that supplied biolimiting elements (P, Fe), and by the development of episodic oxygen depleted conditions. These combined factors led to increased organic carbon sequestration in the basin that resulted in a TOC content of up to 1.7%. The results also reveal that restricted marine basins can also produce environments that independently at the local scale replicate the effects of global forcing mechanisms.
- 2) The supply of critical nutrients to the basin from adjacent terranes stimulated sustained *in situ* primary productivity that greatly influenced the overall sedimentation rate. Extremely high productivity of calcareous nannoplankton generated a mass accumulation rate of at least ~5.0 cm/kyr from the latest Barremian to the lowest Aptian highlighting the role of phytoplankton in the

sequestration of not only organic but also inorganic carbon. Comparative studies with modern restricted basins revealed the unique character of the Organyà Basin in which the biogenically produced CaCO₃ dominated the sediment content instead of siliciclastic material.

- 3) Here I report the first recorded occurrence of roveacrinids in Barremian–Aptian sediments along the northern margin of Iberia. Their presence in the periodically eutrophic and oxygen-restricted environment of the El Pui sediments concurs with previous indications that these taxa are associated with extreme environments not suitable for high diversity planktonic communities. Low diversity of all forms of organisms in the El Pui sediments concur with such interpretation because phototrophs represented by calcareous nannoplankton together with heterotrophic microscopic planktonic roveacrinids and minuscule ammonoids dominated the ecosystem of the Organyà Basin at that time.
- 4) In the upper 155 m of the El Pui sequence, physiographic factors coupled with high sediment accumulation rates and sea level fluctuations induced a particular sedimentary response of the semi-restricted Organyà Basin that contrasts with the general view of enhanced OM preservation confined to anoxic conditions. Regional factors caused favorable depositional conditions for the export and preservation of OC in the sediment in the absence of an anoxic water column.

In addition to the major conclusions my dissertation research has contributed to the investigation of restricted basins of the Lower Cretaceous as follows:

- a) My study is the first to examine the geochemistry of the El Pui section, and it provides significant new data (geochemical, petrographic, stratigraphic,

mineralogical, and paleontological) concerning oceanographic conditions around the Barremian-Aptian boundary that may have an extended applicability for global interpretation.

- b) I have generated a high-resolution $\delta^{13}\text{C}_{\text{org}}$ profile for the extended El Pui section that improves the present knowledge of the isotopic variability of the global carbon reservoir from the late Barremian to the middle Aptian, and better defined carbon isotopic C-segments serve as an additional means for chemostratigraphic correlation and relative chronology. Using the $\delta^{13}\text{C}_{\text{org}}$ curve produced in this dissertation a more precise Barremian/Aptian boundary has been proposed for the El Pui section. The $\delta^{13}\text{C}_{\text{org}}$ has also been used to identify the interval corresponding to OAE1a and provide new details on the isotopic characteristics of each C segment.

In summary, the results of my dissertation provide valuable new data to further our understanding of the modern Earth system response to global environmental changes and the role of semi-enclosed basin in carbon sequestration. Such results have also economical implications as they expand the present knowledge of depositional conditions in marginal basins and their relationship with the development of hydrocarbon source rocks.

APPENDICES

APPENDIX 1

Appendix 1 Sample code, stratigraphic height and Total Carbon (TC), Total Inorganic Carbon (TIC), Total Organic Carbon and $\delta^{13}\text{C}_{\text{org}}$ of all the samples analyzed for the dissertation research. The precision of the laboratory analyses are also included.

Sample ID	Height (m)	TC(wt%)	TIC(wt%)	TOC (wt%)	$\delta^{13}\text{C}_{\text{org}}$ (‰)
C-10-01	0.0	63.6	60.1	0.4	-25.51
C-10-02	0.3	67.7	63.1	0.6	-25.28
C-10-03	0.6	71.8	71.3	0.1	-25.54
C-10-04	0.7	79.1	70.5	1.0	-25.54
C-10-05	1.2	75.3	68.9	0.8	-25.38
C-10-06	1.7	76.3	71.3	0.6	-25.18
C-10-07	1.8	60.0	54.6	0.7	-25.01
C-10-08	1.9	65.4	60.8	0.6	-25.33
C-10-09	2.3	66.4	63.5	0.3	-25.32
C-10-10	2.6	67.8	63.4	0.5	-25.32
C-10-11	2.8	71.9	63.9	1.0	-25.11
C-10-12	2.9	70.4	64.5	0.7	-25.12
C-10-13	3.8	67.2	65.4	0.2	-25.22
C-10-14	4.3	74.4	67.8	0.8	-25.18
C-10-15	4.7	49.2	45.5	0.4	-23.87
C-10-16	4.9	67.0	57.9	1.1	-24.26
C-10-17	5.4	54.7	43.8	1.3	-24.33
C-10-18	5.8	57.8	50.1	0.9	-24.36
C-10-19	6.1	61.7	47.2	1.7	-25.20
C-10-20	7.2	77.9	66.7	1.3	-24.91
C-10-21	8.0	75.5	73.7	0.2	-24.20
C-10-22	8.5	84.0	78.3	0.7	-24.46
C-10-23	9.0	72.3	65.3	0.8	-24.66
C-10-24	9.6	83.1	79.6	0.4	-24.73
C-10-25	10.3	84.9	74.5	1.2	-24.93
C-10-26	10.8	81.8	75.3	0.8	-24.92
C-10-27	10.8	80.4	75.7	0.6	-24.67
C-10-28	11.5	75.6	68.6	0.8	-24.27
C-10-29	12.2	57.9	51.6	0.8	-23.83
C-10-30	13.0	48.9	43.5	0.6	-22.79
C-10-31	13.7	79.7	66.7	1.6	-23.99
C-10-32	14.3	79.4	74.2	0.6	-22.57
C-10-33	14.7	83.3	77.6	0.7	-24.05
C-10-34	14.8	71.6	61.5	1.2	-24.17

APPENDIX 1 continued...

Sample ID	Height (m)	TC(wt%)	TIC(wt%)	TOC (wt%)	$\delta^{13}\text{C}_{\text{Org}}$ (‰)
C-10-35	15.1	71.3	63.4	1.0	-24.18
C-10-36	15.2	66.6	61.9	0.6	-24.11
C-10-37	15.5	82.7	74.0	1.0	-24.46
C-10-38	15.9	87.1	84.0	0.4	-24.10
C-10-39	16.1	92.5	86.1	0.8	-24.10
C-10-40	16.4	89.6	85.1	0.5	-23.19
C-10-41	16.6	84.2	66.1	1.0	-23.31
C-10-42	16.8	85.8	81.3	0.5	-24.09
C-10-43	17.0	86.4	83.4	0.4	-23.68
C-10-44	17.2	85.7	81.5	0.5	-23.79
C-10-45	17.4	74.1	67.1	0.8	-23.21
C-10-46	17.6	75.2	70.5	0.6	-23.97
C-10-47	18.0	91.3	82.4	1.1	-23.90
C-10-48	18.2	82.6	70.1	1.5	-23.15
C-10-49	18.3	82.6	71.0	1.4	-23.59
C-10-50	18.6	82.5	72.5	1.2	-24.00
C-10-51	18.8	76.6	71.3	0.6	-23.78
C-10-52	19.1	76.4	72.5	0.5	-23.97
C-10-53	19.7	73.8	66.9	0.8	-23.85
C-10-54	19.7	72.7	69.5	0.4	-23.40
C-10-55	19.9	87.0	83.6	0.4	-23.61
C-10-56	20.2	82.1	78.8	0.4	-24.01
C-10-57	20.5	85.3	78.8	0.8	-23.95
C-10-58	20.8	84.6	82.9	0.2	-24.15
C-10-59	21.1	85.5	84.3	0.1	-23.96
C-10-60	21.4	80.1	77.6	0.3	-24.16
C-10-61	21.8	74.2	71.4	0.3	-24.15
C-10-62	22.0	78.8	74.7	0.5	-24.15
C-10-63	22.3	73.7	71.1	0.3	-24.06
C-10-64	22.8	77.3	74.4	0.3	-24.20
C-10-65	23.3	74.2	69.8	0.5	-23.95
C-10-66	24.0	79.8	77.4	0.3	-24.26
C-10-67	24.2	80.7	77.5	0.4	-24.18
C-10-68	24.5	85.0	78.3	0.8	-23.89
C-10-69	24.9	85.8	82.1	0.5	-24.23
C-10-70	25.5	89.7	81.0	1.0	-24.19
C-10-71	26.1	89.8	87.6	0.3	-24.24
C-10-72	26.3	86.0	83.5	0.3	-24.42

APPENDIX 1 continued...

Sample ID	Height (m)	TC(wt%)	TIC(wt%)	TOC (wt%)	$\delta^{13}\text{C}_{\text{Org}}$ (‰)
C-10-73	26.6	84.7	83.5	0.1	-24.31
C-10-74	26.9	86.8	80.2	0.8	-24.07
C-10-75	27.0	81.8	81.1	0.1	-24.24
C-10-76	27.5	84.0	82.2	0.2	-23.45
C-10-77	27.7	83.8	70.8	1.6	-23.37
C-10-78	28.0	77.4	77.4	0.1	-24.04
C-10-79	28.4	86.0	75.0	1.3	-24.09
C-10-80	28.7	84.2	75.2	1.1	-24.15
C-10-81	29.5	87.1	80.4	0.8	-24.19
C-10-82	29.9	82.7	81.4	0.2	-24.28
C-10-83	30.5	85.0	70.6	1.7	-24.37
C-10-84	31.1	84.8	74.0	1.3	-24.19
C-10-85	31.3	79.4	74.1	0.6	-24.14
C-10-86	31.9	82.2	75.9	0.8	-24.12
C-11-87	32.3	79.2	73.1	0.7	-24.35
C-11-89	32.9	78.9	73.0	0.7	-24.47
C-11-91	33.5	76.8	70.3	0.8	-24.50
C-11-93	35.6	73.2	67.5	0.7	-24.29
C-11-95	36.2	77.5	71.5	0.7	-24.15
C-11-97	37.1	80.2	76.2	0.5	-24.35
C-11-99	37.5	84.5	80.7	0.5	-24.35
C-11-101	38.3	83.3	79.2	0.5	-24.35
C-11-103	39.4	82.3	78.1	0.5	-24.27
C-11-105	40.5	80.3	74.1	0.7	-24.20
C-11-107	41.5	88.3	85.3	0.4	-24.08
C-11-109	41.8	89.6	80.9	1.0	-24.25
C-11-111	42.3	84.8	80.8	0.5	-24.27
C-11-113	42.7	85.0	81.7	0.4	-24.33
C-11-115	43.1	85.2	81.3	0.5	-24.32
C-11-117	43.6	84.9	80.7	0.5	-24.42
C-11-119	43.9	82.0	77.3	0.6	-24.50
C-11-121	44.4	80.4	75.7	0.6	-24.50
C-11-123	45.0	80.7	75.9	0.6	-24.39
C-11-125	45.5	78.3	74.0	0.5	-24.05
C-11-127	45.8	76.6	72.1	0.5	-23.98
C-11-129	46.3	74.9	70.0	0.6	-24.13
C-11-131	46.9	78.9	75.3	0.4	-24.17
C-11-133	47.3	77.8	73.7	0.5	-24.12

APPENDIX 1 continued...

Sample ID	Height (m)	TC(wt%)	TIC(wt%)	TOC (wt%)	$\delta^{13}\text{C}_{\text{Org}}$ (‰)
C-11-135	48.0	79.6	75.0	0.6	-24.03
C-11-137	48.7	67.4	61.5	0.7	-23.90
C-11-139	49.5	72.1	67.6	0.5	-24.18
C-11-141	50.3	74.4	71.0	0.4	-24.19
C-11-143	50.8	72.6	68.5	0.5	-24.20
C-11-145	51.3	70.8	67.9	0.4	-24.10
C-11-147	51.6	81.5	77.7	0.5	-23.79
C-11-149	52.6	70.8	65.0	0.7	-23.44
C-11-151	54.3	59.4	52.9	0.8	-23.98
C-11-153	55.1	70.2	63.5	0.8	-23.53
C-11-155	55.6	72.4	66.4	0.7	-23.82
C-11-157	56.3	58.4	52.6	0.7	-24.27
C-11-159	57.0	63.6	57.9	0.7	-24.55
C-11-161	57.9	72.1	65.5	0.8	-24.15
C-11-163	58.3	74.9	68.4	0.8	-24.10
C-11-165	59.1	76.1	71.6	0.5	-24.20
C-11-167	60.3	81.2	76.5	0.6	-24.43
C-11-169	62.0	66.6	59.6	0.8	-24.62
C-11-171	63.1	83.7	79.4	0.5	-24.50
C-11-173	63.6	78.1	72.5	0.7	-24.20
C-11-175	64.0	75.5	69.2	0.8	-24.03
C-11-177	64.7	75.1	69.6	0.7	-24.58
C-11-179	65.4	73.1	68.5	0.6	-24.32
C-11-181	66.3	87.7	84.4	0.4	-25.25
C-11-183	67.0	86.8	81.5	0.6	-24.55
C-11-185	67.6	75.6	70.4	0.6	-24.60
C-11-187	68.3	85.5	82.5	0.4	-24.81
C-11-189	68.8	83.0	79.4	0.4	-25.47
C-11-191	69.3	83.1	79.8	0.4	-25.42
C-11-193	69.7	87.2	84.3	0.3	-24.90
C-11-195	70.2	83.9	80.3	0.4	-25.52
C-11-197	70.7	73.8	66.9	0.8	-24.45
C-11-199	73.0	82.4	77.6	0.6	-25.93
C-11-201	75.7	65.2	59.6	0.7	-25.95
C-11-203	78.3	64.9	59.1	0.7	-25.89
C-11-205	81.1	63.7	58.1	0.7	-25.36
C-11-207	84.5	70.0	64.9	0.6	-25.33
C-12-208	86.0	74.2	61.9	1.5	-24.84

APPENDIX 1 continued...

Sample ID	Height (m)	TC(wt%)	TIC(wt%)	TOC (wt%)	$\delta^{13}\text{C}_{\text{Org}}$ (‰)
C-12-209	86.6	80.5	64.3	2.0	-24.73
C-12-210	87.3	58.8	44.7	1.7	-24.08
C-12-211	88.0	75.7	69.0	0.8	-24.48
C-12-212	88.9	58.7	55.6	0.4	-23.95
C-12-213	89.5	61.2	44.5	2.0	-24.22
C-12-214	90.2	57.9	42.8	1.8	-24.32
C-12-215	90.9	57.3	43.2	1.7	-24.44
C-12-216	92.5	71.1	59.8	1.4	-24.13
C-12-217	93.6	64.4	52.9	1.4	-24.18
C-12-218	94.2	63.6	46.2	2.1	-24.78
C-12-219	95.4	65.0	47.8	2.1	-24.33
C-12-220	96.1	77.0	57.1	2.4	-24.03
C-12-221	97.4	93.1	78.9	1.7	-24.70
C-12-222	99.2	68.4	50.8	2.1	-24.04
C-12-223	100.2	65.0	50.3	1.8	-24.24
C-12-224	101.0	65.8	50.6	1.8	-23.98
C-12-225	102.1	68.0	49.6	2.2	-24.16
C-12-226	103.0	61.2	43.4	2.1	-23.76
C-12-227	104.1	62.3	40.9	2.6	-24.13
C-12-228	104.9	58.4	44.1	1.7	-23.78
C-12-229	105.7	65.7	53.5	1.5	-24.22
C-12-230	106.5	60.3	51.7	1.0	-24.17
C-12-231	107.2	64.4	56.2	1.0	-24.02
C-12-232	108.6	90.9	80.0	1.3	-23.78
C-12-233	109.8	86.7	77.5	1.1	-23.67
C-12-234	110.9	83.8	70.4	1.6	-23.78
C-12-235	111.4	77.2	57.4	2.4	-24.26
C-12-236	112.4	74.8	62.5	1.5	-23.96
C-12-237	113.2	77.8	64.7	1.6	-24.10
C-12-238	113.5	73.2	61.3	1.4	-23.99
C-12-239	114.0	87.9	77.6	1.2	-24.04
C-12-240	114.6	80.4	68.5	1.4	-24.11
C-12-241	115.2	79.6	66.6	1.6	-24.05
C-12-242	115.8	77.1	72.0	0.6	-24.00
C-12-243	116.2	72.9	59.7	1.6	-23.89
C-12-244	116.3	78.7	65.0	1.6	-23.75
C-12-245	116.8	65.7	53.5	1.5	-23.93
C-12-246	117.3	82.4	70.3	1.4	-23.80

APPENDIX 1 continued...

Sample ID	Height (m)	TC(wt%)	TIC(wt%)	TOC (wt%)	$\delta^{13}\text{C}_{\text{Org}}$ (‰)
C-12-247	118.1	85.0	76.4	1.0	-24.06
C-12-248	119.6	75.5	62.8	1.5	-23.87
C-12-249	120.0	89.1	63.9	3.0	-23.91
C-12-250	121.9	77.3	63.0	1.7	-24.41
C-12-251	123.0	70.7	59.1	1.4	-24.27
C-12-252	124.2	82.1	58.3	2.9	-24.48
C-12-253	125.1	70.9	56.9	1.7	-24.57
C-12-254	126.4	66.1	63.7	0.3	-24.42
C-12-255	127.7	78.5	73.9	0.6	-24.25
C-12-256	129.2	70.2	58.7	1.4	-24.66
C-12-257	130.0	72.0	57.0	1.8	-24.53
C-12-258	130.4	77.4	59.9	2.1	-24.71
C-12-259	131.6	71.7	57.2	1.7	-24.57
C-12-260	132.0	76.0	55.5	2.5	-24.32
C-12-261	132.6	59.0	49.9	1.1	-24.72
C-12-262	134.4	70.0	57.1	1.5	-24.08
C-12-263	135.2	98.5	64.1	4.1	-24.42
C-12-264	135.9	75.5	56.8	2.2	-24.23
C-12-265	136.3	85.2	69.8	1.8	-24.22
C-12-266	137.0	75.9	64.2	1.4	-24.44
C-12-267	138.0	80.8	68.3	1.5	-24.51
C-12-268	138.7	75.4	64.9	1.3	-24.83
C-12-269	139.9	82.1	62.1	2.4	-24.47
C-12-270	140.6	77.2	62.7	1.7	-24.46
C-12-271	141.4	73.7	62.5	1.3	-24.60
C-12-272	142.0	77.6	67.7	1.2	-24.66
C-12-273	143.5	85.3	71.6	1.6	-24.67
C-12-274	144.1	85.0	71.4	1.6	-24.58
C-12-275	144.7	89.9	77.6	1.5	-24.58
C-12-276	145.2	93.8	75.8	2.2	-24.49
C-12-277	146.0	87.7	71.9	1.9	-24.52
C-12-278	147.7	76.0	64.7	1.4	-25.03
C-12-279	148.4	69.7	52.4	2.1	-25.40
C-12-280	149.4	95.9	71.5	2.9	-25.58
C-12-281	150.1	81.9	67.9	1.7	-25.14
C-12-282	150.9	93.6	80.2	1.6	-25.53
C-12-283	151.4	76.1	61.7	1.7	-25.55
C-12-284	151.7	80.2	64.0	1.9	-25.22

APPENDIX 1 continued...

Sample ID	Height (m)	TC(wt%)	TIC(wt%)	TOC (wt%)	$\delta^{13}\text{C}_{\text{Org}}$ (‰)
C-12-285	152.1	72.8	63.5	1.1	-25.18
C-12-286	152.7	92.2	78.9	1.6	-26.00
C-12-287	153.0	94.1	80.8	1.6	-25.99
C-12-288	153.6	90.1	78.6	1.4	-26.05
C-12-289	154.1	99.1	83.3	1.9	-25.76
C-12-290	154.4	82.9	70.8	1.5	-25.86
C-12-291	155.1	82.9	76.6	0.8	-25.70
C-12-292	155.4	84.9	71.9	1.6	-25.38
C-12-293	155.8	90.0	75.8	1.7	-25.63
C-12-294	156.4	87.7	70.8	2.0	-25.55
C-12-295	156.6	91.8	78.0	1.7	-25.59
C-12-296	156.9	90.1	90.0	0.0	-25.58
C-12-297	157.3	92.8	77.7	1.8	-25.56
C-12-298	158.1	92.7	76.9	1.9	-25.35
C-12-299	158.7	93.4	76.8	2.0	-25.23
C-12-300	158.9	84.5	69.1	1.9	-25.40
C-12-301	159.4	88.9	76.3	1.5	-25.78
C-12-302	159.8	91.3	80.6	1.3	-25.66
C-12-303	160.2	92.7	76.1	2.0	-25.58
C-12-304	160.8	97.6	80.7	2.0	-25.68
C-12-305	161.3	96.4	81.1	1.8	-25.22
C-12-306	161.6	98.2	87.1	1.3	-25.46
C-12-307	162.0	93.9	80.6	1.6	-25.31
C-12-308	162.4	85.1	71.5	1.6	-25.36
C-12-309	163.1	82.2	68.5	1.6	-25.16
C-12-310	163.5	95.1	78.2	2.0	-25.59
C-12-311	163.9	87.5	74.9	1.5	-25.84
C-12-312	165.3	93.4	85.8	0.9	-26.57
C-12-313	165.9	91.8	85.6	0.7	-26.93
C-12-314	166.4	94.2	87.3	0.8	-26.97
C-12-315	166.9	96.4	86.1	1.2	-26.87
C-12-316	167.2	96.5	83.3	1.6	-27.13
C-12-317	167.5	97.5	82.9	1.8	-27.20
C-12-318	168.1	99.6	84.2	1.8	-27.23
C-12-319	168.5	99.3	84.9	1.7	-27.22
C-12-320	169.0	97.7	86.0	1.4	-26.97
C-12-321	169.4	98.3	86.6	1.4	-27.06
C-12-322	169.9	97.1	88.2	1.1	-26.92

APPENDIX 1 continued...

Sample ID	Height (m)	TC(wt%)	TIC(wt%)	TOC (wt%)	$\delta^{13}\text{C}_{\text{Org}}$ (‰)
C-12-323	170.3	96.4	83.4	1.6	-26.65
C-12-324	170.6	97.6	86.3	1.4	-26.85
C-12-325	171.0	97.8	84.4	1.6	-27.13
C-12-326	171.4	98.5	84.9	1.6	-27.23
C-12-327	171.7	98.2	83.6	1.8	-26.80
C-12-328	172.1	98.2	84.3	1.7	-26.85
C-12-329	172.6	98.5	85.3	1.6	-26.96
C-12-330	173.2	93.1	79.5	1.6	-26.50
C-12-331	173.8	95.1	85.3	0.2	-26.60
C-12-332	174.0	94.1	88.6	0.7	-26.73
C-12-333	174.5	99.5	93.2	0.8	-26.82
C-12-334	175.1	94.8	80.8	1.7	-26.80
C-12-335	176.0	95.5	84.0	1.4	-26.87
C-12-336	177.1	98.0	92.9	0.6	-26.54
C-12-337	178.0	92.5	88.4	0.5	-26.57
C-12-338	178.4	94.1	88.3	0.7	-26.99
C-12-339	178.6	96.8	89.6	0.9	-26.61
C-12-340	178.9	98.9	88.2	1.3	-26.74
C-12-341	179.4	96.9	83.0	1.7	-26.50
C-12-342	180.6	100.7	85.7	1.8	-27.11
C-12-343	180.8	96.6	85.7	1.3	-27.11
C-12-344	181.6	99.2	88.8	1.2	-27.14
C-12-345	181.9	100.2	98.3	0.2	-27.18
C-12-346	182.0	95.5	89.1	0.8	-27.10
C-12-347	182.4	99.2	86.8	1.5	-27.05
C-12-348	182.8	94.8	83.1	1.4	-27.19
C-12-349	183.2	98.8	85.0	1.7	-27.26
C-12-350	183.6	93.6	81.1	1.5	-26.99
C-12-351	183.8	95.4	80.6	1.8	-27.07
C-12-352	184.2	92.4	87.5	0.6	-27.31
C-12-353	184.6	91.1	79.3	1.4	-27.10
C-12-354	185.2	93.9	81.1	1.5	-27.27
C-12-355	185.7	94.6	82.4	1.5	-27.17
C-12-356	186.0	96.9	84.3	1.5	-27.34
C-12-357	186.2	96.3	83.4	1.6	-27.50
C-12-358	186.7	97.0	86.0	1.3	-27.60
C-12-359	187.3	94.5	81.8	1.5	-27.37
C-12-360	187.6	94.4	84.7	1.2	-27.64

APPENDIX 1 continued...

Sample ID	Height (m)	TC(wt%)	TIC(wt%)	TOC (wt%)	$\delta^{13}\text{C}_{\text{Org}}$ (‰)
C-12-361	187.9	94.2	82.0	1.5	-27.50
C-12-362	188.3	91.1	86.1	0.6	-27.03
C-12-363	188.7	92.6	80.3	1.5	-26.13
C-12-364	189.1	95.1	81.5	1.6	-27.28
C-12-365	189.2	89.8	76.8	1.6	-27.30
C-12-366	189.4	98.8	81.8	2.0	-26.42
C-12-367	189.6	89.8	71.4	2.2	-27.29
C-12-368	190.0	90.1	77.3	1.5	-27.40
C-12-369	190.3	94.9	81.7	1.6	-27.38
C-12-370	190.8	93.9	80.6	1.6	-27.62
C-12-371	191.0	92.1	79.0	1.6	-27.75
C-12-372	191.4	91.7	77.8	1.7	-27.59
C-12-373	191.6	93.7	79.6	1.7	-27.46
C-12-374	192.0	96.5	82.7	1.6	-27.37
C-12-375	192.4	82.9	69.7	1.6	-27.35
C-12-376	192.8	79.9	73.9	0.7	-27.33
C-12-377	193.1	98.6	86.2	1.5	-27.69
C-12-378	193.4	88.9	75.7	1.6	-27.16
C-12-379	193.6	85.8	74.0	1.4	-26.29
C-12-380	193.8	93.6	79.5	1.7	-27.29
C-12-381	194.0	92.5	82.3	1.2	-27.32
C-12-382	194.1	97.9	88.7	1.1	-27.37
C-12-383	194.4	96.0	84.7	1.4	-26.96
C-12-384	194.5	93.3	83.9	1.1	-27.45
C-12-385	194.8	98.1	85.7	1.5	-27.46
C-12-386	195.2	93.3	83.6	1.2	-27.44
C-12-387	195.5	95.8	83.8	1.4	-27.28
C-12-388	195.8	94.1	82.1	1.4	-27.25
C-12-389	196.2	98.8	83.3	1.9	-27.47
C-12-390	196.3	93.9	84.4	1.1	-27.09
C-12-391	196.5	95.2	82.0	1.6	-27.25
C-12-392	196.7	95.9	93.2	0.3	-27.28
C-12-393	196.9	93.5	81.6	1.4	-27.30
C-12-394	197.1	95.5	82.3	1.6	-27.41
C-12-395	197.4	98.9	86.5	1.5	-27.71
C-12-396	197.8	93.9	81.8	1.4	-27.11
C-12-397	198.0	95.3	82.5	1.5	-27.59
C-12-398	198.2	95.4	84.4	1.3	-27.17

APPENDIX 1 continued...

Sample ID	Height (m)	TC(wt%)	TIC(wt%)	TOC (wt%)	$\delta^{13}\text{C}_{\text{Org}}$ (‰)
C-12-399	198.4	95.9	82.8	1.6	-27.43
C-12-400	198.6	99.9	86.7	1.6	-27.78
C-12-401	198.8	98.7	88.3	1.2	-27.95
C-12-402	198.9	87.7	74.7	1.6	-27.76
C-12-403	199.0	98.2	86.1	1.4	-27.85
C-12-404	199.4	95.9	82.0	1.7	-27.80
C-12-405	199.5	95.4	81.8	1.6	-27.40
C-12-406	199.8	94.2	82.9	1.3	-27.43
C-12-407	199.9	93.3	80.6	1.5	-27.78
C-12-408	200.2	96.6	83.4	1.6	-27.73
C-12-409	200.6	94.4	82.6	1.4	-27.71
C-12-410	200.7	91.7	83.7	1.0	-27.54
C-12-411	200.8	96.7	86.4	1.2	-27.69
C-12-412	201.0	97.0	85.2	1.4	-27.73
C-12-413	201.1	89.4	78.0	1.4	-27.45
C-12-414	201.3	86.0	74.1	1.4	-27.24
C-12-415	201.5	97.8	88.3	1.1	-27.54
C-12-416	201.6	94.7	87.1	0.9	-27.50
C-12-417	201.7	93.9	82.0	1.4	-27.41
C-12-418	201.8	87.7	72.3	1.8	-27.17
C-12-419	202.0	96.8	84.7	1.5	-26.92
C-12-420	202.1	84.7	75.2	1.1	-27.38
C-12-421	202.2	96.5	83.7	1.5	-27.46
C-12-422	203.1	96.4	81.9	1.7	-27.30
C-12-423	203.3	95.7	86.0	1.2	-27.25
C-12-424	203.4	98.7	85.4	1.6	-27.42
C-12-425	203.7	97.9	80.6	2.1	-27.56
C-12-426	203.8	93.9	81.3	1.5	-27.42
C-12-427	204.0	94.4	81.3	1.6	-27.20
C-12-428	204.5	90.6	76.4	1.7	-26.72
C-12-429	205.1	88.9	76.5	1.5	-26.41
C-12-430	205.3	94.7	81.3	1.6	-26.39
C-12-431	205.6	92.0	79.7	1.5	-26.75
C-12-432	205.8	99.1	87.1	1.8	-26.64
C-12-433	206.4	90.5	77.4	1.6	-26.67
C-12-434	206.7	96.1	82.9	1.6	-26.82
C-12-435	207.9	88.8	75.8	1.6	-25.99
C-12-436	208.2	92.4	76.9	1.9	-26.22

APPENDIX 1 continued...

Sample ID	Height (m)	TC(wt%)	TIC(wt%)	TOC (wt%)	$\delta^{13}\text{C}_{\text{Org}}$ (‰)
C-12-437	208.8	96.9	83.5	1.6	-25.31
C-12-438	209.4	78.0	66.6	1.4	-25.04
C-12-439	209.9	84.2	71.0	1.6	-24.36
C-12-440	210.2	89.6	75.2	1.7	-24.08
C-12-441	210.6	93.4	80.0	1.6	-23.82
C-12-442	211.0	96.2	89.5	0.8	-23.84
C-12-443	211.4	95.4	82.0	1.6	-23.68
C-12-444	211.6	81.7	70.9	1.3	-23.72
C-12-445	211.8	90.0	82.7	0.9	-23.92
C-12-446	212.1	93.2	83.0	1.2	-24.18
C-12-447	212.7	79.6	72.6	0.8	-24.30
C-12-448	212.9	78.9	69.8	1.1	-24.06
C-12-449	213.1	90.0	77.6	1.5	-24.32
C-12-450	213.4	83.1	74.6	1.0	-24.20
C-12-451	213.8	80.8	69.9	1.3	-24.21
C-12-452	214.1	83.4	71.4	1.5	-24.24
C-12-453	214.7	83.0	70.2	1.5	-24.10
C-12-454	215.2	81.3	74.5	0.8	-24.02
C-12-455	215.7	82.8	73.3	1.1	-24.04
C-12-456	216.2	81.0	71.8	1.1	-23.94
C-12-457	216.8	77.2	71.3	0.7	-24.29
C-12-458	217.4	86.3	83.7	0.3	-24.23
C-12-459	218.1	76.0	64.3	1.4	-24.30
C-12-460	218.9	66.3	56.3	1.2	-24.21
C-12-461	220.1	92.3	61.0	3.8	-23.94
C-12-462	220.9	67.1	54.8	1.5	-24.32
C-12-463	221.5	71.2	58.9	1.5	-24.18
C-12-464	222.2	83.7	68.5	1.8	-24.34
C-12-465	222.9	81.7	72.1	1.2	-24.29
C-12-466	224.4	76.8	66.4	1.3	-24.33
C-12-467	225.1	72.3	60.4	1.4	-24.78
C-12-468	225.6	81.2	67.8	1.6	-24.51
C-12-469	226.3	78.4	64.2	1.7	-24.34
C-12-470	227.0	75.6	63.2	1.5	-24.21
C-12-471	227.5	69.2	56.3	1.5	-24.29
C-12-472	228.3	70.2	59.1	1.3	-24.60
C-12-473	228.8	75.5	59.5	1.9	-24.62
C-12-474	229.6	67.1	57.6	1.1	-24.31

APPENDIX 1 continued...

Sample ID	Height (m)	TC(wt%)	TIC(wt%)	TOC (wt%)	$\delta^{13}\text{C}_{\text{org}}$ (‰)
C-12-475	230.5	65.0	54.0	1.3	-24.24
C-12-476	231.8	67.8	55.9	1.4	-24.01
C-12-477	233.3	77.9	57.1	2.5	-23.95
C-12-478	234.9	76.7	70.8	0.7	-22.98
C-12-479	236.9	72.8	60.7	1.5	-22.83
C-12-480	240.0	65.8	52.3	1.6	-22.76
Pressicion		±2%	±2%		±1.2

APPENDIX 2

Appendix 2 Major and trace element concentrations of all samples analyzed for the El Pui section. The average standard deviation is reported as the average for each element.

Sample Id	Height	Al	Si	P	Ti	V	Cr	Fe	Co	Ni	Cu	Th	U	Mo
Units →	(m)	(ppm)	(ppm)	(ppm)	(ppt)	(ppm)	(ppm)	(ppm)	(ppm)	(ppm)	(ppm)	(ppm)	(ppm)	(ppm)
C-10-02	0.3	34128	73233	282	1.7	39.7	34.0	13.9	1.5	15.7	7.9	4.6	1.3	N/A
C-10-08	1.9	40709	88241	413	1.7	36.7	63.9	13.5	3.4	76.6	15.4	5.2	1.7	N/A
C-10-14	4.3	27479	56871	342	1.3	35.0	68.7	11.1	3.1	99.7	9.9	4.3	2.2	N/A
C-10-18	5.8	49042	95678	424	2.1	57.9	87.2	21.7	6.3	102.3	16.3	6.1	2.4	N/A
C-10-21	8.0	21214	44051	285	1.0	27.2	39.0	8.9	1.7	43.9	5.8	2.8	0.7	N/A
C-10-25	10.3	16712	35954	253	0.9	21.7	20.3	7.5	0.6	8.2	4.3	2.6	1.2	N/A
C-10-28	11.5	24259	51435	268	1.2	29.4	51.5	10.4	4.1	60.1	7.7	3.4	0.9	N/A
C-10-31	13.7	27995	55525	384	1.2	39.3	56.4	10.5	5.4	73.8	13.1	3.7	3.5	N/A
C-10-34	14.8	32049	61787	292	1.5	37.7	37.4	11.3	1.7	35.2	7.4	4.8	1.3	N/A
C-10-37	15.5	18804	43613	189	1.2	22.6	38.4	6.7	2.6	57.9	5.1	3.0	0.8	N/A
C-10-40	16.4	10004	23431	222	0.4	15.4	26.4	5.2	1.8	40.4	4.7	1.4	0.9	N/A
C-10-43	17.0	13610	27662	200	0.6	18.8	44.7	5.7	1.2	29.4	5.8	1.9	0.7	N/A
C-10-47	18.0	14985	30373	227	0.6	18.6	26.3	5.7	1.2	33.3	5.7	2.0	1.0	N/A
C-10-50	18.6	24234	44120	294	1.1	32.0	38.9	8.8	2.3	58.0	7.1	3.2	1.4	N/A
C-10-54	19.7	31230	60739	320	1.4	38.3	55.1	12.2	2.4	77.4	9.4	3.9	1.3	N/A
C-10-57	20.5	14090	27649	138	0.7	17.9	23.8	6.0	1.0	32.2	4.7	1.8	0.5	N/A
C-10-61	21.8	26127	49551	269	1.2	33.1	31.3	9.3	1.6	22.8	11.5	3.3	0.9	N/A
C-10-65	23.3	28409	52535	326	1.2	36.0	37.5	10.2	1.6	48.2	8.7	3.7	1.0	N/A
C-10-69	24.9	16054	30797	147	0.7	20.9	23.9	6.8	1.0	23.3	5.0	1.9	1.0	N/A
C-10-71	26.1	10541	22594	194	0.4	16.0	27.6	4.5	1.5	43.4	5.8	1.4	1.2	N/A
C-10-75	27.0	16955	31833	170	0.8	21.7	28.5	6.3	1.2	22.5	5.5	1.9	1.0	N/A
C-10-83	30.5	21860	43243	250	1.0	31.3	28.6	8.1	1.1	14.7	6.7	2.7	1.5	N/A
C-11-87	32.3	15909	29714	169	0.6	19.6	22.7	5.7	5.0	15.5	4.1	1.5	0.6	0.7
C-11-93	35.6	21294	39148	176	0.8	25.7	27.0	7.5	4.9	13.5	6.2	1.8	0.7	0.6
C-11-97	37.1	14086	27633	153	0.6	17.5	18.2	5.2	2.1	11.4	3.9	1.3	0.5	0.7
C-11-105	40.5	15812	31318	159	0.5	20.1	23.7	5.2	1.0	31.2	5.4	1.5	0.8	1.9
C-11-107	41.5	7078	13801	112	0.3	10.5	14.0	3.4	1.4	17.0	3.0	0.6	0.7	1.1
C-11-109	41.8	5978	12407	107	0.2	8.4	11.4	2.9	1.1	11.7	2.1	0.5	0.3	0.7
C-11-115	43.1	26880	50055	187	0.9	30.5	32.4	9.6	9.3	32.8	6.3	2.2	0.5	1.1
C-11-123	45.0	15257	29319	213	0.6	20.1	24.1	5.5	1.6	36.5	5.3	1.2	0.5	2.1
C-11-131	46.9	16263	30532	205	0.6	19.7	28.3	5.5	3.7	17.2	5.5	1.5	0.4	0.8
C-11-137	48.7	22550	43729	172	0.9	29.4	34.5	7.8	1.6	43.8	7.3	2.2	0.8	2.8
C-11-145	51.3	18049	35716	219	0.7	26.8	29.9	6.5	1.6	38.5	7.3	1.9	1.0	2.8
C-11-153	55.1	22287	43135	199	0.9	26.3	32.2	8.0	6.9	43.4	4.4	2.1	0.4	2.1
C-11-165	59.1	17659	33279	174	0.7	21.0	19.6	6.7	2.2	13.4	5.4	1.6	0.4	0.5
C-11-175	64.0	19728	38301	187	0.7	24.1	27.5	7.0	4.2	25.8	11.3	1.9	1.0	1.3
C-11-181	66.3	10726	20635	114	0.4	14.2	18.8	3.7	4.0	13.1	4.0	0.9	0.5	0.9
C-11-185	67.6	18289	34596	173	0.7	22.0	22.2	7.9	3.0	20.2	6.3	1.5	0.5	0.8

APPENDIX 2 continued...

Sample Id	Height	Al	Si	P	Ti	V	Cr	Fe	Co	Ni	Cu	Th	U	Mo
Units →	(m)	(ppm)	(ppm)	(ppm)	(ppt)	(ppm)	(ppm)	(ppm)	(ppm)	(ppm)	(ppm)	(ppm)	(ppm)	(ppm)
C-11-197	70.7	21001	39068	193	0.8	23.2	26.6	7.2	2.1	14.9	7.4	2.2	0.6	0.6
C-11-203	78.3	8369	17797	138	0.3	12.0	11.8	3.5	2.5	9.4	4.7	0.8	0.5	0.5
C-11-207	84.5	23672	46212	229	0.8	27.1	24.1	8.1	4.8	15.8	6.4	2.0	0.5	0.3
C12-208	86.0	34572	84381	448	1.3	49.0	47.5	14.7	23.2	39.8	12.2	4.9	1.5	1.7
C12-211	88.0	30907	94243	325	1.3	41.6	46.8	16.0	14.7	48.8	9.7	5.1	1.4	2.6
C12-214	90.2	55646	124440	383	1.9	66.8	66.7	23.5	13.2	50.5	14.3	6.9	1.6	1.3
C12-217	93.6	47407	98239	281	1.7	51.0	68.6	16.7	15.1	71.4	9.0	5.5	1.1	3.8
C12-220	96.1	35720	78423	313	1.4	40.3	51.4	13.7	11.1	65.8	9.0	5.1	1.3	3.3
C12-223	100.2	45325	94834	236	1.8	48.7	54.6	15.5	13.5	42.0	9.9	6.1	1.2	2.0
C12-226	103.0	53753	113991	440	1.9	48.5	69.5	19.9	18.5	60.4	9.7	6.7	1.5	2.1
C12-229	105.8	47540	110842	273	1.7	52.5	56.0	17.8	12.6	61.0	12.1	6.3	1.2	2.0
C12-232	108.6	15776	45858	211	0.7	18.1	22.6	6.5	6.1	26.9	5.2	2.1	0.8	1.2
C12-235	111.4	41399	93357	285	1.8	45.9	78.4	14.9	29.9	65.0	9.3	5.5	1.2	2.4
C12-238	113.5	37903	87061	346	1.3	44.0	66.8	14.1	18.8	67.8	11.7	5.1	1.3	3.1
C12-241	115.2	32984	84512	294	1.1	36.7	53.6	12.4	19.9	49.7	9.1	4.0	1.2	2.0
C12-244	116.3	26267	80343	260	1.2	29.7	46.9	10.8	11.4	41.2	7.5	4.2	1.0	1.9
C12-247	118.1	24712	68018	238	0.9	31.2	43.9	11.1	7.5	57.8	8.3	3.2	1.2	3.3
C12-250	121.9	35944	86263	355	1.4	40.7	51.2	14.2	23.3	44.0	16.3	4.4	1.1	1.5
C12-253	125.1	38933	91279	293	1.3	44.2	62.5	16.3	21.2	60.9	10.2	5.3	1.2	3.6
C12-256	129.2	38765	97404	309	1.5	45.7	62.3	15.6	20.6	69.0	10.9	4.8	1.0	2.3
C12-257	130.0	11295	34052	122	0.4	14.3	17.1	3.9	2.3	13.7	2.9	1.1	0.6	1.3
C12-257A	130.0	11729	35139	130	0.5	13.6	14.5	4.1	1.8	12.5	1.9	1.2	0.7	1.1
C12-259	131.6	38507	94352	312	1.4	45.7	60.0	16.3	16.5	73.8	9.6	4.9	2.3	5.0
C12-259A	131.6	39606	91863	319	1.3	46.4	59.5	17.7	12.9	76.5	9.9	6.0	2.9	3.8
C12-262	134.4	34671	97373	229	1.6	41.6	73.1	17.5	21.7	99.1	10.8	4.8	1.1	5.5
C12-265	136.3	27438	74775	246	0.9	34.9	37.8	12.9	9.2	46.1	8.0	3.6	1.1	2.5
C12-268	138.7	34701	83180	249	1.3	43.4	57.0	15.0	12.3	63.8	9.6	4.0	0.9	3.3
C12-271	141.4	34833	97086	269	1.4	39.2	58.9	14.1	22.2	57.8	9.1	4.3	2.2	3.3
C12-274	144.1	26093	78941	333	0.9	31.4	60.4	11.6	13.6	47.0	11.2	3.0	1.2	2.9
C12-277	146.0	23210	76071	255	1.1	28.6	34.9	10.2	12.2	38.1	5.5	3.6	1.2	1.9
C12-280	149.4	23989	55470	212	1.4	34.2	37.6	9.8	9.2	34.9	6.3	4.0	1.0	2.4
C12-283	151.4	38630	89951	209	1.5	51.3	63.9	12.0	15.7	38.9	10.3	6.0	3.4	5.0
C12-284	151.7	31649	72908	301	1.1	40.4	50.9	12.0	15.3	52.4	20.3	5.2	4.0	9.0
C12-285	152.1	43719	106061	230	1.8	50.4	72.6	15.6	18.6	63.6	10.4	5.9	3.0	5.7
C12-286	152.7	13939	32815	162	0.4	16.7	26.9	7.7	8.2	34.1	6.4	1.8	0.9	8.4
C12-290	154.4	28162	63803	152	1.1	37.8	40.1	8.4	7.2	29.9	8.2	3.9	0.9	2.1
C12-293	155.8	19300	43860	169	0.7	24.9	31.0	6.8	5.8	30.2	6.8	2.7	1.2	2.5
C12-296	156.9	20732	47854	290	0.6	24.4	29.2	6.9	9.4	20.7	8.3	2.7	1.1	1.4
C12-299	158.7	16005	38771	135	0.9	19.4	26.9	7.6	10.4	30.3	6.2	2.5	1.1	8.4
C12-302	159.8	18771	43242	147	0.6	21.7	26.8	6.0	6.4	22.2	4.3	2.4	0.9	1.8

APPENDIX 2 continued...

Sample Id	Height	Al	Si	P	Ti	V	Cr	Fe	Co	Ni	Cu	Th	U	Mo
Units →	(m)	(ppm)	(ppm)	(ppm)	(ppt)	(ppm)	(ppm)	(ppm)	(ppm)	(ppm)	(ppm)	(ppm)	(ppm)	(ppm)
C12-303	160.2	20559	47029	148	0.6	24.1	29.2	6.5	4.2	20.3	4.8	2.7	1.1	1.3
C12-306	161.6	14686	34731	148	0.5	18.5	21.7	4.9	3.4	15.9	2.7	2.0	0.7	1.1
C12-309	163.1	31568	77488	184	1.2	39.5	41.1	9.6	13.2	28.2	6.3	4.0	1.3	1.1
C12-312	165.3	15697	38818	152	0.7	15.5	25.6	6.2	13.3	24.8	5.8	2.5	0.6	1.3
C12-315	166.9	9977	31067	97	0.4	14.6	20.9	4.4	4.2	25.0	3.4	1.4	0.9	2.3
C12-318	168.1	9573	28347	95	0.4	14.2	24.4	4.2	4.8	30.9	3.4	1.3	0.5	3.1
C12-321	169.4	7179	25592	75	0.3	10.8	19.8	3.8	15.0	30.6	3.0	1.0	0.5	2.7
C12-324	170.6	10561	32507	78	0.3	13.9	24.0	5.5	7.2	36.8	4.3	1.3	0.9	3.3
C12-327	171.7	8752	30283	73	0.3	12.2	17.5	3.8	6.2	22.4	2.8	1.3	0.6	2.5
C12-333	174.5	9336	27708	114	0.3	13.6	17.5	4.5	6.3	18.2	3.1	1.0	0.7	1.6
C12-336	177.1	13576	40800	86	0.5	21.6	24.7	5.9	6.1	28.6	4.6	1.7	0.8	2.3
C12-339	178.6	10260	28039	74	0.4	16.4	22.5	5.1	4.0	24.8	3.9	1.2	0.9	1.8
C12-342	180.6	8939	26189	140	0.4	13.6	16.3	4.0	6.7	19.3	2.5	1.0	0.6	0.9
C12-345	181.9	7398	22653	84	0.3	9.1	15.5	3.6	4.9	19.3	2.1	0.9	0.5	1.5
C12-348	182.8	13112	35219	80	0.5	19.4	22.7	5.5	4.9	23.9	3.8	1.4	0.6	1.4
C12-351	183.8	16665	44840	92	0.6	25.6	28.7	6.0	4.0	25.2	3.7	1.9	0.8	1.3
C12-360	187.6	12757	34307	89	0.5	18.8	26.7	4.8	5.3	24.8	3.3	1.5	0.6	1.0
C12-363	188.7	11139	31576	63	0.4	16.1	23.3	4.0	4.4	20.2	3.2	1.3	0.4	1.0
C12-366	189.4	13666	36552	88	0.5	20.3	26.2	5.5	8.6	22.9	3.3	1.4	0.6	1.4
C12-369	190.3	12596	35703	83	0.6	19.3	29.9	6.0	13.2	39.3	3.5	1.4	0.7	1.7
C12-372	191.4	18699	53138	102	0.8	25.6	33.1	6.1	20.9	27.2	3.3	2.1	0.7	1.3
C12-375	192.4	29686	83392	212	1.5	46.5	57.3	11.8	28.6	48.3	7.5	3.2	1.3	2.2
C12-378	193.4	21738	58256	121	1.0	33.9	39.8	7.7	11.6	25.8	5.0	2.3	0.9	1.6
C12-381	194.0	19275	54036	117	0.9	29.4	35.1	6.6	18.0	18.5	4.5	2.0	0.9	0.8
C12-384	194.6	15585	33276	127	1.1	31.3	36.7	7.6	22.1	28.2	10.7	1.5	1.0	0.5
C12-387	195.5	13069	30821	131	0.6	23.6	25.6	5.5	19.4	17.5	2.7	2.0	0.8	0.3
C12-390	196.3	16798	35618	126	0.9	31.9	35.9	7.8	8.5	23.3	7.3	1.4	0.7	1.4
C12-393	196.9	14524	33190	184	0.8	24.5	24.6	5.9	10.2	16.3	3.5	2.0	0.6	0.6
C12-396	197.9	15559	33874	172	0.9	30.4	35.0	7.4	10.0	23.5	6.5	1.4	1.0	0.7
C12-399	198.4	13680	29042	282	0.7	21.7	24.6	7.2	16.2	22.5	4.4	1.7	0.9	0.9
C12-401	198.8	7721	16809	103	0.7	14.1	23.4	5.3	18.7	19.9	4.7	0.7	0.6	0.6
C12-404	199.4	14562	29824	204	0.6	24.1	24.3	6.3	11.4	19.8	3.7	1.7	1.2	1.0
C12-406	199.8	16561	36802	263	0.9	30.4	33.7	6.5	10.3	16.2	7.5	1.5	0.8	0.7
C12-412	201.0	25416	51523	162	1.5	39.0	64.7	8.3	14.7	29.4	8.2	2.5	1.1	1.2
C12-414	201.3	27268	56546	224	1.3	42.8	43.3	10.7	13.9	28.5	5.9	3.3	1.0	1.2
C12-417	201.7	17078	43417	266	0.9	34.4	48.7	7.8	19.6	22.3	8.4	1.7	0.8	0.9
C12-422	203.1	15561	31466	116	1.0	24.7	31.0	7.7	7.8	23.6	7.5	1.4	0.8	1.0
C12-425	203.7	16472	35539	192	0.8	22.2	24.6	7.4	10.1	19.9	3.9	2.5	1.0	1.0
C12-428	204.5	20739	44507	154	1.1	28.9	40.5	11.9	10.3	23.4	13.8	1.9	0.9	2.3

APPENDIX 2 continued...

Sample Id	Height	Al	Si	P	Ti	V	Cr	Fe	Co	Ni	Cu	Th	U	Mo
Units →	(m)	(ppm)	(ppm)	(ppm)	(ppt)	(ppm)	(ppm)	(ppm)	(ppm)	(ppm)	(ppm)	(ppm)	(ppm)	(ppm)
C12-434	206.7	16074	33063	133	0.8	19.5	29.0	6.1	8.5	18.9	5.7	1.3	0.6	0.6
C12-439	209.9	30822	62606	246	1.4	31.3	43.9	14.0	13.0	24.3	6.9	3.5	1.2	0.7
C12-449	213.1	23064	50544	151	1.1	33.2	36.9	14.5	30.8	29.3	4.8	2.9	0.9	0.7
C12-458	217.4	30470	60152	286	1.2	36.7	38.1	13.3	8.8	20.2	4.3	3.3	0.8	0.9
C12-471	227.5	51471	93983	425	1.7	75.6	69.6	21.6	20.4	41.7	9.3	5.3	1.2	0.5
C12-477	233.3	49841	95192	450	1.7	71.7	59.8	22.5	21.0	36.8	8.0	6.1	1.5	1.0
Ave. Std	→	2382	4781	43	0.2	12.1	5.4	1.2	2.0	7.0	1.6	0.4	0.2	0.2

APPENDIX 3

Appendix 3 Semi-quantitative bulk mineral composition of selected samples along the stratigraphic log.

Sample Id	Height (m)	Clay	Quartz	K-feldspar	P-feldspar	Calcite	Dolomite	Pyrite/Marc.
C10-04	0.7	5%	17%	0%	5%	72%	1%	1%
C10-17	5.4	12%	25%	0%	5%	51%	2%	5%
C10-19	6.1	15%	25%	0%	7%	52%	1%	0%
C10-31	13.7	13%	14%	0%	6%	64%	1%	1%
C10-58	20.8	7%	9%	0%	3%	78%	3%	1%
C10-77	27.7	5%	7%	1%	2%	84%	1%	1%
C10-85	31.3	6%	10%	1%	3%	76%	3%	1%
C11-109	41.8	3%	6%	1%	2%	86%	1%	1%
C11-169	62.0	9%	14%	0%	5%	72%	0%	1%
C11-205	81.1	9%	17%	2%	5%	65%	1%	0%
C12-211	88.0	6%	15%	2%	4%	66%	1%	3%
C12-229	105.8	13%	22%	2%	7%	51%	1%	0%
C12-249	120.0	8%	15%	2%	4%	66%	1%	1%
C12-252	124.2	12%	17%	2%	5%	56%	3%	3%
C12-288	154.1	4%	8%	1%	2%	82%	2%	1%
C12-326	171.4	2%	7%	1%	3%	85%	1%	1%
C12-376	192.8	3%	13%	1%	3%	76%	1%	1%
C12-408	200.2	2%	6%	0%	2%	87%	2%	1%
C12-412	201.0	3%	7%	1%	3%	83%	2%	1%
C12-415	201.5	2%	5%	1%	2%	86%	1%	2%
C12-416	201.6	3%	9%	1%	1%	83%	2%	1%
C12-431	205.6	2%	7%	1%	2%	83%	1%	1%
C12-435	207.9	3%	8%	1%	3%	79%	2%	1%
C12-437	208.8	2%	7%	1%	4%	84%	1%	1%
C12-441	210.6	2%	7%	1%	5%	79%	2%	2%
C12-445	211.8	2%	8%	2%	5%	79%	1%	0%
C12-446	212.1	2%	6%	1%	4%	85%	1%	1%
C12-461	220.1	7%	15%	2%	3%	65%	2%	3%
C12-471	227.5	3%	13%	2%	3%	75%	2%	2%
C12-478	234.9	10%	13%	2%	3%	67%	1%	1%

APPENDIX 4

Appendix 4 Pristane/phytane ratio of all samples analyzed for n-alkane composition with the corresponding stratigraphic level.

Sample	Height (m)	Pr/Phy
C10-04	0.7	1.5
C10-05	1.2	2.2
C10-17	5.4	1.7
C10-19	6.1	1.6
C10-20	7.2	2.5
C10-23	9.0	1.9
C10-25	10.3	1.4
C10-31	13.7	1.6
C10-34	14.8	1.8
C10-41	16.6	1.6
C10-48	18.2	1.5
C10-50	18.6	1.6
C10-58	20.8	0.9
C10-70	25.5	1.7
C10-77	27.7	0.9
C10-79	28.4	1.6
C10-80	28.7	1.6
C10-83	30.5	1.6
C10-87	32.3	2.1
C11-109	41.8	1.2
C11-117	43.6	1.6
C11-149	52.6	1.4
C11-175	64.0	1.7
C11-199	73.0	1.1
C12-227	104.1	1.2
C12-249	120.0	1.3
C12-252	124.2	1.1
C12-261	132.6	1.3
C12-263	135.2	1.3
C12-287	153.0	1.4
C12-314	166.4	1.1
C12-337	178.0	1.1
C12-349	183.2	0.7
C12-405	199.5	0.8
C12-460	218.9	1.8
C12-470	227.0	1.6

VITA

YOSMEL SANCHEZ HERNANDEZ

Born, Mayabeque, Cuba

- 1997-2002 B.S., Nuclear Engineering
Higher Institute of Nuclear Sciences and Technology
Havana, Cuba
- 2002-2005 Specialist in Oil Well Drilling and Oil Production
Higher Polytechnic Institute Jose A. Echeverria
Havana, Cuba
- 2005 Oil Production Engineer
Cuban Petroleum Company
Matanzas, Cuba
- 2006-2009 Adjunct Faculty and Math Tutor
Miami Dade College
Miami, Florida
- 2009 -2014 Doctoral Candidate
Teaching Assistant
Florida International University
Miami, Florida
- Summer 2012 Dissertation Evidence Acquisition Fellowship
Miami, Florida
- May 2013 Outstanding Student Paper Award (OSPA) recipient at the
AGU Meeting of the Americas, Cancún
- Summer 2013 Professional Intern. ExxonMobil
Operations Geologist
Houston, Texas
- February 2014 Awarded best PhD geosciences presentation at the
scientific symposium of the Earth & Environment
department of Florida International University.
- March 2014 First place in the Bio-Geosciences oral presentations
Scholarly Forum. Florida International University

PUBLICATIONS AND PRESENTATIONS

Sanchez-Hernandez, Y., Maurrasse, FJ-MR., Moreno-Bedmar, J., Sen, I., (September, 2011) *Preliminary Interpretation of the Cabó Section, Sierra de Prada, South - Central Pyrenees, NE Spain*. The 8th Romanian Symposium on Paleontology, Bucharest, Romania.

Sanchez-Hernandez, Y., Maurrasse, FJ-MR., (May, 2013). *Episodic Enhanced Carbon Sequestration from Late Barremian to Early Aptian in a Restricted Marine Basin: The Organyà Basin*. AGU Meeting of the Americas, Cancun, Mexico. Oral Presentation: Control ID 1667837.

Sanchez-Hernandez, Y., Maurrasse, FJ-M.R., (October, 2013). *Mechanisms of Organic Carbon Sequestration During the Early Aptian in the Restricted Organyà Basin*. GSA Annual Meeting, Denver, CO. Oral presentation. Paper No. 303-5.

Sanchez-Hernandez, Y., Maurrasse, F. J-M.R., 2014. *Geochemical Characterization and Redox Signals from the Latest Barremian to the Earliest Aptian in a Restricted Marine Basin: El Pui Section, Organyà Basin*. *Chemical Geology* 372, 12-31.

Sanchez-Hernandez, Y., Maurrasse, F. J-M.R., Melinte-Dobrinescu, M.C., He, D., Butler, S.K., 2014. *Assessing the Factors Controlling High Sedimentation Rates from the Latest Barremian–Earliest Aptian in the Hemipelagic Setting of the Restricted Organyà Basin, NE Spain*. *Cretaceous Research* 51, 1-21.